2017

THE IMPACT OF WATER INJECTION ON SPARK IGNITION ENGINE PERFORMANCE UNDER HIGH LOAD OPERATION

Jeremy Worm
Michigan Technological University, jjworm@mtu.edu

THE IMPACT OF WATER INJECTION ON SPARK IGNITION ENGINE PERFORMANCE UNDER HIGH LOAD OPERATION

By

Jeremy Worm

A DISSERTATION

Submitted in partial fulfillment of the requirements for the degree of

DOCTOR OF PHILOSOPHY

In Mechanical Engineering-Engineering Mechanics

MICHIGAN TECHNOLOGICAL UNIVERSITY

2017

This dissertation has been approved in partial fulfillment of the requirements for the Degree of DOCTOR OF PHILOSOPHY in Mechanical Engineering-Engineering Mechanics.

Department of Mechanical Engineering – Engineering Mechanics

Dissertation Advisor:	*Dr. Jeffrey D. Naber*
Committee Member:	*Dr. Darrell Robinette*
Committee Member:	*Dr. Jason Blough*
Committee Member:	*Dr. Scott Wagner*
Department Chair:	*Dr. William W. Predebon*

Dedication

I dedicate this dissertation to my loving wife Jennifer. Without her unwavering support and encouragement this would not have come to completion.

Contents

List of Equations

List of figures

List of tables

Preface

During the process of completing this dissertation, a journal publication was produced and published in SAE Journal of Engines (Worm 2017). That publication focuses on a portion of the work included in this dissertation. This dissertation includes little text from the publication, but does include multiple figures and tables with only subtle changes. All figures and tables that are reproduced are acknowledged in the figure / table captions.

Some of the work contained within this dissertation was produced collaboratively with Joel Duncan, Michigan Tech APS LABS Staff Engineer, as Mr. Duncan assisted extensively in the experimental setup and data collection efforts. Furthermore, the image shown in Figure 17 was obtained by Mr. Duncan, and Mr. Duncan generated *Figure 46*, Figure 54, and Figure 55. Some of these figures were used in the publication referenced above (Worm 2017), of which Mr. Duncan was a co-author.

Acknowledgements

This work has come to fruition through the immense support of many individuals, all of which deserve tremendous gratitude.

The project was made possible through the support of Nostrum Energy, the project sponsor. The support of Nostrum Energy was far reaching; not only in the form of initial funding, but also throughout the project. Nostrum's engagement in the project was appreciated, and in fact was the most engaged and enthusiastic sponsor I have worked with in over 10 years of being a Principal Investigator at APS LABS. I sincerely wish to thank the whole team at Nostrum Energy including Sam Barros, Frank LoSrudato, Bill Atkinson, and Brian Eggart for making this project possible.

Joel Duncan, Research Engineer at APS LABS was instrumental in making this project a success. The value of his skill and expertise in engine assembly cannot be overstated. Mr. Duncan stuck it out with me in this project from the very beginning to the very end. This included celebrating the milestones and wins, but also the many late nights, broken parts, and general frustrations. Creating and operating this testbed, on the ragged edge of sending parts flying across the testcell, is not for the faint of heart. Those kinds of experiences that turns expensive parts and instrumentation into unique paperweights tends to create either friends or enemies, so I am glad to say the latter was formed. I owe Joel a beer,…or six.

There were so many individuals that provided technical assistance, it is impossible to list them all. Tucker Alsup, Research Engineer at APS LABS is always eager to help anyone in need. He has a wealth of technical knowledge and skill, and is the person you want to have in the passenger seat when your vehicle breaks down on a two-track dirt road. Simon Wang, PhD candidate at APS LABS is a whiz at using MotoTron, and it really showed when it was time to control the water injectors. Uwe Ostmann of Xtreme DI was instrumental in getting the engine running with the Bosch controller, working tirelessly with me to debug some seemingly simple problems that proved to be quite challenging. I

think Uwe and I may have set a record for the amount of data sent via text message between two people. I also had the opportunity to meet Billy Godbold, Derrick Hubbard, and Chris Sulewski all from Comp Cams when it came time to ponder increased fuel pump lift and valve actuation. Their professionalism, responsiveness, and knowledge made for a great experience. Hugh Blaxill from Mahle Powertrain came through as he always does with great knowledge and insight. It is always a pleasure to talk to Hugh. Ryan Graham and the entire crew at ZZ Performance was great to meet and talk with throughout the project. So much insight, and so willing to share it; greatly appreciated. Craig Giraud at A&D Technologies was critical in assisting with commissioning of the new CAS system. Craig really understands how important his role is the success of his customers, and it shows. Getting into the lube side of things was a really nice unexpected benefit of this project, and through that, I got to know Lake Speed Jr. of Driven Racing Oil. Lake is a lubrication expert with a passion for engines; what a perfect combination. Lake was eager to share his knowledge with me, and I very much look forward to working with Lake again in the future. I've known Steve Bethel of Leadfoot Engineering since about 2004, and I am so glad I do. Steve is the world's foremost expert on pistons, so when inevitably I needed help with pistons, there was nobody else I wanted to talk to. An amazing wealth of information, and his skills are in such high demand, and yet so willing to help me with this project. I'm also glad I had others like Paul Dice and Duane Bucheger at APS LABS as well, both of whom were also eager to help. Dr. Scott Miers of APS LABS is always a pleasure to talk to. I had some great technical conversations w/ Scott during the course of this project, and I really appreciate his willingness to help me learn. The help and encouragement that Tina Sarazin provided throughout the entire project was very much appreciated. The engine R&D community is a small town, and I can't wait to work with all of these individuals again on a future project.

I wish to thank my committee consisting of Dr. Darrell Robinette, Dr. Jason Blough, and Dr. Scott Wagner, who were all an absolute joy to work with. They all took time out of their busy schedules to meet with me and provide valuable feedback. They were willing to receive updated drafts (nightly as the defense approached), and be flexible in their

schedules, the whole while providing encouragement. I sincerely appreciate their efforts in this; something they were not required to do, but chose to do. Truly a group of accomplished researchers and "doers" you want on your team.

I am privileged to have had the opportunity to have Dr. Jeffrey Naber as my Advisor. The technical conversations with Dr. Naber were truly fun, and valuable. The technical discussions inspired and reminded me why I became an engineer in the first place, something that is all too often easy to forget. Dr. Naber's knowledge in engines, combustion, and thermodynamics is unrivaled, and it is always a joy and privilege to engage in a deep technical discussion. I've been a research engineer at APS LABS for over 10 years now, so Dr. Naber is so much more than just my advisor, he has been my manager, my mentor, and most importantly my friend.

As much as all of these individuals helped me in the professional aspects of the project, I can never forget the support that I had outside of the office and lab in getting to this place. This support came in many forms. From the standpoint of earlier influences, my grandma grew up dirt poor on a farm during the great depression when she had to leave school permanently during the 8th grade. This was not something she wanted to do, but had to do. Because of this, she always instilled upon me the value of education. Meanwhile my grandpa was known for keeping and repurposing items. As a child, I found these caches of parts and pieces that were scattered throughout his barns and outbuildings, which many people would classify as "junk", to be rather inspirational. As I grew, my mom and dad always gave me the freedom to tinker with things in the garage. At an early age I was making various gadgets, and these progressed to building lawnmowers and go karts, then snowmobiles, then demolition derby cars, then finally I bought my first vehicle when I was 15, and proceeded to restore it since I couldn't drive it (much) until I was 16. I was pretty sure I wanted to be a mechanic, as I enjoyed working on cars, and thinking about how they ran. It was around this time that my Dad, a life-long heavy equipment mechanic, and a damn good one, planted a different seed by asking me if I would rather fix the cars that other people designed, or be the person designing and developing the cars. That seed

obviously took hold. I started dating my wife in high school (we actually met in 8th grade, but it wasn't until 11th grade that I convinced her I wasn't a complete weirdo), and from day 1 she supported this notion of me being an automotive engineer. After high school we moved to Michigan Tech, and she worked two jobs; cleaning hotel rooms in the morning and making pizza in the evening (washing her hands in between) to cover the bills while I worked toward my BSME. By the time I got my BSME she had worked her way up to hotel management and I was an engineer at GM, where I could not have asked for a better technical experience learning from some of the best engineers in the business. GM was good to me, and I learned so much there. After we moved back to Michigan Tech with me as a research engineer, my wife and I discussed me getting a PhD, and she supported it fully. It has been a long hard road since that initial conversation. My boys gave me motivation through my desire to show them that hard work pays off, and in setting an example to achieve an education. They sacrificed in the form of lack of my time as I completed this degree. From my wife's perspective I can only imagine how hard it is taking care of two boys, a dog, and a house, while encountering numerous life events (some good, some bad) while your partner is working late in the office or on a business trip. However, she not only handled it like the true champion she is, but found the stamina to encourage and motivate me through it all. There were many late nights I was in the lab kicking and cussing at a test engine that would not start, while at the same time she was home kicking and cussing at the snowblower engine that would not start in the middle of a blizzard. Words don't describe the sacrifices she made, and the strength she needed to have for me to get this degree.

God has surrounded me with an amazing network of old friends, new friends, and family who have made this possible, and I am grateful for that.

List of Abbreviations

AEAP – Average Exhaust Absolute Pressure

AIS – Air Induction System

AKI – Anti-Knock Index

APSRC – Advanced Power Systems Research Center

APS LABS – Advanced Power Systems Labs

ASTM – An International organization for the standardization of test procedures

ATDC – After Top Dead Center

$ATDC_{ge}$ – After Top Dead Center Gas Exchange

BDC – Bottom Dead Center

BMEP – Break Mean Effective Pressure

BTDC – Before Top Dead Center

CA – Crank Angle

CAC – Charge Air Cooler

CA50 – Crank Angle where 50% of the fuel mass has burned

CAD – Crank Angle Degree (the primary reference used throughout this document)

CAD – Computer Aided Design

CFR – Cooperative Fuels Research

CI – Compression Ignition

CO – Carbon Monoxide

COTS – Commercial Off The Shelf

C_p – Specific heat capacity at constant pressure

CR – Compression Ratio

C_c – Specific heat capacity at constant volume

DI – Direct Injection

DIVVT – Dual Independent Variable Valve Timing

DLC – Diamond Like Coating

E0 – Refers to fuel with 0% Ethanol fraction

E10 – 10% Ethanol mixed with 90% gasoline

E85 – 85% Ethanol mixed with 15% gasoline

ECU – Electronic Control Unit

EES – Engineering Equation Solver

EGR – Exhaust Gas Recirculation

EGT – Exhaust Gas Temperature

EMOP – Exhaust Maximum Open Point

EOI – End of Injection

ESN – Engine Serial Number

ETC – Electronic Throttle Control

EVO – Exhaust Valve Opening

GE – Gas Exchange

HC – Hydro-Carbon

HEV – Hybrid Electric Vehicle

IC – Internal Combustion

ID – Inside Diameter

ICED – Internal Combustion Engine

IMOP – Intake Maximum Open Point

IVC – Intake Valve Closing

KLSA – Knock Limited Spark Advance

LBT – Leanest for Best Torque (referring to A/F)

LFE – Laminar Flow Element

LHU – 3 digit RPO code designating a particular model GM engine in the Ecotech family

LIVC – Late Intake Valve Closing

LSPI – Low Speed Pre-Ignition

MAF – Mass Air Flow

MAP – Manifold Absolute Pressure

MBT – Maximum Brake Torque

MFB – Mass Fraction Burned

MON – Motor Octane Number

MTBE – Methyl Tertiary Butyl Ether

MY – Model Year

n – Polytropic Index

NA – Naturally Aspirated

NO_X – Oxides of Nitrogen

NVH – Noise Vibration and Harshness

OEM – Original Equipment Manufacturer

ON – Octane Number

PID – Proportional Integral Derivative; a closed-loop control strategy

PPR – Pulse Per Revolution

PWM – Pulse Width Modulated

RBT – Richest for Best Torque (referring to A/F)

RO – Reverse Osmosis

RON – Research Octane Number

RPM – Revolutions Per Minute

RPO – Regular Production Order

SAE – Society of Automotive Engineers

SCFM – Standard Cubic Feet per Minute

SI – Spark Ignition

SOI – Start of Injection

SPI – Stochastic Pre-Ignition

TBI – Throttle Body Injection

TDC – Top Dead Center

TEL – Tetraethyl lead

TWC – Three Way Catalyst

V_c – Clearance Volume

V_d – Displaced Volume

VVA – Variable Valve Actuation

VVT – Variable Valve Timing

WOT – Wide Open Throttle

ZDDP - Zinc Dialkyldithiosphosphate

γ – Ratio of Specific Heat Capacities

ω – Humidity Ratio

Abstract

An experimental effort has been completed in which water injection was investigated as a means of enabling increases in engine output and high load efficiency. Water was injected into the intake port of a direct fuel injected, 4-cylinder, boosted engine with dual independent variable valve timing. The water was shown to increase volumetric efficiency and decrease the onset of knock which in turn enable more optimal combustion phasing. Both of these affects resulted increases in load of up to 5.5% at the same manifold pressure as the baseline case. The advancement of combustion phasing, combined with elimination of fuel enrichment resulted in an increase in full load thermal efficiency of up to 35%. Analysis is provided around these affects, as well as the phase transformation of water throughout the engine cycle.

1 Introduction

The 4-stroke Spark Ignition (SI) engine has been in use since the late 1800's (Heywood 1988). Following intense development during World War I, the SI Engine became the dominant automotive propulsion device.

The modern SI Engine has many strengths:

- It is highly scaleable,
- It operates over a wide range of ambient temperature (-40°C to 50°C typical),
- It operates over a wide range of ambient pressure (below sea level to the highest inhabited regions),
- Service life is typically as long or longer than the equipment being powered,
- Capable of meeting stringent emissions standards,
- Acceptable power density,
- Acceptable Noise, Vibration, and Harshness (NVH) levels,
- Acceptable thermal efficiency,
- Relatively low manufacturing cost,
- Highly recyclable with a relatively low fraction of hazardous or rare materials,
- Established manufacturing, service, and operating infrastructure.

Because of these and other strengths, the SI Engine is poised to remain a significant technology for at least several decades to come.

1.1 Load Control in SI Engines

In the SI engine, combustion of homogeneously mixed air and fuel, is initiated with a spark which is discharged at a pre-determined point in the cycle, generally 5° to 50° Before Top Dead Center (BTDC), depending on operating conditions. Following the spark discharge, a flame propagates through the unburned fuel – air mixture, eventually oxidizing >95% of the fuel mass that was trapped in the cylinder (Heywood 1988).

As the Hydro-Carbon (HC) based fuel oxidizes to less reactive compounds such as CO_2, and H_2O, thermal energy is released from the breaking of the Hydrogen – Carbon bonds. The energy released through this exothermic reaction increases the temperature in the cylinder, and subsequently the pressure. The high pressure gas is expanded as the piston descends the cylinder during the expansion stroke. This expansion is primarily where work is extracted from the working fluid[1].

By this account, it becomes apparent that increasing the amount of work extracted from the cycle, requires the oxidation of additional fuel (all else being equal). However, to sustain combustion, the ratio of air to fuel must be within a range around the stoichiometric air to fuel ratio. Engine researchers and developers will often refer to air fuel ratio relative to the stoichiometric air to fuel ratio, equation 1.

Equation 1: Lambda

$$\lambda = \frac{\left(\frac{A}{F}\right)_{actual}}{\left(\frac{A}{F}\right)_{Stoichiometric}}$$

Furthermore, for optimal performance of exhaust aftertreatment catalysts the air to fuel ratio must be very close to stoichiometric.

This implies that increasing load requires the mass of fuel *and* mass of air must be increased in proportion to each other. In practice an SI engine employs a throttle valve to regulate the flow of air into the cylinder during the intake stroke. The air mass is measured, and an appropriately proportioned mass of fuel is injected. Opening the throttle valve allows more air, and thus more fuel, to enter the cylinder, thus temperature and pressure is higher

[1] The use of the word "primarily" is used here to acknowledge that work can be extracted during the intake stroke as well, however, this is insignificant compared to the work extracted during the expansion stroke.

following combustion, more moles of molecules are available to expand, resulting in more work to be extracted.

During operation, the dynamic load range of an engine can be adjusted from zero[2] to the point where the throttle valve is fully open or Wide Open Throttle (WOT). At WOT, it can be assumed that the pressure in the cylinder following the intake stroke is near atmospheric. As such, the ideal gas law (Equation 2: Trapped Air Mass) provides a first approximation of the mass of air that can be trapped in the cylinder (and proportionally the mass of fuel).

Equation 2: Trapped Air Mass

$$\frac{PV}{RT} = m$$

Where:

P=Pressure

V=Volume

m=Mass

R=gas constant

T=Temperature

1.2 Methods of Increasing Load

If a particular vehicle application requires more load than a given engine can produce at WOT, then an examination of equation 1 suggests that either the volume in the cylinder must be increased or the pressure at Intake Valve Closing (IVC)[3].

[2] The work extracted from the gas during the expansion stroke is equal to the work required for the other three engine strokes and the mechanical friction of the engine.

[3] R is constant for air. T can't be reduced below ambient.

1.2.1 Increased Displacement

Indeed, increasing the displaced volume of the engine is an effective method of increasing trapped mass under WOT conditions, and thus dynamic load range of the engine. This method of increasing load capacity comes with a penalty. When the load demand is not high, the engine must be throttled, potentially heavily, and this leads to additional pumping losses, and a reduction in engine efficiency. There are however many technologies in production today to mitigate these effects. The most common of these technologies include cylinder deactivation (a form of variable displacement), and variable valve timing.

1.2.2 Increased Pressure (Boosting)

Alternatively, an engines displaced volume can remain fixed, and the intake charge can be boosted to increase the mass trapped in the cylinder at IVC. Boosting is most commonly accomplished through either a compressor driven from the engines cranktrain (supercharging) or a compressor driven from a turbine which extracts energy from the engines exhaust stream (turbocharging). Electrically assisted boosting (e-boost) is becoming increasingly popular, and can be a variant on either of these traditional technologies.

1.2.3 Limitations of Boosting

In theory, boosting an engine is a simple means of increasing load, with subsequent increases in boost resulting in proportional increases in load. However, a practical limit is reached. Increases in boost level leads to increased pressure and temperature in the unburned fuel and air mixture. If left at a high enough temperature for a long enough period of time, the unburned mixture will auto-ignite. The auto-ignition event is a near instantaneous release of heat in the end-gas zone (unburned zone). This rapid heat release

leads to a locally high temperature and an oscillating pressure wave. The high temperature and oscillating high pressure can lead to catastrophic engine damage[4].

The onset of auto-ignition, most commonly referred to as "knock" in the engine R&D community is dependent on the time-temperature history of the unburned end-gas during the compression and expansion strokes.

Furthermore, different fuels behave differently relative to their tendency to auto-ignite. The metric that serves as a proxy for the tendency of a particular fuel to auto-ignite is the fuels Octane Number (ON). The ON can be given as either the Motor Octane Number (MON) or Research Octane Number (RON), with the difference resulting from differences in operating conditions and control parameter settings during the engine tests that assess ON. A metric that the consumer is more accustomed to seeing is the fuels Anti-Knock Index (AKI). AKI is the average of the RON and MON, as shown in Equation 3: Anti-Knock Index.

Equation 3: Anti-Knock Index

$$AKI = \frac{RON + MON}{2}$$

1.2.4 Auto-Ignition Mitigation Techniques

The knock limit can be deterred, albeit incrementally, through several means, however, all with their drawbacks. These methods will be briefly introduced.

1.2.4.1 Fuel

Purely from the perspective of the engine developer, perhaps the easiest way to increase engine dynamic range with boost beyond the auto-ignition limit is with increases in fuel

[4] Although one can envision mechanical limitations as well, modern materials and manufacturing advancements have made mechanical limitations secondary to the combustion limitations (auto-ignition), and thus mechanical limitations are ignored in the context of this discussion.

ON. However, this is not trivial from the perspective of the fuel chemist. Keeping the discussion focused on HC based liquid fuels, there are practical limits for ON, and these limits are even more difficult to achieve when constraints prohibit the use of toxic additive such as tetraethyl lead (TEL) and Methyl Tertiary Butyl Ether (MTBE). Therefore obtaining fuels with an AKI significantly greater than today's common pump fuels results in substantial increases in cost, which the average consumer is not willing to accept.

1.2.4.2 Combustion Phasing

A longstanding and common technique for mitigating knock is to retard combustion phasing via retarded spark timing. By phasing combustion later in the cycle, the temperature of the end-gas is reduced, effectively delaying the onset of auto-ignition. This technique comes with multiple disadvantages. Foremost is a reduction in thermal efficiency (Worm 2013, Worm 2013). Furthermore Exhaust Gas Temperature (EGT) can increase significantly as less work is extracted prior to Exhaust Valve Opening (EVO). This increase in EGT results in a practical limit whereby further retarding of combustion phasing results in EGT levels that are damaging to exhaust valves, turbochargers, catalyst substrates, and other components.

1.2.4.3 Fuel Enrichment

Often used in conjunction with combustion phasing retard is fuel enrichment, whereby under heavy load lambda is decreased (fuel rich mixture). In a fuel rich condition, charge cooling is increased through the enthalpy of vaporization of additional fuel in addition to a reduced adiabatic flame temperature. The reduced end-gas temperature delays the onset of auto-ignition. The resulting reduction in burned gas temperature is used to counteract the increasing EGT resulting from retarding of combustion phasing. The negative impact of enrichment is a reduction in thermal efficiency.

1.2.4.4 Exhaust Gas Recirculation

As a diluent, Exhaust Gas Recirculation (EGR) is effective at reducing knock tendencies. Although effective in enabling MBT combustion phasing in moderate load throttled operating conditions, EGR is fundamentally difficult to use for extending the dynamic load

range of the engine simply because of the need to move gas from the relatively low pressure exhaust tract to the relatively high pressure intake tract. Furthermore EGR reduces volumetric efficiency, being directionally incorrect for increasing the engines load range.

1.2.4.5 Valve Timing

Valve timing, and in particular IVC can have a profound impact on the onset of knock. Holding the intake valve open deeper into the compression stroke delays the point at which compression begins, reducing the cumulative time-temperature history of the unburned gas. However, this significantly reduces volumetric efficiency. Because of this, there is a point of diminishing returns in terms of trying to trap more charge mass, while at the same time trying to reduce the charge time – temperature history with Late Intake Valve Closing (LIVC) (Worm 2007).

1.2.4.6 Compression Ratio

The engines geometric Compression Ratio (CR), Equation 4: Compression Ratio, can be reduced. This serves reduce the pressure during compression, leading to a reduction in unburned gas temperature. However, there is a well understood relationship between geometric compression ratio and cycle efficiency (Heywood 1988), Equation 5: Ideal Cycle Efficiency. In this sense, reducing CR to mitigate knock may well result in a beneficial tradeoff under high load operation whereby combustion phasing can be run closer to optimal. However, assuming a conventional cranktrain assembly, the CR is reduced across the entire engine operating regime. Therefore although the tradeoff may be positive under high load, cycle efficiency will be reduced at all other operating conditions.

Equation 4: Compression Ratio

$$CR = \frac{V_c + V_d}{V_c}$$

Where:

V_c = Clearance Volume

V_d = Displaced Volume

Equation 5: Ideal Cycle Efficiency

$$\eta = 1 - \frac{1}{CR^{\gamma - 1}}$$

Where:

γ = Ratio of Specific Heat Capacity of the working fluid

1.2.4.7 Water Injection

Another alternative for knock mitigation is injection of water into the Air / Fuel mixture, either upstream of the inlet valve, or directly in-cylinder.

Water is effective at sequestering knock through multiple mechanisms. With a latent heat of vaporization of 2257 kJ/kg (Cengel 2008) water has the effect of substantially cooling the charge air as the liquid water vaporizes. Furthermore the water vapor acts as a diluent in the combustion process, sequestering knock reactions in much the same way as cooled EGR gas.

1.3 Motivation

The current trend in the automotive industry is to downsize the engine with boosting devices added to maintain the load range the consumer expects. However, as previously discussed, in practicality there is an upper limit in boost / load due to the onset of combustion knock. Technologies and techniques currently employed to extend that limit are incremental at best, and moreover, result in notable decreases in thermal efficiency. In fact, evidence suggests that even at the degree of downsizing common with many production engines today, real-world fuel consumption is actually worse than it would be with a larger displacement conventionally sized engine (Bassett 2016). The reasons for this are likely 1) excessive spark retard to control knock, and 2) excessive fuel enrichment also to limit knock, and to limit high EGT resulting from the spark retard. As discussed, both spark retard and fuel enrichment have a detrimental impact on engine efficiency.

Without a paradigm shift, the current trend in downsizing and boosting will reach a plateau, where additional increases in boost pressure are simply not practical with any level of spark retard and fuel enrichment due to knock and pre-ignition limitations. Water injection has the potential to provide knock relief without the efficiency loss that comes with other knock mitigation techniques (excluding high-octane fuels), and therefore, has the potential to be that paradigm shift needed to avoid a plateau in engine specific output. A basic understanding of the operating characteristics of Internal Combustion (IC) engines and automotive systems, indicates several potential benefits of water injection as an enabler for extending the high load limit:

- Water is readily abundant and posses no adverse health or environmental effects. Due to its abundance, one can easily conceive technologies for in-situ water reclamation from engine exhaust, HVAC condensate, or rain
- Technology required for injecting water parallels well established hardware and software utilized for injecting fuel
- Water injection has the potential to squelch knock without negative impacts to engine efficiency

In due diligence it should be noted that there are potential negatives as well, which may include:

- Freezing of water in cold climates
- Lack of lubricity and potential corrosion issues in the supply, injection system, power cylinder, and turbocharger
- Limitations on mixing and vaporization leading to deterioration in combustion.

Although water-injection, as a concept, does have a relatively long history[5], there is evidence to suggest this concept has the potential for significant improvement in engine operation. Considering the potential to drive a paradigm shift, the ease of implementation, and seemingly solvable negatives, it is felt that water injection warrants a significant study

[5] This will be elaborated upon further in the literature review section.

to fully understand the details by which water interacts with the compression, combustion, and expansion processes.

1.4 Goals and Objectives

The overall goal of this research is to examine water injection as an enabler for increased engine BMEP and full-load efficiency relative to best-in-class engines as of the 2017 Model Year.

The specific objectives of this proposed research include:

1. Develop a multi-cylinder, boosted, high output SI Engine testbed
   1.1. Develop a robust, repeatable, and accurate experimental testbed to quantify and understand the thermodynamic and combustion related impacts of water injection on the 4-stoke spark ignited engine cycle.

2. Quantification of impacts
   2.1. Validate conclusions of previous researchers indicating injection of water significantly reduces knock tendencies. This objective establishes a foundation upon which all subsequent aspects of this research can be built.
   2.2. Demonstrate operation at manifold pressure levels corresponding to that of a current best in class BMEP production engine, but with ***87 AKI*** "Regular" fuel, and ***stoichiometric*** lambda. This objective is included because even at current best in class BMEP levels, operation on regular fuel and at lambda = 1 would be considered a significant result.
   2.3. Demonstrate operation at manifold pressure levels at least 10% greater than that of a current best in class BMEP production engine, with 91 AKI "Premium" fuel, and stoichiometric operation. This objective provides credibility to the previously made assertion that water injection could be the paradigm shift needed to continue

to push specific output increasingly higher. Although considered premium, 91 AKI is a consumer grade fuel, so demonstrating operation on pump fuel and lambda = 1 at higher than production manifold pressure is considered a significant result.

2.4. Quantify the impact of water injection on engine performance metrics including thermal efficiency, MEP, etc. Like objective 2.3, demonstrating a quantified efficiency improvement lends credibility and underscores the relevance of the research.

2.5. Increase the level of understanding regarding how water injection affects the engine operating cycle.

2 Literature Review

2.1 Trends in Downsizing and Boosting

(Bassett 2016) points out that downsizing with boosting has been a clear trend in the automotive sector since the turn of the millennium. The driving factor has been improvement of part load efficiency in the load range found on regulated drive cycles. For a given automotive platform (i.e. road load on a drive cycle), a smaller engine will operate less throttled than a larger engine, thus there will be efficiency gains due to a decrease in pumping work. Depending on how the downsizing is implemented, it may be accompanied by frictional improvements as well. However, as noted in the previous discussion, in order to maintain customer expected performance targets the smaller engine must be boosted to increase its specific output. Furthermore, as noted, there exists a limit on boost whereby further increases in boost lead to retarded combustion phasing and enriched lambda in order to avoid knock and control EGT, thus reducing efficiency. This may lead one to suspect that although a downsized boosted engine may achieve improved low load efficiency such as on regulated drive cycles, it may come at the cost of reduced high load efficiency when compared to a larger displacement engine.

(Bassett 2016) goes on to make an analysis from which some predictions can be made. By scaling data from a 3.2L Naturally Aspirated (NA) engine, (Bassett 2016) predicts that 24 bar BMEP is about the practical upper limit with current conventional engine technology including single stage pressure charging systems. In other words, one should not expect to see production engines exceeding 24 bar peak BMEP significantly without a major shift in engine technology or development and adoption of cost effective high-octane fuels.

Moreover, as shown in Figure 1, (Bassett 2016) claim that even if engines are pushed beyond 24 bar BMEP to approximately 32 bar peak BMEP, a point of diminishing returns is reached in terms of reductions in fuel consumption / CO_2 on regulated test cycles. (Bassett 2016) explains that this point of diminishing returns is reached from a number of

factors including reductions in base engine compression ratio (to mitigate high load knock), and increasing friction.

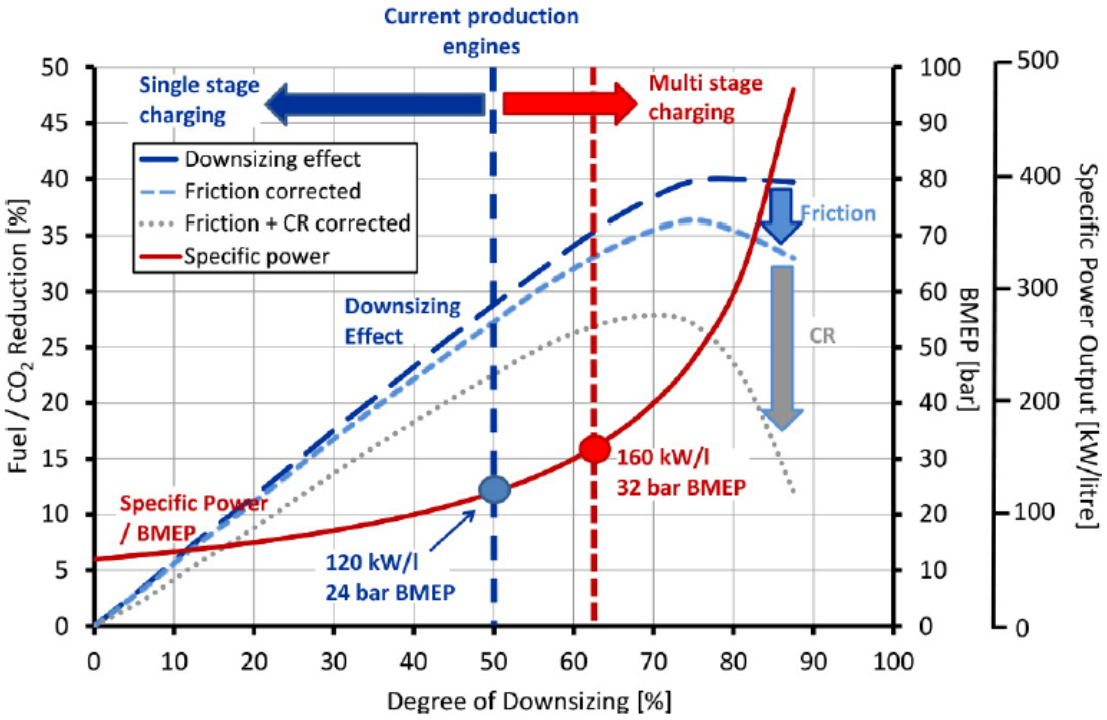

Figure 1: Estimated limit in output with current conventional pressure charging systems, and point of diminishing returns in terms of fuel consumption. Reproduced by permission from SAE International Journal of Engines via Copyright Clearance Center, *Heavily Downsized Gasoline Demonstrator* (SAE Int. J. Engines 9(2):2016, doi:10.4271/2016-01-0663, 2016, pg 2). See. Copyright documentation, 9Appendix F.

Although the (Bassett 2016) conclusions are reasonable given a fundamental understanding of SI IC Engines, the point of diminishing returns may in fact be lower than predicted by (Bassett 2016) as evidenced by at least one study. (Mock 2013, Tietge 2016) have identified real world data suggesting that indeed there is a point of diminishing returns in terms of downsizing and boosting. (Mock 2013) examined fuel consumption on regulated drive cycles compared to real world driving for the same vehicle, and have found that there is a growing trend where real world driving results in higher fuel consumption than the regulated cycles. They have shown the discrepancy between on-cycle and on-road CO_2 (in the US derived from fuel consumption data) was below 10% in 2001, and by 2011 it rose

to approximately 25%[6]. (Mock 2013) goes on to suggest at least one factor explaining this discrepancy may be a correlation with the trend in downsizing and boosting, as pointed out previously. This suggests that although engine downsizing is effective at reducing pumping losses and improving on-cycle efficiency, the higher loads encountered in real world driving, push the engine into a boosted region, wherein combustion phasing is becoming increasing retarded from MBT, and lambda may be enriched for knock control or hardware protection, thus leading to a loss of efficiency in real world driving conditions.

The results of the (Bassett 2016) work and the findings of (Mock 2013) may leave one curious as to where the bulk of current engines fall relative to peak BMEP. When examining engine trends, a rich pool of information can be found in the annual datasets compiled and published through Ward's Auto in collaboration with Mahle (Ward's Auto 2017). A new database is released annually for each new Model Year (MY). The data is primarily focused on engine architecture and manufacturing details, but does include thermodynamic parameters such as peak torque, displaced volume, and Compression Ratio. The report was copied into an MS Excel spreadsheet to allow for calculations and graphs to be made. Brake Mean Effective Pressure was calculated from the data according to Equation 6.

Equation 6: Brake Mean Effective Pressure

$$BMEP = \frac{\tau * n * 2\pi}{V_d}$$

Where :

τ = Brake Torque

n = Crank Revolutions per Cycle (2 for a 4 - stroke engine)

V_d = Displaced Volume

Using the Ward's / Mahle report for the 2017 MY light duty vehicles (Ward's Auto 2017), several interesting observations can be made. By looking simply at peak BMEP, it can be

[6] It should be noted that in 2008 in the US, additional test cycles were added to better account for discrepancies, however, Mock's 2013 study should include this.

shown that there are a fair number of engines achieving greater than ~25 bar peak BMEP, as shown in Figure 2[7].

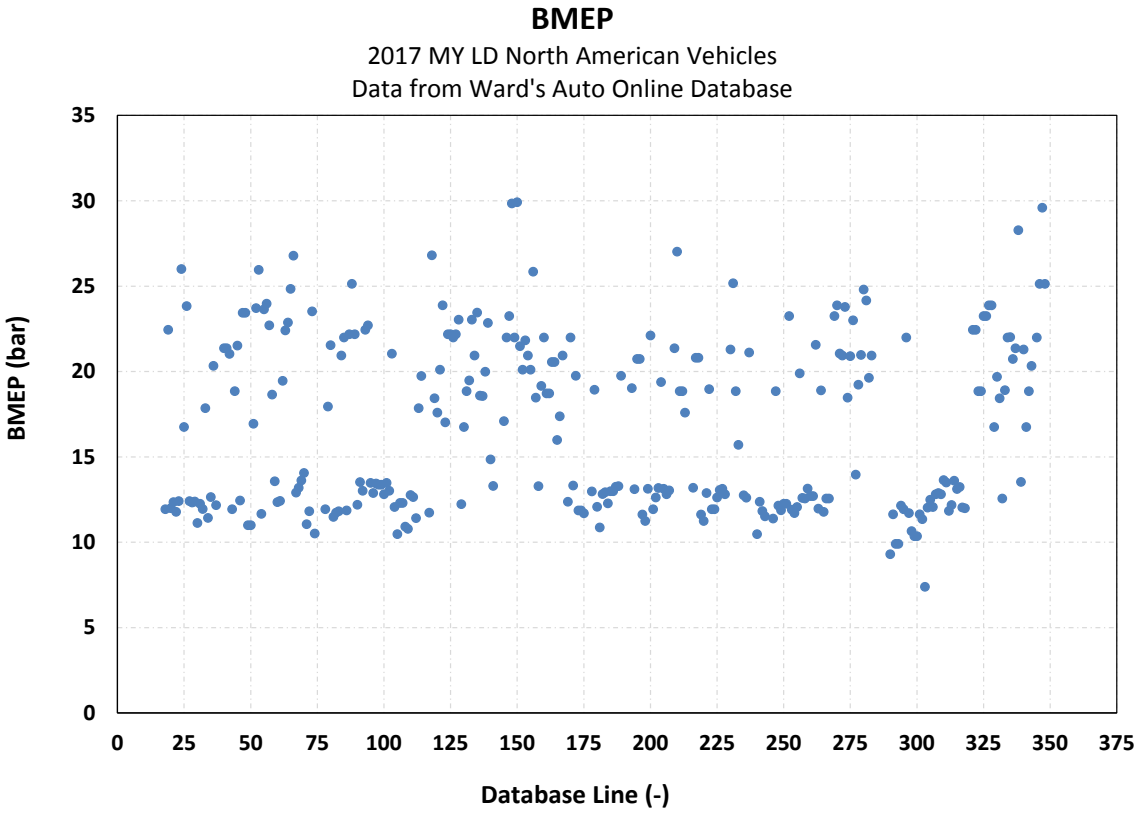

Figure 2: Peak BMEP for engines in 2017 MY Light Vehicles. Data from the 2017 Ward's / Mahle Light Vehicle Engines report (Ward's Auto 2017).

At the onset, this may appear to contradict the relatively recent (2016) claim by (Bassett 2016) that peak BMEP on production engines is not likely to exceed ~24 bar BMEP. However, one must dig deeper. By cross plotting the BMEP against CR, as in Figure 3, some aspects of the engine's technology level begin to appear.

[7] Upon initial plotting of the 2017 MY data in the Ward's / Mahle database, there were three engines which stood out from the trend when examining multiple parameters. These engines were examined further by looking at other publically available data including the OEM's websites, and vehicle reviews published by Car and Driver and MotorTrend. Upon further investigation, it was concluded there were errors in the data published by Ward's / Mahle. The errors are related to unit conversion issues, and transposing units for brake torque. For all subsequent discussions and plotting in this section, the corrected database is being used.

First, the Compression Ignition (CI) engines are clearly grouped for all CR's greater than 15:1. The CI engines alone, account for at least 5 of the datapoints greater than 25 bar BMEP.

Next, a small group of engines can be identified with a relatively high CR (~13:1), yet with a relatively low peak BMEP. These are likely "high efficiency" engines, such as those employing Late Intake Valve Closing (LIVC) timing or similar strategies. These types of engines are often found in Hybrid Electric Vehicles (HEV), where the electric propulsion system can be used for load leveling, lowering the requirements for peak engine BMEP.

Beginning with CR at ~12:1 and below, two more groups of data appear; a high BMEP and a low BMEP group, with the separation between the two groups being ~15 bar BMEP. The high BMEP group is formed from boosted engines (primarily turbocharged, but may include supercharged engines), while the low BMEP group is formed from Naturally Aspirated (NA) engines. To substantiate this claim, several specific data points within each of these two groups, but along the boundaries were investigated deeper, and confirmed to indeed be NA and Boosted engines respectively.

Finally, in Figure 3 it becomes apparent (and illustrated by the straight line) that there is a correlation between peak BMEP and CR. As peak BMEP is increased, base engine CR decreases in order to suppress high load knock. Recalling previous discussion, including that of Bassett et al., there will be a loss of efficiency, as CR is decreased to limit knock, and furthermore, this corroborates Mock et al.'s claim that as the number of boosted engines increase, the deviation between on-cycle and real-world fuel consumption increases.

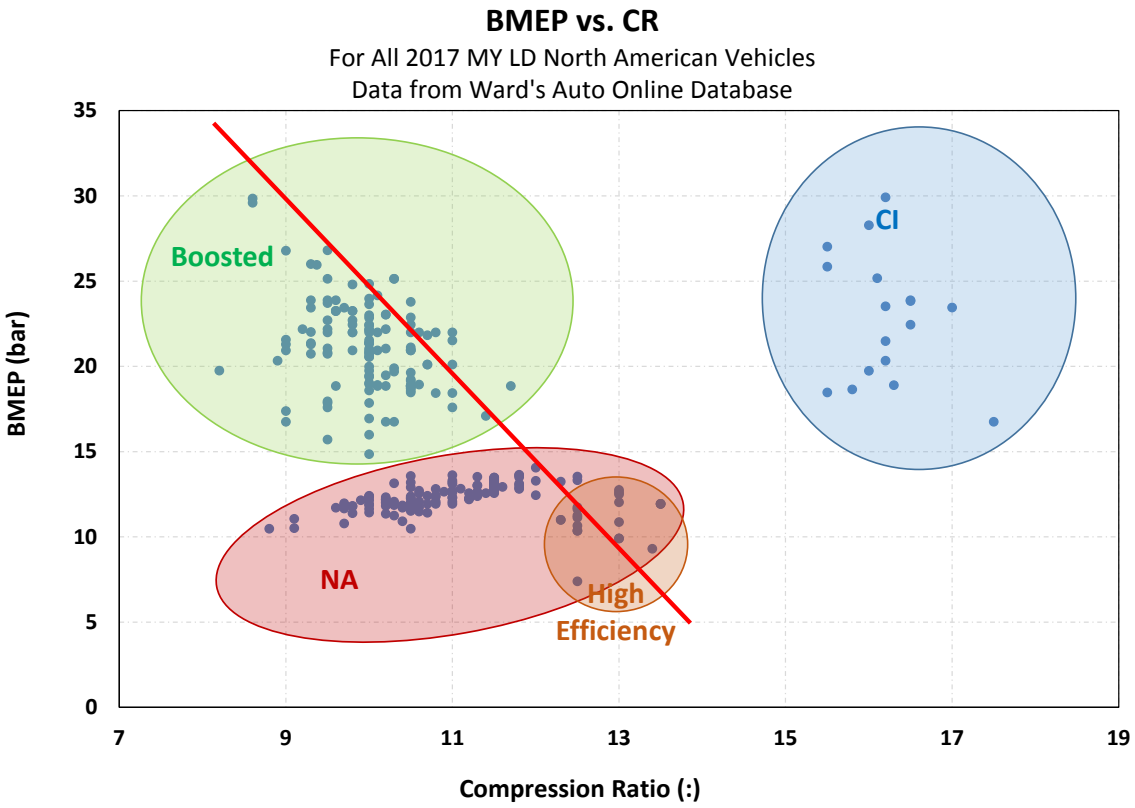

Figure 3: BMEP as a Function of Compression Ratio for 2017 MY Light Vehicles. Data from the 2017 Ward's / Mahle Light Vehicle Engines report (Ward's Auto 2017).

The discussion thus far of the 2017 MY LD Vehicle data has not fully addressed the apparent discrepancy between Bassett et al.'s claims that ~24 bar BMEP should be considered the upper limit for production engines, and the fact that Figure 2 and even Figure 3 shows a large number of engines greater than 24 bar BMEP. Separating the CI engines, partially explains this discrepancy, but not entirely, as there are still 15 engines in the 2017 MY with a CR < 15.0:1, and a BMEP greater than or equal to 24.0 bar.

Taking another cut through the data, Figure 4 plots only those engines that have a CR < 15.0:1, and BMEP greater than or equal to 24.0 bar BMEP against annual sales volume. Here it can be seen that of the 12 SI engines with BMEP above 24.0 bar, only one has an annual sales volume even approaching 100,000 units, with the remainder being significantly below this, and 10 engines being at or below 17,000 units. To put this into

perspective, the engine with the highest sales for MY 2017 is 1,012,000. The highest BMEP engine (29.8 bar) has only 17,000 sales, and one of the engines (26.8 bar BMEP) has a sales volume of only 100 units.

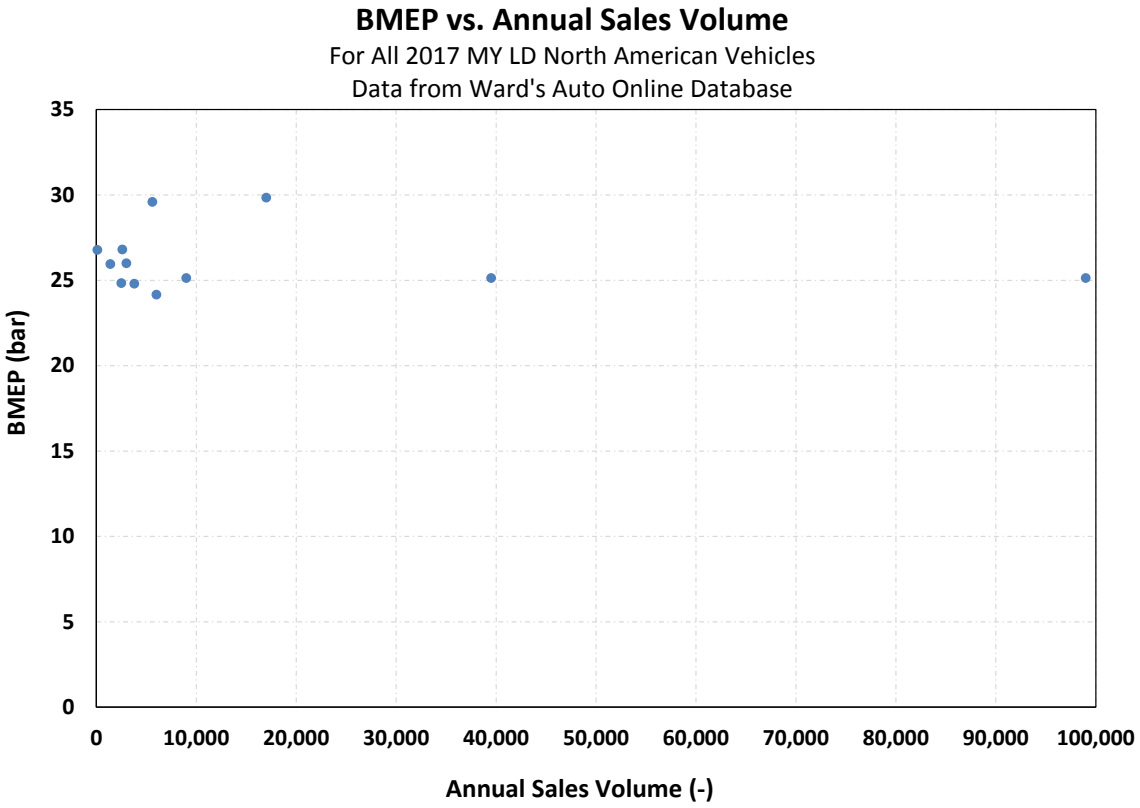

Figure 4: BMEP as a function of Sales Volume for 2017 MY Light Vehicles. Data filtered for CR < 15.0:1, and BMEP > 24.0. Data from the 2017 Ward's / Mahle Light Vehicle Engines annual report (Ward's Auto 2017).

What these low sales volumes suggest is this subset of engines with BMEP greater than or equal to 24.0 bar, are likely installed in specialty vehicles catering to a niche market. These types of vehicles are typically not the primary transportation vehicle for a family or even an individual, and as such, owners are more accepting of unique requirements, perhaps filling with premium fuel for example. Additionally, these low production volume vehicles may have a relatively high initial sales price to cover increased content such as Direct Injection, piston oil squirters, Variable Valve Actuation (VVA) technologies, and not only one, but perhaps multiple pressure charging devices.

Going beyond the data found in the Ward's / Mahle database, an additional deep dive was conducted on these 12 engines, using data found through multiple web-based datasets (Driver 2017, MotorTrend 2017). This deeper investigation was done to try to explain why there are 12 MY 2017 engines with BMEP greater than what Bassett et al claim is the practical limit. Specifically, factors other than those found in the Ward's / Mahle database were required. The results of this investigation can be summarized in Table 1.

In Table 1 it can be shown that when looking at the 2017 MY engines with BMEP greater than 24.0; ALL of the engines employ some form of pressure charging (as expected), Direct Injection (and some use dual fuel systems), and some form of VVA. Furthermore, MOST of the engines have multiple boosting devices (two turbochargers or a turbocharger and supercharger), and most require premium fuel. Only one of the engines, the GM LTG utilizes only a single pressure charging device AND does not require premium fuel.

Table 1: Summary of 2017 MY LD Engines with BMEP Greater Than 24.0 bar.

OEM	Model	Disp (L)	Code	CR	BMEP	Fuel Type	Technology Level	Cost	Additional Notes
FCA	Alfa Romeo Giulia Quadrifoglio	2.9	NA	9.3:1	26.0	Prem	DI/DOHC/4vpc/2TRBO/IntVVT/RF (single-scroll IHI manifold integrated)	$73,595	No Ref to Water Injection Found
FORD	Focus RS	2.3	NA	9.37:1	26.0	Prem	DI/DOHC/4vpc/TRBO/Int/Ti-VCT/BT	$36,995	No Ref to Water Injection Found
FORD	Edge Sport, Fusion Sport; Lincoln Continental, MKX	2.7	NA	10.0:1	24.0	Prem	DI/DOHC/4vpc/2TRBO/iVCT/RFF	$41,795	No Ref to Water Injection Found
FORD	F-150 Raptor	3.5	NA	10.0:1	24.8	Reg	DI-SFI/DOHC/4vpc/2TRBO/INT/TiVCT/RFF	$50,560	No Ref to Water Injection Found
FORD	Ford GT	3.5	NA	9.0:1	26.8	Prem	DI-SFI/DOHC/4vpc/2TRBO/Int/TiVCT/RFF	$453,750	No Ref to Water Injection Found
GM	Buick Regal; Cadillac ATS, CTS, CT6; Chevrolet Camaro. Malibu	2.0	LTG	9.5:1	25.1	Prem rec./not req.	DI/ETC/DOHC/4vpc/TRBO/Int/VCT/RFF	$27,990	No Ref to Water Injection Found
BMW	i8 Hybrid	1.5	B38K15TO	9.5:1	26.8	Prem	DI/DOHC/4vpc/TRBO/VVTL	$144,395	No Ref to Water Injection Found
DAIMLER	Mercedes CLA45 AMG	2.0	NA	8.6:1	29.8	Prem	DI/ETC/DOHC/4vpc/TRBO/Int/VI/Sp-St	$50,875	No Ref to Water Injection Found
PORSCHE	911 Turbo, Turbo S	3.8	NA	9.8:1	24.8	Prem	DI/ETC/DOHC/4vpc/2TRBO/Int/DOHC/VCT	$160,250	No Ref to Water Injection Found
PORSCHE	Panamera Turbo	4.0	NA	10.1:1	24.2	Prem	DI/ETC/DOHC/4vpc/2TRBO/Int/VVTL/VCI/CD	$147,950	No Ref to Water Injection Found
VOLVO	S60, V90, XC60, XC90	2.0	B4024t27, B4204T27	10.3:1	25.1	Reg	DI/DOHC/4vpc/VVT/TRBO/SPR/int	$34,945	No Ref to Water Injection Found
VOLVO	S60, V60, XC60,	2.0	B42044T43	8.6:1	29.6	Reg	DI/DOHC/4vpc/VVT/TRBO/SPR/int	$60,000	No Ref to Water Injection Found. Polestar Versions. Polestar re-develops Volvo vehicles with performance enhancements.
VOLVO	XC90	2.0	B42044T35	10.3:1	25.1	Reg	DI/DOHC/4vpc/VVT/TRBO/SPR/int	$53,295	No Ref to Water Injection Found

Another goal of this deep dive was to see if any of these 2017 MY production, high BMEP engines have incorporated water injection, or simultaneous injection of gasoline and Ethanol or Ethanol / Gasoline Blends (e.g. E85). In examining these 12 engines, no reference to water injection has been found or simultaneous injection of multiple fuel's has been found, although there is reference to two fuel systems (DI and SFI) on two of the engines.

In summary, the data from (Ward's Auto 2017) does support (Bassett 2016) and (Mock 2013, Tietge 2016) in that with current ***mainstream*** technology levels there appears to be

an upper limit on BMEP (of the 12 engines with BMEP greater than 24, only one engine uses a single pressure charging device and regular fuel). The data suggests the current engine population is approaching that limit now, and that as BMEP levels increase, a corresponding drop in CR can be found, which will lead to a decrease in engine efficiency across the full load range. Furthermore, this all supports the statements made by this author previously, that if this trend in downsizing and boosting is going to continue with any practical success, there must be a paradigm shift in engine technology, with the implication that water injection could be that shift. The fact that none of the 12 engines with BMEP greater than 24 BMEP have any reference to water injection, indicate that this technology is not being used in production currently, and continues to support the assertion that it could provide the shift discussed.

Finally, the preceding data and discussion illuminates that the current best-in-class BMEP falls in the range of 25 bar BMEP to 30 bar BMEP, with the absolute highest for the 2017 MY being 29.8 bar BMEP. This distinction is important here, as it establishes the best-in-class targets that need to be exceeded to meet objectives 2.3 and 2.4 of this research.

2.2 Water Injection

Referring back to the previous discussion, water injection has the potential to suppress knock, without requiring spark retard or fuel enrichment (or a lesser degree of retard and enrichment), which again, is the motivation of this research. It must be acknowledged that the concept of water injection is not new. Many modern authors identify the application of water injection on reciprocating piston engines as beginning in the 1940's. This author found evidence that water injection was being studied on reciprocating piston aircraft engines at least as early as the late 1930's (Kuhring 1938) and continued through the 1940's (Rothrock 1942) for example. Additional work continued through the years that followed (Porter 1950, Nicholls 1968, Weatherford 1970, Lestz 1972, Tsao 1984, Lanzafame 1999) to list some examples. Furthermore, although the highest BMEP engines in 2017 do not appear to employ water injection, there is a precedence of water injection in production,

albeit on a limited capacity. Known applications are the 1962 Oldsmobile, a Chrysler V8, and a Saab Turbo (Brooke 2015).

Water injection is experiencing renewed interest now (Boretti 2012, Bhagat 2013, Soyelmez 2013, Berni 2015, Busuttil 2015, Fu 2015, Kim 2016, Iacobacci 2017, Rohit 2017, Worm 2017) presumably with correlation to the increasing trend toward highly boosted downsized engines (Mock 2013, Tietge 2016).

Although this work is focused specifically on the injection of water into the engine as a separate fluid stream, it must be noted here that alternatively water can be introduced concurrent with the fuel. In this method, the water and fuel are pre-mixed as a homogeneous emulsion (Peters 1976, Harrington 1982, Tsao 1984). One can easily appreciate the allure of greatly reducing, if not completely eliminating an entire hardware subsystem, and control subsystem. However, a major challenge is the lack of stability in the water – fuel emulsion (Lanzafame 1999). One may also speculate a general lack of controllability in terms of both water fraction and water timing with emulsions.

Furthermore, this work is focused specifically on the impacts of water injection on engine performance. However, this is not necessarily the only motivation for the study of water injection. Some researchers have studied water injection as a means to reduce, or eliminate the engines external cooling system (Lanzafame 1999), while others have focused their attention on the significant reductions in Oxides of Nitrogen (NO_X) emissions that accompany water injection (Wang 2009). An interesting example of applying water injection specifically for NO_X reduction can be found in (Nande 2008) because the fuel was Hydrogen (H_2). With H_2 as the sole fuel, Hydro-Carbon (HC) and Carbon Monoxide (CO) emission are fundamentally zero[8], so the only regulated toxic emissions is NO_X.

[8] Excluding any potential affects due to lube oil entering the combustion chamber, or exhaust tract through valve seals.

Finally, it should be noted that water injection is not exclusive to spark-ignited engines, as many researchers have looked at applying water injection to Compression Ignition (CI) engines, with the primary objective being NO_X reduction. Some examples include (Odake 1991, Miayamoto N. 1995, Kohketsu S. 1996, Mello J. P. 1999, Walsh 1999). Again, the focus of the current work is injection of water as a separate fluid stream into a Spark-Ignited Engine for the benefit of improving full-load engine output.

2.2.1 Water Injection Effects on Knock

When examining how water injection improves engine output, perhaps the most widely known benefit of water injection is the ability of water injection to subdue the onset of auto-ignition or knock. It is customarily assumed that auto-ignition follows an Arrhenius function. It is assumed auto-ignition occurs when the actual elapsed time that the unburned mixture has been under elevated temperature is equal to the kinetic based induction time for that mixture, Equation 7. In other words, the unburned mixture will auto-ignite when the integral reaches unity (Heywood 1988).

Equation 7: Onset of Knock

$$\int_{t=0}^{t_i} \frac{dt}{\tau} = 1$$

Where :
τ = Induction Time
t = Time

Researchers have investigated the induction time, finding it to be a complex function of not only chemical kinetics, but also engine dependent mechanical and thermodynamic factors (Livengood J. C. 1955). To account for these complexities, several empirical correlations have been developed (By 1981). The most extensively vetted correlation (Heywood 1988), is shown in Equation 8 (Douaud A. M. 1978).

Equation 8: Empirical Correlation of Induction Time

$$\tau = 17.68\left(\frac{ON}{100}\right)^{3.402} p^{-1.7} \exp\left(\frac{3800}{T}\right)$$

Where :

τ = Induction Time (ms)

ON = Octane Number

p = absolute pressure in atm

T = Temperature in K

When water is injected as a liquid (either in the intake port, or directly into the cylinder), it is vaporized, and the energy to vaporize the liquid comes largely from the fuel and air mixture during the intake stroke, and potentially even through the compression stroke and well into the combustion process. As the energy is transferred from the unburned mixture to vaporize the water, the unburned mixture is cooled. From Equation 8, it can be shown that decreasing Temperature (T), leads to an increase in the induction time, thus taking longer for the integral of Equation 7 to reach unity, having the overall impact of reducing the knock tendency of the engine.

The amount of energy that can be transferred from the unburned mixture, and the resulting drop in temperature can be significant. Table 2 compares the enthalpy of vaporization for several liquid fuels to that of water (Cengel 2008). Interestingly, there are very inconsistent reports of enthalpy of vaporization of several of these substances found in the literature (Boretti 2012, Kale V. 2012, Kim 2016, Iacobacci 2017), therefore table is based on data originating with fundamental references. Here it can be shown that although the alcohols Ethanol and Methanol have very high enthalpy of vaporization compared to petroleum based fuels, water has over twice the enthalpy of vaporization of methanol, and over 7 times the enthalpy of vaporization of iso-octane. This high enthalpy of vaporization results in the cooling of the end gas that suppresses knock. By suppressing knock, combustion

phasing can be run at, or at least closer to, MBT, and the suppression of knock enables operation at high loads (i.e. boost pressures).

Table 2: Enthalpy of Vaporization Comparison[9]

	Substance				
Property	E0 Gasoline	Iso-Octane	Ethanol	Methanol	Water
Enthalpy of Vaporization (kJ/kg)	350[10]	306	839	1100	2257

Several researchers have observed that water injection reduces knock tendency but two researchers, (Lanzafame 1999), and (Brusca 2003) took the knock mitigation effects of water injection a little further. They looked at deriving an "Effective" Octane Number (ON). Essentially a measure representing what the ON of a fuel would need to be to have the same anti-knock qualities as a lower ON fuel in conjunction with water injection. They utilized a Cooperative Fuels Research (CFR)[11] engine running the same ASTM test procedures that would be used to determine the ON of an unknown fuel. Figure 5 is from (Lanzafame 1999), where the baseline fuel was virgin naptha. Here it can be seen that both the Research and Motor methods of determining ON show a significant increase when even just moderate amounts of water are injected. This further corroborates the discussion of water injecting improving the knock tolerance in an engine.

[9] Data from Cengel, Y. A., Boles, M.A. (2008). Thermodynamics An Engineering Approach, McGraw-Hill Inc.

[10] Heywood, J. B. (1988). Internal Combustion Engine Fundamentals. New York, McGraw Hill, Inc.

[11] This is a standardized engine used internationally for determining the Octane Number of fuels.

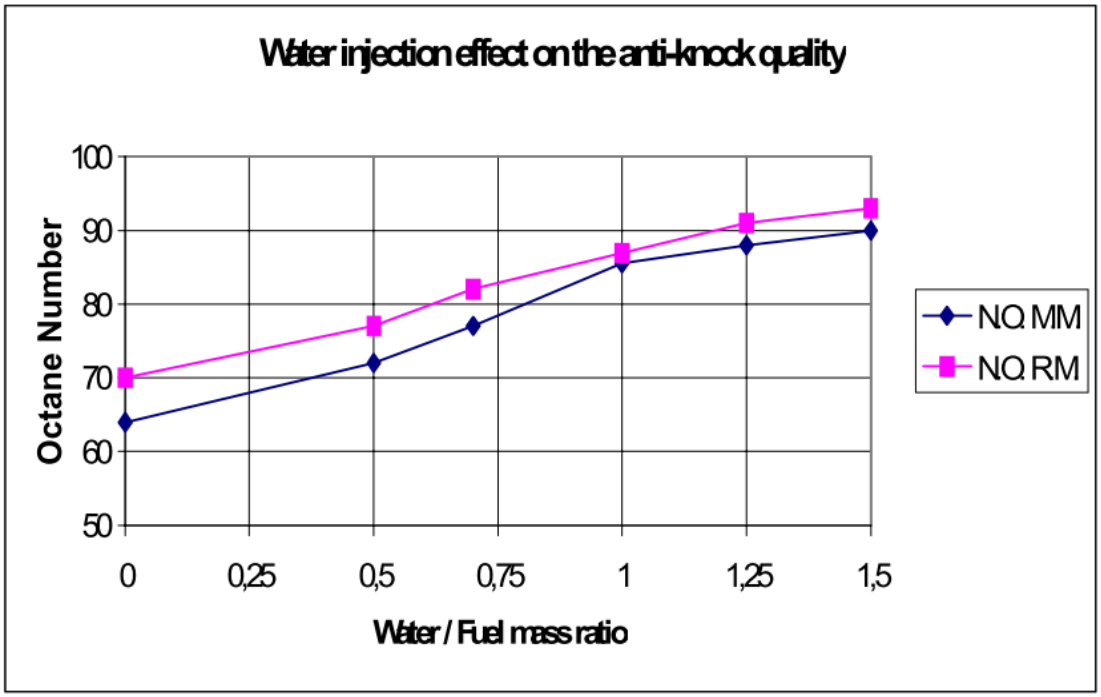

Figure 5: The impact of water injection on the "Effective" ON of a fuel. Figure taken from (Lanzafame 1999).

2.2.2 Water Injection Effects on Volumetric Efficiency

In addition to suppressing knock and allowing more optimal combustion phasing, the charge cooling effect of water injection also serves to densify the fresh air charge enabling more charge air mass to be trapped in the cylinder for a given manifold pressure. This allows more fuel to be injected, ultimately introducing more energy to the system, and increasing engine output. In this case the charge cooling manifests itself as an increase in volumetric efficiency. In order to impact volumetric efficiency, the water must be injected, either in-cylinder or in the intake port, prior to Inlet Valve Closing (IVC).

Although charge cooling, and the subsequent influence on volumetric efficiency and knock tolerance are large factors in terms of water injections impact on engine output, other factors must be considered as well.

2.2.3 Water Injection Effects on Compression Work

Several researchers (Lanzafame 1999, Brusca 2003, Kim 2016) point out a reduction in compression work due to charge cooling effects, but with no explanation or reasoning why. Although this conclusion may very well be true, it warrants further consideration. Simply stating that charge cooling reducing compression work may lead one to surmise that colder gases lead to lower pressure and as a result require less work to compress.

In a closed system, compression work can be defined as the integral of pressure with respect to volume as shown in Equation 9.

Equation 9: Work in a closed system with a moving boundary

$$W = \int p dv$$

Where :
W = Work
p = Pressure
v = Volume

From Equation 9 it is shown that it is not the pressure that determines the compression work, but rather the overall pressure – volume history over the compression stroke. In considering the impact of water, one must first determine what to hold fixed in the comparison; mass, or pressure. If considering throttled, part-load operation, holding mass fixed is likely the most appropriate comparison (to maintain near fixed engine brake torque), and when holding mass constant, pressure at the start of the compression stroke will be lower, so the integral of Equation 7 will indeed tend to finish lower. However, if one is considering water injection for increasing engine output (as is the objective here) pressure at the start of compression is likely to remain constant[12]. If the pressure at the start of compression is the same, then it is not immediately clear that the compression work will be reduced.

[12] For example, atmospheric for a Naturally Aspirated engine, or at a fixed boost pressure.

Assuming isentropic compression, the relationship between pressure and volume is given by Equation 10[13].

Equation 10: Pressure - Volume Relationship for Isentropic Compression

$$\left(\frac{P_2}{P_1}\right)=\left(\frac{V_1}{V_2}\right)^{\gamma}$$

Where :
P = Pressure
V = Volume
γ = Ratio of Specific Heats

If P_1 is assumed to be constant even after water addition, then what impacts compression work is where P_2 ends after the compression stroke. Rearranging Equation 10 for P_2 results in Equation 11:

Equation 11: Pressure - Volume Relationship for Isentropic Compression Arranged for P2.

$$P_2 = P_1\left(\frac{V_1}{V_2}\right)^{\gamma}$$

The ratio of specific heat, γ, for water vapor at 300 K is 1.327 vs 1.400 for air at the same temperature (Cengel 2008). Therefore, if ignoring temperature effects, the introduction of water vapor will decrease γ for the mixture. Since the ratio V2/V1 is constant, and with the assumption that P1 is constant, one would indeed conclude that P2 will decrease resulting in a reduction of compression work. However, even if holding P1 fixed, the

[13] The relationship is the same for a non-isentropic compression, however, in a real-world, non-isentropic compression process, γ, is replaced with the Polytropic Index, sometimes labeled as n.

temperature of the charge will be decreased due to the charge cooling effect. When temperature is considered, it can be shown that γ increases with decreasing temperature. At least directionally, this would counteract the γ decrease from the change in mixture composition.

To further compound this thermodynamic analysis, one must be clear in how they define the limits of integration for compression work. If compression work is defined as taking place until TDC, then the timing of the spark and the early burn phase must be considered[14]. This is important because if the water injection is enabling advanced combustion phasing, then it is directly affecting the pressure –volume history during the compression stroke.

This discussion illustrates why it is felt that although water injection will certainly change compression work, it is difficult to say generically that compression work will be reduced. One must carefully consider the water fraction, charge gas temperature, and load control strategy. This discussion assumes that all of the water is vaporized prior to IVC. If water is vaporizing *during* compression, the situation is further complicated.

2.2.4 Water Injection Effects on Expansion Work

The thought of liquid water vaporizing after IVC is interesting from an expansion perspective as well as from a compression perspective. Water vaporizing during expansion or even late in combustion has the potential to affect expansion through the generation of steam, while not significantly impacting compression or combustion. This case is particularly interesting when considering Direct Injection of water. In this case water could be injected into the burned gas zone during and immediately after combustion with the sole purpose of vaporizing into steam and increasing expansion work. This perspective is not addressed in the existing literature.

[14] Assuming ignition occurs BTDC.

2.2.5 Water Injection Effects on Combustion

The actual combustion process must also be considered. Water vapor has a relatively high specific heat capacity. Table 3 compares the constant pressure (C_p), and constant volume (C_v) specific heats capacity for water vapor to that of other working fluids pertinent to engine operation. Data taken from (Cengel 2008).

Table 3: Heat Capacity Comparison for Fluids of Relevance to Engine Operation.[15]

	Property		
Substance	**C_p (kJ/kg-K)**	**C_v (kJ/kg-K)**	**γ (kJ/kg-K)**
Air	1.005	0.718	1.400
CO_2	0.846	0.657	1.289
N_2	1.039	0.743	1.400
H_2O Vapor	1.8723	1.4108	1.327

Table 3 shows that whether it is as constant pressure or constant volume-like conditions, the specific heat capacity of water vapor is significantly higher than air. Likewise it is significantly higher than CO_2 and N_2 with the implication being that water vapor has a specific heat capacity greater than EGR which could be considered an alternative diluent. With an increased heat capacity, the water vapor acts as a heat sink for both the burned and unburned gas. This is good for suppression of knock and NO_X, as well as being directionally correct for reducing heat loss to the coolant, but does reduce the adiabatic flame temperature which combined with the overall dilution of oxygen and fuel, slows down flame propagation. So, although combustion phasing can be shifted more optimally and there may be less energy lost to the coolant, it comes at a price in the form of longer overall combustion duration. Previous researchers have observed reduced burn rate (Kim 2016, Iacobacci 2017).

[15] Data taken from Cengel, Y. A., Boles, M.A. (2008). Thermodynamics An Engineering Approach, McGraw-Hill Inc.

The discussion so far has been centered primarily around the thermodynamics of the engine and combustion process. Kinetics should also be considered. (Wang 2009) suggests that at temperature levels expected near the flame and in the burned gas region, H_2O may undergo dissociation into H and OH radicals. (Wang 2009) goes on to say that the OH radical may play a role in the suppression of NO_X but gives little insight (nor do others) into how these radicals may impact other aspects of the combustion process.

2.2.6 Water Injection Effects on Ideal Cycle Efficiency

The ratio of specific heat capacity, γ, also impacts the ideal cycle efficiency according to Equation 5. In reviewing Table 3, it is evident that the addition of water vapor to the cylinder will decrease the overall γ, and from Equation 5, it is shown that a reduction in γ will decrease the ideal cycle efficiency. This is yet one more example where the net effect is a tradeoff of several competing factors.

It should also be noted that researchers have observed in increase in unburned HC emissions from the engine when water injection is being used (Lestz 1972, Kim 2016, Iacobacci 2017). The increase in HC is likely due to reduced in-cylinder temperature with increased quench layer thickness. Although this observation is somewhat expected, what is not addresses sufficiently in the literature is that this increased HC has to be accompanied by a reduced combustion efficiency. If the HC hadn't escaped the combustion chamber, it would have oxidized, and thus contributed to the net in-cylinder heat release and work production.

2.2.7 Summary of Existing Literature

As discussed in this section, many researchers have studied water injection. However, when filtering through the literature to match relevant prior work to the objectives of the current research, the pool shrinks considerably. Table 4 has been created to summarize the literature that directly relates (Lanzafame 1999, Brusca 2003, Soyelmez 2013, Busuttil 2015, Kim 2016, Iacobacci 2017). Table 4 includes only experimental work published

within the past 20 years. The table is filtered to include only projects in which the primary objective was examining either high-load operation or knock mitigation, and with Hydro-Carbon based fuels. Furthermore the table excludes studies where the water was introduced as part of a fuel emulsion, and does not include studies on CI engines.

As shown in Table 4, when applying these filters, the body of literature is greatly reduced. Moreover, when examining the specific design space these researchers were operating in, it becomes clear that no other researcher has load as high as is intended with this project, nor speeds as fast. By speed and load alone, this proposed research breaks new ground, but more than just that, as recently as 2017, others have identified that there are significant gaps in the experimental results and analysis in this area (Rohit 2017).

Table 4: Summary of Most Closely Related Literature.

Reference	Type of Water Injection	Engine Architecture	Air Induction	Fuel Induction	Fuel	CR	Water / Fuel	Speed (RPM)	Load	Limitations
Lanzafame 1999	Port	CFR Single Cylinder 2 valve / cylinder	Naturally Aspirated	Carbureted	Gasoline	Varied During Test	0 - 1.5	900	0 BMEP (1)	No Load
Brusca 2003	Port	CFR Single Cylinder 2 valve / cylinder	Naturally Aspirated	Carbureted	Gasoline	Varied During Test	0 - 2.0	900	Unspecified	No Load
Soyelmez 2013	Port	4-cylinder 1.3L	Naturally Aspirated (2)	Unspecified	Liquefied Petroleum Gas	7.8:1	0.125 to 0.5	1000 - 4500	WOT, 9 bar BMEP nominal	Combustion / cylinder pressure data not available
Busuttil 2015	Port	1-cylinder 0.59 L Air Cooled Industrial Engine	Boosted (4)	Port Injection	Gasoline (5)	4.97:1	0.0 to 1.3	1600 - 2000	WOT, 9 bar BMEP nominal	Combustion / cylinder pressure data not available
Kim 2016	Direct	4-cylinder 1.6 L	Naturally Aspirated (3)	Port Injection	Gasoline	13.5:1	0.0 to 2.5	1500 - 3000	WOT, 9.25 bar BMEP nominal	Low Speed & Load
Iacobacci 2017	Port	2-cylinder 0.875L	Turbocharged	Port Injection	Gasoline	10.0:1	0.1 to 0.3	3500 - 4500	WOT, 15 bar NMEP nominal	

NOTES:
Only includes engine studies (i.e. excludes combustion vessel)
Only includes SI
Does not include emulsions
Only includes studies that looked at knock and performance benefits (i.e. some only looked at Nox reduction)
Only includes relatively modern work
(1) Assumed to be 0 brake load, as authors note "A dynamometer was not used in this testing."
(2) Unspecified; inferred based on BMEP under WOT
(3) Not explicitly specified. A Turbocharcher appears in a schematic in the paper, plots of WOT BMEP is more inline with Naturally Aspirated engines.
(4) Boosted w/ shop air to 120 kPa Absolute
(5) Unspecified, but inferred to be gasoline based upon the context of the paper, engine architecture, etc.

3 Research Methodology

The bulk of this research will be supported by experimentation. First principals thermodynamic and thermochemical analysis will be carried out on experimental data and known fluid properties as needed, as will 1-D computer simulation to develop a deeper and more fundamental understanding of the impacts of water injection.

3.1 Base Engine

The engine platform chosen for this work is the General Motors Ecotec, specifically RPO code LHU. This is a Spark-Ignited, 2.0L 4-cylinder engine with a turbocharger, Direct Injection (DI) of fuel, and Dual Independent Variable Valve Timing (DIVVT). This platform was selected for several reasons:

- The technology level (DI, Turbocharged, DIVVT) is representative of most other highly boosted production engines,
- At 25 bar BMEP (SAE_International 2004, Joss 2011), the production brake output is at the upper most end of current production engines. This suggests the platform has sufficient hardware strength for testing at least across the load spectrum for current production engines, and implies it is a suitable starting point for increasing load beyond current production levels.
- Availability of production level parts through an extensive network of Original Equipment Manufacturer (OEM) dealers and aftermarket automotive parts retailers.
- This platform has a strong following in the motorsports industry, and therefore, there exists a wide selection of racing components intended to provide additional strength in high load operating conditions.

Additional details on the LHU engine platform are shown in Table 5.

Table 5: Details of the Engine Testbed. Reprinted with permission Copyright © 2017 SAE International. Further Distribution of this material is not permitted without prior permission from SAE. See 9Appendix F for further details.

LHU Engine Specifications		
Base Engine	Configuration	Inline 4-Cylinder, Pent-Roof Central Spark Plug
	Displacement	1998 cc
	Bore	86.0 mm
	Stroke	86.0 mm
	CR	9.2:1
	Valvetrain	4-Valve / Cyl, DIVVT, 50° CAD Authority Intake & Exhaust
	Fuel System	Direct Injection (Wall Guided)
	Induction	Twin Scroll Turbocharged

3.2 Fuels

Three main fuels and a supplemental fuel have been selected to meet the objectives of this investigation, each with a different octane rating as defined by the fuels Anti-Knock Index (AKI). A fuels AKI is the average of the fuels Research Octane Number (RON), and Motor Octane Number (MON), as shown in Equation 3.

A pump grade "Regular" fuel with an AKI of 87 was used in conjunction with water injection, to assess the potential of water injection. A pump grade "Premium" fuel with an AKI of 91 was used for the baseline testing of the production configuration. This particular engine is rated as "Premium Recommended", not "Premium Required", however it was felt the premium fuel would provide some margin of safety for knock when running production spark timing during baseline testing. This fuel was also used for testing at loads greater than 300 kPa MAP. Both of these fuels were sourced from a local filling station under the "Freedom" brand.

VP Racing Fuels VP110 is an off-road only race fuel that was used to assess the potential if knock is not limited by fuel properties. The race fuel includes tetraethyl lead[16], and has an AKI of 110. This VP Racing Fuel was also purchased from a local filling station.

416 L of each of these three fuels were procured at the beginning of the project. It was estimated that this quantify of fuel was sufficient to meet all scheduled testing, ensuring that all test data would be run on a consistent batch of fuel.

Testing at boost levels exceeding production boost revealed the engine was knock limited even on the 110 AKI fuel. In an attempt to reach MBT, even if it required the most exotic fuel possible, a small drum (114 L) of "VP Import" was purchased directly from VP Racing fuels. This fuel has an AKI of greater than 120, and contains Methyl Tertiary Butyl Ether (MTBE).

Samples of each of the pump grade fuels were pulled and delivered to Paragon Laboratories in Livonia MI for detailed property analysis (Pangborn 2016). VP Racing fuels was contacted for specifications of the VP 110 and VP Import (Fuels 2014, Fuels 2016). In supplying specifications, VP Racing fuels provided assurance that their fuels have very tight batch to batch tolerances on properties (Taylor 2016). A summary of the most pertinent properties are shown in Table 6. Full property reports are included in Appendix D.

[16] It was known at the onset of the project that the tetraethyl lead would deteriorate the performance of the wide band and narrow band O2 sensors used. It was felt the onset of sensor deterioration could be identified with careful control charting. The O2 sensors did show a degradation in performance approximately halfway through the project, and were replaced.

Table 6: Summary of Fuel Properties. Reprinted with permission Copyright © 2017 SAE International. Further Distribution of this material is not permitted without prior permission from SAE. See 9Appendix F for further details.

		91 AKI Pump	87 AKI Pump	110 AKI Race	120+ AKI Race
Fuel Specification	RON	94.8	90.6	113	128.8
	MON	88.4	85	107	124.6
	AKI (R+M/2)	91.6	87.8	110	126.7
	SG @ 15.6°C	0.7216	0.7186	0.73	0.744
	LHV (MJ/kg)	43.88	42.068	41.03	40.83
	WT% O2	0.0	3.92	NA*	3.63

** Advertised as a Non-Oxygenated Fuel*

3.3 Experimental Test Matrix

With the objectives of this work centered around demonstrating and quantifying the potential for water injection to lead to a paradigm shift in engine downsizing / boosting, all testing was conducted at WOT operation. The range of speeds selected for testing is 2000 RPM, 3000 RPM, 4000 RPM, and 5000 RPM. The 2000 RPM and 3000 RPM points probe the impact on low-end torque, the 4000 RPM point represents the peak torque speed of the base engine, and the 5000 RPM point probes the impact on high-end torque. Speeds below 2000 RPM were not considered because 1) by far the major market penetration in the automotive sector in the U.S. is automatic transmissions, and due to the torque converter, an automatic transmission vehicle spends very little time at engine speeds below 2000 RPM, ***when at WOT***, and 2) there is an increased risk of driveline resonance related issues when operating engines on a dynamometer at speeds below 2000 RPM. Speeds greater than 5000 RPM were not considered because 1) there is an increased risk of catastrophic engine failure as engine speed increases, and 2) higher test speeds place increased demand

on the fuel system, external boost system, cooling system, test cell ventilation, and combustion analyzer (increased processor demand).

Within this range of speeds, all testing was conducted at steady state[17]. For all testing, intake and exhaust cam timing was set at the production calibration values for full load at each speed, which are calibrated by the OEM for peak volumetric efficiency. Depending on the test, lambda was run at either the production calibration value, or lambda = 1. For nearly all tests, combustion phasing was adjusted by setting the CA50 point to 10° ATDC to approximate MBT (Worm 2013), or Knock Limited Spark Advance (KLSA)[18].

Testing began at production WOT boost levels to address objective 2 and its associated sub-objectives. The work done at the production boost levels can be categorized primarily into three separate tests. Test 1, the baseline testing was conducted with all control setpoints as-calibrated in the production controller, and without water injection. As the name implies, this test was run to establish a detailed performance analysis of production hardware and control settings to serve as a baseline to which further comparisons can be made.

Test 2 was conducted with 110 AKI fuel, and still without water injection. Lambda remained enriched, as-calibrated in the production ECU, while spark timing was adjusted to achieve a target CA50 of 10° ATDC or KLSA. This test was conducted in an effort to identify the upper limit of performance, if knock was not constrained by fuel characteristics.

Test 3 was with 87 AKI fuel. Port water injection was enabled for this test. Lambda was adjusted to 1.0, and spark timing was adjusted to achieve a target CA50 of 10° ATDC or

[17] As will be discussed later, the external boost system did not have sufficient capacity to supply the engine at all speeds and loads indefinitely. However, the boost system capacity was sufficient to get to the speed / load setpoint, make control setting adjustments, stabilize the engine, and record data, therefore, it is reasonable to consider all data to have been recorded at steady state.

[18] For this testing, borderline knock was defined as having a peak to peak of 400 kPa resulting from the ringing in the pressure trace.

KLSA. This test was the first probe to assess the potential for water injection as a paradigm shift, by running a "regular" fuel, but moreover, doing it with lambda = 1.0.

A summary of these tests is shown in Table 7.

Table 7: Summary of the major tests conducted at production boost levels. Reprinted with permission Copyright © 2017 SAE International. Further Distribution of this material is not permitted without prior permission from SAE. See 9Appendix F for further details.

Test No.	Fuel	Water Injection	Spark Timing / Combustion Phasing	Intake / Exhaust Cam	Lambda
1	91 AKI	None	Production	As-calibrated	As-calibrated
2	110 AKI	None	10° CA50 or KLSA	As-calibrated	As-calibrated
3	87 AKI	Port Injection	10° CA50 or KLSA	As-calibrated	1.0

Once the tests summarized in Table 3 were complete at production boost levels, testing continued with the boost level incrementally increasing for subsequent sets of tests. This was done out of necessity, as setpoints for control parameters were unknown, thus it was easier to make small incremental changes in boost level. Additionally, it was felt that if a hardware failure did occur as a function of a load threshold (not due to aging and wear affects), at least data would exist up to that load threshold.

For the testing at the production and elevated boost levels, the water injection rate was chosen in a quasi-realtime fashion with the primary target being achieving MBT CA50, or as close as possible to it. While running the engine, an incremental increase would be made in water injection rate, followed by an incremental increase in spark advance up to the onset of knock, at which point another incremental increase in water injection rate would be made. This alternating pattern would be continued until stopped by any one of several

constraints; 1) occurrence of misfire, 2) CA50 = 10° ATDC, or 3) water injection pulse width = 720° (i.e. water injection duration over the full engine cycle or 100% duty cycle).

3.4 Simulation Test Matrix

The 1-D Commercially available engine simulation code GT-Power (Gamma_Technologies 2016) will be used throughout various aspects of this research. The base model used was previously developed by GM, and supplied to APS LABS as part of a previous research project. The model represents a LNF / LHU[19], and was previously calibrated and validated by GM. Starting with the model supplied by GM, several modifications were made:

- Intake and Exhaust valve timing was set to be able to be adjusted by the user through the case setup.
    - This was done to allow easy slewing of cam phasing.
- The exhaust system, which represented a production vehicle, was eliminated, and a model of the APS LABS Test Cell exhaust system was created. The correct test cell exhaust was modeled from the outlet of the engine to the atmosphere outside the building including the drop for the engine on the other end of the dynamometer.
- Load control was modified to be able to run closed loop on Brake Torque.
    - The goals and objectives of the research are based on output torque / BMEP levels, so this change allowed running the model at exactly the target output levels.
- Turbocharger was eliminated.
    - With preliminary probe modeling in GT-Power, it became evident that the production turbocharger would not support the stretch goals of 50 bar BMEP. Subsequent analysis of available turbochargers revealed that

[19] LNF and LHU are the same base engine. LHU was a mid-generation change that simply added E85 capability to the LNF.

achieving 50 bar BMEP would be difficult even with aftermarket racing oriented hardware. Therefore the decision was made to supply boosted air with an external apparatus. An external boost rig would ensure adequate airflow to meet the stretch target of 50 bar BMEP while at the same time separating induction airflow and induction pressure from engine operating parameters such as speed and exhaust enthalpy.

- Fuel Injector flow rate was increased.
    - Running the model with the as-received settings for fuel injector flow resulted in an inability of the engine to meet the load requirement because the fuel injectors were open during the entire cycle. Increasing the flow rate of the injectors resolved this issue.

An image of the top level of the model is shown in Figure 6.

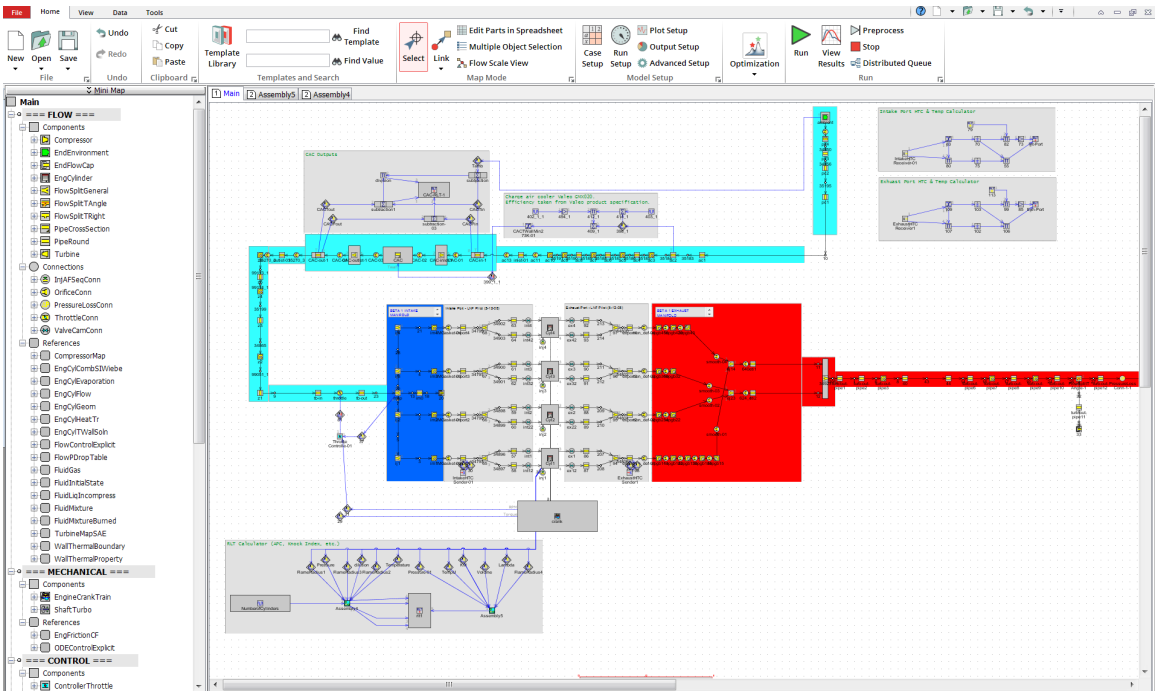

Figure 6: Top level of GT-Power user interface and engine model used for preliminary simulation. Image used with permission from Gamma Technologies Incorporated. See 17 Appendix F for further details.

The GT-Power model was used to predictively design the experimental testbed. Of particular importance was predicting the peak cylinder pressure that should be expected, which drove the piston selection, and the prediction of airflow and pressure ratio requirements which drove the design constraints for the boosting system. These predictions were made by running a test matrix where load was controlled to 800 nm brake torque (50 bar BMEP) at 3000 RPM, with sweeps of combustion phasing, lambda, and CR. Intake Maximum Open Point (IMOP) and Exhaust Maximum Open Point (EMOP) was fixed at the cam phasing producing peak engine output at 3000 RPM. These values were determined by examining the production intake and exhaust camphaser calibrations for an LHU installed in a 2012 Buick Regal. The calibrations were examined using the HP Tuners calibration editing tool. The simulation test matrix is shown in Table 8.

Table 8: Simulation Test Matrix

CR (:)	CA50 (° ATDC)	Lambda (:)	MAP (bar)	H2O Injected (%)	IMOP (°ATDC ge)	EMOP (°ATDC ge)	Speed (RPM)
9.2	10, 20, 30	1, 0.85, 0.7	Closed Loop on Torque	0	101	-106	3000
10	10, 20, 30	1, 0.85, 0.7	Closed Loop on Torque	0	101	-106	3000
11	10, 20, 30	1, 0.85, 0.7	Closed Loop on Torque	0	101	-106	3000
12	10, 20, 30	1, 0.85, 0.7	Closed Loop on Torque	0	101	-106	3000

3000 RPM was selected as the simulation speed because the stretch target of 50 bar BMEP defined by the project sponsor, Nostrum Energy, was intended to specifically be at 3000 RPM. Combustion phasing was swept because of the difficulty in predicting knock tolerance and burn rates. Sweeping combustion phasing, ensured that the actual combustion phasing for high octane race fuel, low octane pump fuel, and various fuels with water injection was comprehended. Lambda was swept to encompass the knock limitations and EGT limitations that were likely to be encountered over the range of fuels tested and with water injection. Finally, CR was swept because of future goals to demonstrate water injection as an enabler for increased geometric compression ratio.

4 Experimental Setup

4.1 Using Simulation Results in Testbed Build

A subset of the simulation results will be shown here, as these results were used in the design and assembly of the engine test bed and ancillary support systems. Figure 7 shows the peak cylinder pressure over the range of operating conditions and parameters simulated. Here it can be seen that as expected, peak cylinder pressure increases with compression ratio. Furthermore, it is shown that within a given compression ratio, peak cylinder pressure also increases when combustion phasing is advanced toward Maximum Brake Torque (MBT)[20], and for a fixed compression ratio and combustion phasing when the Air to Fuel ratio is leaned toward stoichiometric.

[20] MBT can be considered to occur when combustion phasing as indicated by the 50% Mass Fraction Burned location (CA50) is approximately 6° After Top Dead Center (ATDC) to 12° ATDC. For this work it is taken to be approximately 10° (ATDC).

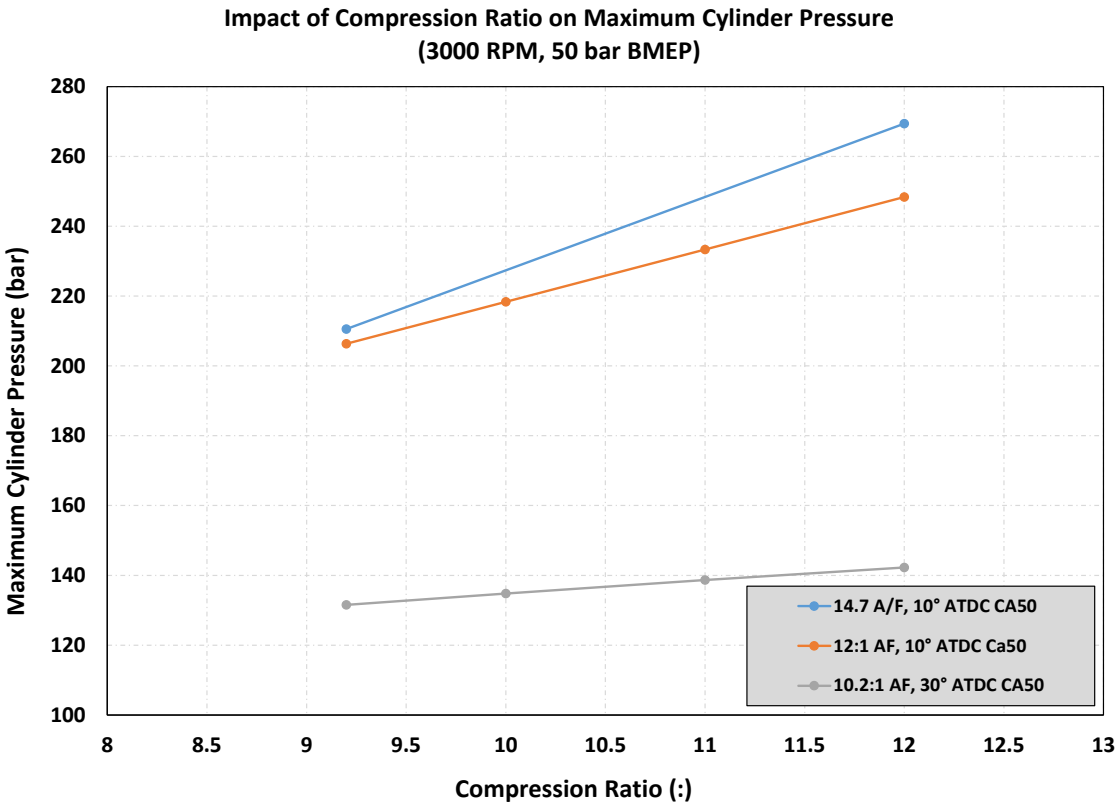

Figure 7: Peak cylinder pressure as a function of Compression Ratio, over a range of combustion phasing and lambda.

Figure 8 shows the pressure ratio[21] vs mass airflow for all operating conditions and parameters simulated. Here it can be seen that the minimum requirement is an airflow of approximately 745 kg/hr at a pressure ratio of 3.7. This corresponds to the highest compression ratio (12.0:1), MBT combustion phasing (CA50 = 10° ATDC), and a 12:1 A/F, and thus high thermal efficiency with a lambda near optimized for peak output. Oppositely, the maximum airflow corresponds to the lowest CR which was the production CR (9.2:1), most retarded combustion phasing (CA50 = 30° ATDC) and an overly rich A/F of 10.2:1. As will be described in more detail in a subsequent section, these results were used to guide the design and selection of a boost system.

[21] Pressure Ratio as used here is defined as intake Manifold Absolute Pressure (MAP) divided by barometric pressure. This metric is chosen here as it is very close to the pressure ratio across the turbocharger compressor. This allows direct comparison with manufacturer published data for commercially available turbochargers.

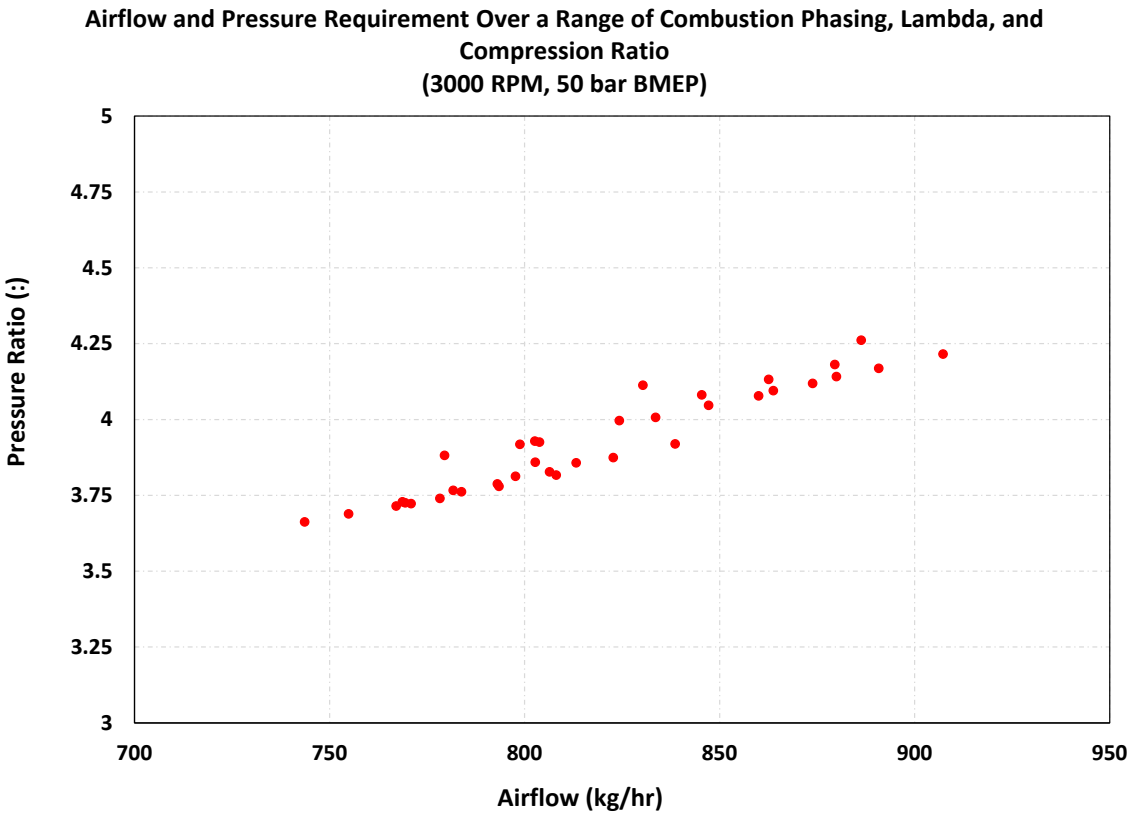

Figure 8: Engine Pressure Ratio (MAP/Baro) as a function of mass airflow rate for all engine operating conditions and geometric parameters simulated.

4.2 Experimental Test Bed

Two separate test engines have been prepared based on the LHU platform. These have been serialized for concise identification and will be referred to as Engine Serial Number (ESN) 01 and ESN02.

4.2.1 ESN01

With the exception of instrumentation, the addition of a water injection system, and installing cylinder head studs when the cylinder head was removed for cylinder head instrumentation, ESN01 remained in an entirely production configuration. ESN01 was purchased as a GM Replacement parts engine. The engine was an assembled long-block. Any additional components needed for testing (e.g. Air Induction System, etc.) was

purchased through a GM Dealer. This engine was used to 1) calibrate and validate the control system, water injection system and other aspects of the test bed and 2) investigate the impact of water injection up to current production boost levels. Specifically this engine is being used to meet previously stated objective 2 with boost greater than production.

4.2.2 ESN02

ESN02 is being used to meet Objective 2 with high boost levels, and thus is being utilized at boost levels significantly higher than current production. As such, this engine has been assembled with aftermarket and fabricated components as required to 1) reach output levels significantly higher than current production, and 2) maintain durability when operating at these high load conditions.

Architecturally and dimensionally, ESN02 maintains the production specifications. However, various components were changed for improved strength and durability under high load operation. The most noteworthy of these components and modifications will be discussed.

4.2.3 Fasteners

The production LNF / LHU engine utilizes bolts to fasten the cylinder head to the engine block. The head bolts are a torque-to-yield design that can only be used one time, and must be replaced anytime the cylinder head is removed and re-installed. During reinstallation of the cylinder head to the block for both ESN1 and ESN2, the production head bolts were replaced with studs manufactured by ARP. Replacing the cylinder head bolts with studs was a technique the author started using while doing engine development at GM, and found it to be quite advantageous. The studs were used for three reasons. 1) It was felt that the cylinder head would likely be removed many times over the course of this project. Since the studs remain in their elastic region they do not need to be replaced upon reinstallation. This saves time and money in the long run. 2) When installing bolts in the cylinder lock, the steel bolt tends to gall and wear the aluminum threads in the block. Within as little as

3 or 4 installations the threads in the block can be compromised to the point of failure requiring either tedious and questionable thread repair or a replacement of the entire block. Since the stud remains seated in the block, and at the interface between the stud and block is in pure tension during tightening (as opposed to tension and sliding for a bolt), the stud does not damage the block threads. Where the nut interacts with the stud is steel on steel, and therefore a very robust joint. All of this allows for the cylinder head to be repeatedly removed and reinstalled without issue. 3) Finally, the studs from ARP provide a larger clamp load compared to the production bolts. This is synergistic in this case as the expected significant increases in cylinder pressure will act to lift the cylinder head from the block, potentially failing the fastener, head, head gasket, block deck, or other issues. The stronger ARP head studs will be directionally correct for preventing these failure modes. An image of the head studs (taken from the manufacturers website) is shown in Figure 9.

ARP bolts were also used for the connecting rods. ARP studs / bolts were investigated for the main bearings, however, ARP does not make an off the shelf main stud / bolt kit, so production fasteners were used in this location.

Figure 9: The cylinder head studs used for ESN01 and ESN02. Image reproduced under permission of Automotive Racing Products, ARP. See 17 Appendix F for further details.

4.2.4 Pistons

The objectives of this research including increasing output, running lambda = 1, and advancing combustion phasing will have an impact on the cylinder pressure profile, including the peak cylinder pressure. Although gas temperature certainly plays a role, one of the primary parameters that correlate to the durability of a given piston design in an application is peak cylinder pressure (Bethel, 2016). It is the peak cylinder pressure that leads to a bending force around the top piston ring land and around the wrist pin boss (as well as the wrist pin itself). Conversations between the project sponsor Nostrum Energy LLC and Mahle Powertrain indicated that the production pistons, (produced by Mahle) cast with a hypereutectic aluminum alloy, are expected to fail catastrophically if exposed to sustained operation with peak cylinder pressure above 150 bar (Blaxill 2015).

Referring again to Figure 7, it becomes apparent that with all but the most retarded combustion phasing and overly rich lambda, the peak cylinder pressure far exceeds the 150 bar bogey suggested by Mahle Powertrain as the upper limit for which the production cast hypereutectic pistons can be expected to run without failure. Because failure of the piston directly results in catastrophic failure of the entire engine, and quite possibly much of the instrumentation, it was apparent that ESN02 must be assembled with a piston stronger than the production units. It was felt that a forged aluminum piston, with thicker critical sections would meet the cylinder pressure targets.

Several aftermarket custom piston manufacturers were identified, and discussions begun to investigate potential suppliers. Suppliers that were identified and contacted included:

- JE Pistons
- Carrillo
- Wiseco
- Diamond Racing Products
- Leadfoot Engineering
- Mahle Motorsports

Of these suppliers, Wiseco and Carrillo were both the lowest cost, and shortest leadtime. Wiseco was chosen initially as the supplier, with Carrillo added later as a parallel path when issues with design and leadtime arose with Wiseco.

With the supplier(s) chosen, several design requirements were established based on both meetings with the project sponsor, and through conversations with Steve Bethel of Leadfoot Engineering (Bethel 2016). A Summary of these design requirements are shown in Table 9.

Table 9: Piston Design Requirement Summary.

	Supplier	
Design Requirement	**Wiseco**	**Carrillo**
OK to run to 5000 RPM	NA	TBD
OK to run to 300 Bar Peak Pressure	NA	TBD
NO DI Bowl	Confirmed	TBD
NO Gas Ports	Confirmed	TBD
11.0:1 Design Intend CR	Confirmed	TBD
Dimensionally Equivalent to Wiseco 9.2 Piston	Confirmed	TBD
3D Rendering Provided	Confirmed	TBD
2618 Material	Confirmed	TBD
NO Ceramic Coating	Confirmed	TBD
DLC Top Ring	Not Available	TBD
Coated Skirt	Confirmed	TBD

The reasoning behind the design requirements shown in Table 9 is as follows:

- The requirement to be able to run to 5000 RPM was based simply on the fact that the desired test matrix included test points up to and including 5000 RPM. With strength a primary factor, the concern was that piston weight may increase significantly, which may in turn limit the maximum engine speed due to inertial loading.
- The requirement to operate at 300 bar peak cylinder pressure comes directly from Figure 7 where it can be seen that peak cylinder pressure is well over 200 bar even at the production CR of 9.2:1 and can approach 300 bar at 12.0:1 which was considered to be the highest CR possible due to geometric limitations. 300 bar was chosen to provide a small factor of safety, and to account for knock and pre-ignition.
- For the 11.0:1 CR only, the characteristic bowls in DI pistons were removed. These bowls are primarily to enhance cold start performance and since this engine is intended only for steady state dynamometer operation the bowls are not necessary. Moreover, the bowls impose additional limitations on the ability to increase CR significantly beyond the production 9.2:1.

- It was specifically requested that gas ports NOT be included in the design. This refers to ports around the periphery of the piston that port cylinder gases to the back side of the top piston ring. The intention of the port is to increase the gas force applied to the back side of the piston ring. However, these ports have been deemed to provide no measurable improvement in piston ring seal or stability at speeds less than approximately 7000 RPM, and can potentially lead to thermal non-uniformity of the piston crown (Bethel 2016). Because of the lack of benefit, and potential issues created, the requirement was to omit the gas ports.
- Two CR's were ordered. A 9.2:1 to maintain consistency with the production CR, and a higher 11.0:1 CR. Wiseco had determined that 12.0:1 was the absolute maximum that was geometrically possible with this engine configuration, and it was determined that 11.0:1 would result in a geometrically simpler design with less surface area and potential for flame quenching, while keeping peak cylinder pressure slightly lower. A requirement was that the 11.0:1 CR piston must be dimensionally similar to the already in production Wiseco production replacement 9.2:1 CR piston.
- It was required that a 3D rendering be provided. The piston manufacturers were not willing to provide original Computer Aided Design (CAD) files, but agreed to a rotatable pdf file.
- 2618 aluminum allow was required for the forgings due to the allows proven high strength (Bethel, 2016).
- The requirement was made to NOT have a ceramic coating on the top (or any other part) of the piston. This decision was made to stay consistent with current production technologies.
- The requirement was made to NOT require a Diamond-Like-Coated (DLC) top piston ring[22]. This was partially because of the desire to maintain current production technologies, but also because of concerns that the DLC ring may quickly wear the bore wall.

[22] Although this was the case during the initial build, a mid-project rebuild did include DLC top rings.

- To maintain consistency with current production technology, a graphite based coating on the piston skirt was required.

As mentioned previously, Wiseco already had a 9.2:1 CR piston in production that met all design requirements listed in Table 9 (except that they included DI bowls). A set of these pistons was purchased, and arrived quickly. These were the pistons installed in ESN02. One minor issue encountered during engine assembly was that the aftermarket forged pistons were extremely close to contacting the piston squirters. See Figure 10. The solution to this issue was to simply slightly twist and bend the oil squirter tube to provide additional clearance.

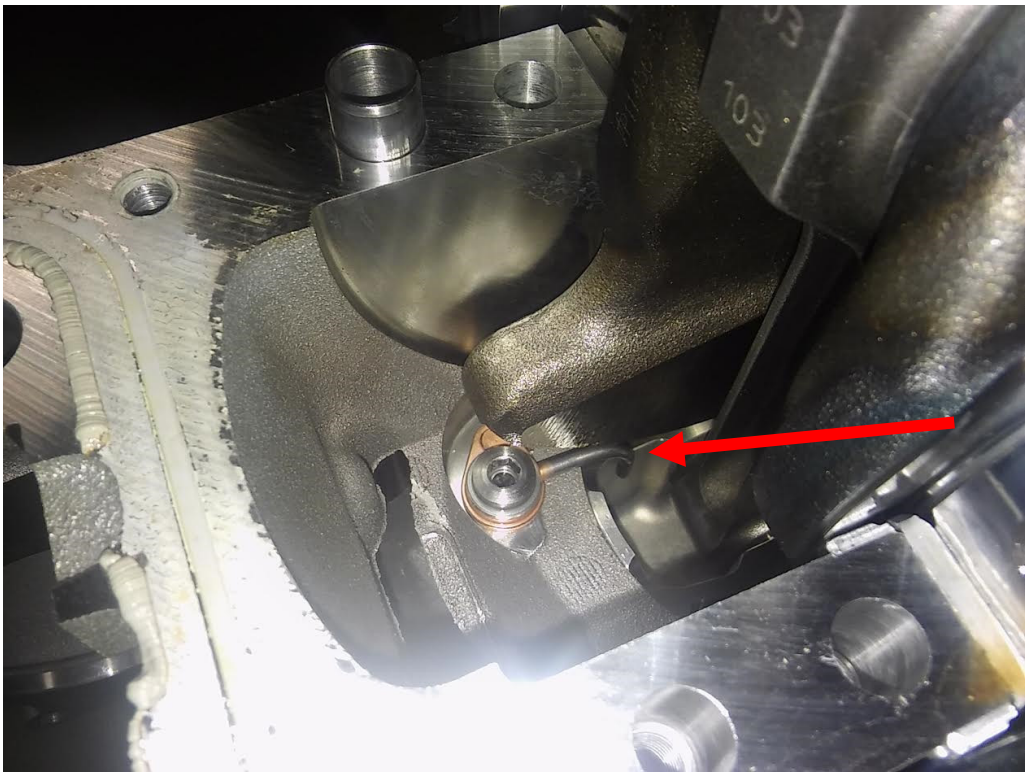

Figure 10: Clearance between the piston oil squirter tube and aftermarket piston (arrow) was nearly zero. Additional clearance was obtained by slightly twisting and bending the oil squirter tube.

Two iteration rounds were required with Wiseco to achieve the target high CR of 11.0:1. The first iteration resulted in a 9.6:1 CR, while the second iteration was just below 11.0:1. Figure 11 shows a picture of the first and second design iterations for the 11.0:1 piston on the left and right respectively. Figure 12 shows the production 9.2:1 piston, the Wiseco 9.2:1 piston, and the 2nd (final) iteration of the Wiseco 11.0:1 piston from left to right respectively.

Figure 11: Comparison between 1st iteration (Left), and 2nd iteration (Right) of the Wiseco 11.0:1 CR pistons.

Figure 12: Comparison between production 9.2:1 CR Piston (Left), Wiseco 9.2:1 CR Piston (Middle), and Wiseco 2nd iteration 11.0:1 CR Piston (Right).

4.2.5 Fuel Pump

Much consideration has been given to the high pressure fuel pump. Although objectives 2.3 and 2.4 refer to a target BMEP of 10% greater than production there was an underlying goal to demonstrate operation at considerably greater BMEP, as much as 100% greater than the baseline production engine. Ignoring differences in thermal efficiency a 100% increase in output will require a 100% increase in injected fuel mass. Although the production fuel pump undoubtedly is capable of providing some overhead capacity, it was strongly felt the production pump would not be capable of supplying fuel at a 100% mass increase.

Several options were considered for delivering a substantial increase in fuel to the cylinder. Options not selected will be mentioned here for completeness, however, in the interest of brevity will only be discussed at a high level.

- Addition of a 2nd pump, driven from the same cam lobe, installed on the top of the cam cover
- Driving one or more pumps with an electric motor thus increasing pump speed higher than engine speed

Both of these options require significant machining and fabrication effort. Moreover, a piston driven injection pump must be controlled synchronously with engine position, further complicating the setup and operation.

- Supplying fuel from a high pressure accumulator
- Driving a non-synchronous high pressure pump (a hydraulic pump for example)

Although these options were attractive from a pump control perspective, a significant amount of fabrication would still be required, and these options open up some potential safety concerns.

At this point, effort was put into developing a plan to increase the displacement of a single engine driven pump. The pump displacement can be increased by increases in pump stroke and / or pump bore. It was discovered that at least two aftermarket intake camshafts were available with an increase in fuel pump lobe lift (one from ZZ Performance, and another from Comp Cams). Surprising little information was available on these cams, even after discussions with both ZZ Performance and Comp Cams. One of each cam was purchased for further investigation. Upon measurement it was determined that the increased lift is achieved through a reduction of the base circle diameter. The production pump has a small amount of preload when it is fastened tightly to the cylinder head and the pump lobe is on the base circle. The aftermarket cam has the base circle reduced to a point where the pre-load is nearly zero, so further reduction of base circle diameter are not practical. As shown

in Figure 13, the reduction in fuel pump base circle diameter results in a 30% increase in pump lift.

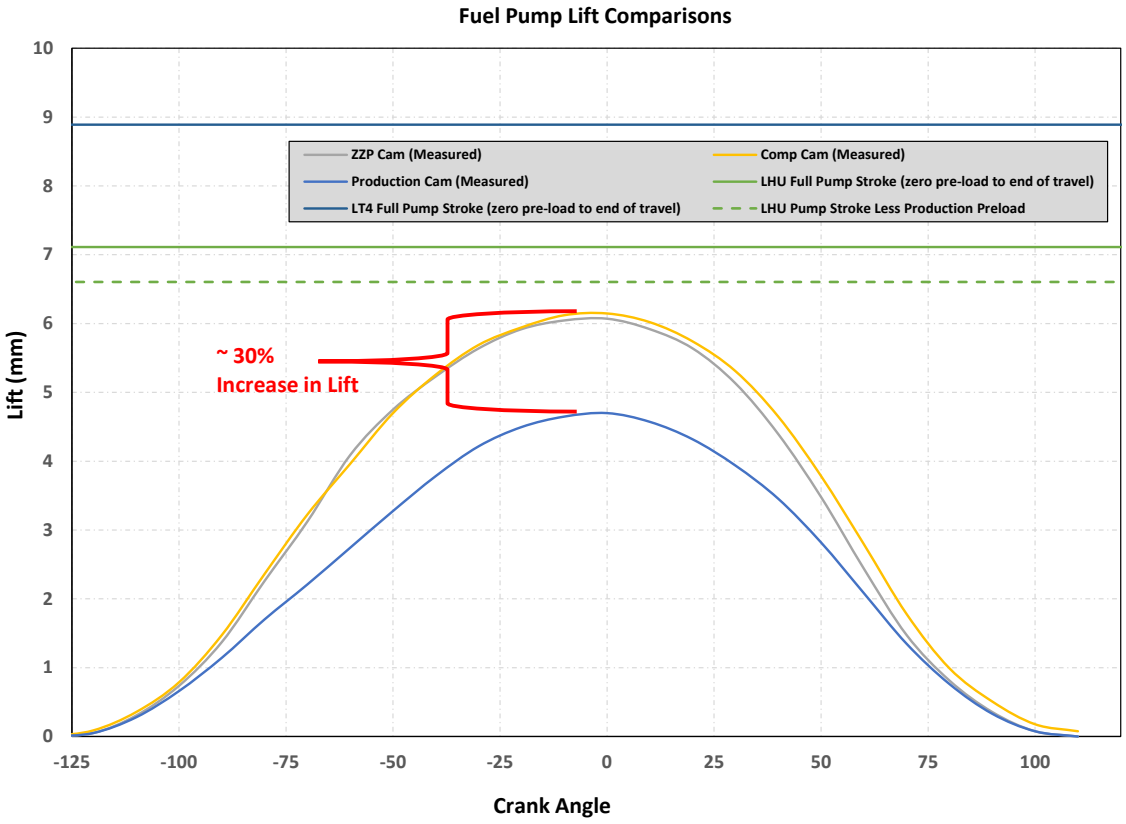

Figure 13: Comparison of Available Options for Fuel Pump Lift.

Targeting more than a 30% increase in injected fuel mass, the production pump was examined in hopes that it might be possible to increase the bore size and fabricate a new piston to match the larger diameter. However, in addition to this being a complicated undertaking, the production pump body is swaged together in such a way to make it unserviceable. A pump from a GM LT4[23] engine was available from the project sponsor. Like the LHU, the pump could not be disassembled to measure the bore. However, the stroke was measured, and it was assumed that the bore was larger than the LHU pump as

[23] Although there has been previous incarnations of the LT4, the 2017 MY LT4 is a supercharged 6.2L V8 producing 485 kW.

it needs to supply considerably more fuel per revolution of the cam. Figure 14 shows the LHU (right) and LT4 (left) pumps.

Figure 14: LHU vs LT4 high pressure fuel pumps.

With confirmation that the LT4 pump would operate at the lift levels of the aftermarket cams (see again Figure 13), plans were developed to adapt the LT4 pump to ESN02. This would require some machining to the cylinder head, and also fabrication of an adaptor plate. However, the larger concern was that the LT4 pump uses an independently sprung follower, while the LHU follower is maintained in contact with the cam lobe by the fuel pump return spring. This results in a much stiffer spring on the LHU pump, and this can be seen in Figure 15.

Since the LHU follower would need to be run with the LT4 pump, a design effort began to retrofit a stiffer spring to the LT4 pump in order to maintain follower contact on the cam lobe. An extensive search of commercially available springs revealed a solution that would dimensionally fit the LT4 pump, and result in closing forces similar to the LHU pump. See the dashed blue line in Figure 15.

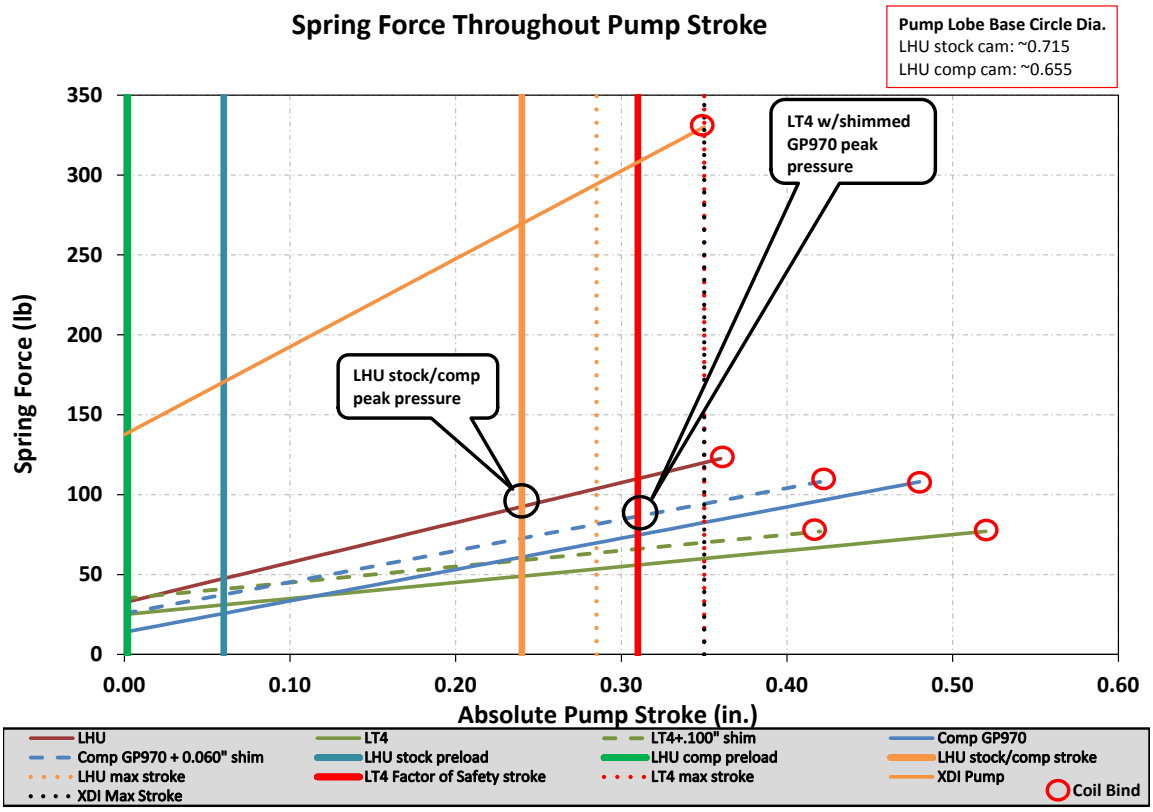

Figure 15: Fuel pump spring comparison.

With plans made to begin adapting the LT4 pump to ESN02, a new option was found. An aftermarket fuel system provider, Xtreme DI, had recently developed an adaption of the GM LT1[24] pump to the LHU platform. Although the fuel requirement of the LT1 is less than the LT4 (339 kW vs 485 kW rated Power), Xtreme DI was able to provide exact bore diameter information on the LT1 pump. Combined with the available high lift aftermarket

[24] Although there has been previous incarnations of the LT1, the 2017 MY LT1 is a Naturally Aspirated 6.2L V8 producing 339 kW.

cam, the LT1 pump would provide nearly exactly the 100% increase in fuel delivery that was being sought, and was chosen as the final solution, and assembled into ESN02. Full details of the fuel pump and cam lift comparison is shown in Table 10.

Table 10: Comparison of high pressure fuel pump options.

RPO	PN	Bore (mm)	Stroke (mm)	Displacement (cc/stroke)
LHU (production)	12658478	9.0	4.5*	0.3*
LHU (comp cam)	12625817	9.0	6.1*	0.4*
LT1 (production)	12625817	10.7	5.7	0.5
LT1 (comp cam)	12625817	10.7	6.1*	0.55
LT4 (production)	12642287	Unknown	Unknown	Unknown

** Measurements made at APS LABS*

Through conversations with Xtreme DI, it was learned that the 6.1mm lift provided by the aftermarket Comp Cam should be considered the absolute maximum lift that the LT1 pump can tolerate without risk of bottoming the piston in the bore. Therefore, if during high load testing it is determined that the 0.55 cc/stroke of the LT1 pump with the high lift Comp Cam is insufficient, further increases in lift through a custom cam grind is not a viable solution. If this case arises, an LT4 pump must be retrofit to the engine.

4.2.6 Intake Cam

Although intake valve lift is not as critical in a boosted application 1) there was a soft goal to produce as much as a 100% increase in output which will require a significant increase in airflow through the valves, and 2) the need for increased fuel pump lift drives the engine build to an aftermarket intake cam. For both of these reasons, an aftermarket intake cam was selected with increased lift compared to the production cam. The comp cams PN 8756

has a peak lift of 10.726 mm vs. the production 10.297 mm providing an increase of 0.43mm peak lift.

4.2.7 Exhaust Cam

To account for the anticipated increase in boost, it was felt exhaust valve lift should be increased to keep pumping work, and potentially residual fraction, reasonable. The Comp Cams PN 8757 has a peak lift of 10.648 mm vs. the production 10.069 mm providing an increase of 0.58mm peak lift. With the increase in intake and exhaust lift, combined with the aftermarket pistons, careful attention was paid to ensure there would not be piston to valve contact within the production range of cam phaser authority. In this regard the valve reliefs cut in the aftermarket pistons were deemed to be acceptable, albeit with less factor of safety than the production hardware. The lift of the production and aftermarket cams, as well as the clearance to the piston is shown in Figure 16. The cams are phased to maximum overlap in Figure 16.

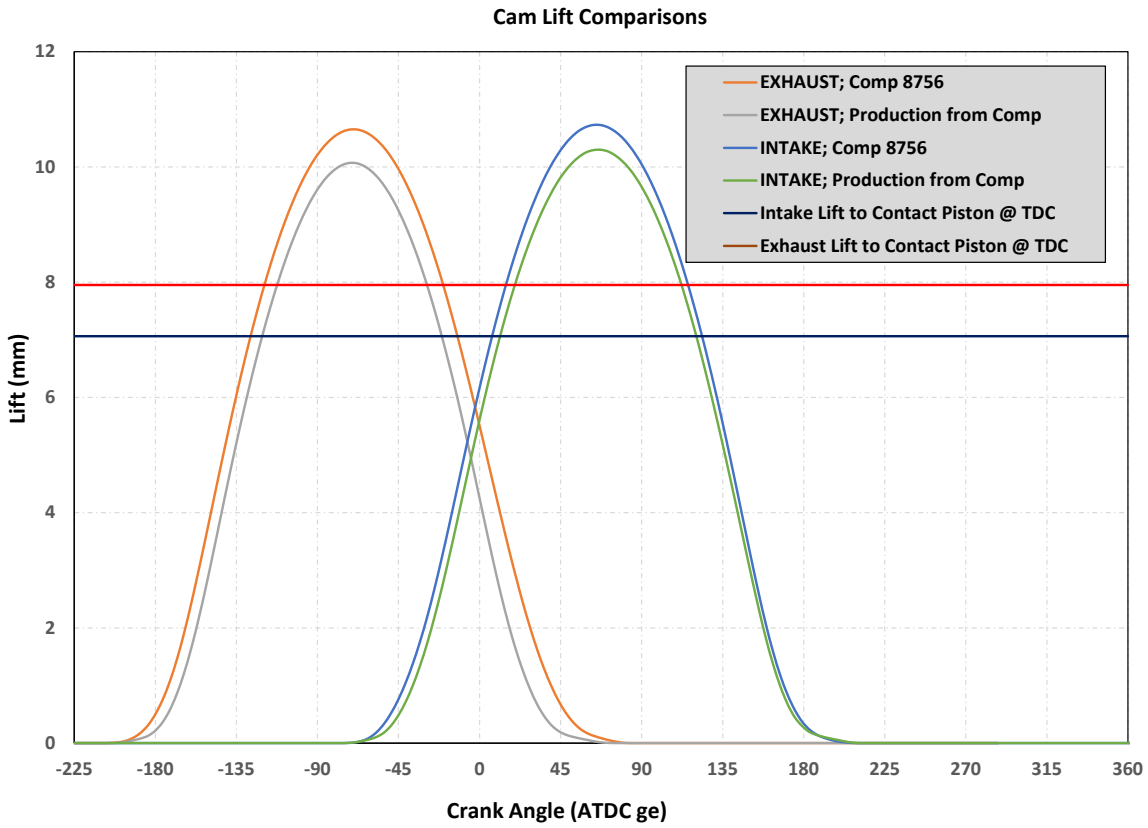

Figure 16: Cam Lift Comparison. Cams phased to maximum overlap.

4.2.8 Valve Springs

With changes planned to valve lift, consideration had to be given to the valve springs to ensure 1) there would not be issues with coil bind and 2) ensure there is sufficient force on the nose and base circle of the cam. However, with plans to significantly increase boost, another consideration was the ability of the springs to keep the intake valves closed with higher than production pressure in the intake manifold pushing on the backs of the valves. Of particular interest was late in the exhaust stroke, when cylinder pressure is lowest and the delta pressure across the valve will be in the direction of forcing the valve open. If this situation occurs, aside from the obvious performance issues, there is a high probability of catastrophic piston to valve contact.

To assess the concern of the high intake pressure pushing the intake valves open, a fixture was designed and built to supply shop air pressure to the intake port. The shop air pressure was adjusted with a regulator, and the pressure at which the valve lifted from its seat was recorded. A dial indicator was used on the valve tip to precisely detect initial valve movement, and a bourdon tube pressure gauge was used to measure air gauge pressure. The fixture used for these measurements is shown in Figure 17.

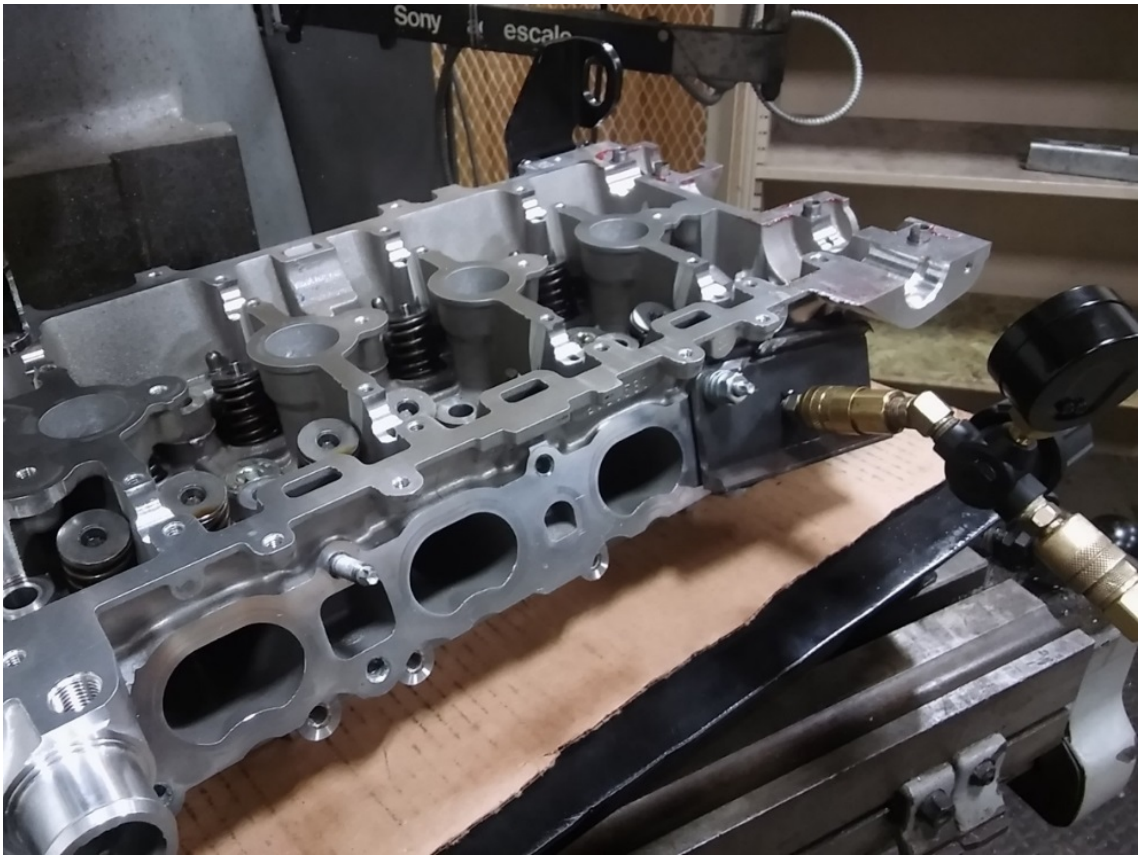

Figure 17: Fixture used to determine the intake boost level that may cause unintended valve opening.

The result of this testing indicated that with production valve springs, the valves began lifting off their seat at 2.2 bar gauge delta pressure, which would correlate to ~2.2 bar boost (assuming cylinder pressure may reach near atmospheric late in the exhaust stroke), and 3.2 bar absolute pressure. Referring again to Figure 8 it is shown that even under the best possible operating conditions, the stretch target of 50 bar BMEP will require manifold

pressure greater than 3.2 bar (recall that the pressure ratio ~ to MAP assuming 1 bar atmosphere, and negligible pressure drop up to and downstream of the compressor. Aside from potential issues with coil bind and valvetrain control, this issue alone necessitated stiffer valve springs.

Aftermarket high tension springs, ZZ Performance PN ZZ-82VS-ECT, were purchased. These springs are advertised as having a spring force on the valve seat of 365 N[25]. Seat lift-off pressure measurements with these springs installed revealed the valves lifted off their seat at 4.3 bar gauge pressure (5.3 bar MAP). Figure 8 suggests this is exactly the worse case pressure requirement and simple hand calculations with assumed thermal efficiency of 20% suggested that the required MAP will exceed 5.3 bar MAP. Therefore a significant amount of additional effort was spent investigating further increases in seated spring force.

Shimming the aftermarket valve springs was considered. However, the lift to coil bind was measured, and determined to be only 2.0 mm beyond the peak lift of the aftermarket Comp Cam. Allowing for a factor of safety to coil bind, only a thin shim, if any, could be used, and this would not significantly increase seat force. Effort was then put into finding another Commercial Off The Shelf spring with greater force. Options were considered from a wide range of engines, including high speed motorcycle engines. However any option found that appeared it would result in greater than 365 N of seated force would have required modifying the cylinder head, running without valve seals, and potential modifications to the valve for different spring retainers and locks. Based on these difficulties, it was decided to proceed with the aftermarket ZZP springs, but keeping this limitation in mind if testing did indeed involve MAP values exceeding 5 bar.

[25] Testing at APS LABS with a valve spring force measurement tool confirmed all springs to be within approximately 1% of the advertised seat force.

4.2.9 Connecting Rods

Aftermarket connecting rods were purchased from ZZP. The connecting rods are forged aluminum, and an H-Beam design both adding to the strength of the connecting rod. As noted in the section on Fasteners, they were purchased with ARP bolts already installed. It is not clear who the manufacturer of these connecting rods is, as ZZP is the distributor, not the manufacturer. ZZP does not provide information on the manufacturer.

4.2.10 Throttle Body

The throttle body in production on the LHU engine uses a digital pulsetrain for throttle position feedback to the engine controller. There were no issues with this for ESN01, which was used for testing with a production controller. However, ESN02 was used with an aftermarket controller and software set. After struggling with throttle control issues, it was discovered that the aftermarket control system was incompatible with the digital feedback of the production LHU throttle body. Some investigation revealed that a pre-2012 MY LNF utilized analog feedback on throttle position, and had the same bolt pattern to the intake manifold. A pre-2012 LNF throttle body was procured from a salvage yard and installed on ESN02. The production LHU throttle had a diameter of approximately 59 mm, while the LNF measured approximately 57 mm.

4.2.11 Boosting System

As discussed previously, GT-Power was used predictively for the development of the engine and other parts of the testbed. The GT-Power simulations were particularly informative in defining the requirements for airflow and pressure required to meet the stretch target of 50 bar BMEP. Referring again to Figure 8, it is seen that the worse case flow and pressure requirements to achieve 50 bar BMEP at 3000 RPM is ~ 912 kg/hr, and a pressure ratio of ~4.26 respectively. After applying a 10% factor of safety and rounding to a typical increment, the boost requirements were 1000 kg/hr and a pressure ratio of 4.75. Figure 8 is replotted in Figure 18, showing the conditions resulting in the minimum and

maximum requirements from the boosting system, and the 10% factor of safety design target.

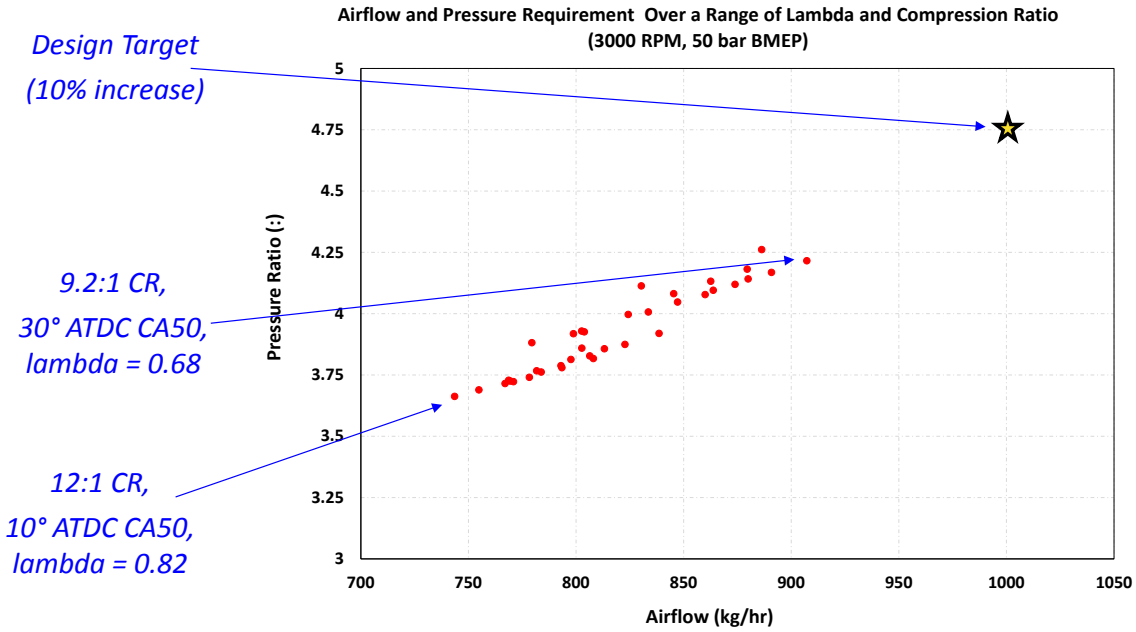

Figure 18: Airflow and pressure ratio requirement to achieve 50 bar BMEP at 3000 RPM over a range of combustion phasings, lambda values, and compression ratios. A factor of safety of 10% is applied to both airflow and pressure ratio for the design of the boosting system.

The first approach to the boosting system was to use a turbocharger, either the production BorgWarner unit, or an aftermarket larger unit. The assumption was made that a particular turbocharger would be limited on the compressor side (either pressure ratio, or total airflow), and not limited on the turbine side[26].

Through conversations with an engineer in BorgWarner's aftermarket turbocharger group, the compressor map for the production turbocharger was graciously provided by BorgWarner, which is included here as Figure 19. In Figure 19, the y-axis is pressure ratio, and although units are not provided for the x-axis, the unit of kg/s is logical, and is assumed

[26] Although one could content that a water injected engine will result in lower exhaust gas temperatures, the total enthalpy may not change significantly because of the increased exhaust mass flow resulting from the water. Therefore, this assumption was held, even for water injection.

to be the unit for the x-axis. The blue lines are contours of efficiency, and the light black curved lines represent shaft speed. The bold black line that runs diagonally across the plot is the surge line. At a given airflow, the compressor will go into a surge condition if the pressure ratio is increased greater than this line (Baines 2005). At best surge results in erratic performance making control of the engine and dyno difficult and making the engine impossible to test. However, prolonged surge can cause catastrophic damage to the compressor blades and in turn catastrophic damage to the engine. Therefore, when selecting a compressor, it is very important to ensure the anticipated operation of the engine requires a pressure ratio below the surge line. In interpreting Figure 19, it becomes immediately apparent that the production turbocharger will not support the 50 bar BMEP stretch target. Not only is the lowest airflow estimated by the GT-Power simulation in Figure 18 ~0.21 kg/s, which is nearly off the map in Figure 19, the minimum pressure ratio shown in Figure 18 (~3.7) is entirely over the surge line at all values of airflow.

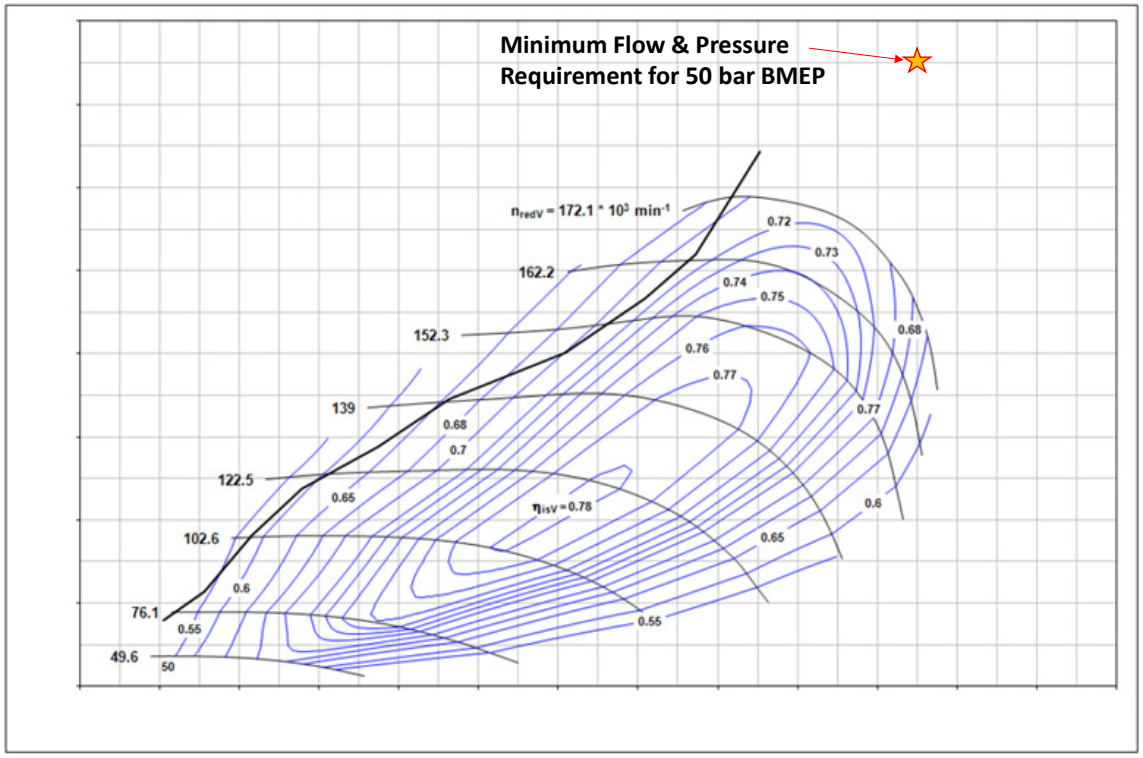

Figure 19: Compressor map for the production LHU turbocharger, the BorgWarner K04-2277D. Image used with permission by BorgWarner. See 17 Appendix F for additional details.

With it apparent the production turbocharger will not support the stretch output goals of this project, a search began for a suitable turbocharger. At the time of ordering test engine hardware, an aftermarket turbocharger was purchased from ZZ Performance. This aftermarket unit was advertised by ZZP as being larger than the production unit, and capable of supporting increases in engine output. Although detailed technical information was not available, it was purchased based on the potential it would support the high output goals of this project. Later, technical information was obtained for this turbo, and it was determined to be a BorgWarner EFR 7163. The compressor map obtained from BorgWarner, (BorgWarner 2015), is shown in Figure 20. Note the data is plotted in English units, however, the requirements for the minimum and maximum boost requirements are placed on this plot. Here it can be seen that even the minimum boost requirement is significantly beyond the surge line.

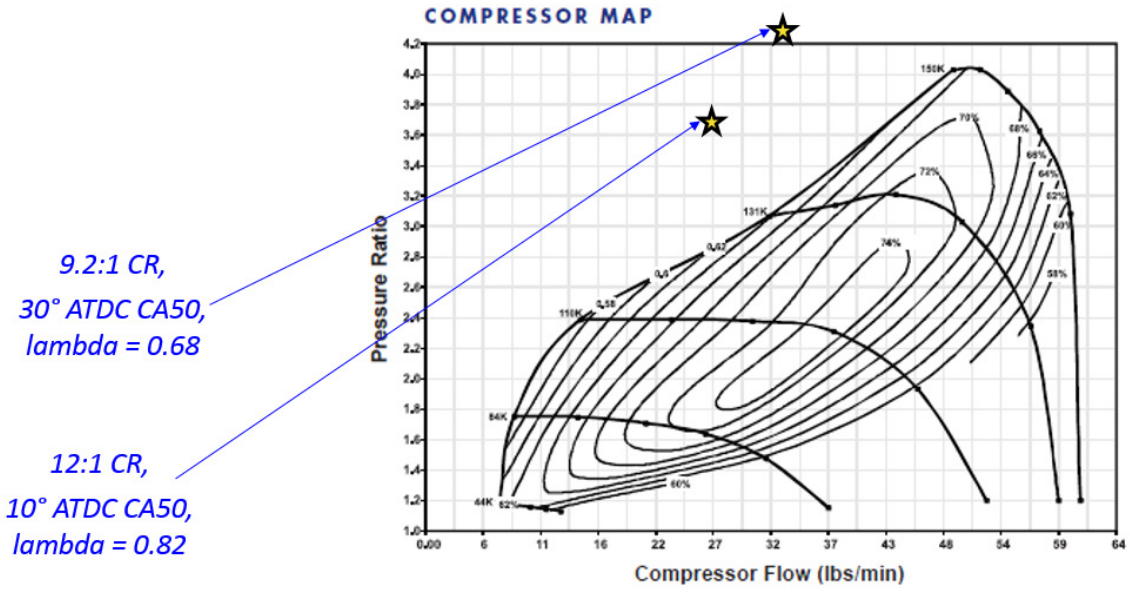

Figure 20: Compressor map for the BorgWarner EFR 7163. Also included the boost requirements for the minimum and maximum cases. Figure used under permission by BorgWarner (http://www.borgwarnerboosted.com). See 17 Appendix F for additional details.

With the aftermarket BorgWarner EFR 7163 sold by ZZP not meeting the requirement, a search for other aftermarket turbochargers began. Garrett, Holset, and BorgWarner were investigated most thoroughly as it was difficult to find engineering data for other manufacturers products. The compressor maps for the best Garrett option, the GTX2860R, and the best BorgWarner option the EFR 7064 are shown in Figure 20 and Figure 21 respectively. Although in both cases the requirement falls on or very close to the surge line, one potential concept could be to create a controlled air leak in the induction path. Such an air leak, if controllable, can shift operation to the right on the compressor map (increased airflow at constant pressure ratio), away from the surge line. This is shown by the horizontal arrows on Figure 22. Because the BorgWarner EFR 7063 has a broader, more horizontal map, it was deemed easier to operate in this way, and was selected as the best possible turbocharger option.

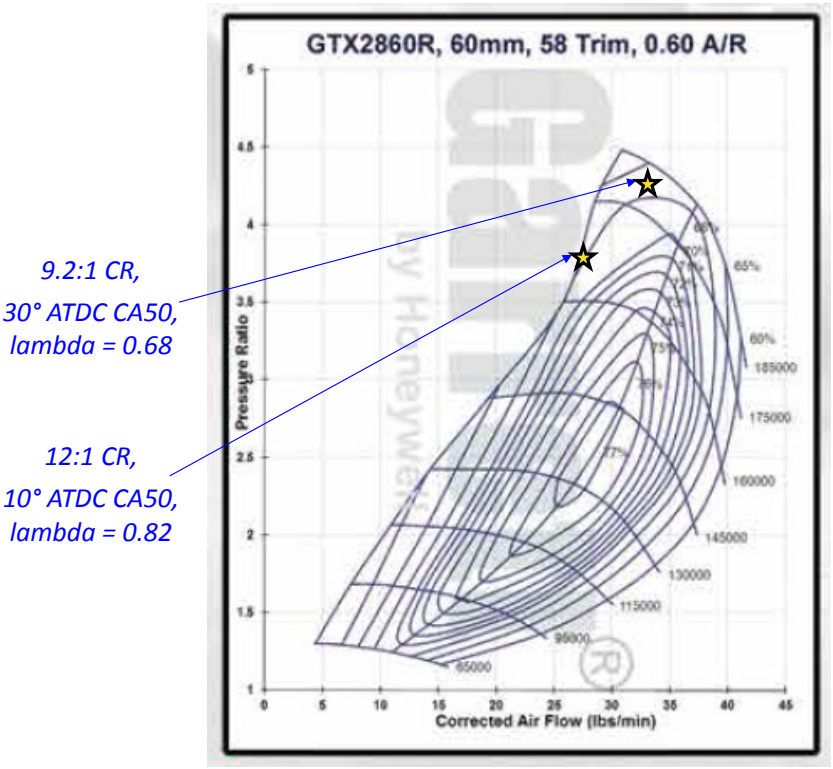

Figure 21: Compressor map for the Garrett GTX2860R turbocharger, the Garrett part that comes the closest to meeting the boosting requirements of this project. Figure used under permission by Garrett division of Honeywell. See 17 Appendix F for additional details.

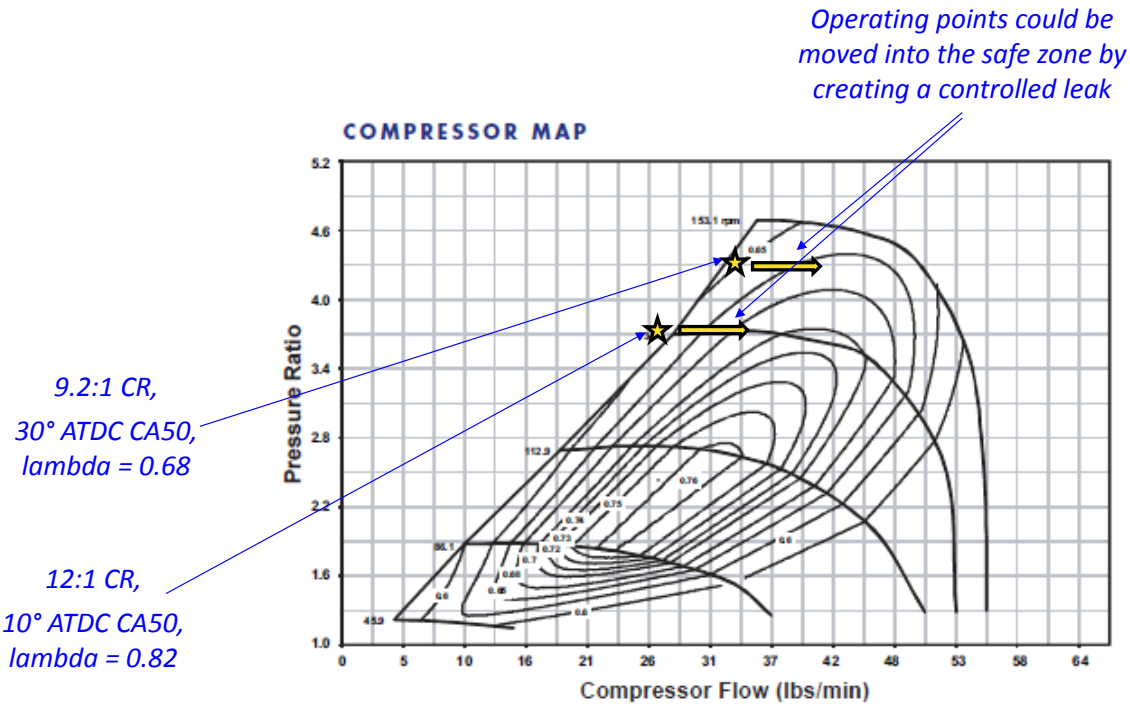

Figure 22: Compressor map for the BorgWarner 7064 compressor, the BorgWarner part that comes the closest to meeting the boosting requirements of this project. Figure used under permission by BorgWarner (http://www.borgwarnerboosted.com). See 17 Appendix F for additional details.

Although the BorgWarner EFR 7063 was the best turbocharger option, it was not without risk, and complexity. Therefore continued effort went into boosting options. One such option is to create boost though an external boost generation apparatus. A scheme such this has the advantage of separating boost generation from engine operation. It was felt this could be a tremendous advantage not only at low speeds, but also over a range of combustion phasings, lambda's, and perhaps most importantly as significant amounts of injected water significantly change exhaust temperature. Several concepts were identified including:

- A centrifugal compressor
- A roots blower
- A screw compressor
- A large displacement engine outfitted with very light valve springs allowing the poppet valves to act as check valves
- The buildings shop air system

All of these options could be driven from either an electric motor controlled with a variable frequency drive, or by coupling the device to the rear side of the dynamometer. Driving the device with a variable frequency drive is considered the best solution as it completely decouples the speed of the device from the speed of the engine. Driving the device with a natural gas powered engine was also considered but abandoned due to complexity.

After speaking with representatives from a number of manufacturers of centrifugal compressors (Paxton, Vortech Automotive, Vortech Industrial, Procharger, etc.) it was determined that a centrifugal compressor does not currently exist that will be the pressure ratio requirement. The concept of arranging two compressors in series was investigated, however, a senior level engineer at Vortech Industrial strongly warned against this concept stating that although it appears straightforward, it would be far more difficult in practice, citing the critical need for significant intercooling between the stages, complications in the control, and complications in the drive as reasons (Endress, 2016). Although he did not defend his position with data, his austere warning was heeded, and this concept was abandoned.

Several companies manufacturing automotive roots blowers were contacted. However, none were able to provide a compressor map, and most went on to state that they do not use, or even generate, compressor maps. At least one manufacturer claimed with confidence their product would meet the performance targets of this project, citing examples where their products are installed on V8 racing engines producing brake power far in excess of the targets of this project. However, when asked what the pressure is

downstream of the compressor on these applications, data was not available. Because of a lack of compressor maps, or even in-use data, these suppliers were not contacted further.

Industrial manufacturers of roots blowers were contacted. A senior level applications engineer at an industrial roots blower manufacturer (PD Blowers) indicated that there is not a roots blower in existence that can generate the pressure ratio required, going on to say a pressure ratio of ~2.5 is the maximum to be expected from any roots blower. When questioned on the feasibility of combining two roots blowers in series, the engineer, without hesitation, stated that the downstream blower would fail. The engineer went on to explain that when under positive pressure, the blower case would balloon, disrupting the high precision clearance between the rotors and case, and rotor to rotor clearances[27] (Endress 2016). Metal to metal contact could result immediately, and if not, the bearings would likely fail quickly. For these reasons, this concept was abandoned.

After some investigation, a screw compressor began to look like a viable solution. Several manufacturers were contacted including Whipple, Lysholm, Kenne Bell, HPS Superchargers AB, Gardner Denver, and Atlas Copco. Quotes were requested from multiple manufacturers, and upon review of quotes it became apparent that the screw compressor solution would be in the $50,000 to $100,000 range, with lead times potentially approaching 4 months. Due to the extreme cost and lead times, this solution was not pursued further.

The concept of using a large displacement engine as an air compressor was considered. To increase efficiency when operating as a compressor, the valves would be disconnected from the camshaft, and light valve springs installed on both the intake and exhaust valves. The theory being that the light spring would allow the valves to float open when the piston travels down the bore, and draw air in from both the intake and exhaust, and close as the piston travels up the bore and cylinder pressure increases. As it is being compressed, the air would flow out the spark plug port. A check valve would be required on the high

[27] The engineer stated that these internal clearances can be 70 microns or less.

pressure line exiting the spark plug port. The engine would be driven from a large electric motor, the back side of the double ended dyno, a second engine, or the engine could be split, whereby a fraction of the cylinders are converted as compressor cylinders and the other half remain functional. Some first principals calculations were performed, which indicated this solution contained merit depending on the displaced volume of the engine and the speed at which it is driven. With used large displacement engines readily available at salvage yards, this option was attractive from a cost perspective, yet with the significant unknowns and risks associated with system integration and implementation, this solution was not pursued further.

Based on the previous discussion, the concept of using shop air was investigated in detail. The air compressor at the Advanced Power Systems Research Center (APSRC) is manufactured by Ingersoll Rand and is sized with an 18.6 kW motor. Although the building air compressor cannot meet the steady state flow requirements of the engine at the highest load test points, it was felt that the engine should not be operated at the highest load test points for long anyhow due to durability concerns, and that the air storage capacity within the building may be sufficient to makeup the difference long enough to collect data at each test point.

A 0-Dimensional model was created of the system including the buildings air compressor, storage volume, and the engine under test. The objective was to determine if this option held merit before continuing down this path. Several different operational scenarios were modeled. A selection of those scenarios is shown in Figure 23. An engine operating condition of 483 kPa of boost pressure at 278 g/s was modeled. This condition matches the design requirement represented by the start Figure 18. The scenario's modeled utilized 4 options for compressors, and 4 options for storage tanks.

The compressor options were:

1. The Ingersol Rand IR25 (25 hp / 18.6 kW) air compressor that was used to supply all of the buildings shop air at the time of this modeling. This compressor is rated at 93 SCFM[28] at 862 kPa.
2. A small portable Craftsman compressor (5 hp / 3.7 kW). This compressor is used for various functions around the shop and in the parking lot. The compressor is rated at 5.8 SCFM at 621 kPa.
3. A supplemental 7.5 hp / 5.6 kW compressor that at the time of this modeling was in the building, but not connected electrically or fluidically to the building.
4. The 7.5 hp / 5.6 kW compressor located on the KRC side of the building. This compressor can be connected to the APSRC side of the building by opening two ball valves (one on the APSRC side of the wall and one on the KRC side of the wall).

The tank options were:

1. The 473L tank that is located near the Ingersol Rand IR25 (25 hp / 18.6 kW) air compressor that was used to supply all of the buildings shop air at the time of this modeling
2. The 100L tank as part of the small portable Craftsman compressor (5 hp / 3.7 kW)
3. The 473L tank that is part of the supplemental 7.5 hp / 5.6 kW compressor that at the time of this modeling was in the building, but not connected electrically or fluidically to the building.

[28] To determine the flow of this compressor, the manufacturer Ingersoll Rand was contacted via phone. The flow was specified as 93 Actual CFM @ 125 psi. This appeared unreasonably high, yet the technician on the phone insisted it was actual CFM, and not standard CFM. Still doubtful, the author asked Joel Duncan (APS LABS Staff Engineer) to call. Mr. Duncan called several days later and talked with a different technician who also insisted the flow was 93 ACFM @ 125 psi, and not 93 SCFM @ 125 psi. However, subsequent approximation based on the bore and stroke and speed of the compressor, and testing all support the compressor flow being 93 SCFM @ 125 psi, and therefore that is the specification that will be assumed correct.

4. The 530L volume that is co-located with the 7.5 hp / 5.6 kW compressor located on the KRC side of the building. This 530L volume is made up of two separate tanks.

In each case, assumptions were made for the additional volume made up from the connecting plumbing. Effects due to pressure drop in the pipes were ignored, as were cooling effects from the expansion of air out of the tanks, and heating effects from the compression of air into the tanks.

As shown in Figure 23, the time to discharge the shop air system is unacceptably low with only the baseline compressor, and receiver tank. However, when adding additional compressors and storage volume to the system, the time to discharge increases as expected. Utilizing all four compressors, and all four tanks resulted in a time to discharge of 50 seconds. Although at first consideration this may seem unacceptable for steady state testing at the level of output corresponding to the 50 second discharge time (50 bar BMEP) the engine is under significant stress and is operating in a thermally challenging situation as well (control of exhaust temperature, coolant temperature, oil temperature, test cell ambient temperature, etc.). Therefore the engine should not, and will not be operated at these extremely high loads for the duration that would be normal under typical steady state dynamometer testing. It is felt that 50 seconds is enough time to get to the target test point, reach some minimal level of stabilization and record enough data for statistical significance (5 – 10 seconds), before the boost pressure begins to fall off.

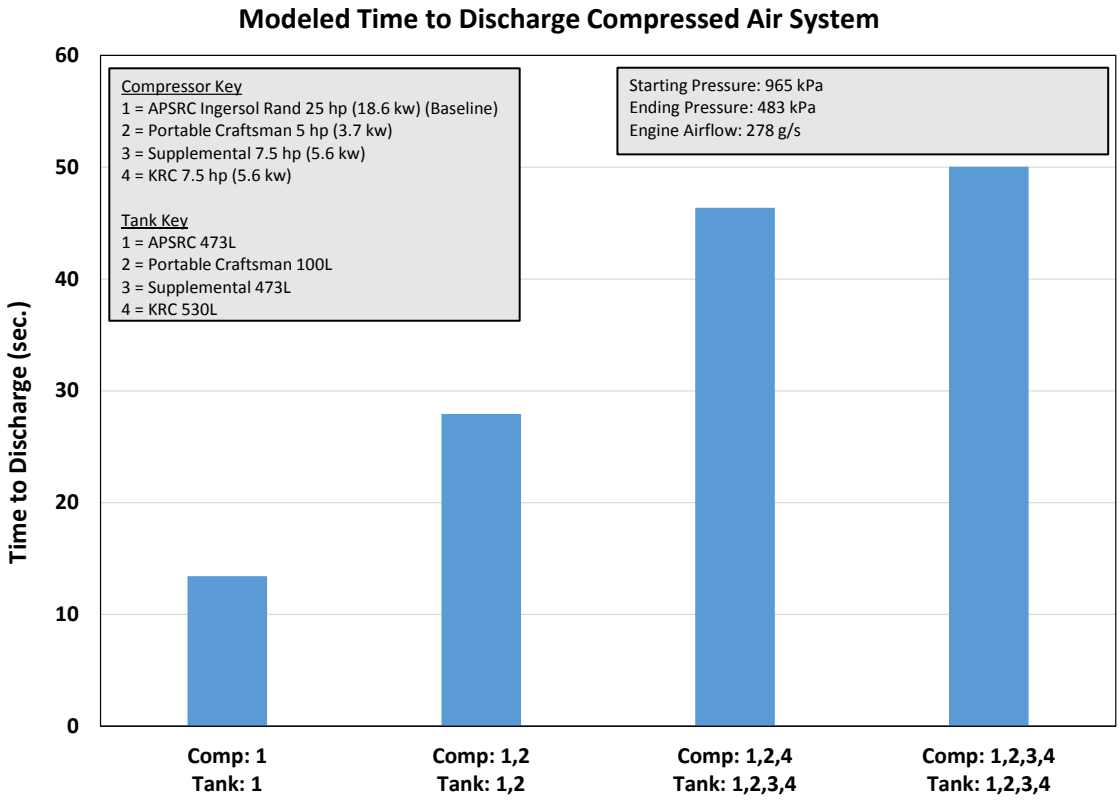

Figure 23: Results from the 0D modeling of the buildings compressed air supply system.

With the results of the 0D modeling indicating that compressed shop air was at least plausible in terms of allowing the engine to meet its boost targets, effort went into designing a system to supply the engine with shop air, and control the boost pressure.

The system was designed to be integral with the building, and universal, such that it can be used to supply boosted combustion air to any engine in the future operating in that same test cell at the APSRC building. Piping was run directly from the buildings main air receiver tank to the testcell control area. Rigid copper tubing was used. Copper was chosen to 1) reduce the risk of rust and scale getting into the engine, 2) it was felt that the smoother walls and the more gradual fitting transitions of copper would reduce pressure loss, and 3) the final installed cost (materials plus installation labor) of copper was only slightly greater than black iron pipe. The nominal diameter of the copper tubing was 50.8 mm resulting in an Inside Diameter of approximately 50 mm.

At the test cell control wall the air first flows through two regulators in series. The first regulator is adjusted to reduce the pressure to close to the desired boost pressure, and the 2nd regulator sets the exact desired boost pressure. Using two regulators provides the same result as a 2-stage regulator, making the final output pressure much more stable with respect to fluctuating pressure at the air receiving tank. This is particularly important in this application because the air compressors won't be able to keep up with the engine demand in steady state the pressure won't simply fluctuate between the turn on and turn off settings of the compressor, but rather will drift from the turn off setting all the way down to a point where boost pressure can no longer be met.

With boost pressure set by the regulators, the air flows through a 3-way ball valve. In one position of the ball valve, a path is created from the regulator set to the engine, allowing the engine to receive boosted air. In the other position, a path is created from an air filter mounted in the test cell mezzanine area allowing the engine to run in a naturally aspirated mode.

When the airflow had to change direction abruptly, a "Y", or "T" was created to serve as a condensate trap. With uncertainty in the amount of condensate that would be trapped, a drain cock was added. A serviceable mesh filter was added in-line just after the air entered the test cell. The mesh filter was arranged with square holes of 0.8mm by 0.8mm. Although this mesh size is considerably larger than a typical engine air filter, it will catch large particles such as rust flakes from iron pipes, pipe tape, etc. Smaller sized dust particles will be filtered out by the paper filter elements on the compressor inlet. The connection between the rigid portion of the boost rig that would be considered a permanent installation in the building and the engine is high pressure rubber flexible hose. The hose is Continental Versaflow with an Inside Diameter of approximately 76mm. The length of hose remains with the engine cart when not in use, and connects to the rigid boost system through a barbed fitting and hose clamp.

On the engine cart, the boosted air flows through an air to water heat exchanger made by Frozen Boost. The water flow through the heat exchanger is regulated with a proportional valve that is controlled a temperature controller made by Omega. If needed, the water source could be either hot or cold, to either cool or heat the incoming boosted air. Two blow-off valves were placed between the heat exchanger and throttle body. The blow-off valves are installed simply to protect the throttle if the throttle were to be suddenly closed while the system is running at boost. The thought was that this scenario could be very likely to take place. If running high levels of boost and the engine begins to pre-ignite or knock heavily, the test cell operator will instinctively close the throttle rapidly. At the levels of boost that are expected, a significant force is created on the closed throttle (in addition to boost pressure upstream, a vacuum will exist downstream), potentially bending or damaging the throttle, and in the worst case, ingesting the throttle or parts of the throttle body into the engine. The blow-off valves are referenced to manifold pressure, so if the throttle were to close creating excessive pressure drop across the throttle the blow-off valves will open, dumping boost air into the atmosphere of the test cell until the test cell operator can turn off the boost supply.

The operating procedure of the boost rig is to motor the engine with the throttle set wide open and the 3-way ball valve set to the Naturally Aspirated (NA) position. Both regulators are adjusted, then the ball valve is switched (engine still motoring) to the boosted position. The flow is allowed to stabilize and the MAP is read in realtime. The 3-way ball valve is switched back to NA and any changes necessary are made to the regulator settings (setting the regulators requires a level of trial and error). Once the desired MAP is achieved motoring, the engine is fired, WOT, NA, then the valve is switched to the boost position, the engine allowed to stabilize for several seconds, then data is recorded.

The boost rig is shown in Figure 24 to Figure 26.

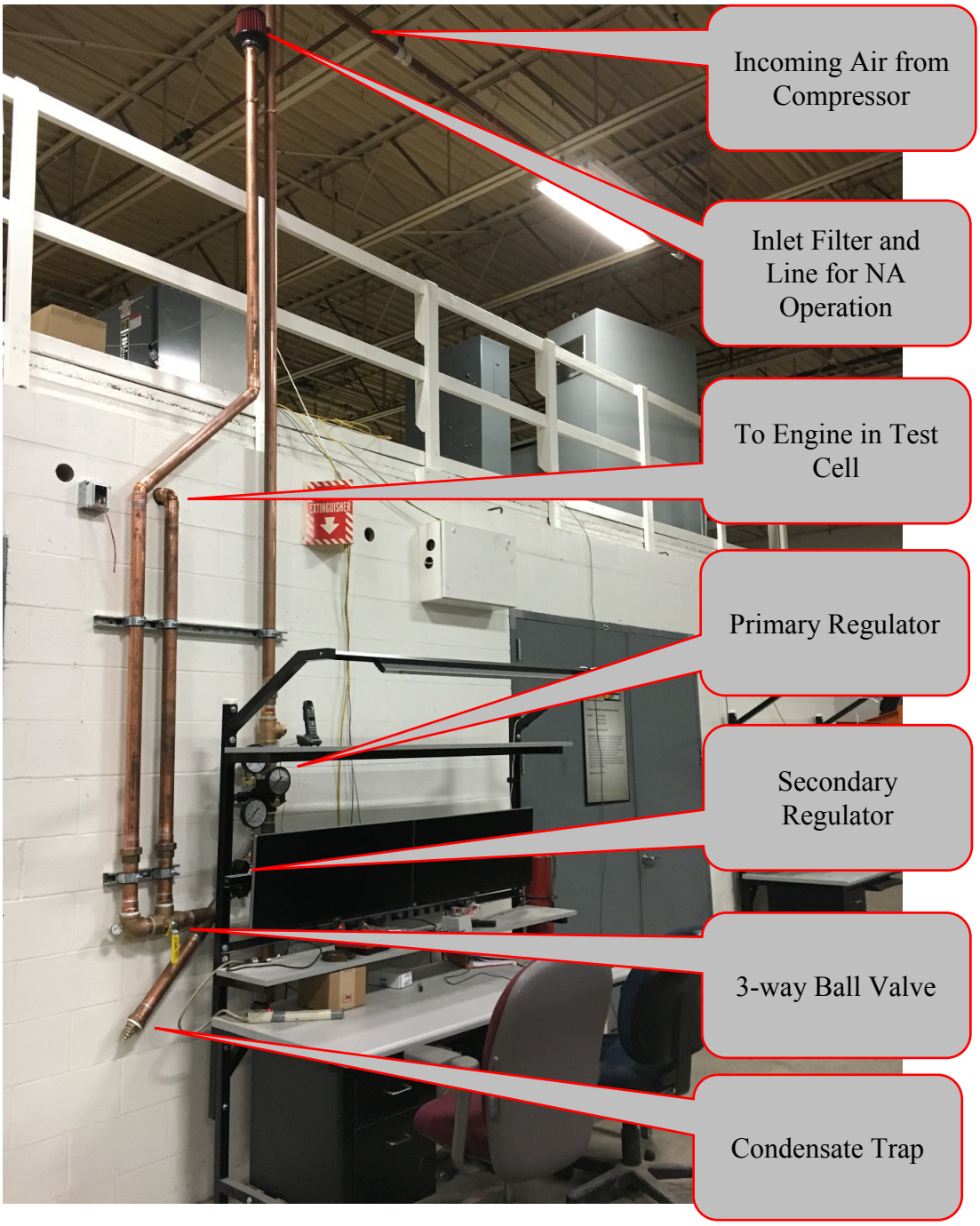

Figure 24: Boost Rig located outside test cell. Rig uses building compressed air.

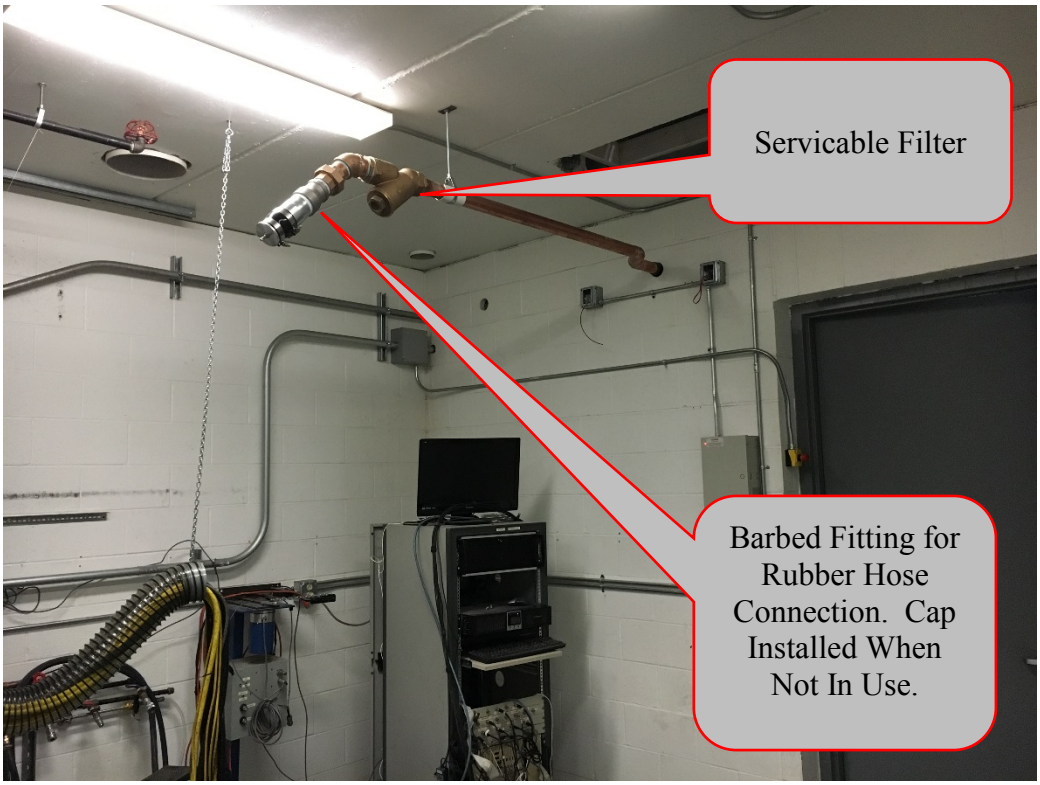

Figure 25: Boost Rig inside Test Cell.

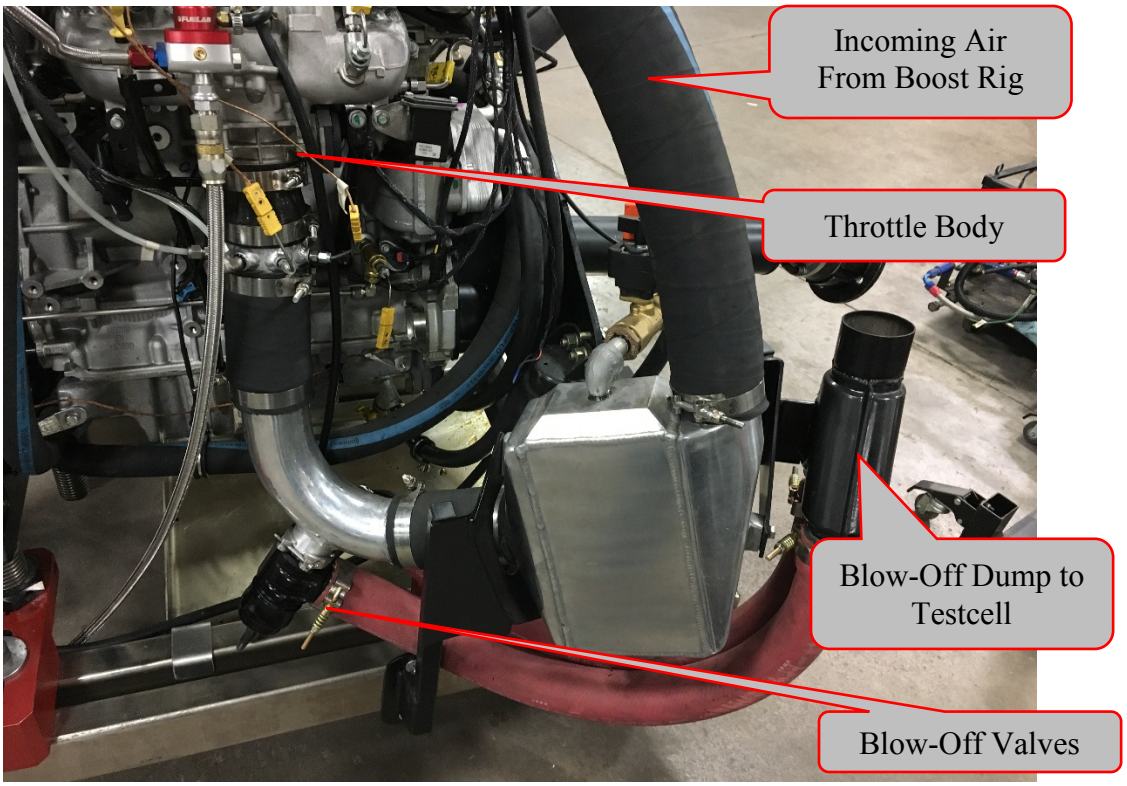

Figure 26: Boost Rig on Engine Cart.

With the boost rig complete, experimental testing was conducted to verify performance. The engine was motored at 3000 RPM, and WOT with the induction system connected to the boost rig. Boost pressure was swept through the range of boost pressure required, as predicted by GT-Power modeling. Three separate compressor / storage volume scenarios were examined. Using the nomenclature in Figure 23, these scenarios were; 1) only the baseline APSRC compressor and air tank (Comp 1 and Tank 1), 2) adding to the baseline the supplemental air tank and the portable compressor / tank assembly (Comp 1, Tank 1, Comp 2, Tank 2, and Tank 3), and 3) adding to the baseline the supplemental air tank, the KRC compressor, and the KRC air tanks (Comp 1, Tank 1, Comp 2, Tank 2, Tank 3, Comp 4, and Tank 4). The results of this test are shown in Figure 27. The results corroborated the modeling data, suggesting that although true steady state testing will not be possible, there would be an adequate amount of time to stabilize the engine and record data.

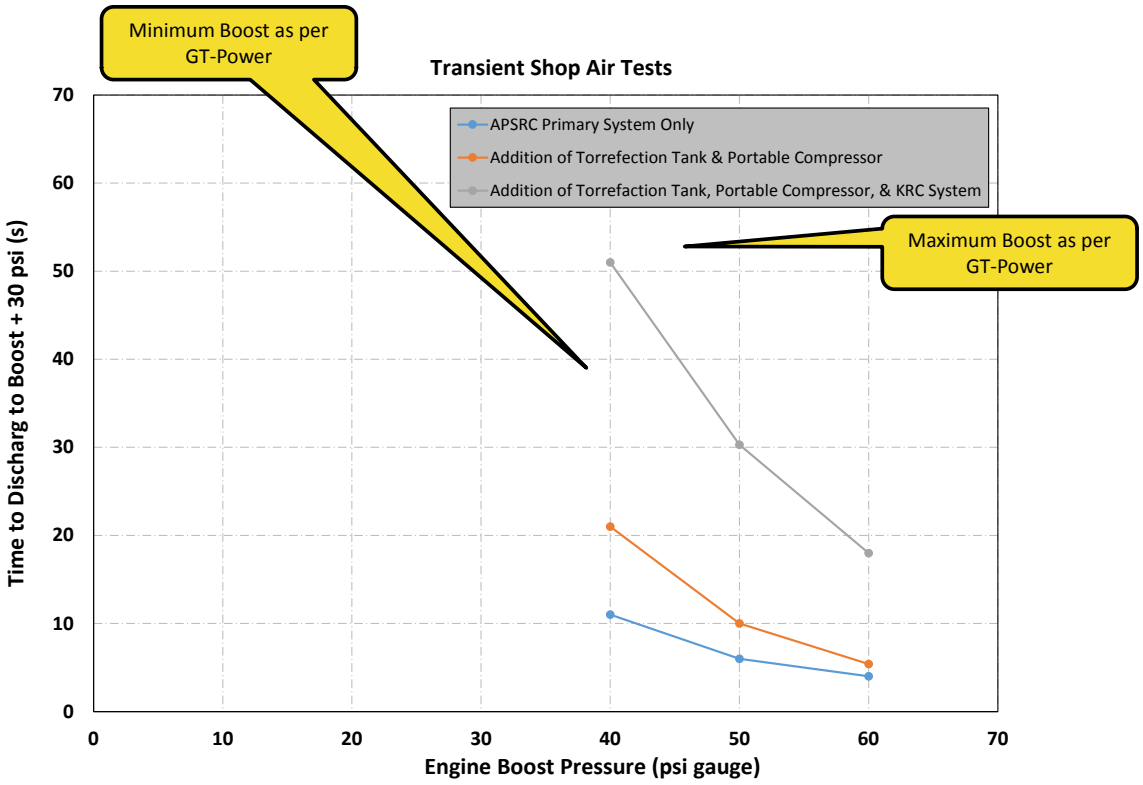

Figure 27: Experimental results of boost rig testing.

4.2.12 Lubrication Oil

Consideration was given to the lubrication oil. The manufacturer specified oil for this application is fully synthetic with a multi-grade viscosity of 5W30. With cylinder pressure expected to be significantly higher than production intent, one concern was that the increased force on the connecting rod could push the oil out of the connecting rod and main bearing leading to bearing failure. It is commonly excepted that a higher viscosity oil will be more likely to maintain hydrodynamic lubrication between the shaft journal and bearing (Speed_Jr. 2015). It is for this reason that many oils intended for racing applications may have a higher viscosity, for example 20W50. However, unlike many conventional racing engines, the LHU / LNF engine relies upon the lubrication system for non-lubrication roles. These non-lubrication functions had to be considered before making a change in oil viscosity. One non-lubricating role is the use of lubricating oil for cooling of the pistons. A concern here is that a significantly higher oil viscosity may reduce the oil jet penetration

distance, thus reducing the amount of oil that reaches the piston, especially at TDC. More of a concern though was the operation of the Variable Valve Timing (VVT) system. Phasing of the camshafts is accomplished by routing lubrication oil through a PWM controlled hydraulic spool valve to an advance or retard chamber in a vane phaser. The author can say from personal experience developing VVT systems at GM, that factors such as pressure, entrained air fraction in the oil, and viscosity can all have a significant impact on the control of the phasers. Since all of these factors are impacted by oil viscosity, there was a feeling of conservatism in changing oil viscosity.

The SAE viscosity rating is applied at 100°C for single grade oils and for the second value of multi-grade oil (Robert_Bosch_Gmbh 1996). Since the testing of this engine was expected to take place at approximately 100°C, it made sense to only consider the second value in multi-grade oil. Operation below 100° would only be light load as the engine is being warmed prior to data collection. The decision was made to switch to a 10W40 viscosity oil. That viscosity is readily available, and it was felt that the slight increase in viscosity at 100°C would be directionally supportive of increasing bearing durability, while not being a significant enough change to adversely affect piston oil squirter or cam phaser performance. The viscosity change can be seen in engineering units in Figure 28, with the data coming from Material Data Safety Sheets (MSDS) obtained from Driven Racing Oil (http://www.drivenracingoil.com/).

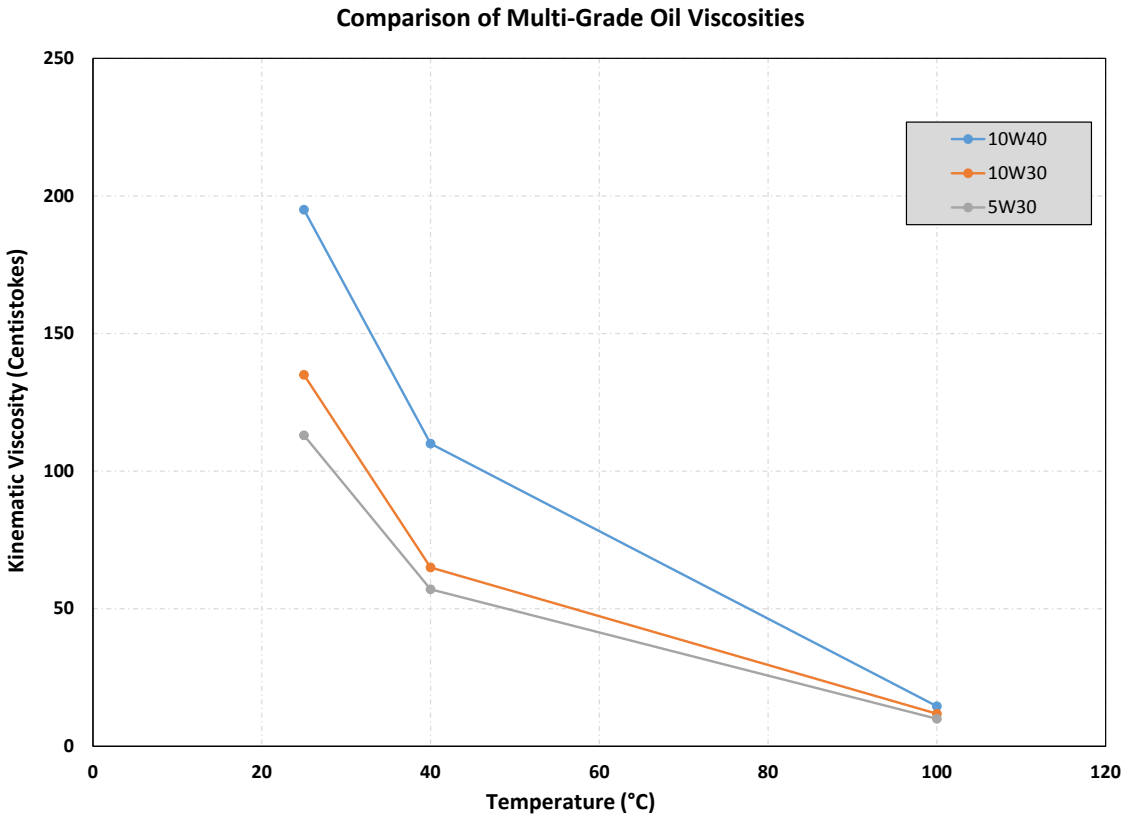

Figure 28: Comparison in viscosity across oil viscosity grades being considered for this project. Data obtained from Material Safety Data Sheets (MSDS) from Driven Racing Oil Website: http://www.drivenracingoil.com/.

Another oil consideration was the additive package. It has long been accepted that Zinc Dialkyldithiosphosphate (ZDDP) when added to engine oil is very effective at protecting metal parts in extreme pressure locations. One particular area are the high stress concentration locations in the valve train. Again, with cylinder pressure expected to increase significantly, the stresses in the valve train were expected to increase. In particular, on the exhaust side instantaneously at Exhaust Valve Opening (EVO). Additionally, recent research has shown ZDDP to be very effective in reducing the component of Low Speed Pre-Ignition (LSPI) and Stochastic Pre-Ignition (SPI) believed to originate from free oil droplets (Ritchie A. 2016). In this case, this is very synergistic. Although a future phase of this work may look at LSPI / SPI, the aim of this research is knock mitigation, therefore PI events only risk damaging or destroying the testbed without adding value to the dataset or research.

In the past ZDDP has been decreased / removed from oil due to it's tendency to poison the three way catalyst (TWC) and Oxygen Sensors. However, ZDDP can still be found in oils intended for off-road racing applications. The oil chosen for ESN02 was Driven Racing Oil XP9 (Speed Jr. 2015). This is a fully synthetic 10W40 oil that contains ZDDP.

4.2.13 Water Injection System

Although the water supply system has been developed to support DI, the scope of this work does not include DI, therefore the ensuing discussion will only focus on PI water. A production Bosch EV14 PI fuel injector has been installed in each of the 4 intake runners. A mounting boss and water rail was designed and fabricated. The mounting boss was fabricated from aluminum, and welded to the aluminum intake manifold. The mounting boss was designed to provide a fastening point for the water rail, which in turn retained the injector. The injector was targeted such that the center of the spray is centered in the intake port, just upstream of the septum. This is the same as would be done for PI fuel. As noted previously, an additional regulator that is referenced to intake manifold pressure is mounted to the engine, and provides the final adjustment of the water pressure. The details of the engine mounted water injection system are shown in Figure 29 and Figure 30. The control system for the water injection will be discussed in the controls section of this document.

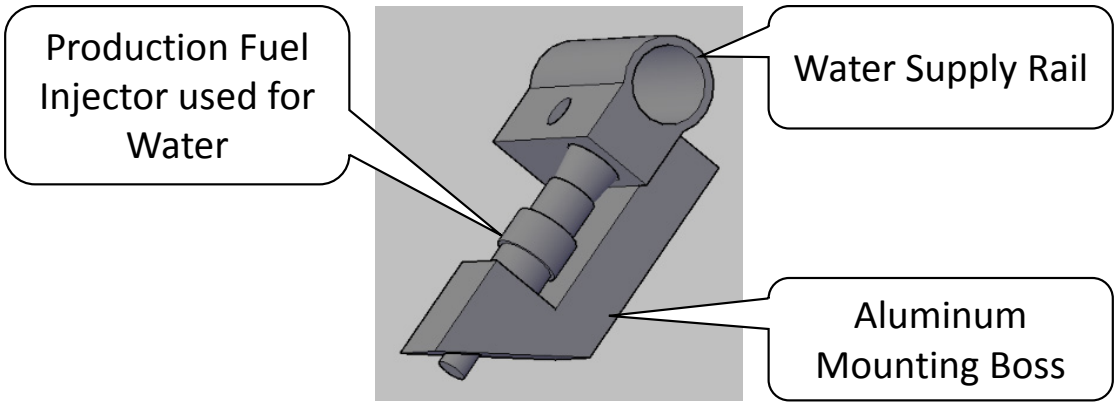

Figure 29: The injector, supply rail, and mounting boss that was designed and fabricated for port injection of water. ***Reprinted with permission Copyright © 2017 SAE International. Further Distribution of this material is not permitted without prior permission from SAE. See 9Appendix F for further details.***

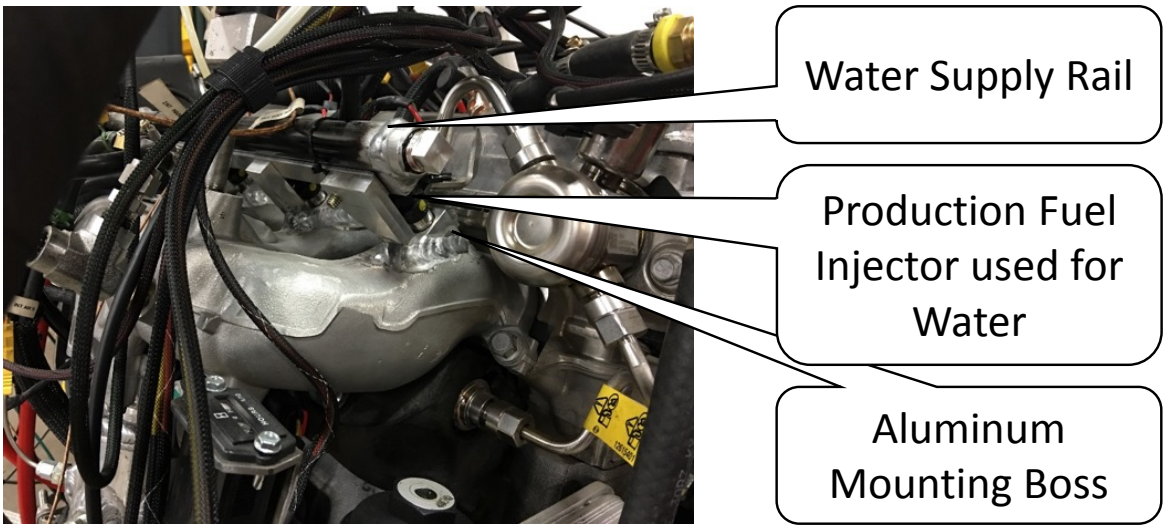

Figure 30: Injector and rail assembly as installed on the engine. ***Reprinted with permission Copyright © 2017 SAE International. Further Distribution of this material is not permitted without prior permission from SAE. See 9Appendix F for further details.***

4.3 Controls

Water injection control was handled separately from engine control, and will therefore be described separately.

4.3.1 Water Injection Control

A MotoTron ECU has been installed to drive the port water injectors. The MotoTron system uses MotoHawk for control algorithm development, and MotoTune for calibration (MotoTron 2007). The controls have been developed to synchronize to engine position using the production crank position sensor. The crank sensor signal wire was tapped and run to the MotoTron controller. In realtime, the user can adjust a parameter which represents the number of crank degrees between the missing tooth of the 58X crank target wheel and TDC of the compression stroke, which times the MotoTron system to actual engine position.

Each of the four injectors can be controlled individually in terms of their Start of Injection (SOI) and End of Injection (EOI), or they can be controlled globally, where the SOI is set, and the injection duration is adjusted through a calibration table. The calibration table allows adjustment of water injector pulsewidth as a function of engine speed and manifold pressure. The code utilizes a digital filter on both speed and MAP to avoid excessive "hunting" within the table.

A camshaft position input is not utilized. The impact of this is that when starting the engine from rest, the MotoTron system may be 360 CA off from actual engine timing. The operating procedure has been to test fire one injector with a short pulse width, then observe in realtime in the CAS system (which includes inputs for all four fuel injectors, all four water injectors, and all four ignition coils), the timing of the water injection. If the water injection is off, the user simply adds or subtracts 360° from the offset between the missing tooth of the crank target wheel and TDC firing.

An image of the MotoTune screen with setpoint parameters and the water pulsewidth calibration table is shown in Figure 31, while Figure 32 shows the MotoTron ECU hardware.

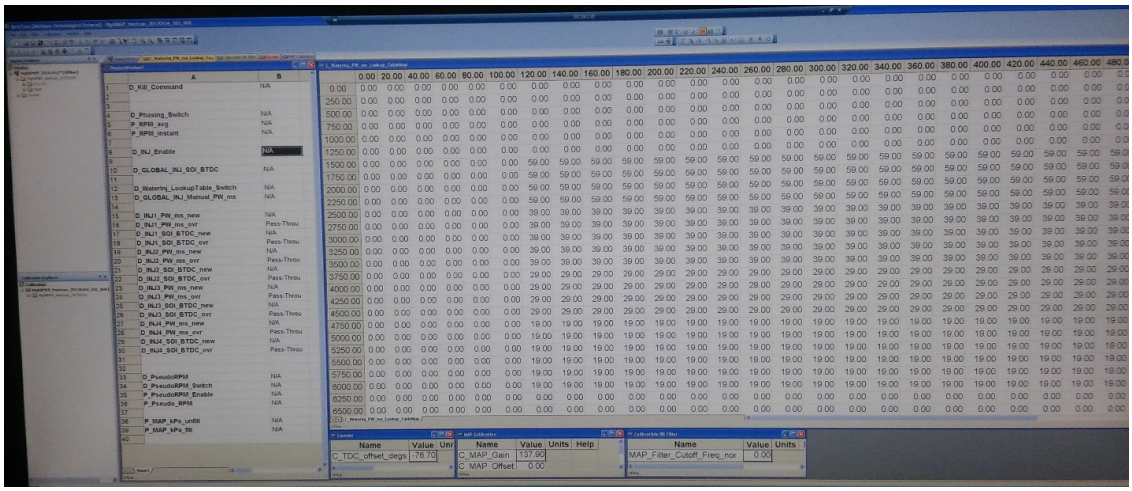

Figure 31: MotoTune screen used for port water injector control. Image used with permission by NewEagle. See 9Appendix F for further details.

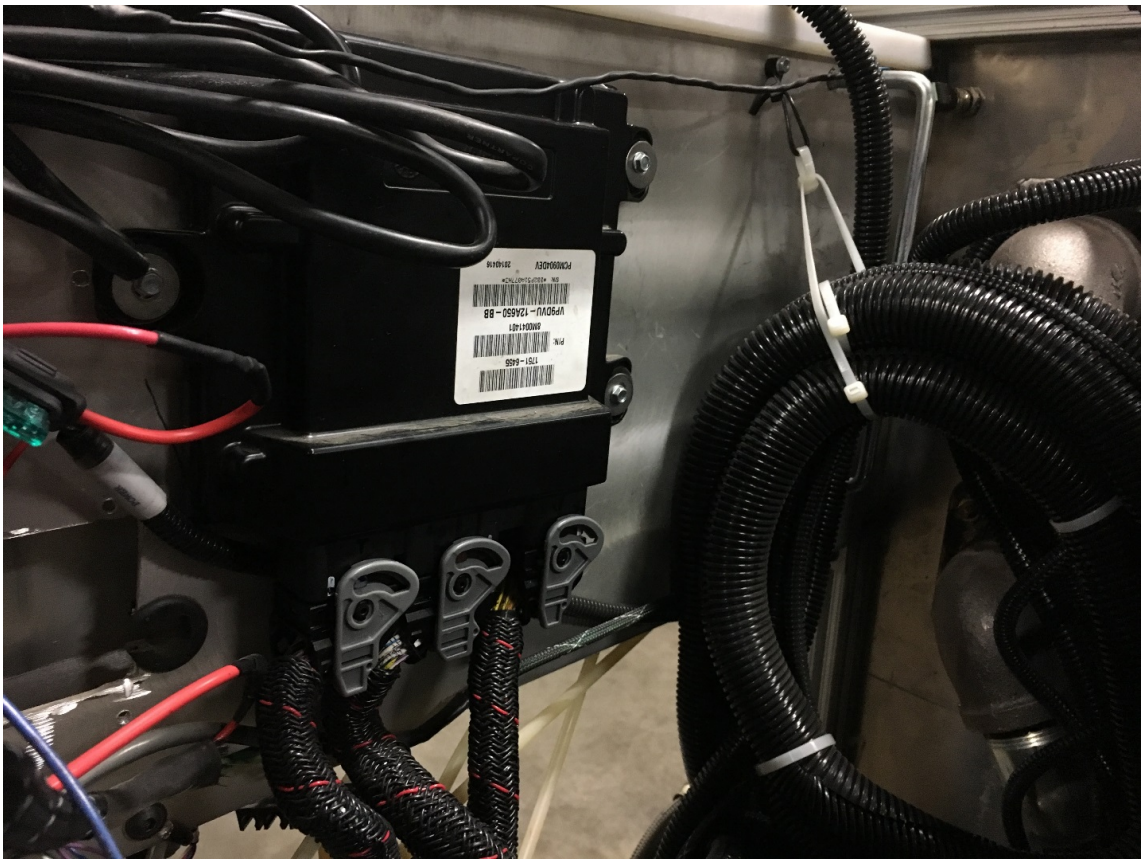

Figure 32: MotoTron ECU Hardware as installed on the engine cart.

It should be noted that the MotoTron ECU hardware does not currently support Direct Injectors. When and if DI water is required as part of this continuing work, a solution will be required for a DI driver. Several hardware solutions were examined as part of this project, however, as of the 2015 – 2016 timeframe, a simple cost effective solution did not exist. However, several solutions appear to be on the horizon.

4.3.2 Engine Control

Engine control was handled by two different systems throughout the project. A production oriented solution was used initially, followed by a fully customized solution as the demands on the engine control system increased.

4.3.2.1 Production Controller

Initially the engine was operated with a production ECU, and an aftermarket calibration tool made by HP Tuners. The production ECU along with a harness created specifically for standalone engine operation was sourced from Alpha Fab Industries. There were many issues with the harness, the controller hardware, and the calibration. These issues had to be sorted out one by one to get the engine to run. In the interest of brevity, these issues will not be discussed individually.

The HP Tuners calibration tool permitted adjustment of critical parameters including spark timing, and lambda as needed. Knock control was disabled via calibration parameters. This was done to achieve consistency in spark timing while testing. Production calibration settings were used for all other parameters including fuel injection timing, fuel rail pressure, cam timing, etc.

Several issues and limitations were found with this system. One issue was that changes could not be made in realtime, but rather a calibration change was made, then the calibration file had to be flashed to the ECU. This required the engine to be shutdown. The entire process was very time consuming, and very difficult when iteratively adjusting multiple parameters such as lambda, spark timing, and water injection rate. Another major issue was that the load axis in the calibration tables that were a function of load did not extend to loads as high as was expected for this project. An example of a calibration table and single point calibration values from the HP Tuners tool, and calibration for this engine are shown in Figure 33.

Figure 33: Example calibration table and single point calibrations taken from HP Tuners interface tool, and the calibration used to run the engine in this testing. Image redacted pending written permission from HP Tuners.

4.3.2.2 Aftermarket Controller

When it became evident that the production controller with HP Tuners would not support the experimental needs of this project, a search began to identify an alternative controls solution. The limiting factor became the Direct Injection system. Many of the control solutions that would be easy to learn and use, for example the Holley Dominator EFI System, did not include integrated drivers for DI injectors, and it was felt they did not have the flexibility to couple with external drivers. Solutions from National Instruments were considered, as the hardware does exist to drive DI injectors, however, it was felt there was too much risk in developing the control algorithms and making all of the hardware work together. The solution chosen was an aftermarket controller made specifically for racing applications by Bosch Motorsports. The controller and harness for this project was purchased through Extreme DI, a distributor of the Bosch Motorsports products.

The Bosch MS 6.3 controller and software supports all of the technology on the test engine including Electronic Throttle Control (ETC), Dual Independent Cam Phasers (for both inline and Vee engines), Turbochargers, and Direct Injection. The Bosch MS 6.3 uses pre-defined algorithms that are defined so generically, such that the user has a very wide range

of configurability in terms of the number of cylinders, crank and cam target wheel configurations, boost control methods, cam control methods, injection parameters, ignition coil parameters, etc. (Bosch 2015).

Although the user doesn't have access to it, the control algorithms are developed in Simulink, and documentation provided to help the user understand how the algorithms operate, in order to customize their calibration. This is not to imply the system is simple. The learning curve was steep, with countless hours into debugging hardware and software issues, and setting up the calibration to be able to run the engine on the dyno. Images of the controller and harness, an example algorithm description, and the calibration interface tool are shown in Figure 34 to Figure 35 respectively.

Figure 34: Bosch Motorsports controller, and flying lead harness prior to beginning installation on the engine.

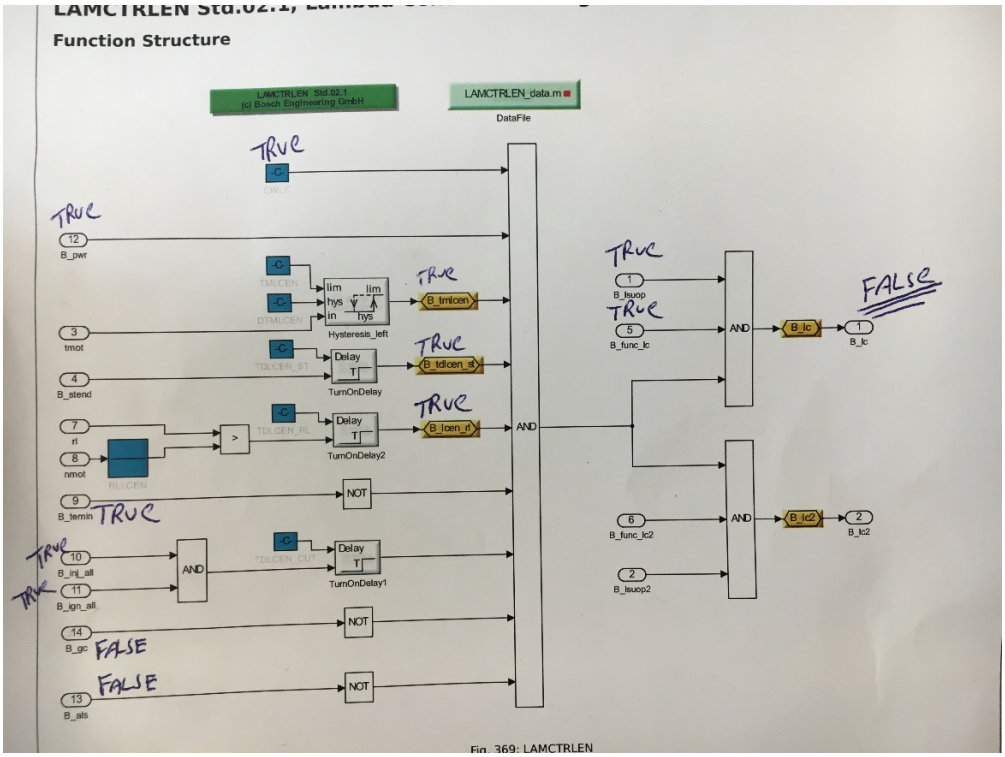

Fig. 369: LAMCTRLEN

Figure 35: Example algorithm description used in the Bosch MS software. Algorithm descriptions were used heavily in the debugging process, as evidenced by the hand written notes on this sheet. Image used with permission by Bosch Motorsport. See 17 Appendix F for further details.

Figure 36: Screen shot of several fueling parameters in the Bosch calibration tool taken while debugging a fuel pump instability issue. Image used with permission by Bosch Motorsport. See 17 Appendix F for further details.

The non-production components used in the assembly of ESN02 are summarized in Table 11.

Table 11: ESN02 Engine Components.

	Component	Manufacturer	Specifications
Base Engine	Piston	Wiseco	Forged Aluminum. No coating or anodizing. 9.2:1 Design intent CR. PN WFLNFP86
	Connecting Rod	Unknown	Forged 4340 Steel. H-Beam Construction. 620 grams vs 580 gram production. ZZP PN ZZ-4340RDS
	Connecting Rod Bolts	ARP	High strength bolts. PN not known.
	Cylinder Head Studs	ARP	High strength studs. Improved clamp load and enables repeated removal of the head w/o damaging the threads in the block. PN 231-4701.
	Intake Cam	Comp Cams	Increased fuel pump lift (via reduced base circle), increased valve lift. PN 8756.
	Exhaust Cam	Comp Cams	Increased valve lift. PN 8757.
	Valve Springs & Retainers	Unknown	High strength material w/ increased seat force. 365N force at seat. ZZP PN ZZ-82VS-ECT
	Exhaust Manifold Studs	Unkown	Facilitates multiple removal of exhaust manifold w/o damaging cylinder head threads. ZZP PN ZZ-EMSNP
	Turbo Delete Exhaust Pipe[29]	APS LABS Custom Fabrication	Steel exhaust pipe fabricated to be installed in place of the turbocharger.
	Blow Off Valves	Turbo Smart	Blow-Off Pressure Adjustable by changing springs, and adjusting spring pre-load. Dual valves installed to ensure adequate relief of boost pressure if needed
	Fuel Pump	Xtreme DI	High Flow Mechanically Driven High-Pressure pump[30]
	Throttle Body	GM	Analog Throttle Body[31]. GM PN 12631187.
	Intercooler	Frozen Boost	Aluminum High Flow Air to Water Intercooler. Model 14.

[29] A Turbocharger was NOT used for high boost operation (additional details will be given in a subsequent section). A custom exhaust pipe was fabricated to be installed in place of the turbocharger.

[30] Additional details will be given in a subsequent section.

[31] Beginning with the 2012 MY the engine control system utilized digital communications with the throttle body. The Bosch controller used with ESN02 requires an analog throttle body. This is a production part for MY 2011 and older.

	Induction Piping	APS LABS Custom Fabrication	Aluminum tube, custom fabricated at APS LABS
	Engine ECU	Bosch Motorsports	Bosch Motorsports MS6.3. A universal controller calibratable for a wide range of engine architectures and technology levels.[32]
	Lube Oil	Driven	PN BR30 – 5W30 break-in oil. High Zinc & Phosphorous. Fast Break-In PN XP9 – 10W40. No Sodium, low calcium based detergent to reduce LSPI. High Zinc and Phosphorous reducing LSPI. Heavy viscosity used for additional component protection.

Like ESN01, ESN02 began as a production GM Replacement Long-Block. However, ESN02 was immediately disassembled and rebuilt with the components shown in Table 11. During the rebuild a detailed set of critical measurements were made. This was done first and foremost to ensure all critical dimensions were within an acceptable tolerance for the anticipated usage, and furthermore, to provide a baseline to assess potential wear or damage during anticipated future disassembly. The critical dimensions for ESN02 during the initial build phase are shown in Appendix A1. It should be noted that plans have been made to do additional testing with ESN02 at 11.0:1 CR. These results are outside of the scope of this PhD Dissertation, however, as it is all part of the larger body of research, it is mentioned here. An analysis of measured compression ratio, using ESN02, with a production piston, the Wiseco piston referred to in Table 11, and a Wiseco piston that was sold to APS LABS as a custom 11.0:1 piston is shown in 9Appendix A.

An image of the assembly of ESN02 is shown in Figure 37. Figure 38 shown the compression ratio measurements being made on ESN02.

[32] Additional details will be given in a subsequent section.

Figure 37: Assembly of ESN02.

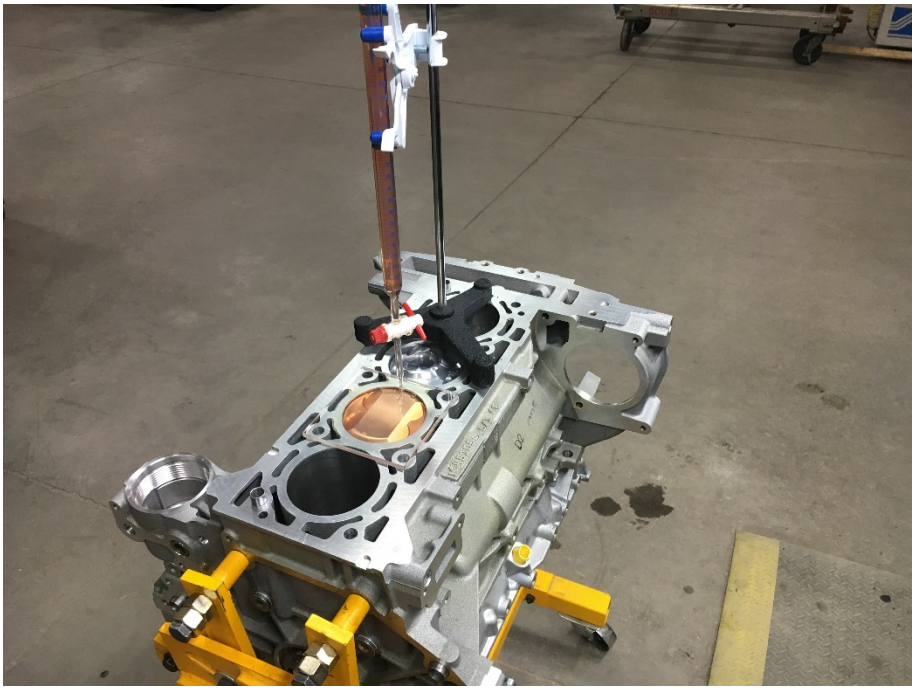

Figure 38: Compression Ratio Measurements being made on ESN02.

4.4 Instrumentation

4.4.1 Test Cell

All engine testing was conducted at the APSRC building in the light duty engine test cell. Data collection was performed during steady state or quasi steady state operation. Load is applied with a GE AC Dynamometer rated at 345 kW absorbing (300 kW Motoring).

4.4.2 Combustion Analysis

Combustion analysis was completed with an A&D Redline II CAS system running CAS version 3.7 software (A&D 2016). Piezoelectric pressure transducers were installed in each cylinder.

All cylinder pressure transducers used were of the 5mm face sealing form factor. Transducers were PCB Model 115A04's for nearly all of the data collected, with occasional use of AVL GH15D pressure transducers. PCB 115A04 transducers were selected because they are the lowest cost cylinder pressure transducers available, and previous work at APS LABS had shown the PCB 115A04's to similar to equivalent transducers produced by AVL and Kistler (Stank 2011). The reason for occasionally mixing transducers is because of numerous transducer failures on both the PCB and AVL transducers. These pressure transducers are prone to failure when exposed to heavy knock, or pre-ignition. The nature of this testing is such that heavy knock and pre-ignition have been prevalent despite efforts to sequester these events. When a PCB transducer would fail, and AVL transducer was installed in it's place until a PCB replacement would arrive. Several of the AVL transducers also failed while installed in the engine. The failure mode is initially a loss of sensitivity (which can impose a significant error in the data, and is difficult to identify without diligent control charting), followed by a complete loss of transducer signal. This is a common problem with engines operating in regimes of heavy knock and / or pre-ignition (Maehling 2017).

Thermal shock of the pressure transducers was of particular concern for this testing as thermal shock can significantly decrease data accuracy and increases in severity with increasing in-cylinder pressure and temperature. Recessed mounting of the transducer (as opposed to flush mounting) helps, although if the passage radius is greater than the flame quench distance (Randolph 1990, Randolph 1990) there may still be opportunity for the flame to reach the transducer diaphragm. Randolph showed that for conditions inside the cylinder of an IC Engine, the quench distance can be as small as 0.2mm. Thus a single hole passage would need to be a 0.4mm diameter or less to be fully effective at quenching the flame. A passage of this size would be not only difficult to machine, but more importantly would lead to significant pressure drop across the passage, especially at times in the cycle when pressure is changing rapidly. Therefore the decision was made to use a larger diameter passage, in conjunction with a dedicated flame arrestor installed between the combustion chamber and transducer diaphragm. Flame arrestors such as this are commercially available from the major cylinder pressure transducer manufacturers.

With the decision made to mount the pressure transducers in a passage with a diameter greater than the quench distance, the recommendations from the transducer manufacturer were given to the machine shop machining the cylinder heads, see Figure 39. Here it can be seen that the recommendation is a 3 mm diameter passage to the combustion chamber with a length between 2.5 and 4.0 mm.

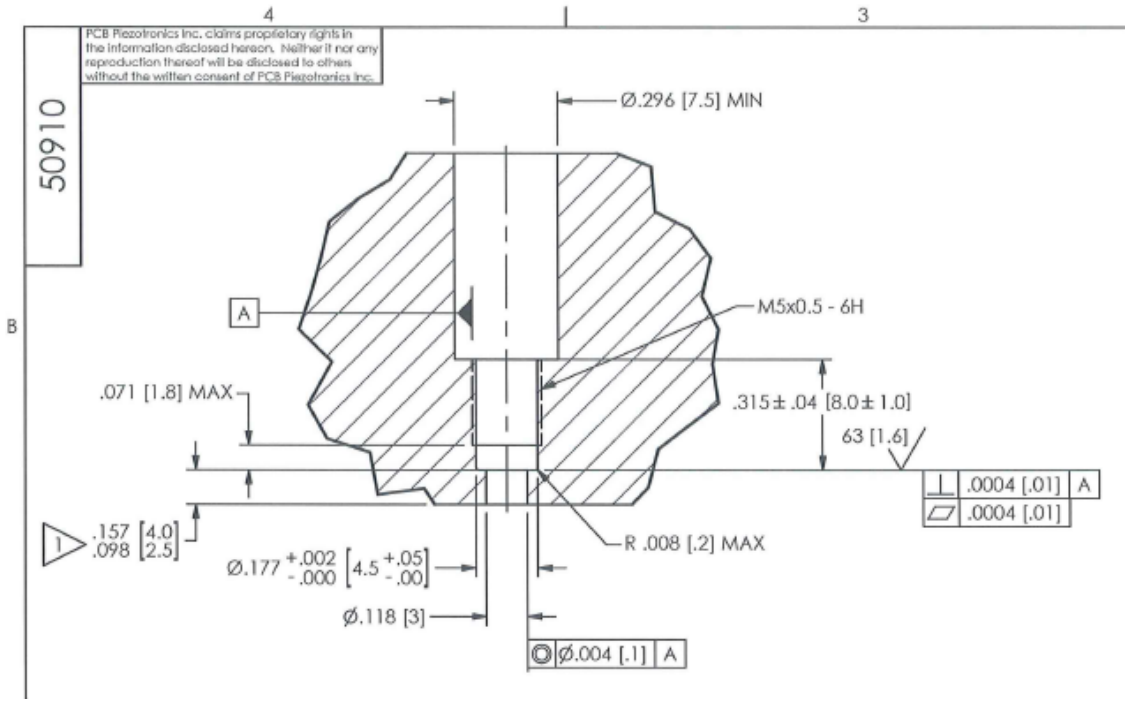

Figure 39: Transducer mounting recommendations provided by the cylinder pressure transducer manufacturer, PCB. Image of drawing and other materials provided courtesy of PCB Piezotronics, Inc. and used with permission. The views expressed in this paper are those of the author and do not necessarily represent views of PCB. I.C.P.®, ICP®, and PCB® are registered trademarks of PCB Piezotronics, Inc. See 17 Appendix F for further details.

The location of the transducer penetration into each cylinder was also selected with thermal shock resistance in mind. Following recommendations of Davis and Patterson, the transducers were located in the end gas region, as far from the spark plug as possible (Davis 2006, Davis 2009).

With the passage in the aluminum cylinder head determined, a stainless steel insert was designed which would hold the transducer, and seal the coolant and oil penetrations. The stainless steel adaptor was threaded into the aluminum cylinder head. Penetrations through coolant and oil were sealed with Loctite 680 bearing retainer, and the surface at the top of the combustion chamber sealed with a copper washer and Loctite 680. A stainless steel tube is press fit into the top of the threaded adaptor, and breaks through the cam cover where it is sealed with RTV gasket sealant.

Once the cylinder heads were received from the machine shop, they were visually inspected. Upon this visual the length of the passage appeared to be longer than the range of 2.5mm to 4.0mm as specified in the technical drawing from the transducer manufacturer (Figure 39). The passage lengths were measured by threading a transducer blank into the stainless steel adaptor, then pushing a 3mm drill through the passage from the combustion chamber side. The depth of the drill was measured, and the depth of the cavity on the transducer blank subtracted to determine the passage length. The passage length was determined to be approximately 7 mm. Note that the passages break into the combustion chamber where there is significant curvature to the chamber. Thus the passage length was taken as the length along the centerline of the passage, Figure 40.

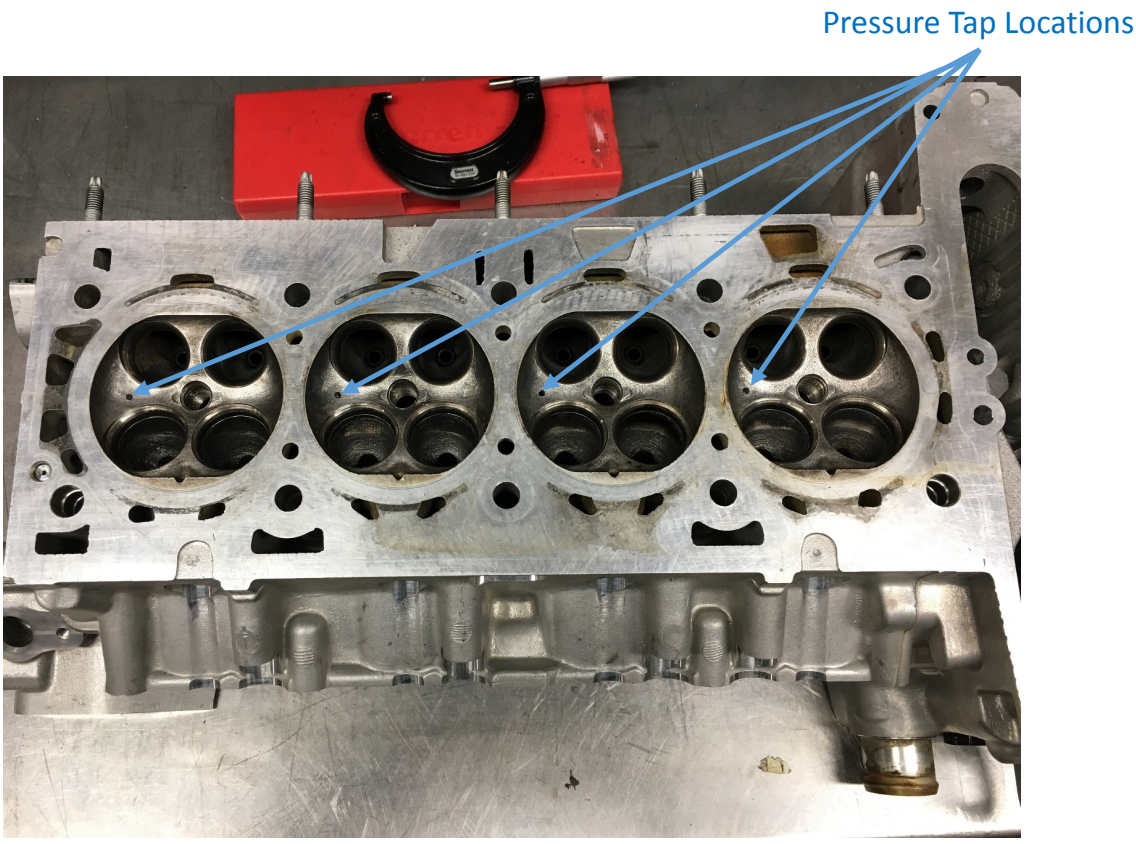

Figure 40: Combustion chamber side of the cylinder head showing the location where the cylinder pressure passages break through into the combustion chamber.

With the passages being longer than expected, a concern was that a Helmholtz resonant frequency would be setup in the passages, which can have negative impacts on data accuracy, and can lead to false detection of knock if the Helmholtz frequency is similar to the knock frequency. To evaluate this potential issue, a simple model was created based on the geometry of the passage, and diaphragm cavity, and based on the expected in-cylinder pressure and temperature. The model is based on the Helmholtz frequency for a volume V connected to an infinitely large volume by means of a passage. A schematic representation is shown in Figure 41.

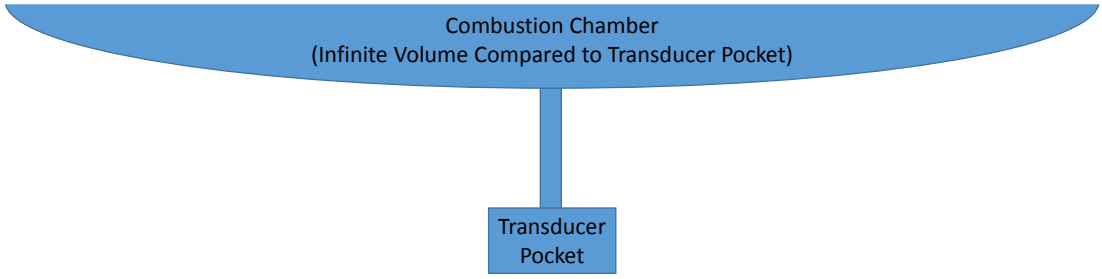

Figure 41: Simplified geometric model of the combustion chamber, passage to the transducer, and transducer tip volume used in the analysis of passage resonance.

For the geometry shown in Figure 41, the Helmholtz frequency is represented by Equation 12 with the speed of sound taken as the speed of sound in an ideal gas with a pressure and temperature representative of in-cylinder unburned gas conditions near TDC. The ratio of specific heats is taken as air. Equation 13 is the speed of sound.

Equation 12: Helmholtz Frequency

$$\omega = \frac{c}{2\pi}\sqrt{\frac{A}{L*V}}$$

Where :
A = Cross Sectional Area of Passage
L = Length of Passage
V = Volume of the Transducer Pocket
c = Local Speed of Sound

Equation 13: Speed of Sound in an Ideal Gas

$$c = \sqrt{\frac{k*p}{\rho}}$$

Where :
k = Ratio of Specific Heats
p = Pressure
ρ = Density

Figure 42 shows the Helmholtz frequency for a 3 mm diameter passage over a range of passage lengths. Again, the conditions are representative of air (unburned mixture) near TDC. The general goal is to have the Helmholtz frequency significantly higher than the response rate of the transducer and even the sample rate, such that any resonant affects are not seen in the data. With a passage length of ~7 mm as was delivered from the machine shop, the Helmholtz frequency has dropped to ~24 kHz, significantly lower than the range in which the PCB specifications would result. This is also below the rated frequency response of the transducer, meaning that the transducer is capable of picking up a pressure frequency in this range.

If time was of no consequence, the cylinder heads would have been sent back to have the sealing surface spot face machined approximately 3 mm or 4 mm deeper to increase the

Helmholtz frequency. However, project timing was very tight, and since the Helmholtz frequency was at least greater than the expected knock frequency, the decision was made to move forward with engine assembly.

As a point of curiosity, the Helmholtz frequency was calculated for a passage 1 mm less than and 1 mm greater than the passage diameter as machined. These results are included here for reference, and are shown in Figure 43. The tabulated data from the Helmholtz frequency calculations are shown in Appendix C.

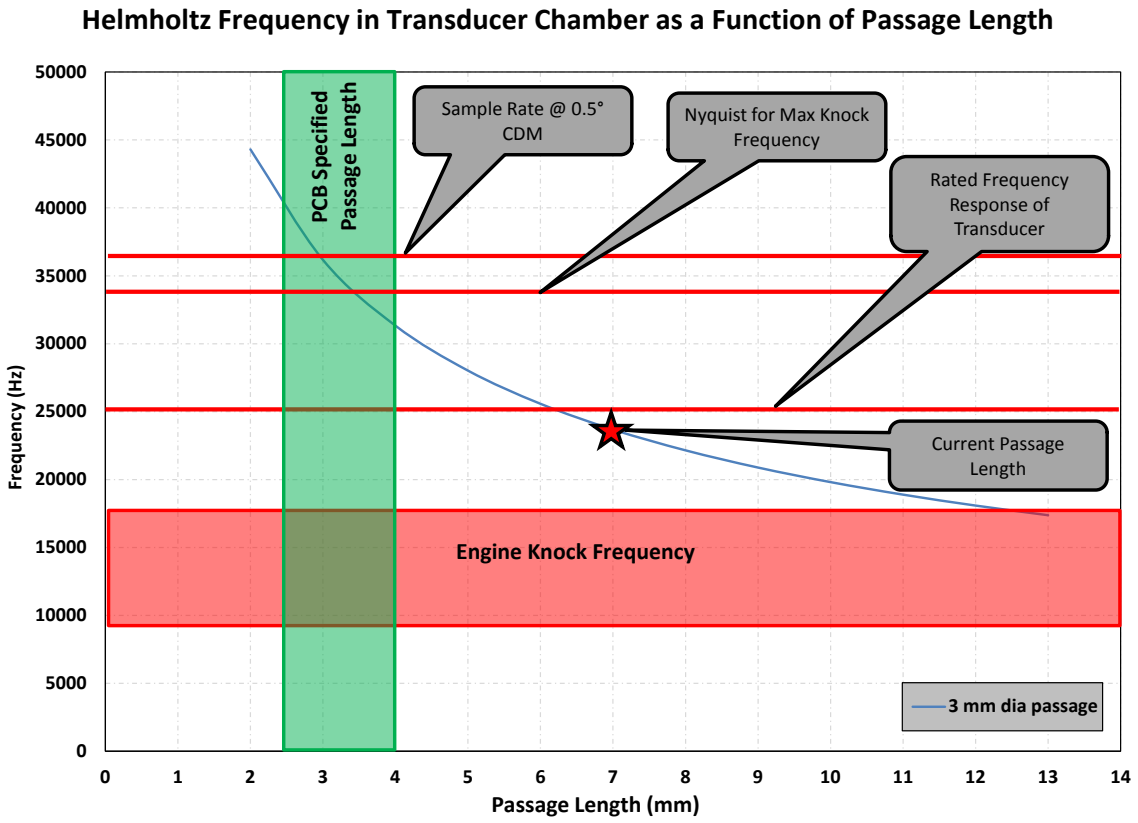

Figure 42: Helmholtz frequency in the transducer adaption passage as a function of passage length. 3mm diameter passage. PCB 115A04 Transducer. Includes Flame Arrestor details.

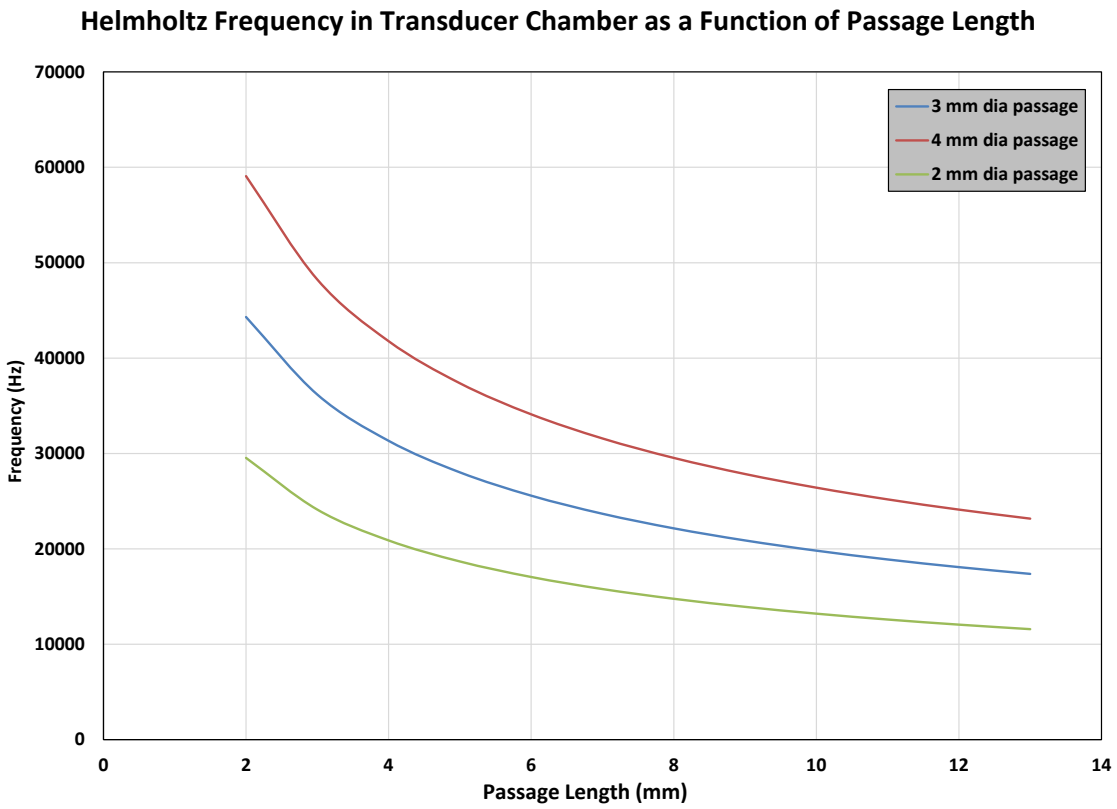

Figure 43: Helmholtz frequency in the transducer adaption passage as a function of passage length for several passage diameters. PCB 115A04 Transducer. Includes Flame Arrestor details.

As discussed, flame Arrestors were initially planned to thermally protect the pressure transducers from thermal shock. However, during initial installation of the PCB transducers, there appeared to be an interference issue with the PCB flame arrestors and PCB transducers. Several of the flame arrestor retaining rings failed while forcing the flame arrestors into the transducer pocket. Therefore the decision was made to begin testing without flame arrestors, as project timing was critical. With testing underway without flame arrestors, they were never used throughout the project.

Other combustion instrumentation included a BEI encoder Model #: XH20DB-37-SS-360-ABZC-28V/V-SM18. This particular encoder has 360 Pulses Per Revolution (PPR) on the clock signal, and 1 PPR on the reset signal. Furthermore, this encoder is designed to be solidly mounted, as opposed to an AVL or Kistler combustion encoder where the encoder

stator is fixed from rotation, but otherwise not rigidly mounted. A mount was designed to affix to the front of the engine block, and be as rigid as possible. To get the encoder axis as close to the crankshaft axis as possible, the encoder mount was designed with slots allowing the encoder to translate in both the X and Y directions. An image of the encoder mount is shown in Figure 44. A small stubshaft was designed that is affixed to the crankhaft. The stubshaft consisted of an aluminum cup with a hole in the center. The crank damper bolt runs through this hole, affixing the cup to the crank damper. The stubshaft is integral with a flat plate that bolts to the cup. Both pieces are piloted to help facilitate a tight centered fit. To compensate for angular difference between the crank centerline and the encoder centerline, a flexible coupling was used. When selecting a flexible coupler, it is important to ensure a coupler is torsionally stiff enough to avoid encoder angular errors.

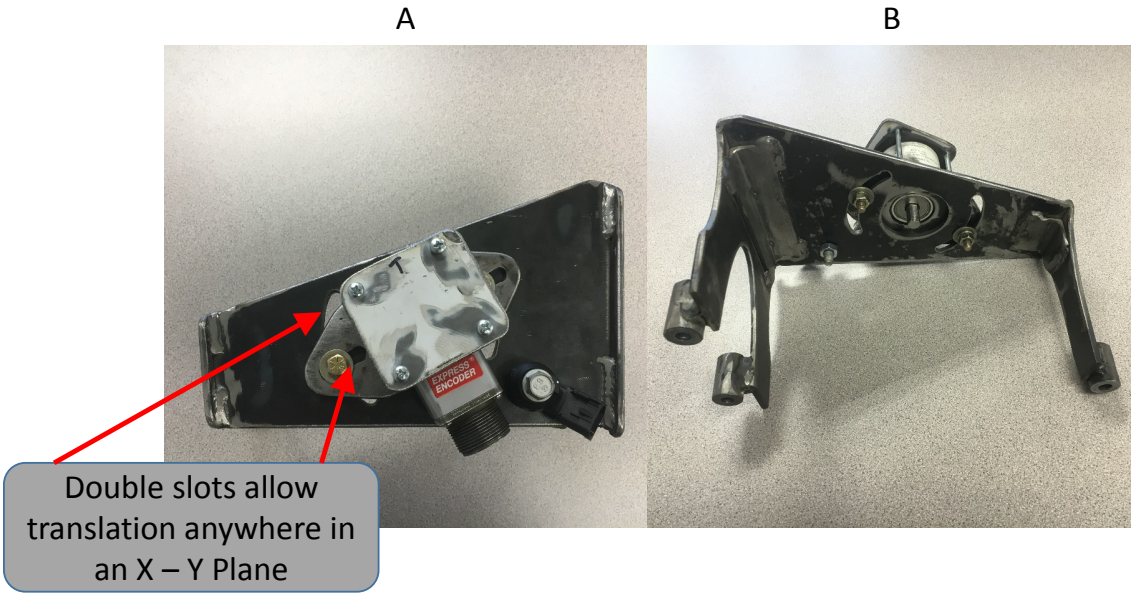

Figure 44: Encoder mounting bracket. Front Side (Left), and back side (Right).

The CAS software performs knock analysis on the digitized signal. Therefore it is important to consider the sample rate resulting from the encoder, the expected knock frequency, and the Nyquist frequency for which the pressure must be sampled at to accurately digitize the knock event. Equation 8 shows the minimum sample rate that

should be used based on the expected maximum knock frequency, and engine speed. Equation 9 shows the actual sample rate based on the encoder clock resolution.

Equation 14: Minimim Sampling Rate for Engine Auto-Ignition

$$f_{\min} = f_{knock} * \alpha$$

Where :

$f_{\min}$ = Minimum Sample Rate

f_{knock} = Expected Maximum Knock Frequemcy

α = Nyquist Oversampling Factor

Equation 15: Actual Sampling Rate

$$f = \frac{PPR * N_{\min}}{60}$$

Where :

f = Sample Rate

PPR = Encoder Pulses Per Revolution

$N_{\min}$ = Engine Speed

Using a Nyuquist over-sampling factor of 2, and assuming a maximum knock frequency of 17 kHz, Equation 8 results in a *minimum* sample rate that should be used of 34 kHz. However when evaluating Equation 9 using the 360 PPR encoder and a minimum engine speed of 1500 RPM (the lowest speed at which testing is expected to occur) the actual sample rate is only 9 kHz.

In these situations the CAS software provides a feature whereby the encoder clock pulse is interpolated by a user input factor (A&D 2016). The required *minimum* interpolation factor is Equation 8 divided by Equation 9, as shown in Equation 10.

Equation 16: Minimum Interpolation Factor

$$f_{\min} = \frac{f_{knock} * \alpha * 60}{PPR * N_{\min}}$$

The result in this case is an interpolation factor of 3.8. For this testing, an interpolation factor of 5 was used, slightly exceeding the minimum. With an interpolation factor of 5, the encoder clock pulse is interpolated to 0.2° increments, which becomes the sample rate. It should be noted that the interpolation factor is a compromise with system performance, as increased interpolation leads to larger raw data files and limitations on the number of realtime calculations that can be displayed and / or the maximum engine speed that can be achieved while displaying realtime calculations. To assist in this, the user can define a window in the CAS software where interpolation is done, so that the entire cycle is not interpolated.

In addition to combustion measurements, several other parameters were measured. Temperature measurements included:

- Exhaust temperature measured at the turbine outlet, turbine inlet, and each exhaust runner ~70mm downstream of the exhaust valves.
- Air temperature was measured at the Laminar Flow Element (LFE), Compressor inlet, Compressor Outlet, Intercooler Inlet, Intercooler Outlet, Throttle Body Inlet, and Throttle Body Outlet for the cases when the Turbocharger was used, and all of the same except for the compressor inlet / outlet temperature when the boost rig was used.
- Fuel temperature was measured at the inlet to the high pressure fuel pump.
- Oil temperature was measured in the oil pan sump (through the drain plug), in the oil main gallery, and at the inlet and outlet of the oil cooler.
- Coolant temperature was measured at the inlet and outlet of the engine.

- Several temperatures on the facility side are measured including ambient test cell temperature, and dynamometer cooling water and lube oil temperature.

Pressure measurements included:

- engine oil pressure measured in the main oil gallery as a gauge pressure,
- engine coolant outlet gauge pressure,
- crank case absolute pressure,
- exhaust absolute pressure measured at the inlet of the turbine, and outlet of the turbine,
- absolute pressure at the LFE
- compressor outlet absolute pressure
- intercooler outlet absolute pressure
- intake Manifold Absolute Pressure (MAP)
- Water Rail absolute pressure

Other measurements included:

- Airflow was measured with a Meriam Laminar Flow Element (LFE) when the turbocharger was used. Airflow was not directly measured when the boost rig was used.
- Fuel flow was measured with an Emerson Micro-Motion Coriolis flow meter.
- Water flow was measured with two Emerson Micro-Motion Coriolis flow meters. One for high pressure DI, and one for low pressure PI.
- Exhaust lambda was measured with an Innovate LC9 lambda meter installed approximately 1m downstream of the turbine
- Various ECU parameters were recorded

The general data acquisition and test cell control system was a National Instruments PXI. This hardware was controlled by Labview code written internally at APS LABS. Cylinder

pressure data was recorded with an A&D Redline CAS II System. The details on the major instrumentation are shown in Table 6.

Table 12: Instrumentation details. Reprinted with permission Copyright © 2017 SAE International. Further Distribution of this material is not permitted without prior permission from SAE. See 9Appendix F for further details.

Instrumentation Specification	
Dynamometer	AC Machine. GE Model 5TKF445DC03A004 345 kW Absorbing / 300 kW Motoring
Combustion	A&D CAS, AVL GH15D Pressure Transducers, BEI Optical Encoder
Flow	Air: Meriam Laminar Flow Element Fuel: Emerson Micro Motion Coriolis Meter Water: Emerson Micro Motion Coriolis Meter
Exhaust	Bosch LSU4.9 wideband lambda sensors
General	Omega Gauge & Absolute Pressures, Temprel Type K Thermocouples, National Instruments PXI Electronic Data Acquisition and test cell control

The setup of ESN01 in the testcell is shown in *Figure 45*.

Figure 45: Engine setup in the testcell. Reprinted with permission Copyright © 2017 SAE International. Further Distribution of this material is not permitted without prior permission from SAE. See 9Appendix F for further details.

4.5 Water Supply System

The system to supply water to the water injection system includes a Reverse Osmosis water filtration system, holding tank, pressurization to either Port Injection (PI) or DI requirements, and flow and pressure metering. Test water is prepared on-site with the Reverse Osmosis (RO) water filtration system. The purified water reduces variability and unknown effects that might otherwise be caused from salts, minerals, and other chemicals in the water supply. The water moves directly from the RO system to a 150 L holding tank.

The high pressure system (for DI) draws water directly from the holding tank and utilizes a pneumatic piston driven pressure booster to send water to a floating piston, Nitrogen pressurized accumulator, then through a high-pressure Coriolis meter and to the engine.

For PI, water is gravity fed from the holding tank to a 45 L pressure vessel by opening a manual valve when needed. The 45 L pressure vessel can be pressurized with standard shop process air (~925 kPa absolute). The air pressure transfers the water through common stainless steel high pressure lines to a low pressure Coriolis meter. The low pressure Coriolis meter has a larger internal diameter, and imposes less pressure drop than the high pressure meter and was added after initial system assembly.

Manual 2-way and 3-way valves are used configure the water supply system for either DI or PI operation. From the RO water filtration system to the engine, all fittings and lines are stainless steel to eliminate corrosion potential, and rated for high pressure to support DI or PI delivery. A detailed schematic of the water supply system is shown in *Figure 46*. Images of the water generation, storage, and pressurization systems are shown in Figure 47.

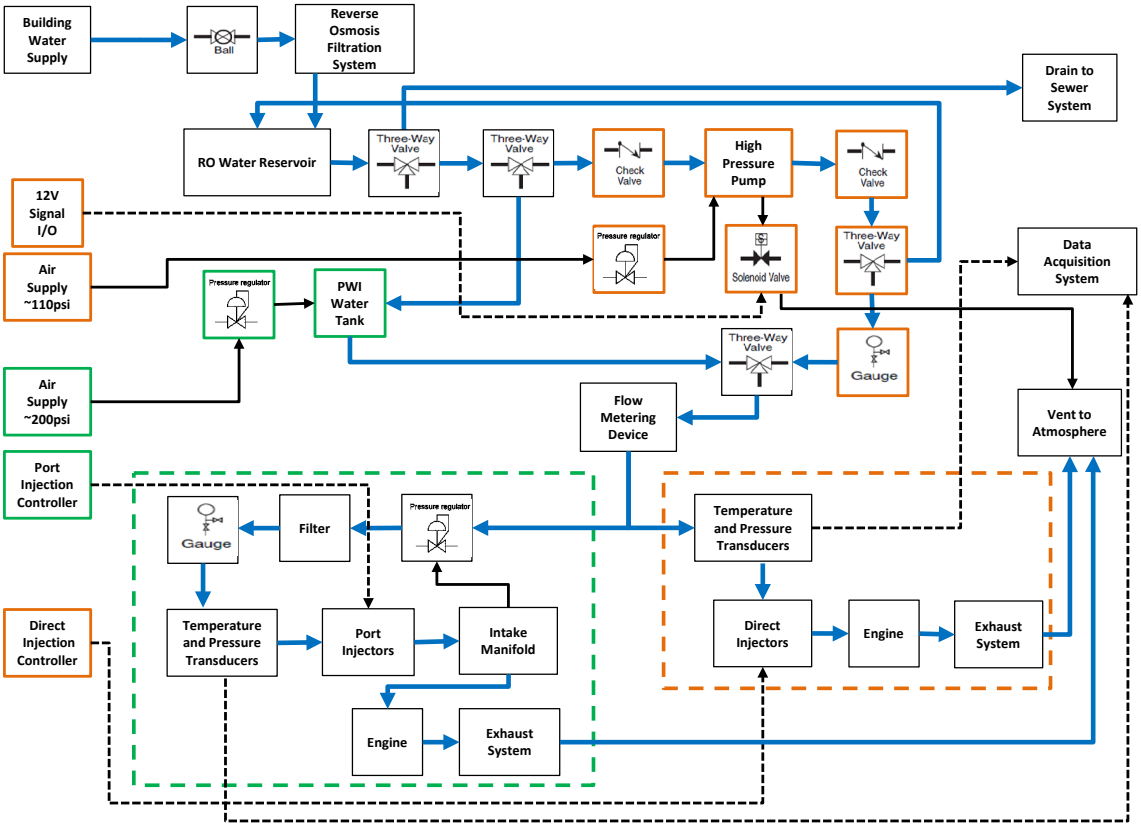

Figure 46: Details of the water supply system. Reprinted with permission Copyright © 2017 SAE International. Further Distribution of this material is not permitted without prior permission from SAE. See 17 Appendix F for further details.

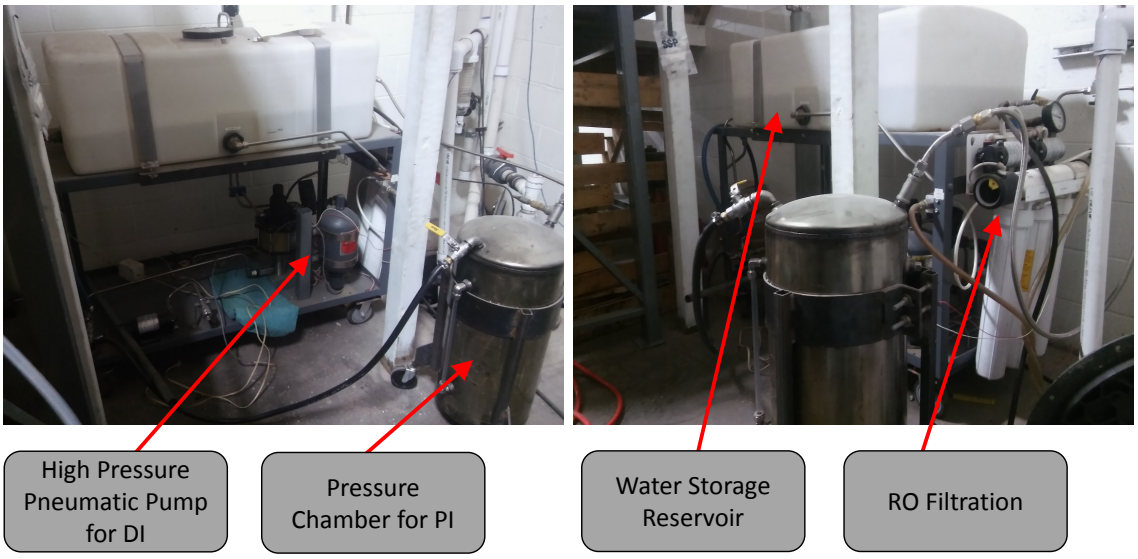

Figure 47: Water Supply System.

It is worth noting that during initial assembly, the system was built with a single Coriolis meter, one rated for high pressure, with the thought being that it could be used to meter water when running DI or PI water. However, it was found that when running PI water, the pressure drop through the thick wall tubing inside the corriolis meter was so substantial (approaching 500 kPa under high water flow conditions) that the pressure remaining in the water rail was too low to sufficiently inject water into the intake port. The design target was for water rail pressure to be 400 kPa greater than MAP, but with pressure drop across the Coriolis meter approaching 500 kPa as MAP was approaching 250 kPa absolute, there was simply not enough pressure at the inlet of the water injector. The low pressure resulted in injection duration of 720° (i.e. 100% duty cycle of the injector), and it was assumed to lead to poor atomization of the water as well.

When the low water pressure issue first appeared, it was not clear if the cause was a sticking pressure regulator[33], the Coriolis meter, excessive line length, a sintered brass filter installed at the inlet of the water rail, or a combination of all of these factors. Initial suspicions were the regulator and / or the sintered brass filter. An experiment was run with the engine operating at high load and high water flow, with the brass filter removed. This had negligible impact on water rail pressure. Next the pressure regulator was bypassed. This had no measurable impact on performance, indicating the regulator was working properly. Finally, an experiment was run to assess the pressure drop across the coriolis meter. The water line was disconnected from the engine, and a valve was installed to terminate the line. A pressure gauge was tee'd just upstream of the valve. Water was discharged into a container for a measured period of time. The pressure was measured at the 45 L water pressurization chamber, and at the valve, and water flow rate was taken as the mass of water flowed, over a period of time. The test was run at several different valve positions, and with and without the flow meter installed (flow meter bypassed). The results, shown in Figure 48, conclusively indicate that the high pressure flow meter was the major cause of low water pressure at the engine.

[33] The pressure regulator used references MAP, and maintains the rail at a constant pressure above MAP. The regulator was sold for fuel injection applications, hence, there was suspicion that the water led to a corrosion issue inside the regulator, causing the regulator to stick.

Because of this excessive pressure drop, an additional low pressure Coriolis meter was sourced. To verify the performance of the low pressure meter prior to purchase, a length of copper tubing of nearly the same ID as the flow meter was bent to what was believed to be the approximate shape of the tube inside the meter, then installed in the position of the meter, see Figure 49. A flow test was run, and the results showed minimal pressure drop across the tubing. Based on this, the low pressure meter was purchased and installed.

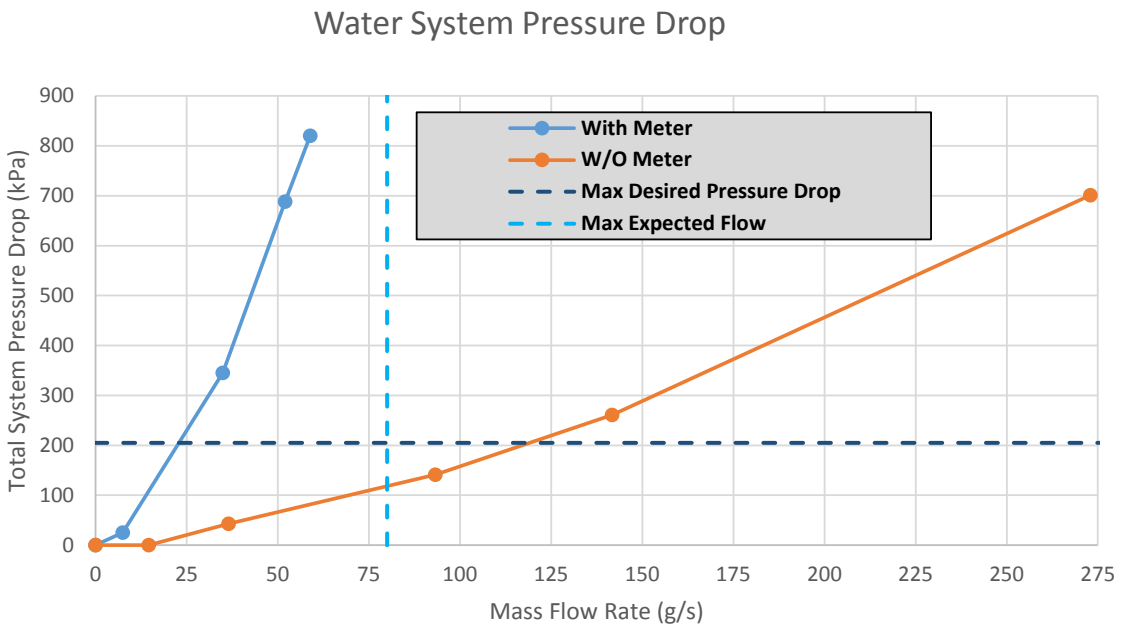

Figure 48: Water system pressure drop with and without the high pressure Coriolis meter in-line.

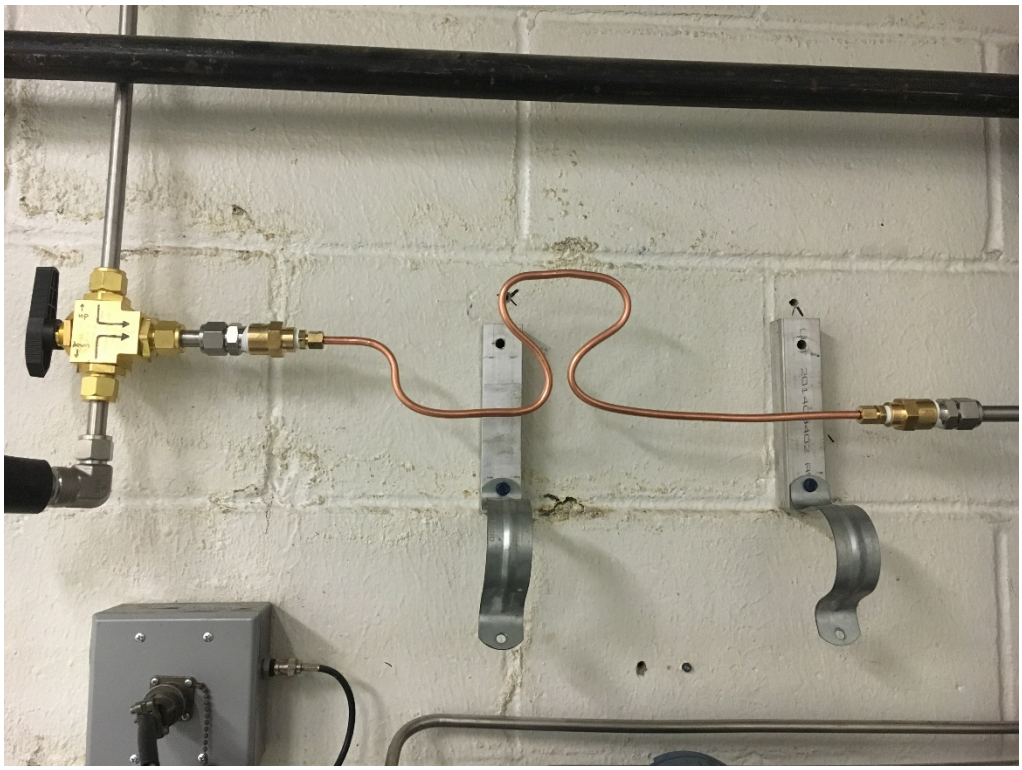

Figure 49: Copper tube used to emulate performance of a low pressure Coriolis meter prior to purchase.

4.6 Supplemental Support Systems

4.6.1 Fuel System

At the onset of testing, an existing APS LABS fuel cart was used to supply fuel to the engines high pressure fuel pump. Three issues were observed with this system. One issue was that with a storage volume of 19L, the tank required refilling quite frequently when operating under high loads. Another issue was that the tank was a fixed component of the fuel system, which in itself posed two difficulties; refilling the tank meant first transferring fuel from a drum in the APS LABS fuel bunker to a hand-carried fuel can, then transferring fuel from the hand-carried fuel can to the fuel system inside the test cell. This resulted in

two different fuel transfers, one of which was inside the lab which increases the risk of a fuel spill or fuel vapor escape inside a hazardous environment.

The second issue was, when switching fuel types, it was necessary to ensure the tank on the supply cart and the hand-carried can were both sufficiently diluted and purged with the new fuel. Finally the third issue was that under high load operation, there was a measureable decrease in fuel pressure at the engines high pressure fuel pump. This was likely due to insufficient fuel pump capacity. The risk with decreased fuel pressure is starvation or cavitation of the high pressure fuel pump. Even if the high pressure pump is able to achieve target fuel pressure, there are certainly control implications. After using the existing cart for several tests at baseline load levels, the decision was made to design and fabricate an improved fuel cart, as it was clear the problems would only be exasperated as load is pushed higher with this project. The fuel pressure with the first fuel cart is shown in Figure 50. The setpoint pressure for this test was 400 kPa. There is evidence here that the drop in supply pressure was already affecting rail pressure, as there is a slight drop in rail pressure at speeds above 4000 RPM, while the calibration did not command a reduction in pressure. With the system unable to meet target fuel pressure at production boost levels, it was felt the system would not keep up with demand at higher than production boost levels. The new fuel cart did deviate from the target fuel pressure, even when boost level was pushed to 300 kPa.

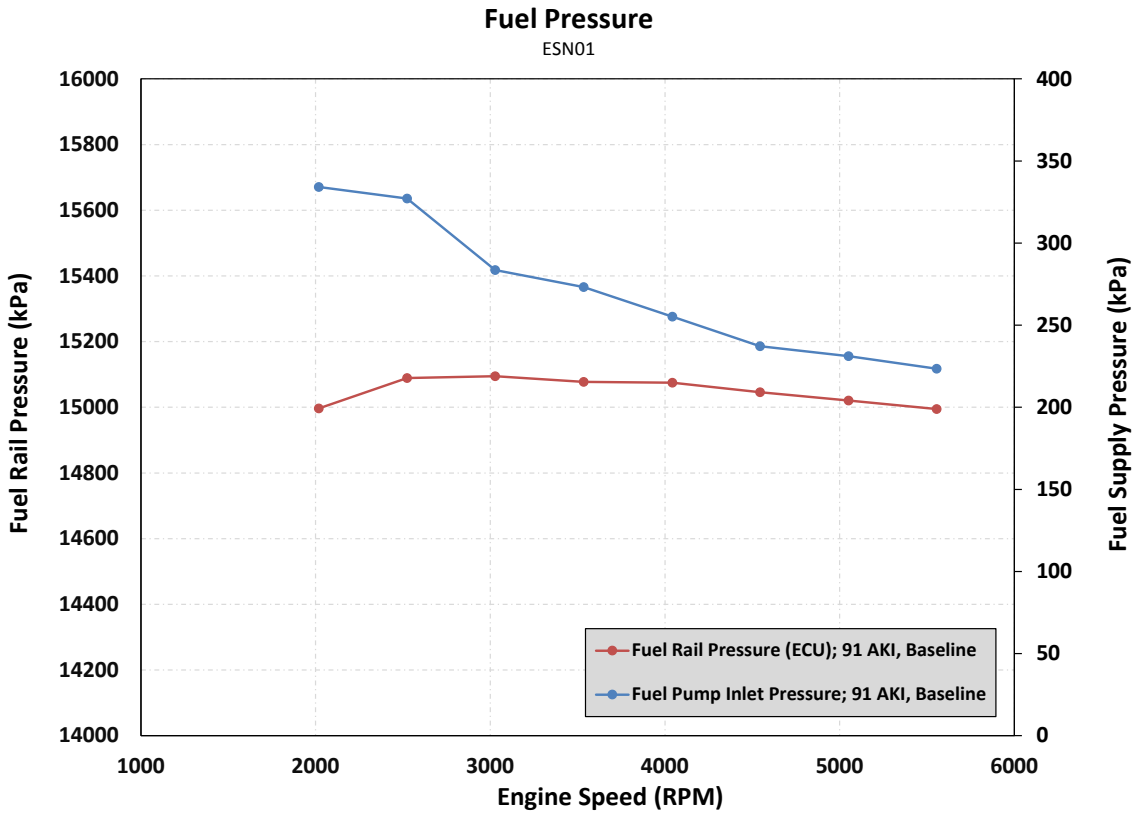

Figure 50: Fuel pressure with the original fuel supply cart. Setpoint was 400 kPa, which was not achieved even at 2000 RPM.

The new cart was designed to accept a Commercial Off The Shelf (COTS) fuel tank intended for racing applications. The COTS fuel tank chosen has a capacity of over 45L, thus extending refill intervals. The design is such that the tank can be brought, full, to the cart on a 2-wheeled hand truck, with a hook type latching mechanism attaching the tank to the cart. This prevents the operator from having to lift and carry a full fuel tank. The fuel lines connect through quick-connect style fittings. The tanks are available in several colors, therefore, three separate tanks were purchased, all of different colors, with each one used exclusively for each of the three types of fuels used in this project[34].

[34] The fuel drums had previously been color coded, and the new tanks were ordered to match the color of the drums to substantially improve the error proofing of accidentally running the wrong fuel on test.

The new cart utilized two high-flow fuel pumps. One pump was the primary pump, and always ran. The second pump was energized through an adjustable pressure switch referenced to MAP, which in turn correlates to fuel demand. When MAP exceeds the switch setpoint, the second pump turns on.

Finally, instead of pulling DC power from the test cell boom box (which lead to blown fuses under high load operation), the new fuel supply cart included its own DC power supply.

4.6.2 Cooling System

Heat from the engine coolant was extracted through a water to water heat exchanger. The heat exchanger is from a production marine application for Detroit Diesel Allison. For this testing, cold building water was allowed to flow through the heat exchanger to the drain system. On the engine side, the production thermostat remained in place and functional, maintaining coolant temperature. Since this testing has concluded, a closed loop water system has been implemented in the building to better conserve water, and retain heat from engine testing during the cold season.

The production oil cooler was retained. However, the "cold" side of the oil cooler was exposed to the same building water as the engine cooling system. A motorized valve was used to limit the flow of cold water through the oil cooler. The valve was controlled from a PID temperature controller made by Omega Engineering. Through this method, a target oil temperature could be established and maintained.

4.6.3 Engine Crank Case Ventilation

To promote consistency in the test data (especially relative to borderline knock), crank case vapors were vented to atmosphere. Partly to avoid discharging liquids to the test cell atmosphere, and partly to quantify the liquid in the crank case blow-by gases, a condensing

unit was designed and fabricated to separate liquids (primarily water) from the crank case vapors.

The condensing unit includes a sight glass to monitor condensed liquid level, a drain plug to purge the condensing unit of condensate, and provisions to pass compressed shop air through the unit, if additional cooling is needed to fully condense liquids. An image of the condenser is shown in Figure 51.

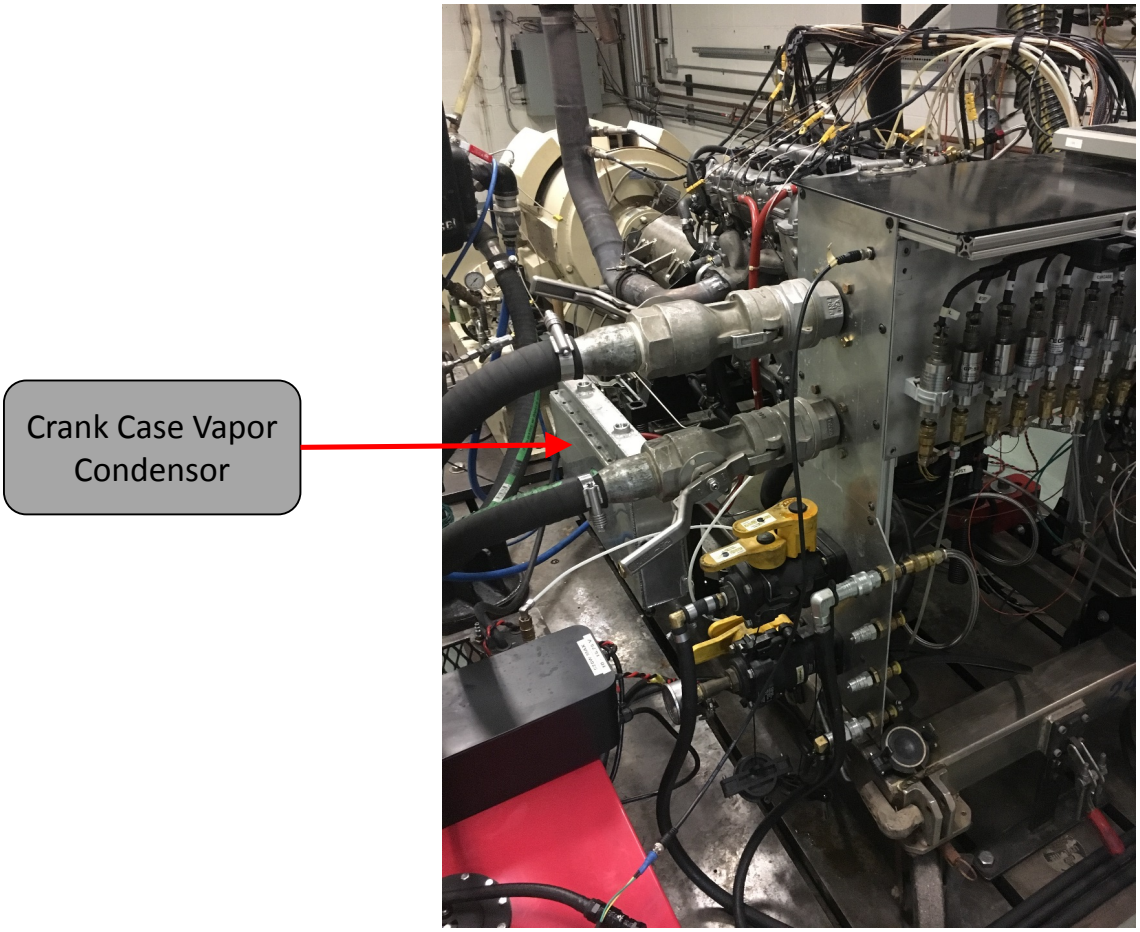

Figure 51: Condenser to separate liquid from crank case vapors prior to discharging to test cell atmosphere.

4.6.4 Test Cell Ventilation

The test cell is ventilated with a large fan installed on the rear wall of the test cell. Makeup air enters through the ceiling. The fan is manually energized. During the warm months of the year, the fan is turned on immediately, and left on for all testing. During the cold months of the year, the fan is used as needed to maintain a consistent test cell ambient temperature.

4.6.5 Engine Exhaust

Engine exhaust is plumbed from the turbine outlet to a Marmon flange located approximately 1 m, straight line distance away. This length of pipe was rigid pipe, and enabled the tapping of temperature, pressure, and lambda measurements. The Marmon flange connects to a mating flange on a length of stainless steel flex pipe. The stainless steel flex pipe connects to rigid pipe along the ceiling of the test cell. This pipe penetrates the rear test cell wall and terminates outside the building. This exhaust system is simple, effective, and does not require the use of additional blowers or fans.

For convenience the image from *Figure 45* is repeated in Figure 52. Here the various instrumentation and support systems are labeled.

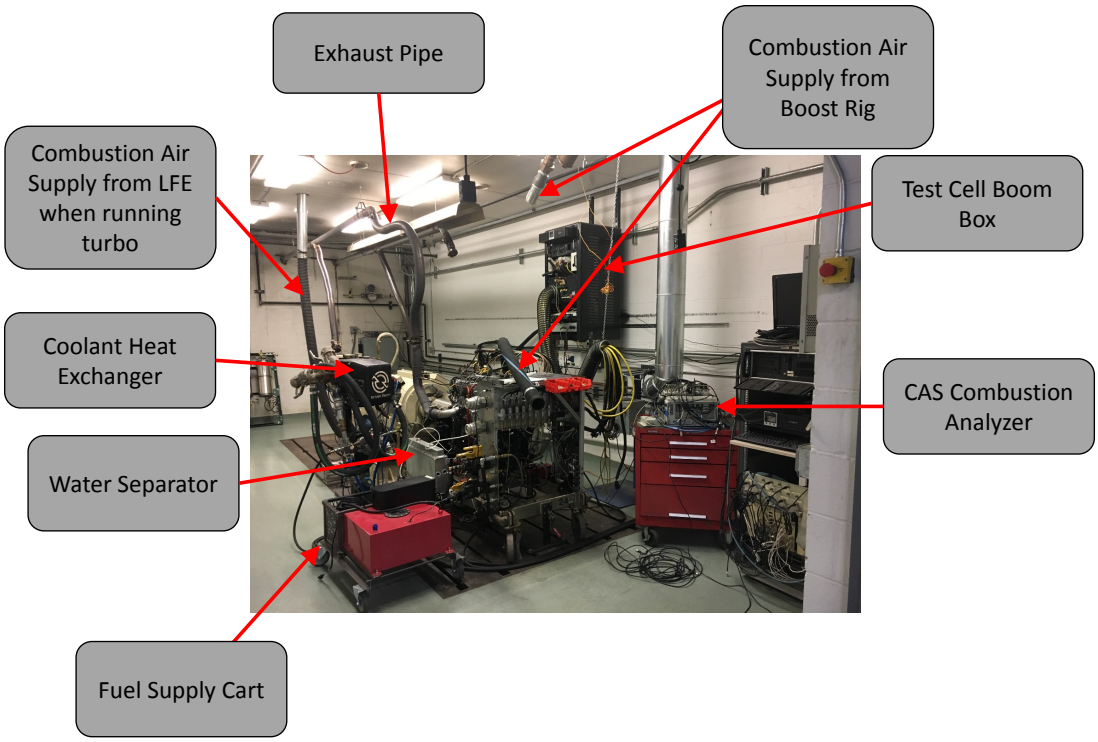

Figure 52: Engine installed in test cell with major support systems.

5 Key Metrics Used for Analysis

Several metrics are key for analysis of this work. These key metrics will be described briefly here to aid in the readers interpretation of the results to follow.

With potential changes to peak load paramount to the discussion, BMEP and NMEP are critical. However, the relationship between IMEP and PMEP is also important as the addition of liquid water, and it's subsequent vaporization are likely to have significant impacts on compression and expansion work, combustion itself, and the pumping process through changes in exhaust enthalpy.

Along the lines of PMEP, average pressures during the pumping process will also be examined. A common metric is Average Exhaust Absolute Pressure (AEAP). This is the average pressure over the exhaust stroke, with the average taken between any two defined points. Although not common, it is reasonable to conceive an equivalent metric on the intake stroke.

The addition of water vapor is expected to have an impact on the ratio of specific heat capacity, γ, of the working fluid. As previously discussed, this is important for many reasons as it impacts the ideal cycle efficiency, and the pressure – volume history on compression and expansion (see Table 3, Equation 5, and **Equation 10**). **Equation 10** is for isentropic compression / expansion. In a real engine there is heat loss, and mass loss, therefore it may be unreasonable to assume the process is truly isentropic, but rather it is assumed to be Polytropic. In this case however, the relationship remains the same, but with γ, replaced by the Polytropic Index, n, as in Equation 17. The Polytropic Index, n, can be solved for from the measured Pressure – Volume data. The Polytropic Index can be used as a proxy for gamma, as it will vary between 1.0 and gamma. If the compression is slow, such that the heat transfer and mass loss are in equilibrium with the rise in pressure due to the change in volume, n will be equal to 1.0. As the rate of compression increases such that the heat transfer and mass loss are negligible over the time scale, then n will

approach γ. Therefore, in this work, examining the Polytropic Index, n, will provide insight into changes in γ.

Equation 17: Polytropic Compression / Expansion Process

$$\left(\frac{P_2}{P_1}\right) = \left(\frac{V_1}{V_2}\right)^n$$

Where :
P = Pressure
V = Volume
n = Polytropic Index

Changes to the combustion process will also be assessed through burn rate parameters including, but not necessarily limited to Mass Fraction Burn (MFB) locations in crank angle. These metrics are often reported following the nomenclature CAXX, where XX is the percentage Mass Fraction Burned. For example CA10 is the crank angle where 10% of the 10% of the fuel mass has burned. For the analysis of this work several MFB locations will be examined, but of particular importance is CA10, CA50, and CA90. CA10 is important as an indicator of the ignition and early flame development period, CA50 is often referred to when specifying the overall phasing of the combustion event relative to engine timing, and CA90 is referred to when examining the end of combustion.

Similarly, burn duration will be examined. Common nomenclature follows the pattern BDXX-XX. For example, BD10-90 is the duration in crank angle between the 10% MFB location and the 90% MFB location. BD10-90 is commonly used to evaluate the overall, or bulk burn duration. BD0-10 will also be examined as the duration of the early burn phase.

Knock metrics will also be important. Several knock parameters have been defined throughout the years in the literature. The combustion analyzer used for this project calculates, and reports many of these parameters, and several were logged during the testing phase of this project. For analysis however, the only knock parameter that will be reported will be knock peak to peak abbreviated pk-pk. This is the amplitude, in units of pressure, the low and high peaks in the pressure signal following auto-ignition.

Finally, efficiency will also be critical, including brake, net, and indicated values. These efficiencies differ by the power term, were the power term is calculated from brake measurements, net indicated, or gross indicated respectively. The primary efficiency parameter that will be used is net thermal efficiency, as described in Equation 18 to Equation 20.

Equation 18: Net Thermal Efficiency

$$\eta_{net\_thermal} = \frac{Power_{net}}{Power_{fuel}}$$

Equation 19: Fuel Energy Expressed as a Rate.

$$Power_{fuel} = \dot{m}_{fuel} * LHV_{fuel}$$

Equation 20: Net Indicated Power.

$$Power_{net} = \frac{NMEP(kPa) * V_d(m^3) * N(\frac{rev}{s})}{Strokes\_per\_rev}$$

Where :

$\dot{m}_{fuel}$ = mass flow rate of fuel

LHV_{fuel} = Lower Heating Value of Fuel

NMEP = Net Mean Effective Pressure in kPa

V_d = Displaced Volume in cubic meters

N = Engine Speed in RPS

The indicated (or gross) thermal efficiency can be calculated by substituting the indicated power instead of net power in Equation 18. The indicated power is obtained by using IMEP instead of NMEP in Equation 20.

Volumetric Efficiency will be important when trying to identify changes in air charge trapping due to charge cooling. Volumetric Efficiency can be defined as the mass of air that is trapped in the cylinder divided by the mass of air that could have been trapped based on the displacement, and the temperature and pressure of the air. When determining the mass of air that could have been trapped, it is important to define the reference point. Taking the atmospheric conditions as the reference point (i.e. barometric pressure and ambient temperature) provides a measure of the overall trapping efficiency of the entire induction system including the air filtering system, pressure charging device, etc. Alternatively, the reference point can be inside the intake manifold, providing a measure of how efficient the port, valve, and valve timing system are at trapping air. Volumetric Efficiency is shown in Equation 21

Equation 21: Volumetric Efficiency

$$\eta_{vol\_ambient} = \frac{m_{trapped}}{m_{ideal}} * 100$$

Where :

$m_{trapped}$ = Mass of Air Trapped in the Cylinder

m_{ideal} = The Ideal Mass of Air That Could Be Trapped at Reference Conditions

The mass of air trapped in the cylinder is calculated from the measured airflow as in Equation 22.

Equation 22: Trapped Air Mass

$$m_{trapped} = \frac{\dot{m}_{air} * 60 * 2 * 1000}{N * Num\_Cyl}$$

Where

$\dot{m}_{air}$ = Mass Flow Rate of Air in g/s

N = Engine Speed in Rev/Min

Num_Cyl = Number of Cylinders

2 is for revolutions per cycle (for a 4 - stroke engine)

60 and 1000 are conversion factors

If the mass air flow rate is not measured directly, or in the case of this work if the airflow might be measured with different instruments and in different locations depending on the experimental configuration, an alternate method can be used to determine the air flow rate. The measured fuel flow rate can be used in conjunction with the measured exhaust lambda, as shown in Equation 23.

Equation 23: Mass Flow Rate of Air Calculated from Mass Flow Rate of Fuel and Lambda

$$\dot{m}_a = \lambda * \left(\frac{A}{F}\right)_{stoich} * \dot{m}_f$$

Where :

λ = Relative Air to Fuel Ratio

$\left(\frac{A}{F}\right)_{stoich}$ = Stoichiometric Air to Fuel Ratio

$\dot{m}_f$ = Mass Flow Rate of Fuel

The ideal mass of air trapped in the cylinder is calculated using the ideal gas law as shown in Equation 24. Again, the values of pressure and temperature depend on the frame of reference.

Equation 24: Ideal Mass of Fuel Trapped

$$m_{ideal} = \frac{P * V}{R * T}$$

Where :

P = Pressure at Reference Condition in kPa

V = Displaced Volume of 1 Cylinder in cubic meters

R = Specific Gas Constant in kJ/kg - K

T = Temperature at Reference Condition in K

Other parameters will be important and will be reported as well, but many of these will be direct measurements. For example, Exhaust Gas Temperature (EGT), or water flow rate, etc.

6 Results

6.1 Preliminary Testing

6.1.1 Engine Break-In

It is critical to condition a new engine prior to testing. This procedure is referred to as engine break-in. When the engine is first assembled the surface roughness of the bearings, valvetrain components, and piston / piston rings / cylinder assembly are all relatively high. This roughness leads to increased friction and reduced sealing of the piston / cylinder assembly and valves and valve seats. Breaking-in the engine is the process of running the engine for a period of time to decrease the affected surface roughness. Scientific testing should not take place prior to break-in as certainly any brake parameters will be erroneous and continually changing because of the friction affects, but also indicated parameters will be impacted because of poor, but changing, cylinder seal, and to a lesser degree combustion chamber metal temperatures. It is generally accepted that break-in is a function of engine cycles and load. Thus to achieve an accelerated break-in the engine should be operated at relatively high speeds, and relatively high loads. A common technique to achieve an accelerated break-in is to operate the engine at WOT with speed alternating between peak torque and peak power. It is also accepted that completion of break-in is signaled by the stabilization of friction and cylinder sealing parameters[35] (Shimizu 1991, Ryu T.-Y. 1997, Schneider 2004, Pathak 2017). Through prior unpublished experience, this author has found that full break-in can take over 40 hours of running at full-load and high speed, however, the majority of the break-in occurs in the 20% of the run time.

In the case of ESN01, in order to keep the project moving in a timely fashion to meet customer deliverable requirements, engine break-in was begun before test-bed debugging was fully complete. Break-in and debugging alternated over the course of multiple weeks.

[35] Cylinder sealing can be assessed by parameters such as peak pressure, Polytropic Compression Index, and motoring IMEP if a combustion indicating system is in-use, but can also be assessed by cylinder leak-down rate and cranking compression pressure using standard automotive service tools.

Although the engine was operated at high speed and load for a cumulative time of over 10 hours of run-time, several parameters including lambda control, intake and exhaust cam positioning, and load were changing over the course of break-in. Data was collected, however, upon analysis of the data, no clear trends can be observed because of inconsistencies in lambda, cam positioning, and load.

In the case of ESN02, once again break-in was completed as fast and efficiency as possible to maintain tight customer timing requirements. As a result, data was not collected during engine break-in. Break-in consisted of operating the engine over a range of speeds between 2000 RPM and 4500 RPM with load > 150 kPa MAP, for a total cumulative run time of > 10 hours.

6.1.2 Measurement Checks

Some of the earliest tests conducted on ESN01 were aimed at validating the instrumentation system, and preparing for future tests that would require external boost. One uncertainty that arises often in engine testing is the confidence in the measurements of fuel and air flow rate. To gain confidence in the airflow measurement the airflow as measured from the production control system[36] was correlated to the airflow as measured from the Meriam LFE installed above the testcell. The engine was operated at a constant 3000 RPM, with load being swept from closed throttle to WOT. These results are shown in Figure 53. Here, fuel flow rate as measured by the Coriolis meter is used as the proxy for load. It can be seen in Figure 53, that very good agreement existing between the LFE and production airflow measurement system, providing confidence in the measurements.

[36] Production GM ECU operated with HP Tuners Calibration editing and monitoring software combined with the production GM MAF sensor installed in the production location in the production Air Induction System (AIS) fixture to the engine in the production X,Y,Z coordinates.

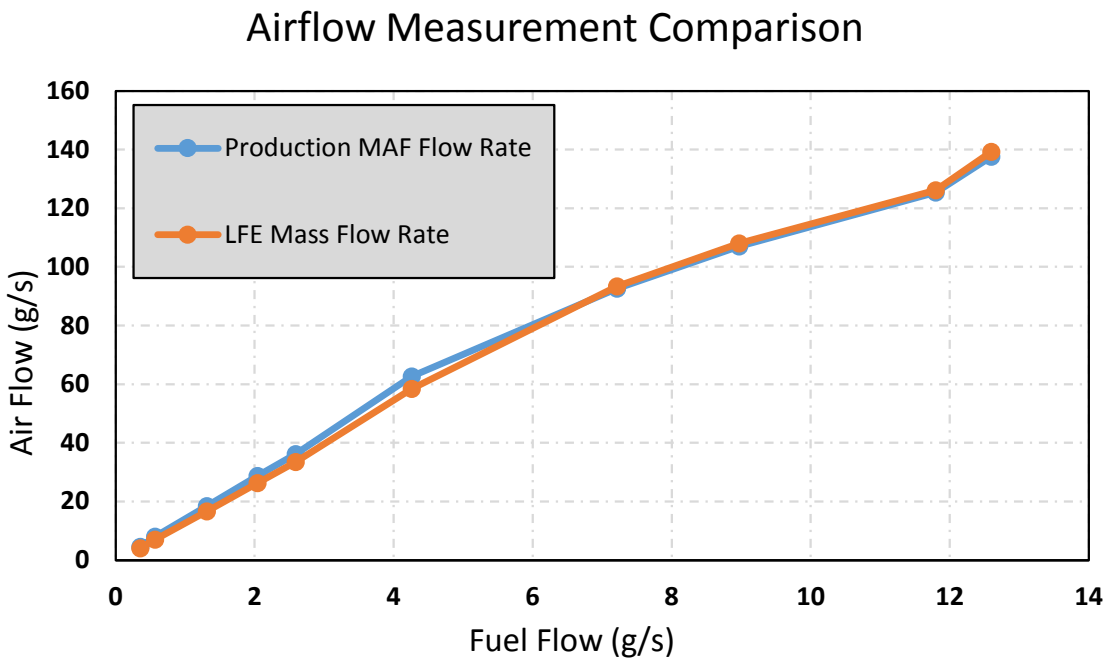

Figure 53: Comparison of airflow as measured with the test cell Laminar Flow Element to airflow as measured with the production Mass Air Flow sensor.

Another area that was investigated early-on was the ability to make accurate airflow measurements with the control system when the MAF sensor was relocated. The motivation here was that the production AIS was only intended for research utilizing the production boosting system up to production boost levels. As previously discussed, an external boost system was developed for research beyond production boost levels. In order for the ECU to monitor airflow with the external boost rig, the MAF sensor would need to be installed in a non-production section of ducting. Any measurement device tends to be sensitive to flow conditions both upstream and downstream of the device, and production MAF sensors are no exception. Therefore to assess and quantify any inaccuracies imposed by relocating the MAF sensor a comparison test was run with the same section of ducting that was intended to be used with the external boost rig. The engine was again operated at 3000 RPM while load was swept from closed throttle to WOT. This test was run first with the production AIS system functional, then repeated with the air flowing through the same section of duct where the MAF sensor was intended to be installed in the external boost system. These results are shown in Figure 54 for the raw output of the sensors and Figure

55 in units of airflow. It can be seen that relocating the MAF sensor had a fairly minor impact on the ECU's measurement of airflow. The difference was measureable however, and used to adjust the frequency vs. airflow calibration table in the ECU software.

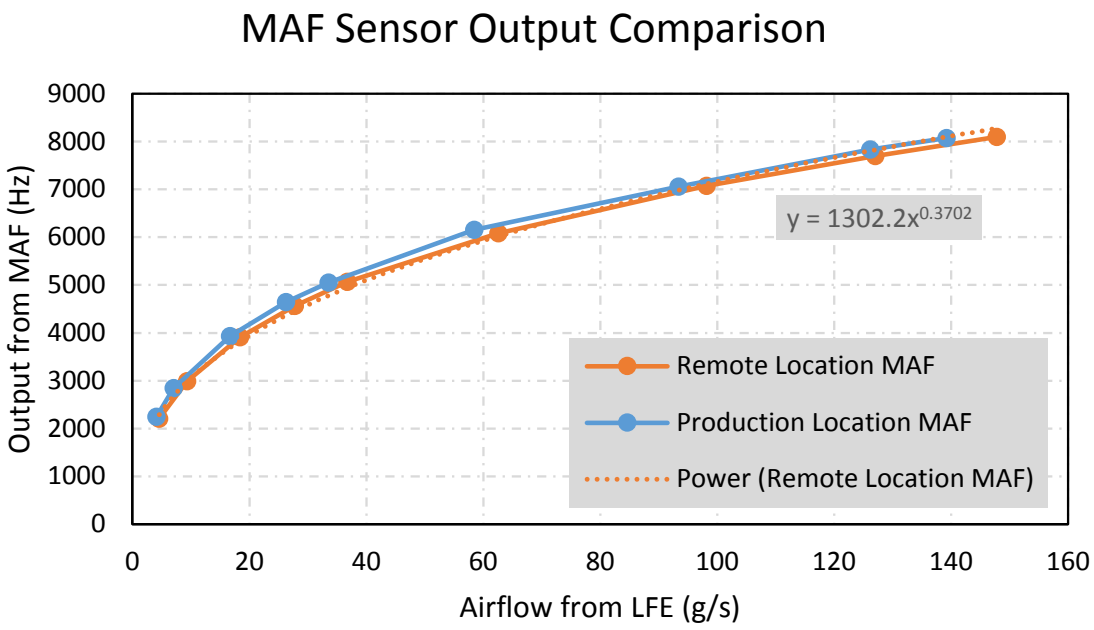

Figure 54: Raw output of production MAF sensor in the production location, compared to a remote mount location as part of the external boost rig.

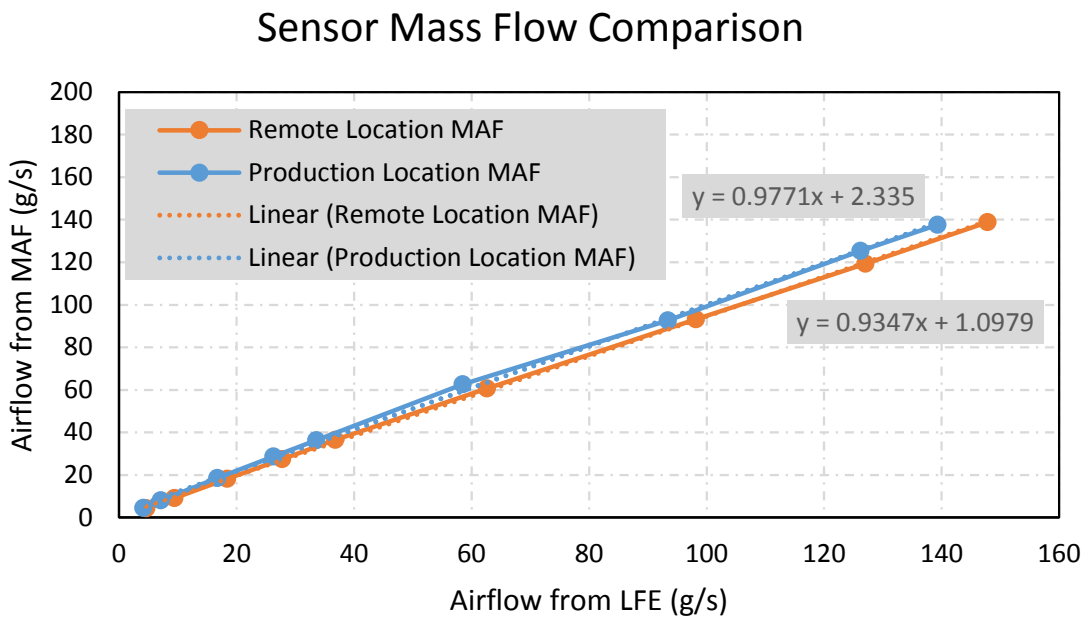

Figure 55: Comparison of processed airflow in engineering units comparing the production location to the remote mount location.

6.1.3 Baseline Checks

With break-in complete, and basic data quality validated the project focus moved on to establishing a baseline. Most fundamental was ensuring that the testbed was representative. The engine build level closely represented a 2012 MY Buick Regal. The basic results for SAE Certified Power testing for this application were purchased from SAE for comparison purposes[37] (SAE_International 2004, Joss 2011) The Certified Power results as obtained from SAE are included in the appendix. A production release calibration for a 2012 Buick Regal was located and downloaded from the HP Tuners online repository (HP_Tuners_User_Community 2016). The 2012 Buick Regal calibration was not used as-is because the calibration had already undergone many modifications to allow the engine to operate properly outside of the full vehicle in a dynamometer test cell environment. However, the 2012 Buick Regal calibration was used to supply the critical

[37] Data was manually digitized from published plots.

calibration tables affecting full load performance including calibrations for lambda, spark timing, intake cam position, exhaust cam position, and turbocharger wastegate control.

This engine as installed in the 2012 Buick Regal is a "Premium Fuel Recommended" application. Therefore baseline tests were conducted with 91 AKI pump grade E0 fuel. The full-load speed sweep is shown in Figure 56. Here it can be seen that full load torque is comparable to the production SAE Certified torque between 3000 RPM and 4000 RPM, and is slightly low below 3000 RPM and above 4000 RPM.

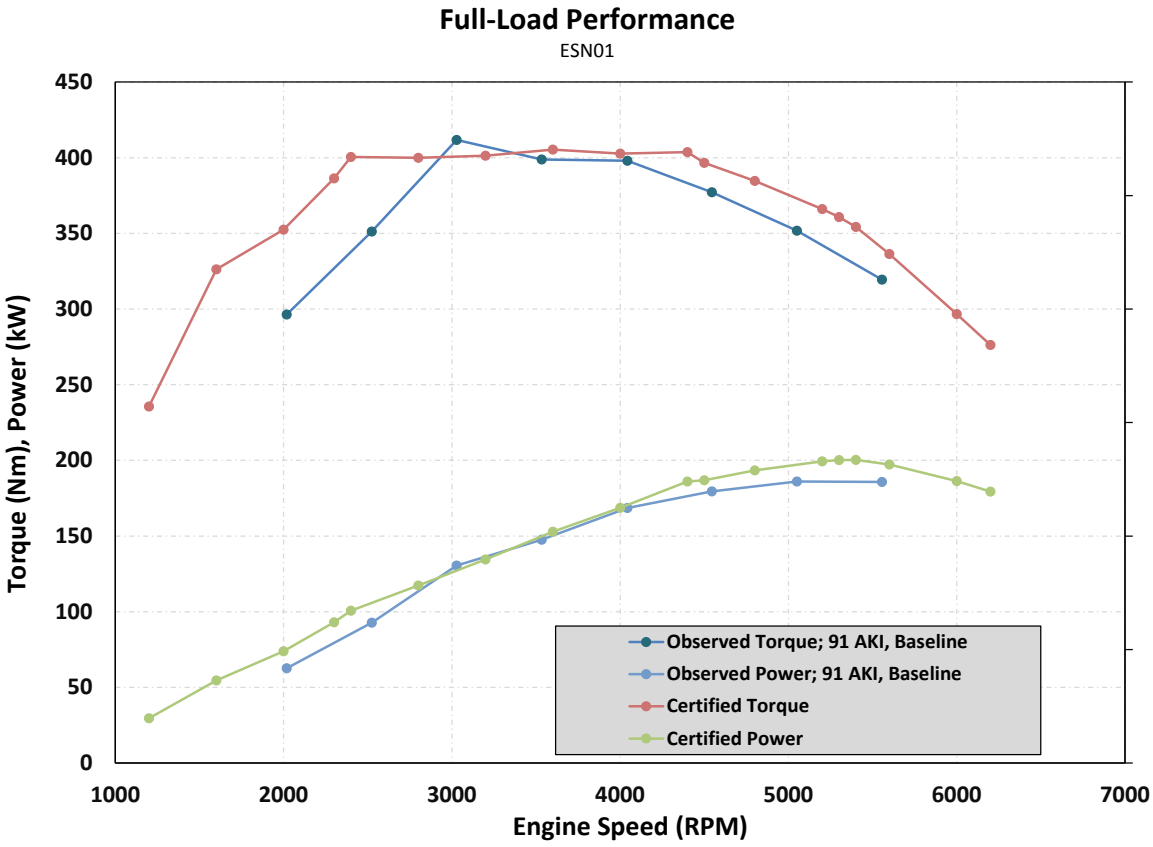

Figure 56: Comparison between full load performance of ESN01 as installed and run at APS LABS compared to the published SAE Certified Power.

Effort was placed on understanding the discrepancies at low and high speed. Because this engine control system uses ETC and operates in a torque based control strategy one

hypothesis for the difference was that the actual throttle position was not being actuated as intended. Figure 57 shows that as-intended, the accelerator pedal was at 100% for the entire test. However, below 4000 RPM, the ECU was throttling the engine. This can also be observed in MAP being less than Boost Pressure[38]. Effort was placed on going through the ECU calibration, and raising torque limits and adjusting other parameters that might have an impact. Test were repeated in the testcell each time a calibration was changed, however, the source of this apparent torque limitation was not found.

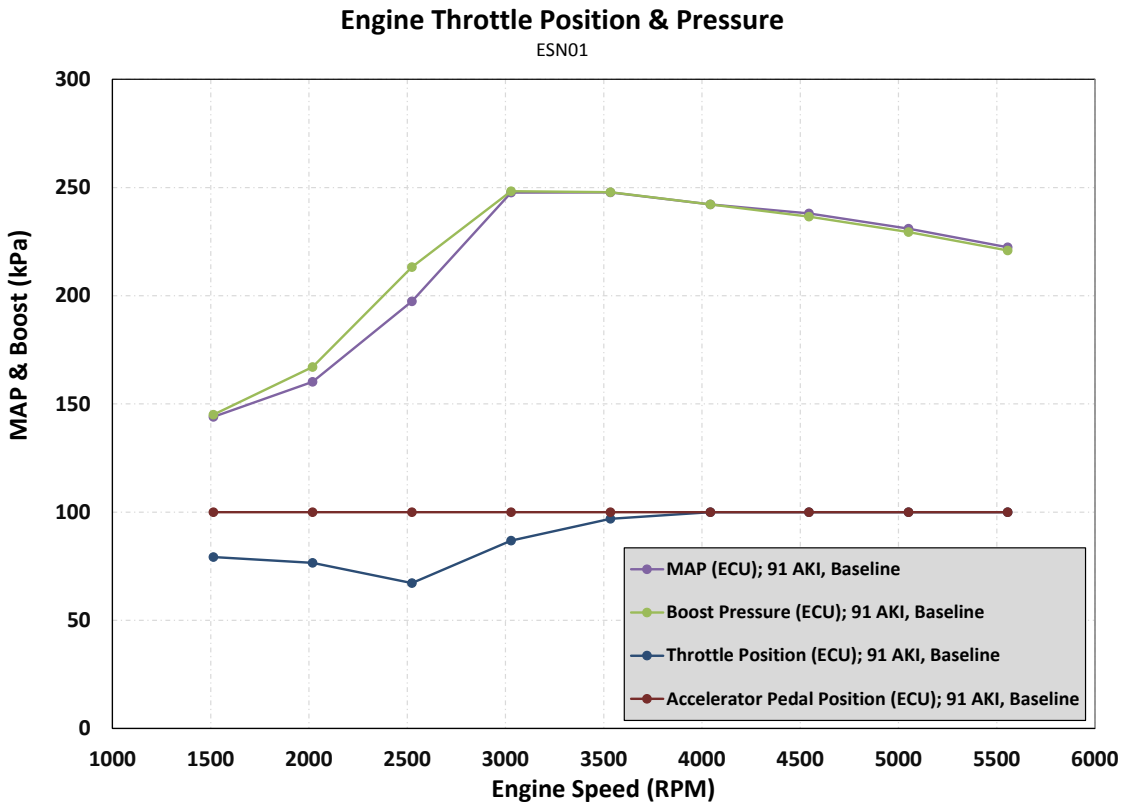

Figure 57: Commanded Load (accelerator pedal), and actual throttle position Manifold Pressure, and Boost during baseline testing.

The environmental conditions that were recorded during the baseline testing are shown in Figure 58. Here it can be shown that the test conditions were relatively close to SAE targets for engine performance testing. The targets are inlet supply pressure of 100 kPa, water

[38] Measured between the intercooler and throttle.

vapor pressure of 1 kPa, and Inlet air supply temperature of 25°C (SAE_International 2004). It is worth noting that the air pressure shown is measured at the LFE, therefore the pressure at the AIS inlet (where the SAE reference is measured) would be slightly lower. The environmental conditions shown here can be used to correct the observed torque using approved correction factors (SAE_International 2004). This was not done here because although it would have increased the torque values because of inlet environmental parameters, the exact production exhaust backpressure settings were not used, so a perfect match would still not be possible.

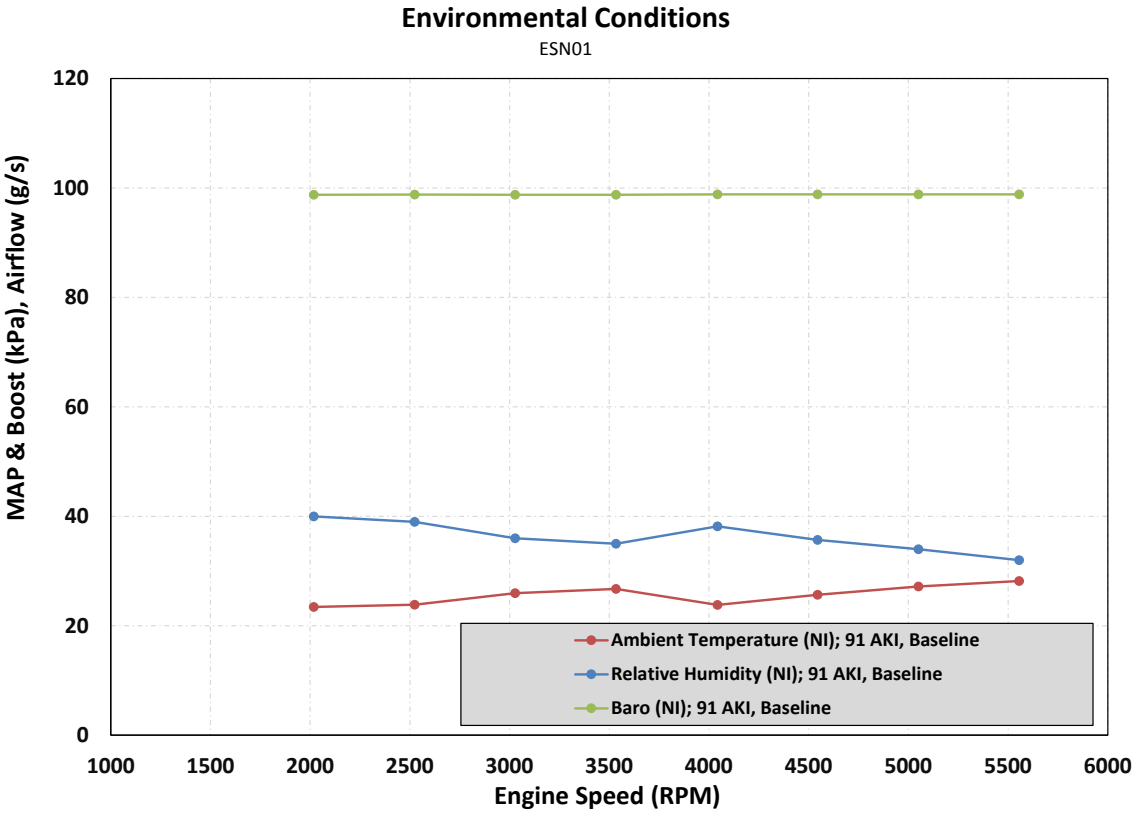

Figure 58: Environmental conditions that were recorded during baseline testing.

At speeds greater than 4000 RPM, the discrepancy in output did not appear to be related to the ECU's torque control, as it is clear the throttle is moving to the 100% open position. It was felt this discrepancy was likely due to subtle differences in spark timing, lambda, or cam position. This detailed data is available in the full SAE Certified Power report, but for

additional cost. It was felt that since the full load torque output was comparable between the baseline ESN01 and the SAE Certified Power results in the range of 3000 RPM to 4000 RPM, it is safe to assume that the 1) the engine hardware is functioning properly, and 2) the testcell and instrumentation is functioning properly. The differences at low and high speed are likely control related differences. Moreover, the majority of the focus with this project will be in the 3000 RPM to 4000 RPM range.

Relative cam timing is shown in Figure 59. These cam positions are calibrated for peak volumetric efficiency by the OEM. These same relative cam positions were used for all subsequent tests regardless of what controller was used, and what level of boost was used.

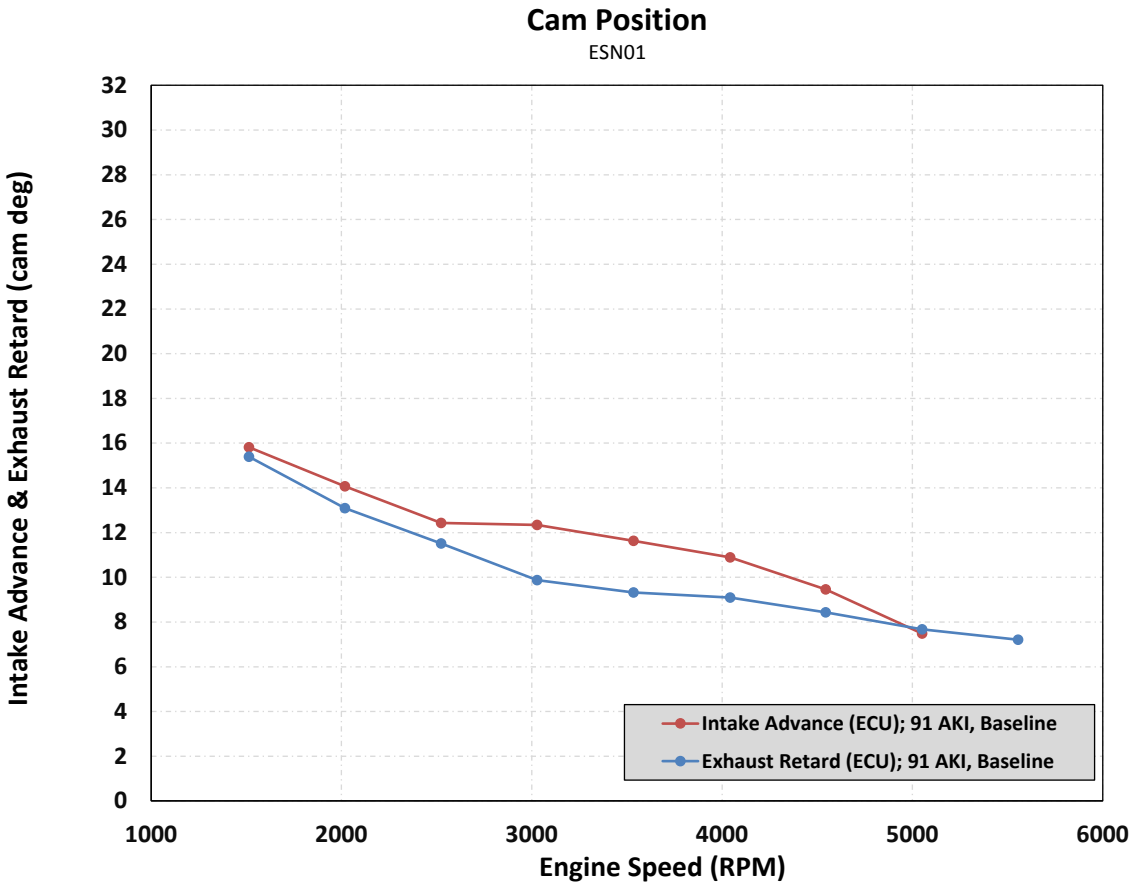

Figure 59: Intake and Exhaust cam position relative to park.

6.1.4 Water SOI Sweeps

A final preliminary test was run prior to water injection testing. The objective of this testing was to determine if the timing of the water injection into the port had an impact on engine operation, and if so, identify the Start of Injection (SOI) timing most appropriate to continue the project with.

For this set of tests the engine was held at 3000 RPM while the throttle was continually adjusted as-needed to maintain 150 kPa MAP. Spark timing was held constant at 11° BTDC. Since the objective was to identify any trends in engine operation with respect to water SOI, the fuel used did not need to be the same fuel as was used in other parts of the testing. Therefore, to conserve the test fuel, this SOI sweep test was run on some EEE E0 Certification fuel that remained at APS LABS from a previous project. The water rail pressure was being controlled by the water pressure regulator, and was set to approximately 400 kPa above MAP[39]. Water injector pulse width was set to a constant 10 ms. At 3000 RPM, 10 ms corresponds to 180° CA according to Equation 25. This injection duration was chosen somewhat arbitrarily to represent what was felt (at the time) to be an example of a relatively long water injection duration.

Equation 25: Crank Angle Duration.

$$\Theta = N * t * \frac{360}{1000 * 60}$$

Where :
Θ = Duration in Crank Angle Degrees
N = Engine Speed in Rev / Min
t = Time in ms

[39] Water rail pressure was not measured for these tests, but was for subsequent tests.

Figure 60 shows that albeit subtle, there is indeed a clear shift in burn rate as indicated by the 50% MFB location and 10% MFB location. The shift corresponds with the intake valve open vs. closed phasing. The burn rate is faster when the water is injected on a closed intake valve, as evidenced by an advancement of CA50 for a fixed spark timing. The fact that CA50 changes more than CA10 indicates the effect continues beyond ignition and flame initiation into the bulk burn phase of combustion.

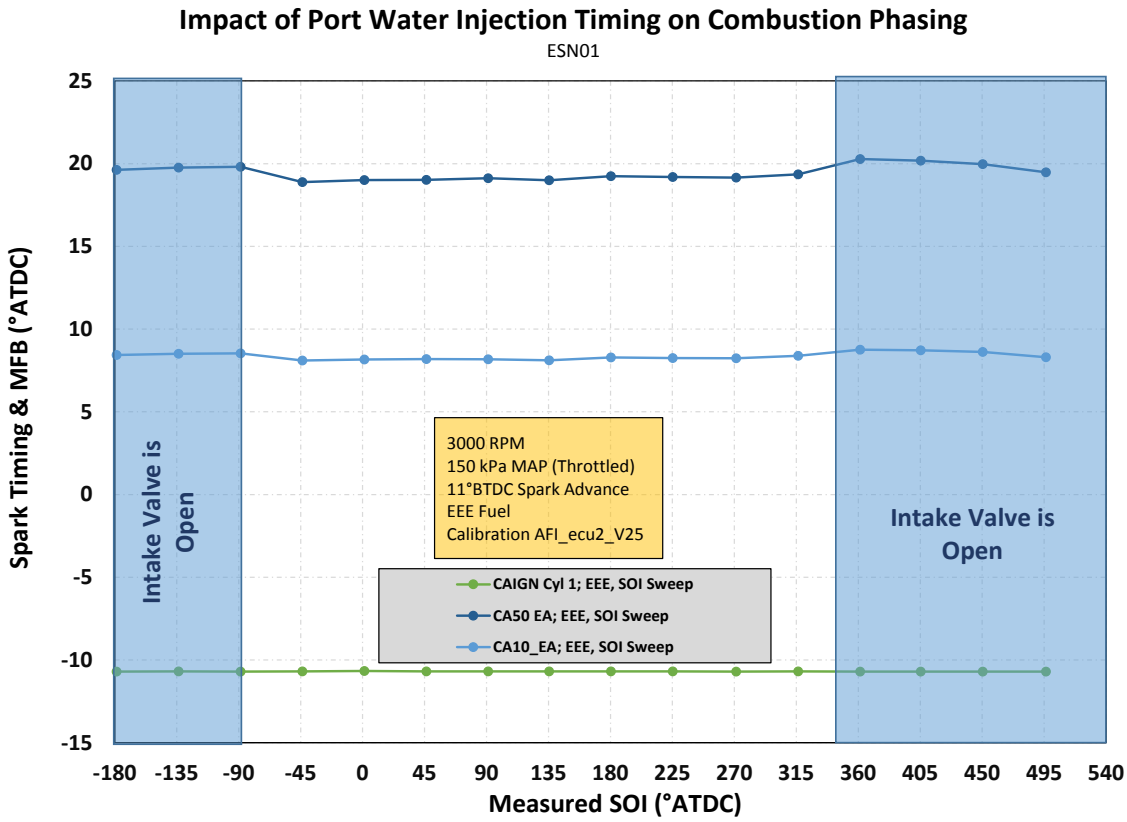

Figure 60: Impact of water injection Start of Injection on CA10 and CA50. 150 kPa MAP.

The implication here is that there is a water preparation effect. Perhaps the water sprayed on the closed intake valve is vaporized better when it enters the combustion chamber. The water sprayed on an open intake valve is likely to vaporize in the cylinder. There may even be impingement implications where the liquid penetration length is sufficiently long such that the liquid water impinges upon, and perhaps pools upon the piston and / or cylinder

wall. This open-valve injection case is likely to have more of a cooling effect on the unburned gases in the cylinder, presumably leading to the lower burn rate. This could especially be true if water is still vaporizing during the combustion process.

The impact on work is shown in Figure 61. Here there is a change in IMEP that corresponds to the difference between open and closed valve injection. This is likely directly resulting from the advancing of CA50 closer to MBT.

It is interesting to note that although NMEP does show the same trend, the trend in NMEP is less pronounced than IMEP. Perhaps due to some competing factors on the pumping side. Exhaust pumping is likely not impacted by water SOI, so if there are any effects, it is likely happening on the intake side.

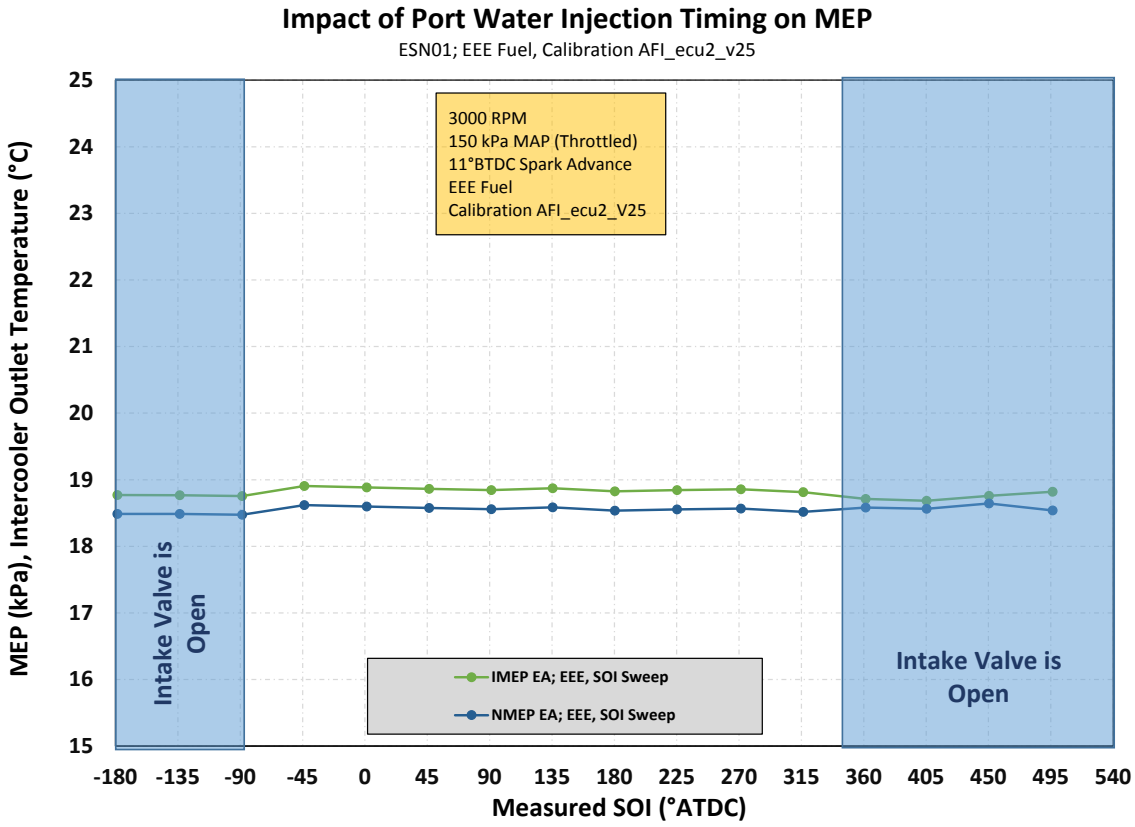

Figure 61: Impact of water Start of Injection timing on Gross Indicated, and Net Indicated Mean Effective Pressure. 150 kPa MAP.

With this preliminary investigation showing that the water SOI does impact combustion the question arose as to if SOI timing also impacts knock tolerance. To assess this, the engine was operated under higher load (250 kPa MAP), and with 87 AKI test fuel. Spark timing was adjusted to put the engine into moderate knock. Once again, water injection duration was held fixed at 10 ms. The impact to combustion phasing and MEP is similar, as shown in Figure 62 and Figure 63; injection on a closed valve advances CA50 slightly for fixed spark timing, and there is a corresponding increase in MEP.

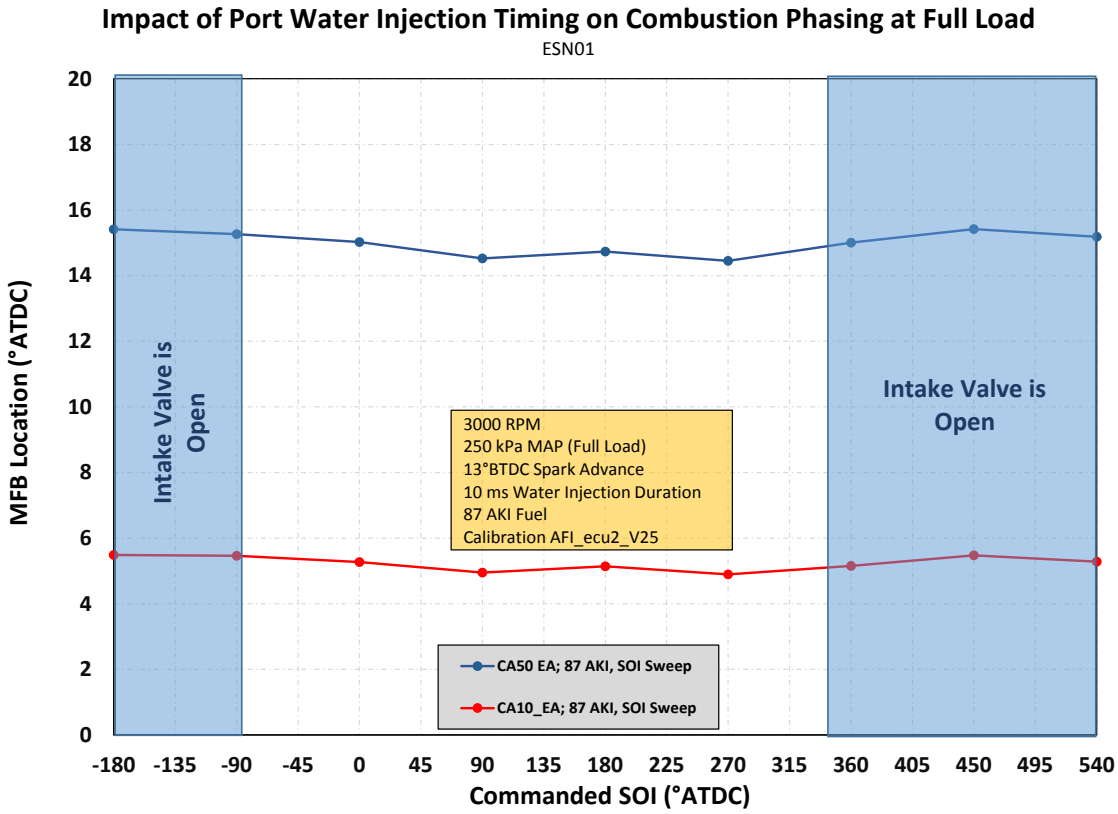

Figure 62: Impact of water injection Start of Injection on CA10 and CA50. 250 kPa MAP.

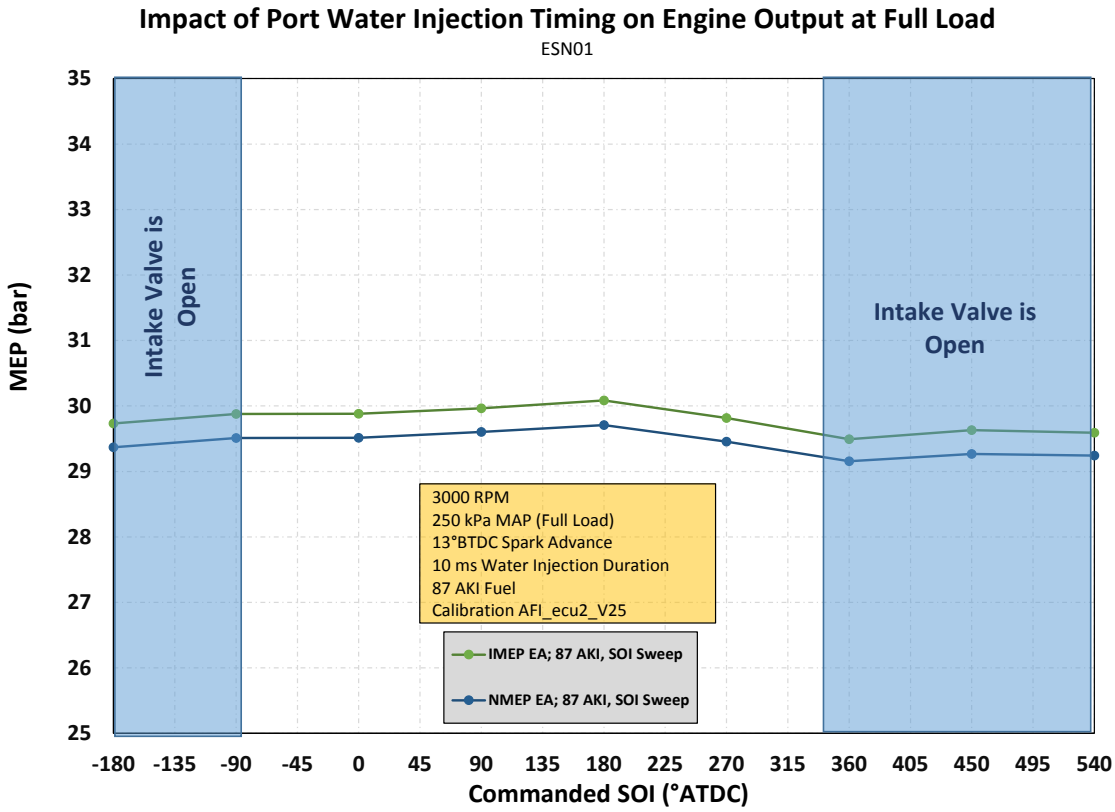

Figure 63: Impact of water Start of Injection timing on Gross Indicated, and Net Indicated Mean Effective Pressure. 250 kPa MAP.

Figure 64 shown the knock peak to peak amplitude. The nominal knock amplitude for this operating condition is 10 bar pk-pk. This knock level produces audile knock that is consistent and can be heard outside of the testcell with the unassisted human ear. This would be considered by many to be "moderate" to "heavy" knock levels. Sweeping water SOI timing influenced the knock severity (as indicated by the peak to peak values). Injection on the closed intake valve clearly shows an increase in knock pk-pk. Surely some of this is due to the shift in combustion phasing alone, but more likely the two effects are inter-related. As discussed previously, the open valve injection leads to vaporization of water in the cylinder, some of which may not fully vaporize until after the valve is closed. The result is colder unburned gas temperature and metal surface temperature. Both will decrease the time-temperature history of the end gas. Clearly this is not stopping the end gas from auto-igniting, but it is delaying the point of auto-ignition to later in the cycle. This results in a decreased peak to peak pressure amplitude because 1) less fuel mass

remains in the end gas for rapid heat release, and 2) combustion chamber volume is larger, so less pressure rise will result for a given energy release.

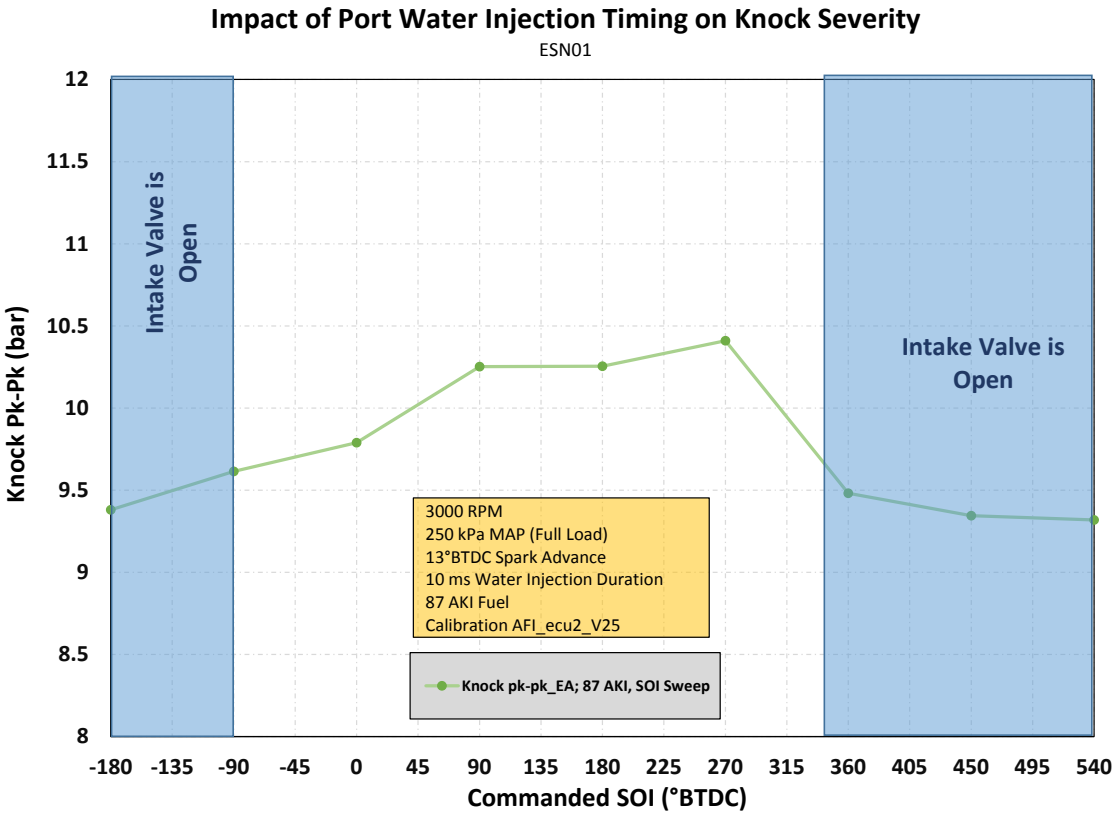

Figure 64: Impact of Water Injection Start of Injection Timing on Knock Peak to Peak Value.

Although this test was run at constant spark timing, an alternate experimental method could be to run the test at a constant knock severity, in which case the reduction in knock pk-pk with open valve injection would enable a corresponding advancing of combustion phasing.

To summarize, this subtest, reveals that the timing of the water injection in the cycle results in a reasonably repeatable affect on combustion. The implication is that open-valve injection is more effective at decreasing in-cylinder temperature as more of the total enthalpy increase of the water comes from the bulk gas and metal inside the cylinder. This negatively impacts combustion, but does have a marked improvement on knock severity.

6.2 Water Injection Testing Results

6.2.1 Production Boost Levels

6.2.1.1 Cycle Summary

Figure 65 compares the four primary test cases that were run at production boost levels. These cases will be elaborated upon further in subsequent discussion, but include a baseline case run with 91 AKI fuel and production fuel enrichment, a non-knocking case run with 110 AKI fuel and production fuel enrichment, a water injected case run with 87 AKI fuel and production fuel enrichment, and a water injected case run with 87 AKI fuel and lambda = 1.0.

In the interest of brevity, the ensemble averaged data is shown only for cylinder 1[40], and only at 3000 RPM full load.

[40] The other engine cylinders shown the same trends and orders.

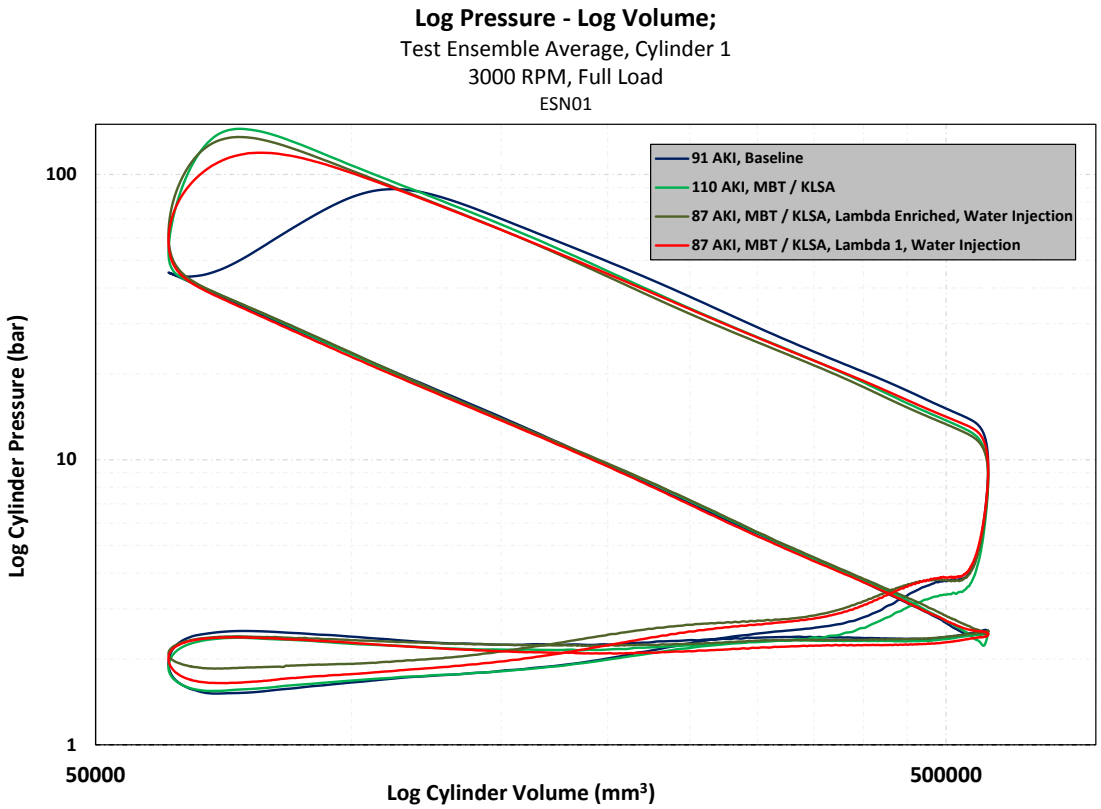

Figure 65: Test Ensemble Averaged Cylinder Pressure. Cylinder 1, 3000 RPM, Full-Load (~250 kPa MAP). All major test cases shown.

In examining Figure 65 there are many differences. Some obvious; for example the retarded combustion phasing found in the baseline case, compared to the advancing of combustion phasing with water injection. Others less so; for example the reduced Polytropic Index on the expansion stroke with water injection compared to the non-water injected cases, or the increase in pumping work found with water injection.

To aid in clarity when interpreting these results, Figure 66 is the same data, but only includes the baseline case compared to the water injected, lambda = 1.0 case.

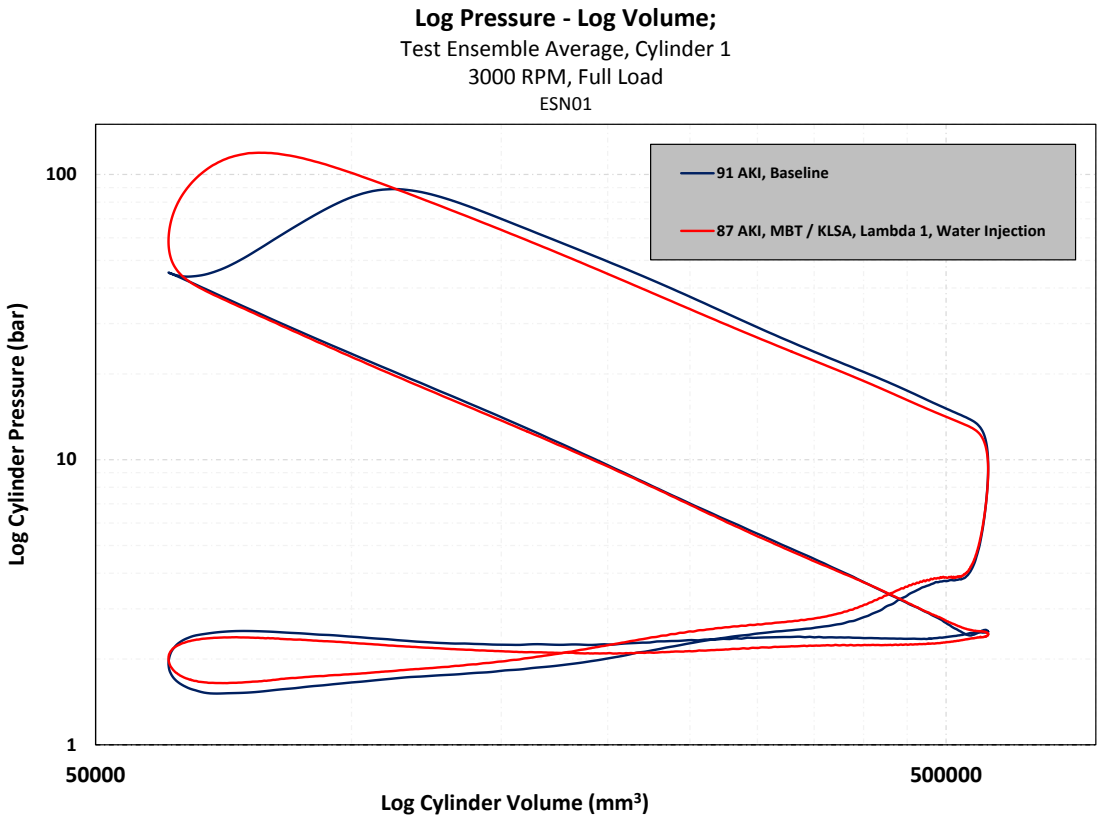

Figure 66: Test Ensemble Averaged Cylinder Pressure. Cylinder 1, 3000 RPM, Full-Load (~250 kPa MAP). Comparison between Baseline and Water Injected, Lambda = 1 case only.

Likewise, Figure 67 shows the same data, but only compares the non-knocking 110 AKI case to the water injected, lambda = 1.0 case. Figure 67 for example shows more clearly a reduced Polytropic Expansion Index and elevated cylinder pressure early in the exhaust stroke. These individual differences will be elaborated upon further through subsequent analysis of metrics specifically developed for detailed causality analysis.

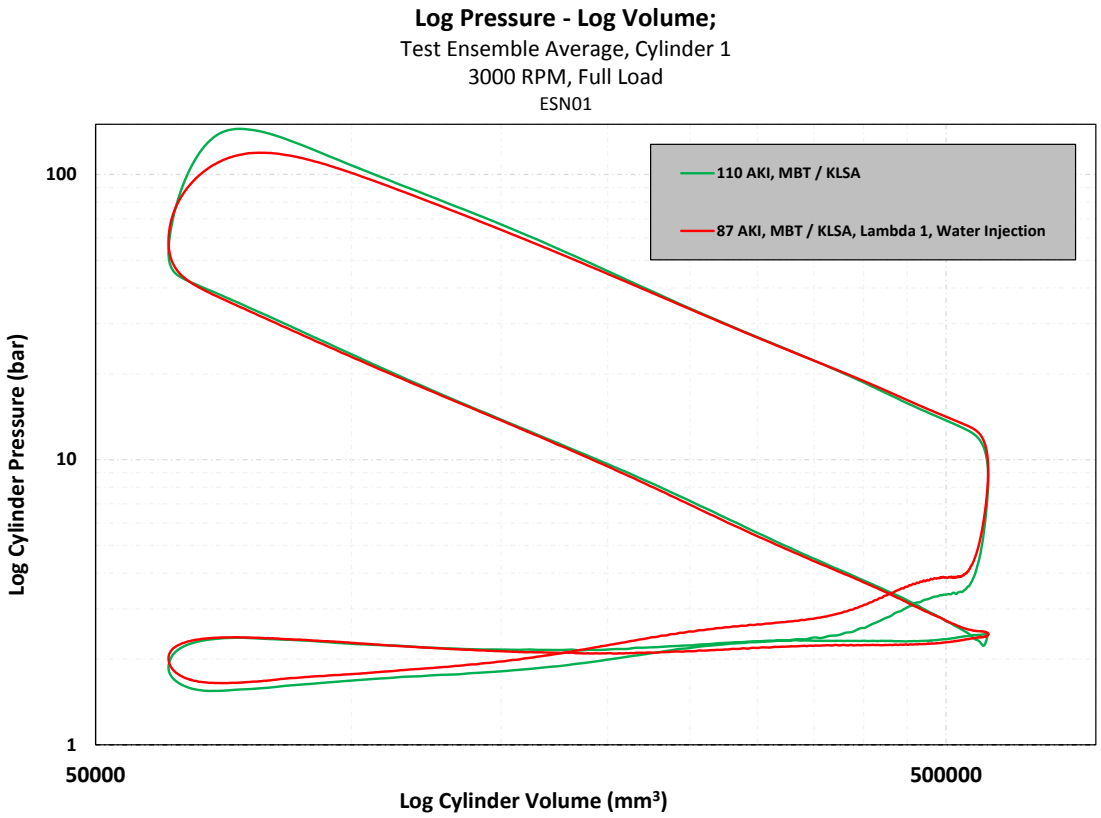

Figure 67: Test Ensemble Averaged Cylinder Pressure. Cylinder 1, 3000 RPM, Full-Load (~250 kPa MAP). Comparison between Non-knocking and Water Injected, Lambda = 1 case only.

6.2.1.2 Operating Parameters

To conduct testing at production boost levels, the production turbocharger and wastegate assembly was used. The production controller actuated the production wastegate and throttle to achieve target boost levels. Figure 68 shows the manifold pressure that was achieved during the three primary tests; baseline, non-knocking fuel, and with water injection, pump regular fuel, and λ=1.0.

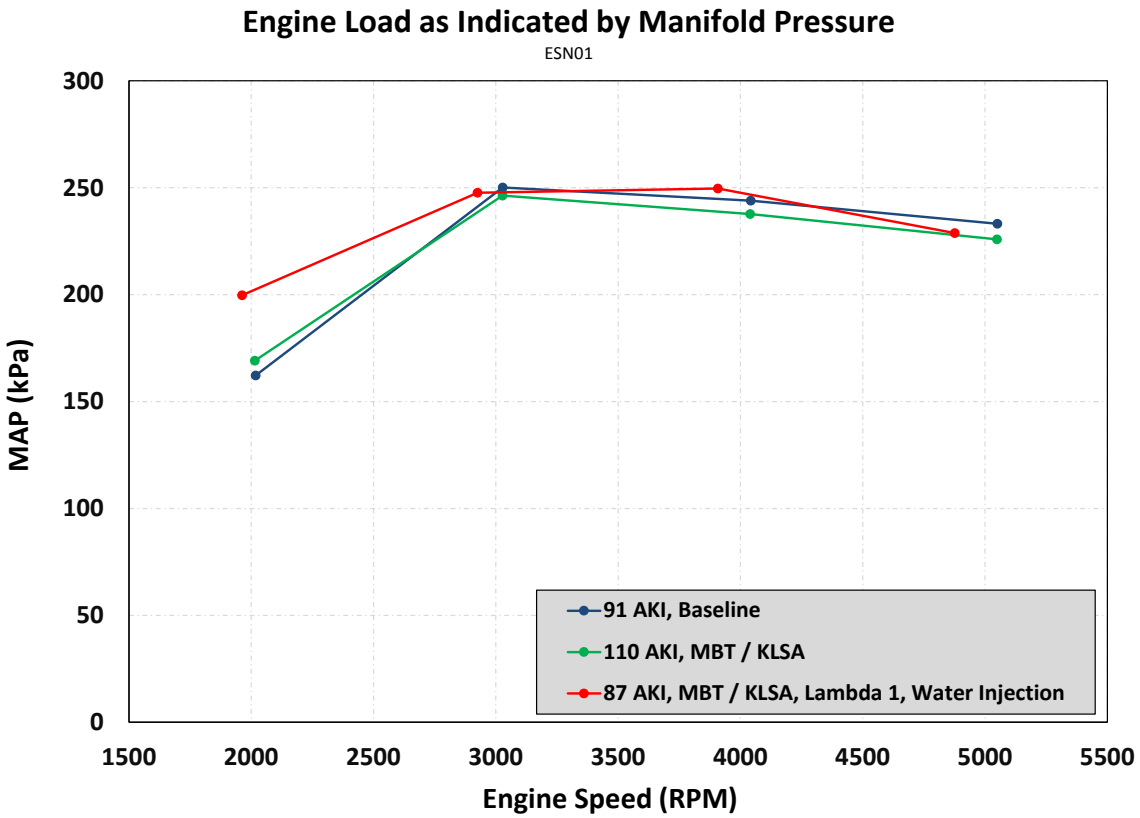

Figure 68: Intake MAP during testing at production boost levels. Reprinted with permission Copyright © 2017 SAE International. Further Distribution of this material is not permitted without prior permission from SAE. See 17 Appendix F for further details.

Exhaust lambda for the tests of interest is shown in Figure 69. Here it is shown that the baseline testing, and the non-knocking fuel testing were run with a commanded lambda equivalent to the production values, as found in the calibration for the 2012 MY Buick Regal.

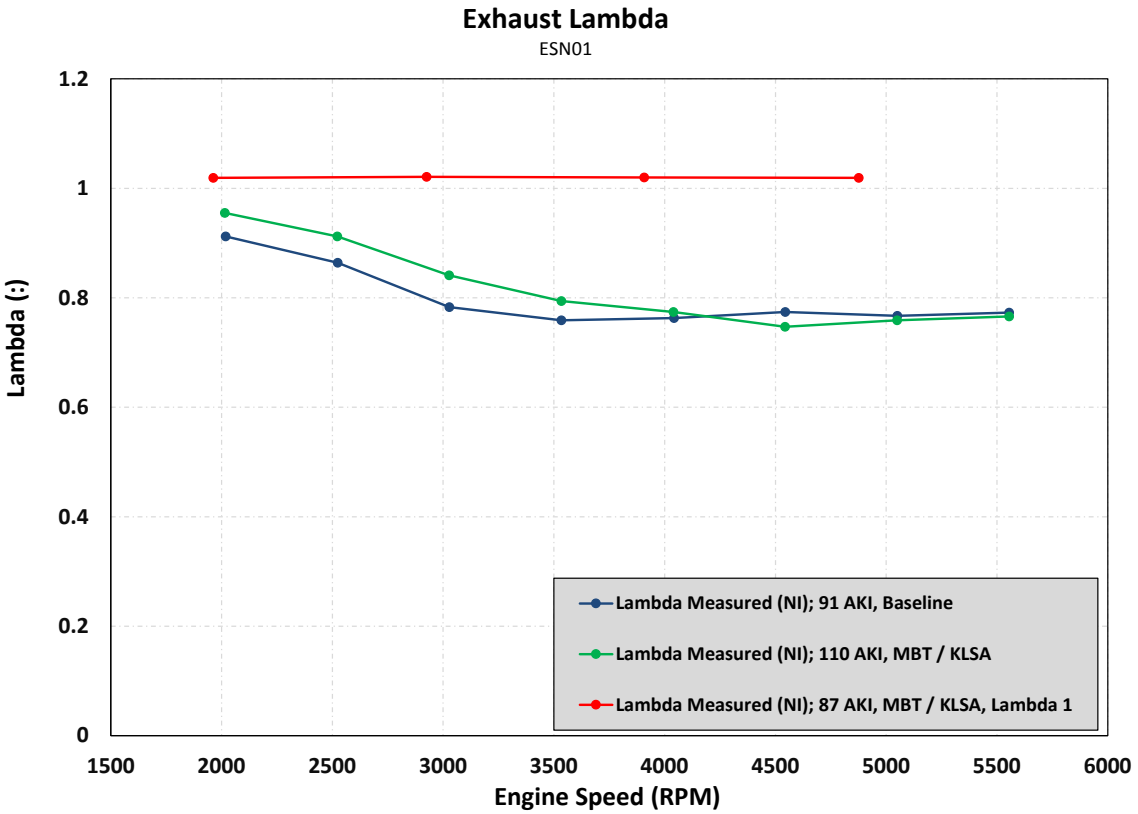

Figure 69: Comparison of Exhaust Lambda, as measured with a Bosch Wide Rang Lambda sensor for the tests of interest.

The fuel flow rate and water flow rate along with the water to fuel ratio on a mass basis are shown in Figure 70 for the test run with 87 AKI Fuel, combustion phasing set to MBT or KLSA, and with lambda = 1. Here it can be seen that the flow rate of water was as much as 4.5 times the flow rate of fuel (at the 2000 RPM point). Recall that the objective of these tests were to attempt to advance the combustion phasing into the 10° ATDC range. To do this requires a significant amount of water, and in fact at 4000 and 5000 RPM, the water injection duration spanned the entire engine cycle (720°). Since the injector was open the entire engine cycle, and the cycle happens over a shorter period of time, the flow rate of water decreased at 5000 RPM compared to 4000 RPM.

Additionally, at 5000 RPM, there was a significant pressure drop across the high pressure Coriolis meter, leaving only ~200 kPa of water pressure at the injectors[41]. Because the injector was open the entire cycle, and water pressure was ~200 kPa compared to the typical injector operating pressure of ~400 kPa, it is expected that not all of the water had evaporated prior to being inducted into the cylinder.

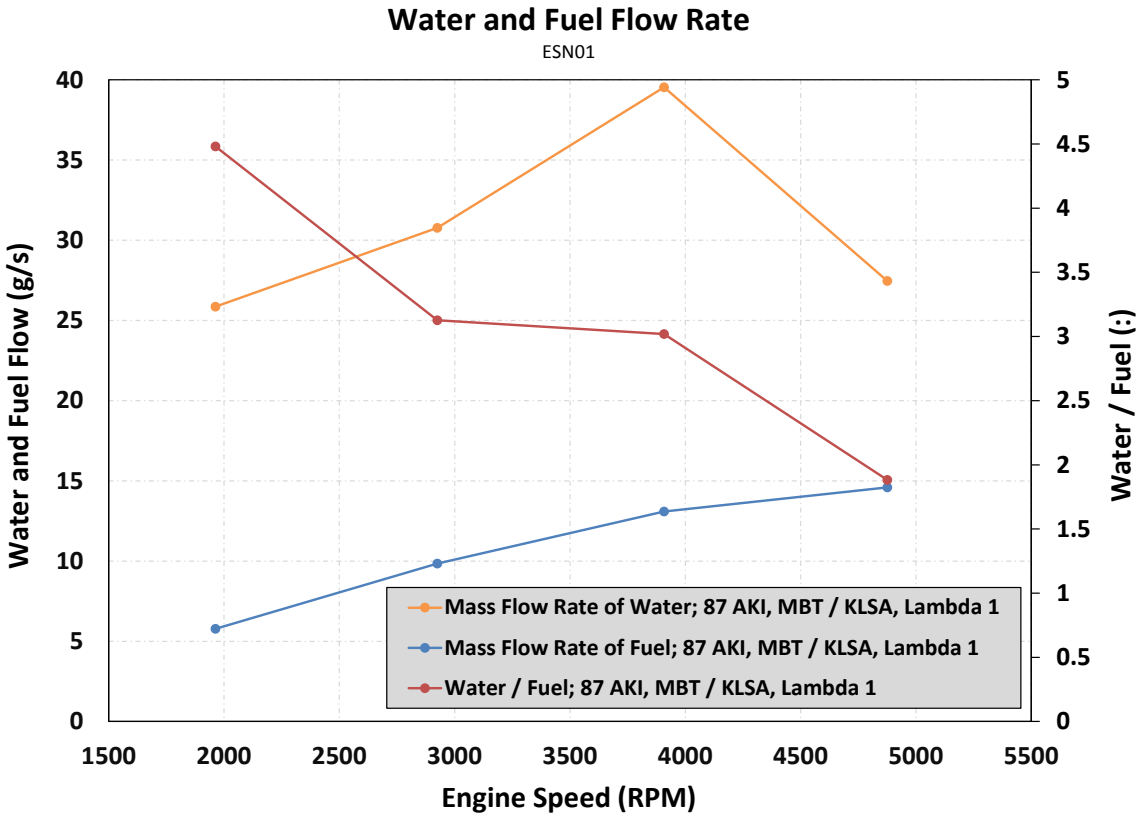

Figure 70: Mass flow rates of water and fuel, and the water to fuel ratio for the test with 87 AKI fuel, MBT or KLSA, and Lambda = 1. Reprinted with permission Copyright © 2017 SAE International. Further Distribution of this material is not permitted without prior permission from SAE. See 17 Appendix F for further details.

Combustion phasing, as indicated by CA50 is shown in Figure 71. The green band indicates the approximate range of CA50 corresponding to MBT. Here it is clear that the

[41] This is the reason a low pressure Coriolis meter was added to the system after this testing at production boost levels. The low pressure Coriolis meter has a larger internal diameter. Subsequent testing with the low pressure Coriolis meter installed has shown negligible pressure drop.

baseline combustion phasing is significantly retarded from MBT due to knock limitations. This directly relates to a loss of cycle efficiency. The higher knock tolerance of the 110 AKI fuel enables MBT, or at least very near MBT operation throughout the speed range. Recall that the 110 AKI Fuel test shown here was run with production calibrated fuel enrichment. With 87 AKI Fuel, and stoichiometric fueling, the addition of water injection enabled CA50 to be advanced to near what was possible with 110 AKI fuel, with the most significant improvements coming at 3000 RPM.

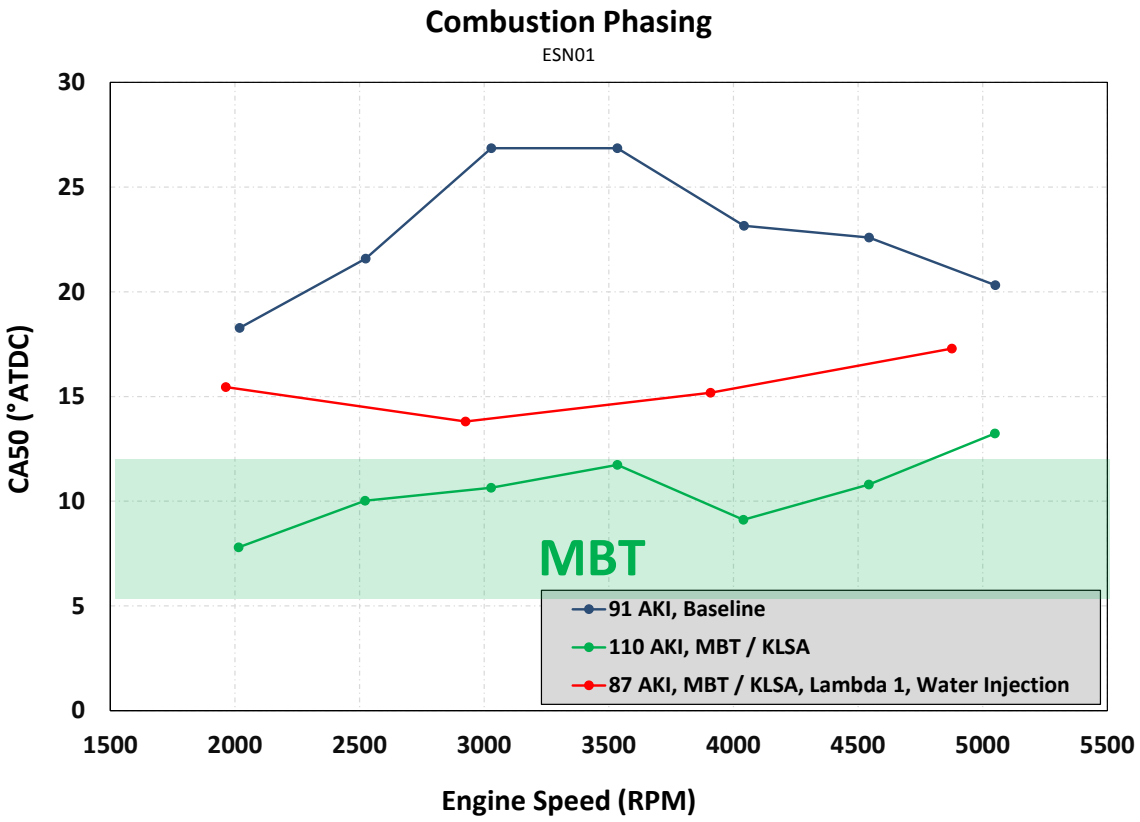

Figure 71: Combustion phasing, as indicated by CA50 during testing at production boost levels. ***Reprinted with permission Copyright © 2017 SAE International. Further Distribution of this material is not permitted without prior permission from SAE. See 17 Appendix F for further details.***

The ignition timing is shown in Figure 72. Here it is interesting to note that although water injection enabled combustion phasing to be advanced to be between the highly knock limited baseline case and the non-knocking case, it required a very significant increase in

spark advance. For example, at 4000 RPM, an advancement of approximately 8° in CA50 required approximately 20° earlier spark timing. Although the relationship between changes in ignition timing and CA50 is not a 1 to 1 due to the change of the burn phases in relation to piston position, this relatively large discrepancy does point to a slowing of the burn rate.

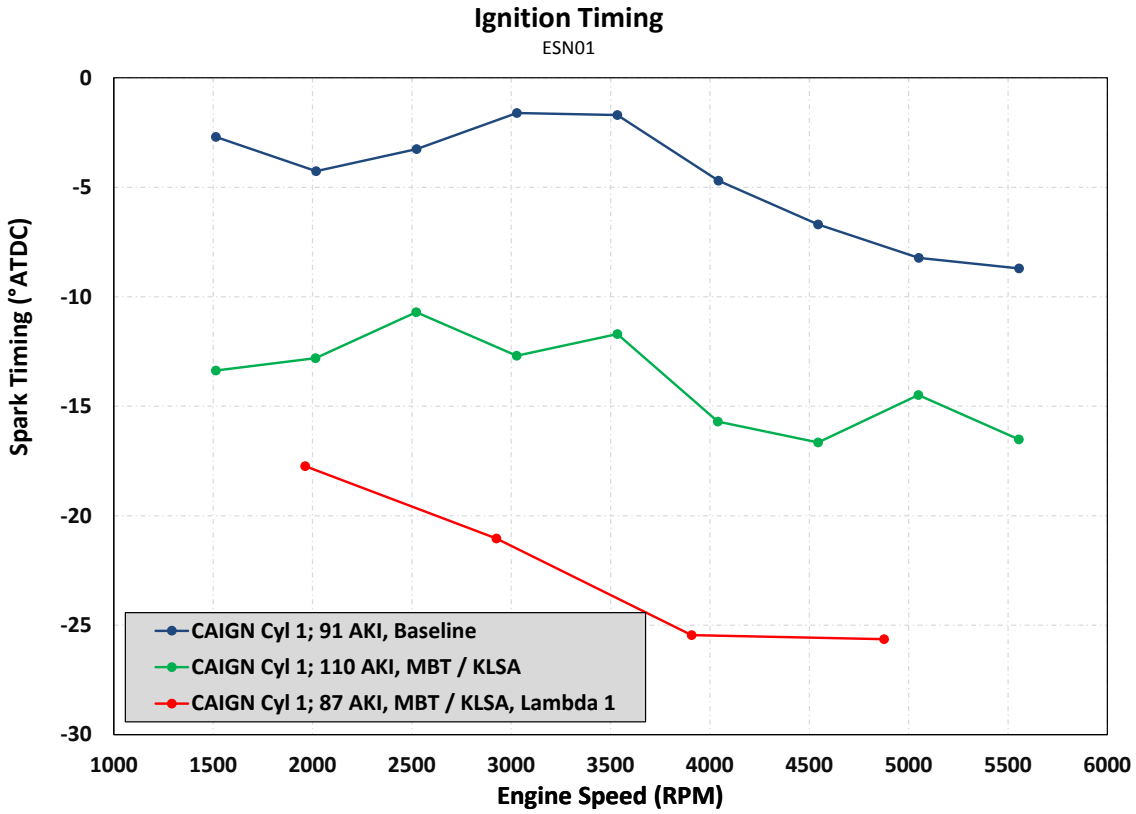

Figure 72: Ignition timing comparison during testing at production boost levels.

6.2.1.3 Combustion and Thermodynamic Effects

Since the relationship between changes in ignition timing and changes in combustion phasing point toward changes in burn rate with water injection, it is prudent to investigate further. Figure 73 shows the bulk burn duration, as indicated by the 10% to 90% burn duration. Here it can be seen that the burn duration does not change significantly between the baseline case with 91 AKI fuel, and the non-knocking case with 110 AKI fuel. However, when water is added, the burn duration increases significantly, nearly doubling

above 3000 RPM. As discussed in the literature review section, previous researchers had also observed an increase in burn duration. Therefore, at least directionally, this was not unexpected.

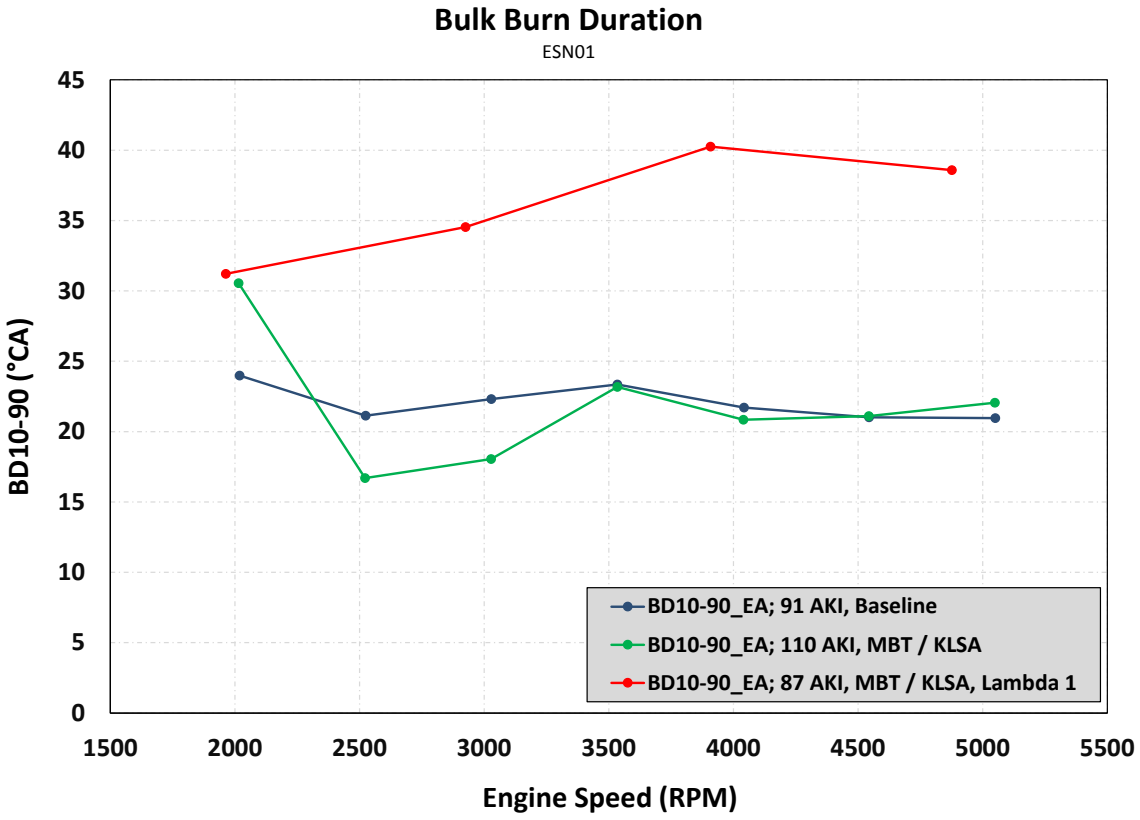

Figure 73: Comparison of bulk burn duration during testing at production boost levels. ***Reprinted with permission Copyright © 2017 SAE International. Further Distribution of this material is not permitted without prior permission from SAE. See 17 Appendix F for further details.***

The early burn duration, as indicated by the 0% to 10% MFB duration is shown in Figure 74. Here it is shown that similar to the bulk burn duration, the early burn duration for the cases with 91 AKI and 110 AKI fuel are similar, while the burn duration for the water injected case is significantly longer. Again, previous researchers reported shifts in CA50 when water was injected, so although they did not report burn duration specifically, these increases in burn duration are not unexpected.

Temperature has a strong influence on chemical reaction rates, and therefore, it is felt here that as the injected water vaporizes and cools the unburned mixture reaction rates and laminar flame speed decreases, leading to increases in burn duration. In addition to the temperature effects, the water vapor will also act as a diluent, which will also slow burn rates. For example, when EGR is added, burn rates slow, even though there is no vaporization and charge cooling taking place.

One other reason that is at least directionally leading to slower burn rates is the timing of the ignition with water injected. As the spark is advanced further from TDC, the ignition and early kernel development occur at an increasingly lower pressure and temperature. The pressure trend is opposite, meaning that the lower pressure actually leads to an increase in burn rate. However, the sensitivity to pressure changes is subtle compared to the temperature effect. As the ignition occurs at lower temperature, the early burn will be reduced as well. Changes to the bulk burn with advancing ignition become more complicated because at least some of the bulk burn occurs near TDC, where temperature is very high, yet at the same time, there is flame quenching that might take place because of the proximity of the piston. An interesting case would be to inject water, but maintain constant spark timing to isolate only the impacts of charge cooling and dilution. Nonetheless, in an actual application, water injection ***would*** be used in conjunction with spark advance, so the impact of advancing spark on burn rate is entirely prudent to examine.

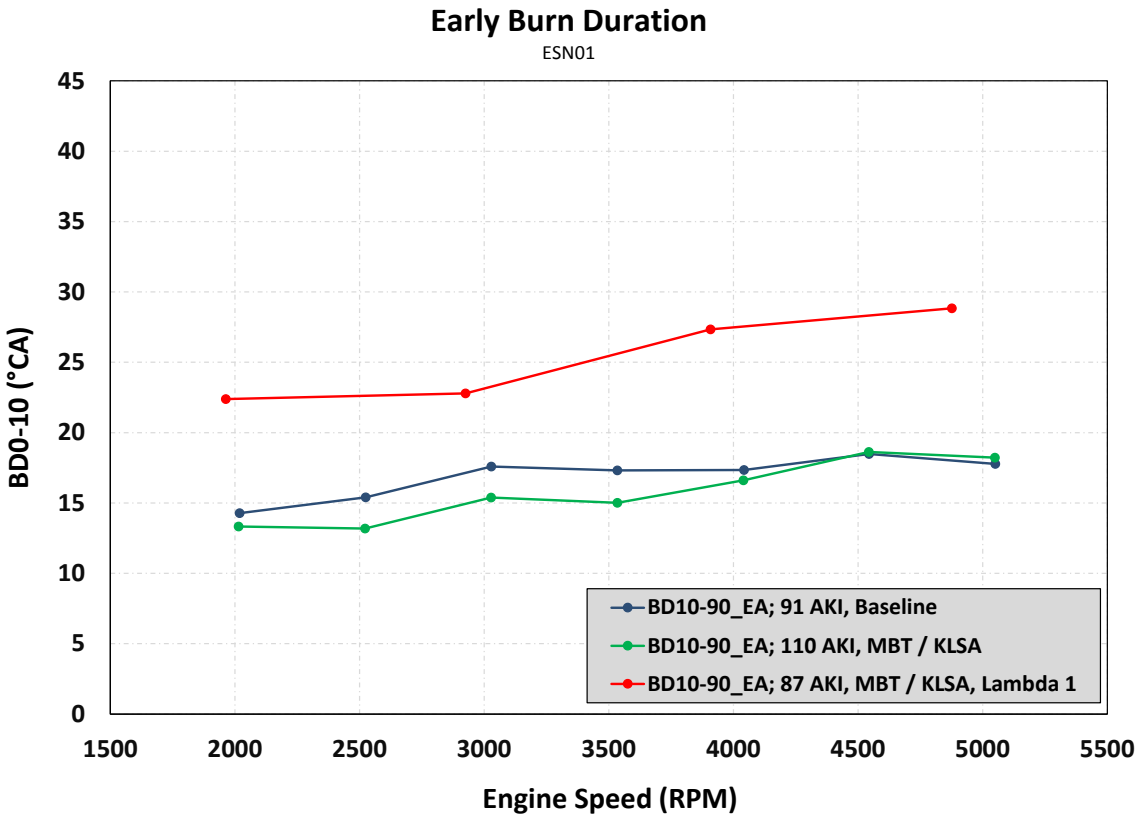

Figure 74: Comparison of early burn duration during testing at production boost levels. ***Reprinted with permission Copyright © 2017 SAE International. Further Distribution of this material is not permitted without prior permission from SAE. See 17 Appendix F for further details.***

Although brake torque was measured, it is not chosen as a primary metric in this study because even slight changes in engine oil temperature can impact friction, leading to variation in brake torque. For this project this is further compounded by the oil dilution that occurred during the water injection tests. The water that migrated to the crankcase formed an emulsion with the oil. This impacted the oil level and entrained air fraction[42]. Furthermore it is assumed to have impacted the viscosity and lubricity of the oil, both of which affect friction. Therefore, Net Mean Effective Pressure (NMEP) is chosen here as the primary indicator of engine output, as NMEP differs from BMEP by only the frictional term FMEP according to Equation 26 and Equation 27.

[42] This statement is made by visual observation of oil level and overall foamy appearance of oil in the crankcase.

Equation 26: BMEP

$$BMEP = IMEP + PMEP + FMEP$$

Equation 27: NMEP

$$NMEP = IMEP + PMEP$$

A comparison of NMEP is shown in Figure 75. Here it can be seen that not surprisingly, the case with non-knocking fuel resulted in NMEP improvements over the baseline at all engine speeds. The change was significant with a peak of 30% improvement at 2500 RPM, but even the smallest improvement was 11% and 6% at 2000 RPM and 5000 RPM respectively. Recalling that the VP110 fuel was run with the same enrichment as the baseline case, and with both fuels being E0, this improvement is entirely related to advancement of CA50. This underscores the importance of combustion phasing in engine performance and efficiency.

The case with water injection resulted in an improvement of NMEP over the baseline case as well. The maximum improvement was 22% at 2000 RPM, with the minimum improvement being 3.6% at 5000 RPM. Recalling that the combustion phasing for the water injected case fell between that of the baseline and non-knocking case, this result is logical.

However, one must consider other factors as well. The water injected case resulted in significantly longer combustion duration which is a negative in terms of cycle efficiency and output. Likewise the charge cooling results in overall lower temperature and pressure, again being directionally incorrect for maximizing output. Therefore, the fact that NMEP

was higher with water injection clearly points to combustion phasing being the dominant factor.

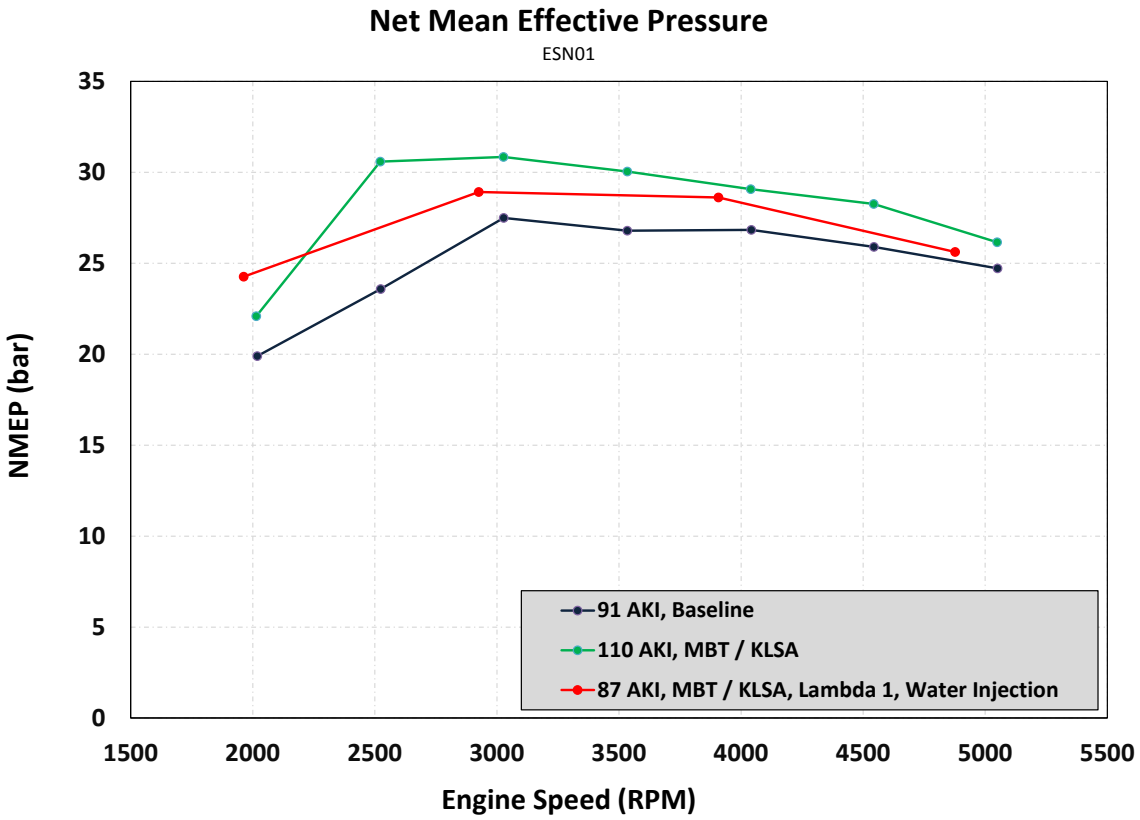

Figure 75: Comparison of NMEP for testing at production boost levels. Reprinted with permission Copyright © 2017 SAE International. Further Distribution of this material is not permitted without prior permission from SAE. See 17 Appendix F for further details.

Since there were slight differences in boost pressure / manifold pressure for the tests being examined, it was felt that the differences in MAP could be skewing the results and impacting conclusions relative to changes in maximum engine output. In an effort to mitigate any effects of variation in MAP, the NMEP was normalized by MAP, resulting in a metric that indicates the NMEP per unit of MAP. These results are shown in Figure 76.

There are at least a couple interesting observations here. First, the rank ordering does not change; the non-knocking 110 AKI test produces the best results. This is likely because it

has the most optimal CA50, and without the negative of longer combustion duration found with the water injected case. However, the water injection case still rank orders higher than the baseline case, which is significant, as it suggests that ***with all else being equal, a production engine, with no other changes, can produce higher output with water injection, and with lower octane fuel, and stoichiometric operation***.

The other interesting point is the trend of all three cases. Since the boost is not constant with engine speeds, normalizing to MAP tends to flatten the NMEP / MAP curve. However, the normalized curve (of all three cases) tends to trend downward with increasing engine speed. This is not the effect of friction, as the metric is NMEP not BMEP, so friction is already separated out. Looking back at the data for CA50, and burn duration do not establish a solid explanation either. Since the normalization is to MAP, this trend could be explained by cylinder trapping changes. This will be evident in looking at volumetric efficiency shortly.

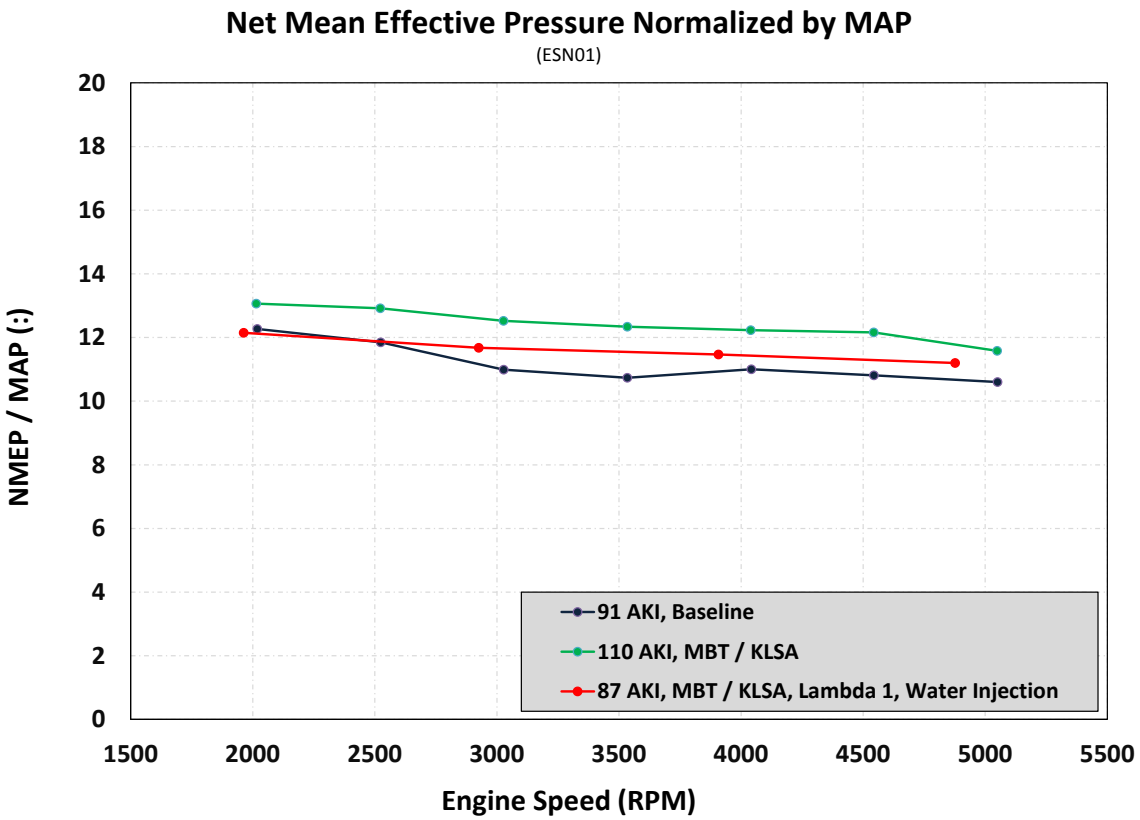

Figure 76: NMEP normalized by MAP. ***Reprinted with permission Copyright © 2017 SAE International. Further Distribution of this material is not permitted without prior permission from SAE. See 17 Appendix F for further details.***

Recalling that the water injection case was run with lambda =1, as opposed to enriched to improve output as was the case with the baseline and 110 AKI tests, may leave one wondering how much the reduction in fuel affected output performance. Figure 77 compares two water injection cases; water injection with 87 AKI fuel, combustion phasing set to MBT / KLSA, and lambda = 1 (the water injection case that has been examined thus far), compared to 87 AKI fuel, combustion phasing set to MBT / KLSA, but with lambda set the same as the baseline and 110 AKI cases. Here it can be shown, perhaps surprisingly, that the enrichment does not improve engine output for the water injection case. One potential explanation for this is that the production calibrated enrichment does not fall between the lambda corresponding to Leanest for Best Torque (LBT), and Richest for Best Torque (RBT) as one would expect, but perhaps richer than RBT for knock control, such that leaning to stoichiometric does not result in a torque change, it just moves to the other

side of the peak. With this being a highly boosted, and knock prone application, it is reasonable that the full load lambda may very well be rich of RBT.

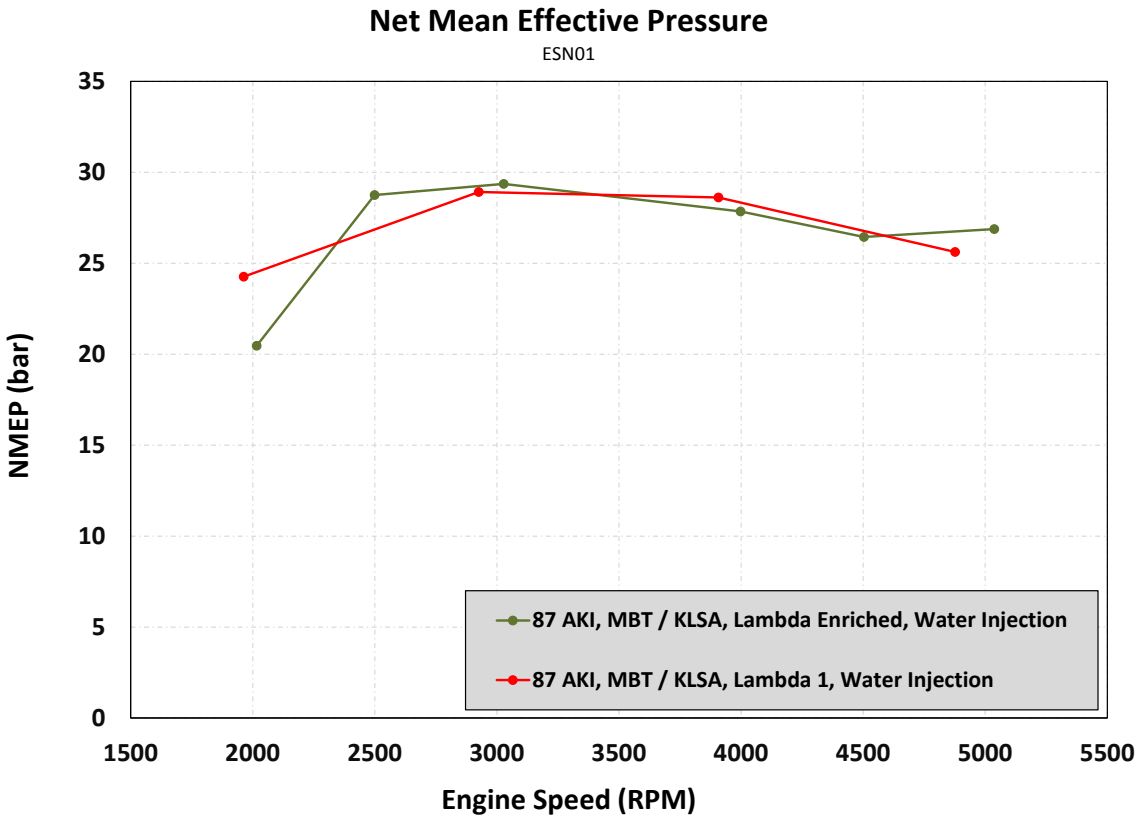

Figure 77: Effect of fuel enrichment on NMEP with water injection.

Although NMEP is a critical metric to look at when rank ordering technology impacts on engine output, additional learnings can be gleaned from other MEP metrics. IMEP is shown in Figure 78. Here the rank ordering is not unexpected; the 110 AKI fuel produced the highest IMEP, the baseline case was the lowest, and the water injection cases were in the middle.

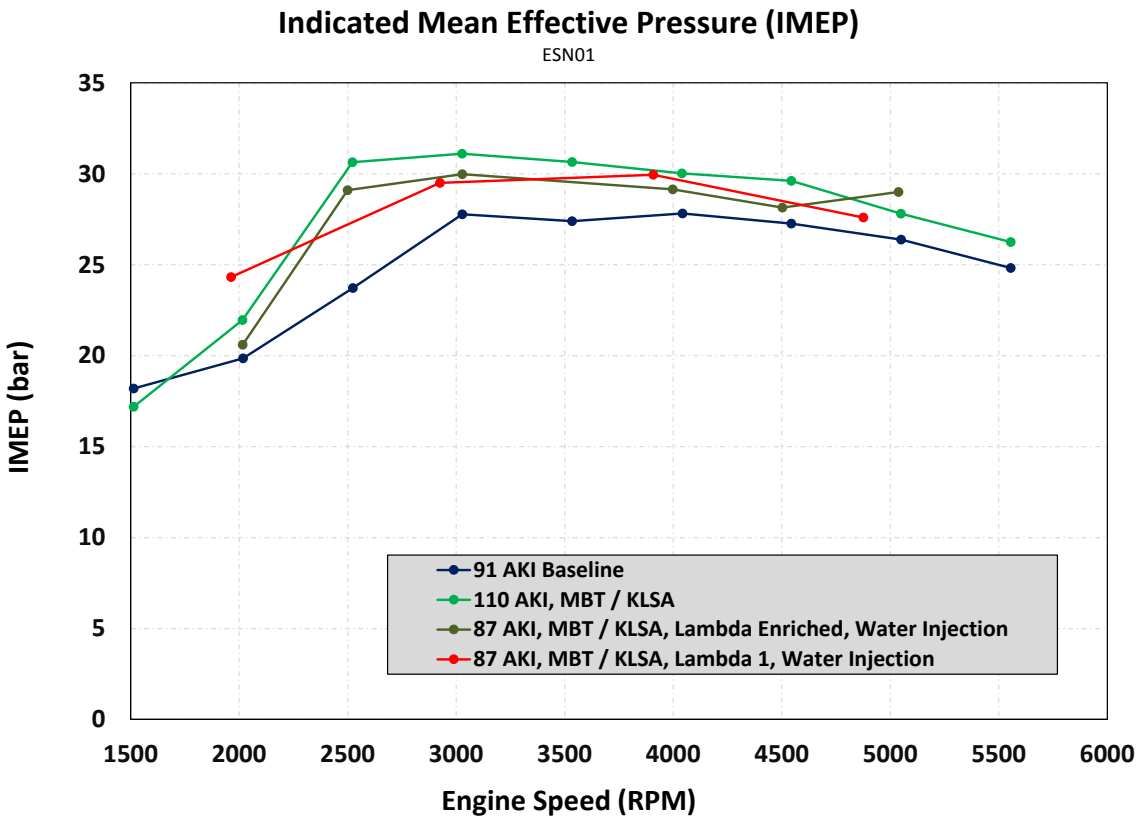

Figure 78: Comparison of Indicated Mean Effective Pressure.

PMEP provides perhaps a more interesting comparison, as shown in Figure 79. Void of combustion variation, the PMEP data is very repeatable, revealing a clear trend. The PMEP in the water injected cases is consistently lower / more negative than the cases without water injection. The more negative PMEP indicates an increase in pumping work, either on the exhaust side, or intake side.

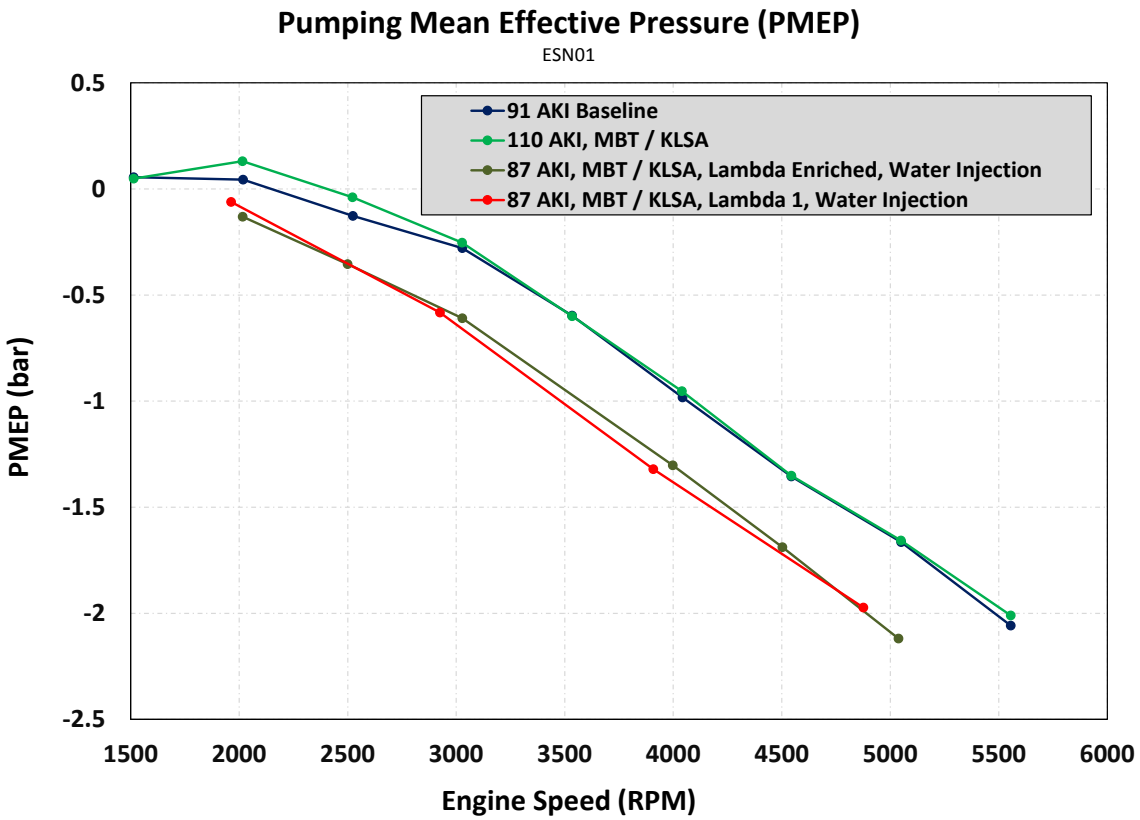

Figure 79: Comparison of Pumping Mean Effective Pressure.

This is put into perspective in Figure 80, where the actual power required to pump air in and exhaust out of the engine is plotted. The rank ordering must be the same as PMEP, however, here this is actual power in units of kW. Generally speaking, the pumping power increases nonlinearly with engine speed, and that the water injection does lead to significantly more power required for pumping. The difference between the baseline case and the enriched water injection case is 3.9 kW at 5000 RPM.

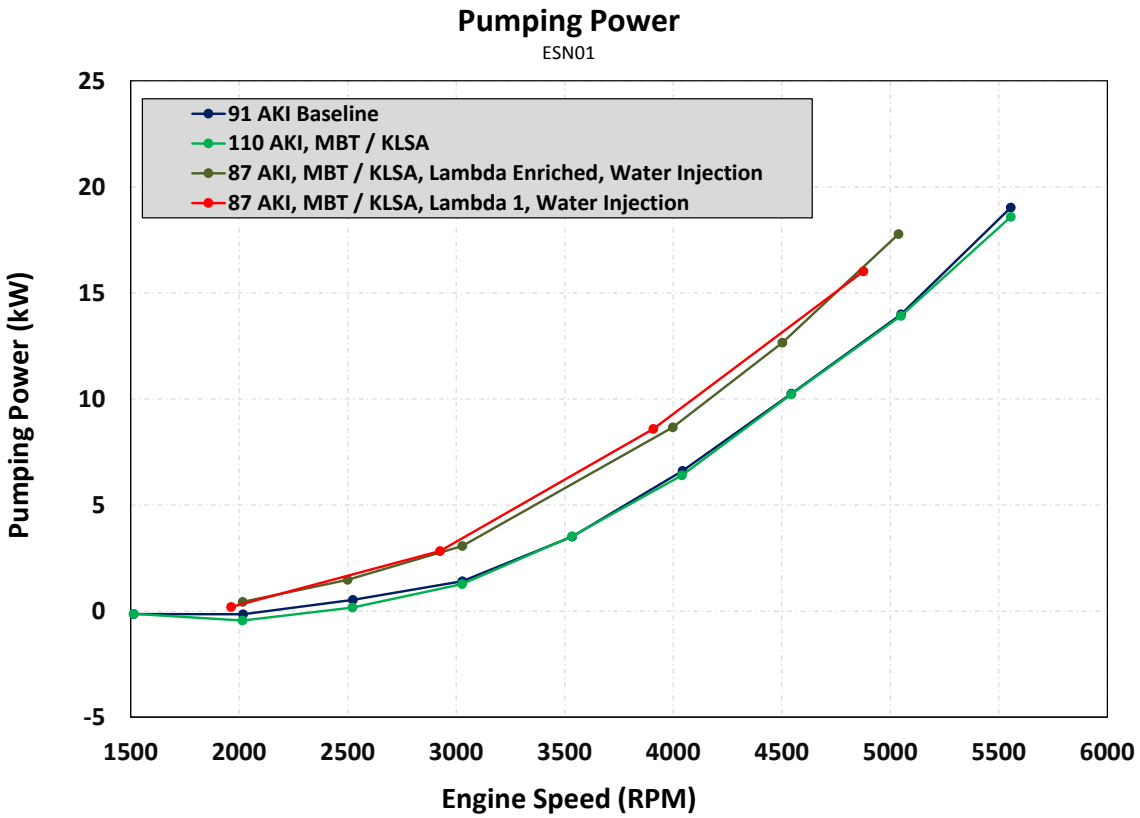

Figure 80: A comparison of the power required for pumping air in and exhaust out of the engine.

Figure 81 begins to dissect the shift in PMEP / pumping work with water injection, as it plots the engine average Absolute Exhaust Average Pressure (AEAP). Here it is shown that the water injection cases result in higher exhaust pressure over the entire speed range tested. These results should be interpreted with caution however. It is tempting to conclude that the change in PMEP in units of pressure, is a direct result of practically the same change in AEAP in units of pressure. This would be a false conclusion, as PMEP is the integral of pressure with respect to volume normalized by displaced volume. What can be concluded though is that PMEP indicates more pumping work with water injection, and AEAP indicates higher exhaust pressure, which is ***directionally*** supportive of an increase in pumping work.

Certainly the gamma and composition of the exhaust gas has an impact on exhaust pumping, and those parameters are impacted by the introduction of water. However, other factors also come into play including the temperature and pressure of the burned gas which are both impacted by the phasing and duration of the combustion event, which are influenced by the water injection.

These pumping and pressure observations are supported by referring again to Figure 66 and Figure 67, both of which show an intake stroke pressure very similar in all cases[43], but with significant differences in exhaust stroke pressure, especially in the early in the exhaust stroke. With the biggest difference in the early portion of the exhaust stroke (see especially Figure 67) it is tempting to surmise that the difference is due to longer combustion duration. Although this may be a contributing factor Figure 66 largely dispels this, as it shows the baseline case, with it's retarded combustion phasing, has higher pressure at blowdown, yet has lower pressure during the early stages of the exhaust stroke compared to the water injected case.

The implication in this is that the water vapor is hindering the blow-down process, but not necessarily the bulk displacement of exhaust gas. This statement is made based on the cylinder pressure in the water injected case being higher than the non-water injected case early in the exhaust stroke, but that difference decreases markedly by mid-stroke where $dV/d\theta$ is maximum (keep in mind Figure 67 is plotted on a Log scale).

This result is logical in that the majority of the water enters the cylinder as a liquid, where it flows well through the intake valves, and leaves the cylinder as a vapor, where it adds to the pressure drop across the exhaust valves, certainly the other factors including the temperature and density are involved, but the increase in mass is likely the driving factor. The vaporization of water in the cylinder will be discussed in detail in a subsequent section.

[43] As it should be, with intake pressure being the controlled parameter amongst tests.

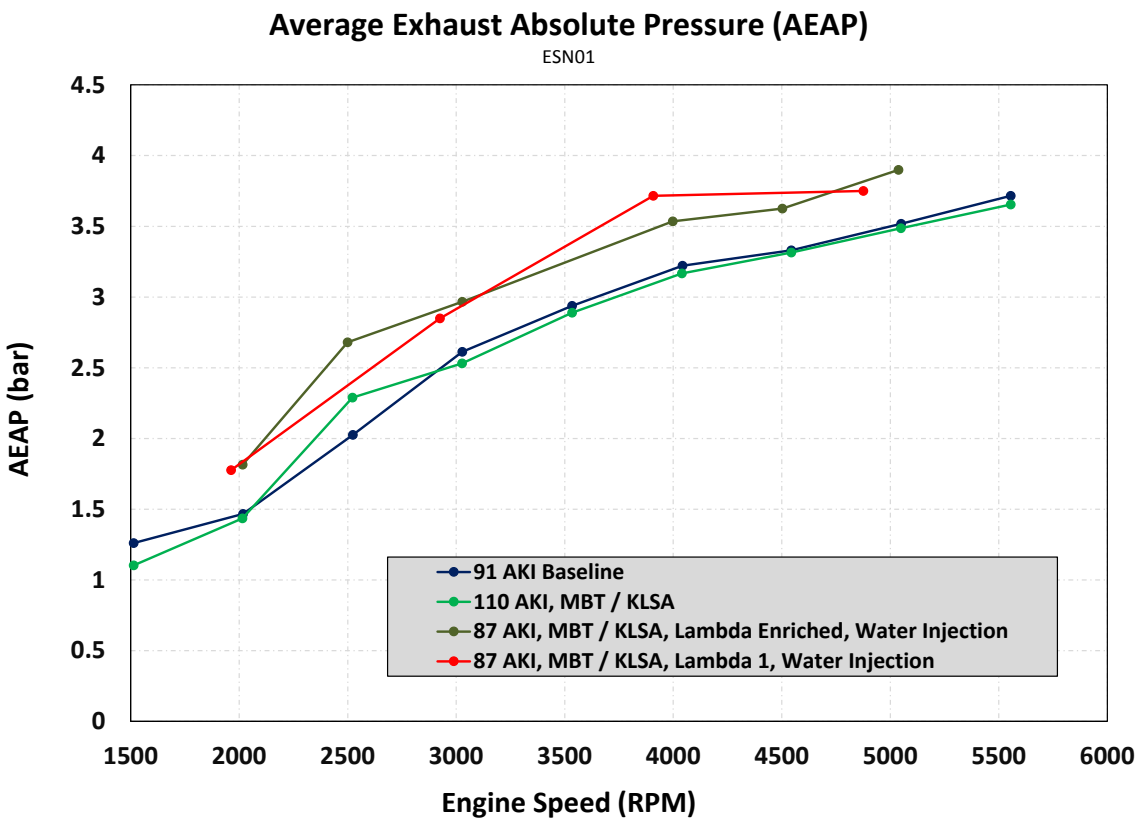

Figure 81: Comparison of Engine Average Exhaust Absolute Pressure (AEAP).

The Exhaust Gas Temperature (EGT) is shown in Figure 82. At least up to 5000 RPM, the rank ordering is as expected. There is a slight decrease in EGT moving from the baseline case to the 110 AKI case. This is a result of the advanced combustion phasing that is possible with the non-knocking 110 AKI fuel. The earlier combustion phasing enables more complete expansion of the burned gas with a corresponding reduction in temperature. There is also likely increased heat transfer to the combustion chamber walls with the advanced combustion phasing, further reducing the temperature of the burned gas by the start of the blowdown event. The water injected case shows a significant reduction in EGT up to 4000 RPM. This is a direct result of the water cooling the unburned and burned gas, and having an increased heat capacity.

At 5000 RPM the EGT of the water injected case is similar to the non-water injected cases. This is a result of at least two additive effects. Referring again to Figure 73 the bulk burn

duration is significantly longer in the water injected case, this results in a reduction in expansion opportunity and heat loss prior to blowdown leading to increased EGT. Moreover, referring again to Figure 70, the water to fuel ratio, and since lambda was constant, the water to air ratio had decreased significantly by 5000 RPM. This decrease in trapped water was a result of flow limitations; the combination of water injectors and water rail pressure did not support any additional water flow with the water injection duration maximized at 720° CA. With water ratio decreased, there was less effect from charge cooling and increased heat capacity to counteract the increased bulk burn duration.

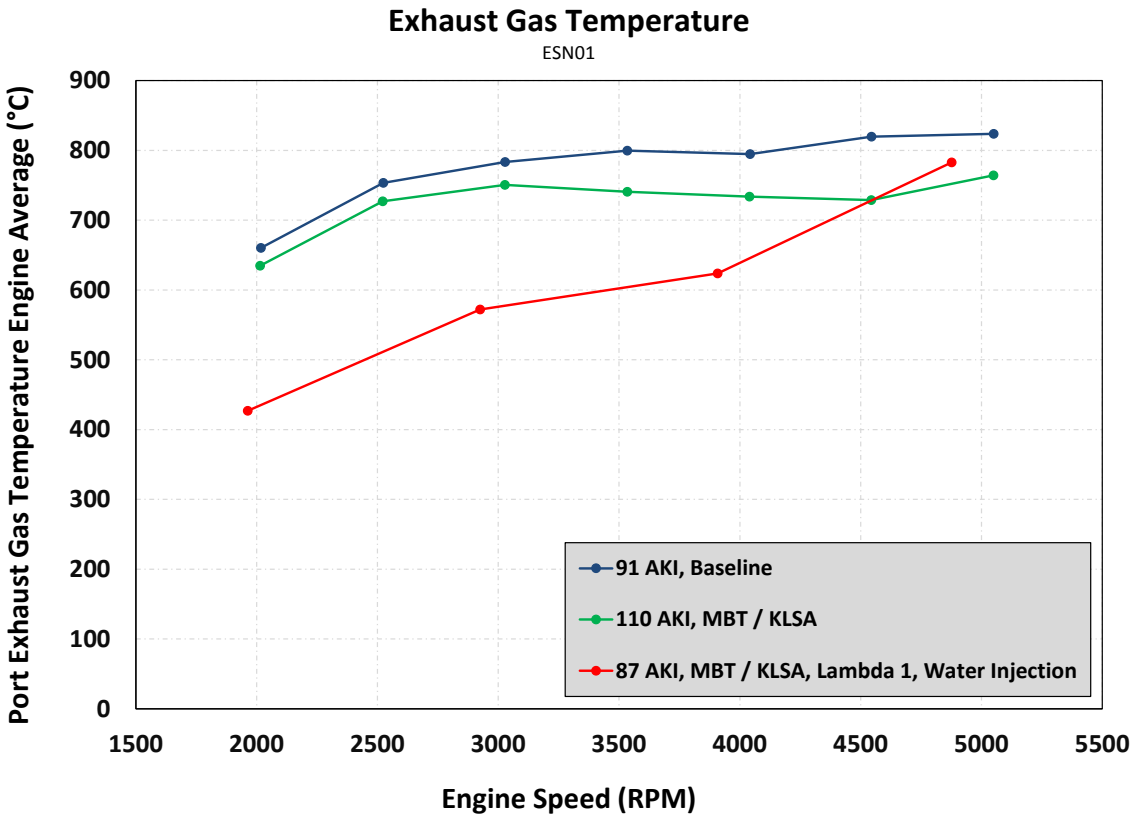

Figure 82: Engine Average Exhaust Gas Temperature measured in the exhaust manifold 15 mm downstream from the cylinder head exit. Reprinted with permission Copyright © 2017 SAE International. Further Distribution of this material is not permitted without prior permission from SAE. See 17 Appendix F for further details.

There are some potential implications of the reduced EGT on turbocharger system performance. The turbocharger turbine extracts exhaust enthalpy to drive the compressor. The enthalpy is a function of temperature, mass flow rate, and composition. As temperature drops, at least in theory, there could be a point where there is not sufficient exhaust enthalpy to drive the compressor. However, in this case, the temperature is dropping because of injection of water, therefore the temperature reduction is accompanied by an increase in mass flow rate, so these two effects counteract each other. In most cases there is an abundance of exhaust enthalpy available for extraction, such that the maximum boost is normally compressor limited, not turbine limited. This combined with the balancing between temperature and mass flow rate suggests this is not likely to be a concern for potential production application, but nonetheless is worth consideration.

As discussed in the Key Metrics section, water vapor is expected to impact the γ of both the unburned and burned gas. The Polytropic Compression / Expansion Index, n, is used as a proxy to assess changes to γ. The Polytropic Compression Index is shown in Figure 83. As a sense check, the data looks reasonable in that all values are below 1.4 (γ for pure air at 25°C). However, perhaps surprisingly, there is not a clear rank ordering, as one might expect. The polytropic index, as shown here is calculated from the cylinder pressure data with the first pressure point taken after the latest Intake Valve Closing (IVC) that was expected during this testing, and the last point take before the earliest ignition point expected during this testing (including part load). To be specific, the calculation window for the Polytropic Compression Index was 90° to 60° BTDC.

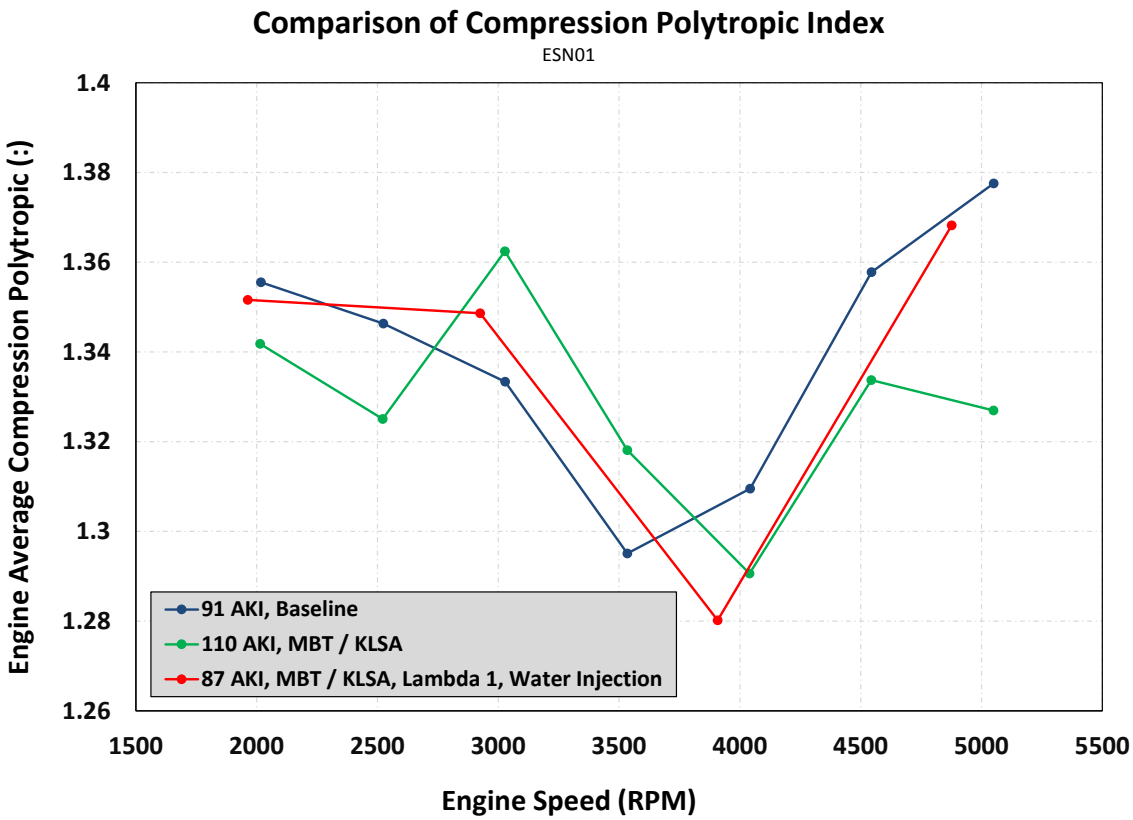

Figure 83: Comparison of Polytropic Compression Index.

Recalling previous discussion, the γ of air will increase as temperature decreases. Although this increase in γ is expected to be subtle compared to the decrease from the additional water vapor, it is at least directionally counteracted the expected decrease in γ. The other thing that needs to be considered is how much water is actually vaporized up to this point in the cycle. The CAC was effective at maintaining relatively low Inlet Air Temperature of near 25°C. Combine this with the fact that the air has a lower water saturation point as the pressure is increased, and recalling that these tests are run at nominally 2.5 bar MAP, may lead one to suspect that the inlet air simply cannot hold a substantial amount of water. Additionally, recall that the water injection duration was either full-cycle (720° CA), or near full-cycle and it is easy to imaging very cold inlet valves and intake port walls. These realizations, combined with the lack of any apparent rank ordering with respect to the Polytropic Compression Index, may lead one to surmise that a relatively small amount of water is vaporized prior to 60° BTDC.

One thing that can be said in certainty is that although several researchers predicted reduced compression work with water injection, these results simply do not support this claim. This is most evident by noting the similarity in slope and magnitude in the compression lines shown in Figure 65.4

The Polytropic Expansion Index is a proxy for the γ of the burned gas, and is calculated on the expansion stroke with the window starting after the longest combustion duration expected is assumed to be over, and before the earliest Exhaust Valve Opening (EVO). A comparison of Polytropic Expansion Index is shown Figure 84. Here, unlike with the Polytropic Compression Index, there appears to be a clear rank ordering present.

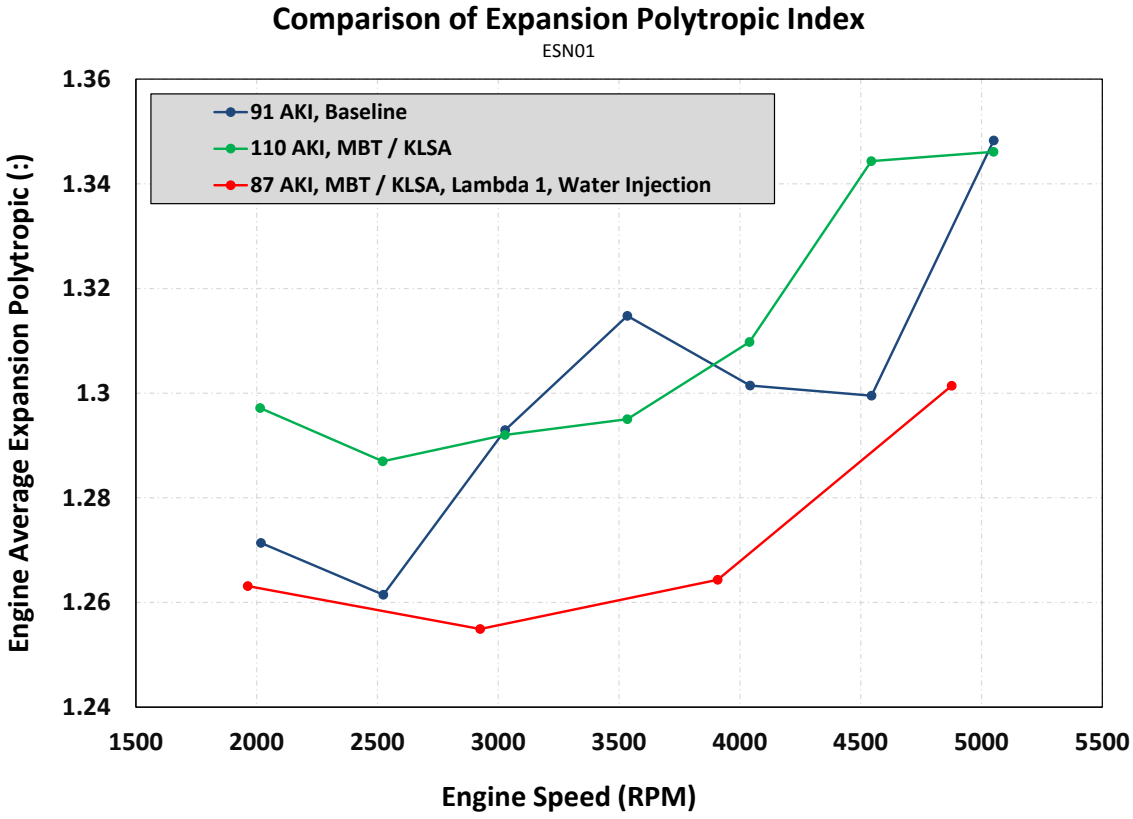

Figure 84: Comparison of Polytropic Expansion Index.

Like on the compression stroke, a cooling of the burned gases would at least directionally tend to increase γ, but here, the polytropic expansion index is significantly lower in the water injected case. The implication being that there is a significant amount of water in a vapor state during the expansion stroke. Together, Figure 83 and Figure 84 suggest that, at least at the inlet air temperature and manifold pressure run during these experiments, ***the bulk of the liquid water vaporizes during the high-temperature combustion process.***

As has been discussed multiple times in this dissertation, the injection of water is expected to impact volumetric efficiency through charge cooling. The volumetric efficiency referenced to ambient conditions is plotted in Figure 85. This overall "system level" volumetric efficiency as referenced to ambient temperature and pressure is well above 100% because the engine is turbocharged. The water injection case results in a significant improvement in volumetric efficiency; on average approximately 25 percentage points. It must be noted however, that the water injection case that has been the primary focus up to this point (the case with lambda = 1) was run with an air to liquid Charge Air Cooler (CAC). The air to liquid CAC enabled lower air inlet temperature at the throttle body, therefore at jjjjleast a portion of the improvement in volumetric efficiency of the system, as the cooler temperature corresponds to densified air.

As a comparison, another case is plotted in Figure 85, this case with 87 AKI fuel, MBT / KLSA, and with water injection, but with the lambda set to match the production calibration. This case is shown here for comparison purposes because it was run with the same air to air CAC as the baseline and 110 AKI cases[44]. Here it can be shown that although lower on average, the water injected case with the air to air CAC resulted in a volumetric efficiency similar to the water injected case with the air to liquid CAC.

[44] The air to air CAC was replaced with an Air to building water CAC after the test case with 87 AKI fuel, MBT/KLSA, production lambda, and water injection. The air to building water CAC was used in conjunction with a closed loop PID controlled water valve to maintain a setpoint inlet air temperature. This was done to improve data consistency, but moreover, as the testing went on, octane lowered, water injected, and with the direction moving toward stoichiometric operation, the engine became increasingly difficult to operate, and at an increasing risk of catastrophic engine failure. Having closed loop control of inlet air temperature allowed faster test stabilization, and made the engine slightly easier to operate.

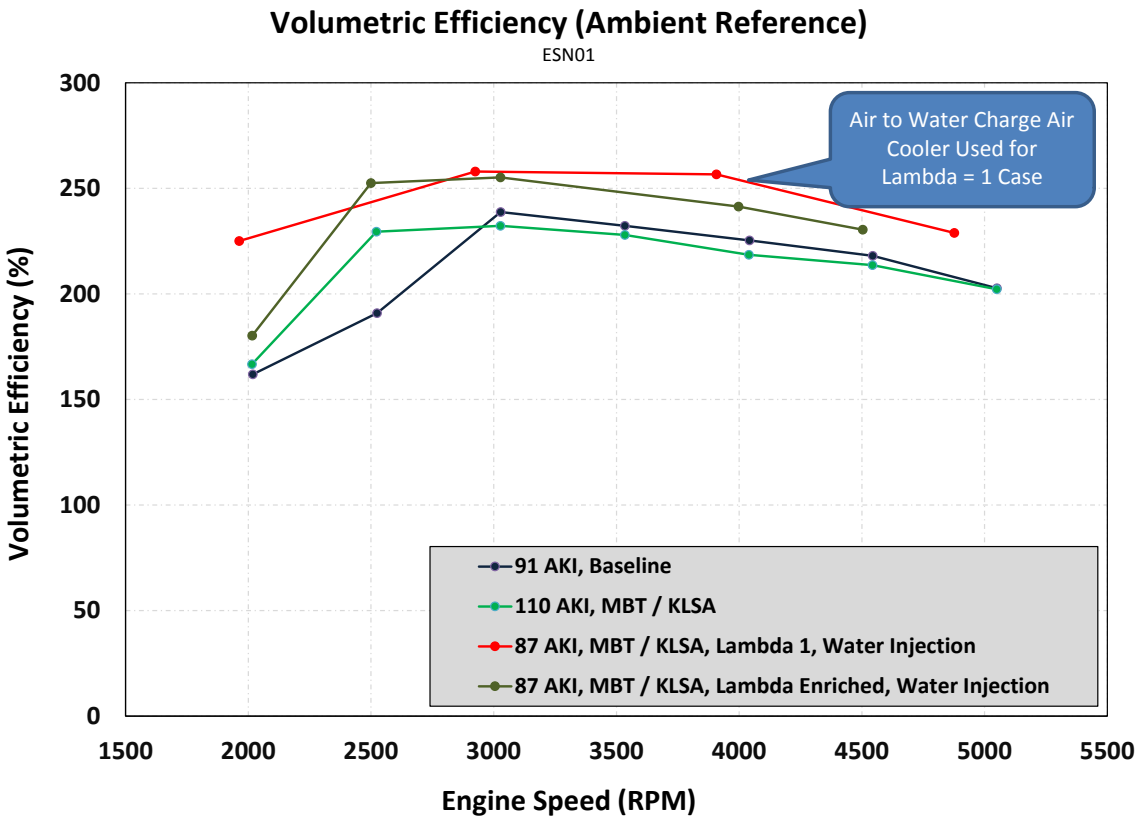

Figure 85: Volumetric Efficiency referenced to ambient temperature and pressure.

Continuing the comparison of volumetric efficiency, Figure 86, examines volumetric efficiency as referenced to conditions (temperature and pressure) inside the intake manifold plenum. Here, the nominal volumetric efficiency is near 100%, as the turbocharger is outside of the analysis volume. The water injected case once again shows the highest volumetric efficiency, but the difference is much smaller than when looking at the whole system. The reason for this may be that the plenum temperature is reduced by the water injection which occurs only slightly downstream of the temperature measurement location. Therefore the ideal trapping at the reference conditions is already rather high because the temperature reference already accounts for some of the cooling. Computing volumetric efficiency referenced to the plenum pressure, but the temperature at the CAC outlet (unlikely to be affected by water injection) would be an interesting comparison. However, unfortunately, the CAC outlet temperature is not available for any of the water injection cases.

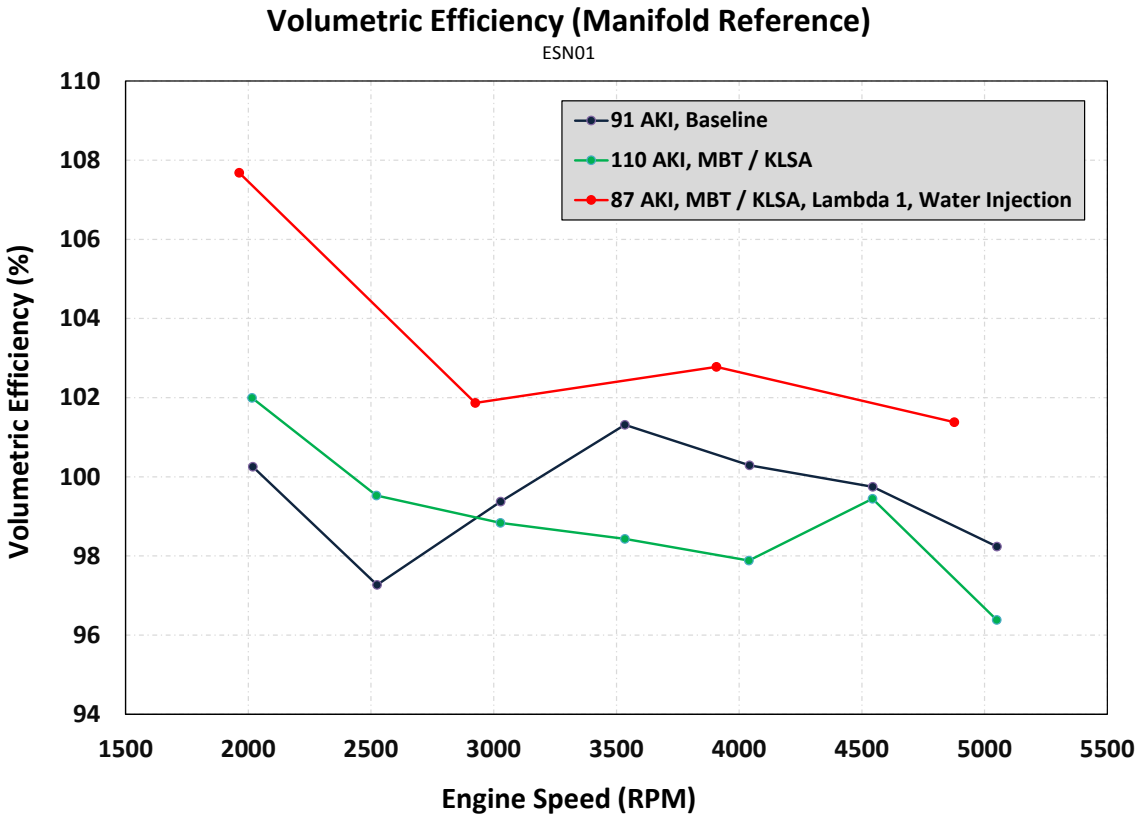

Figure 86: Volumetric Efficiency referenced to conditions in the intake manifold plenum.

It is interesting to compare the volumetric efficiency results with the polytropic index / gamma. Going back to the discussion around Figure 83 and Figure 84 the conclusion was that very little water vaporized prior to start of combustion. Yet the volumetric efficiency shown in Figure 85 and Figure 86 clearly show in improvement in volumetric efficiency. Although this discrepancy is difficult to resolve without further analysis, one obvious explanation may be that volumetric efficiency, through charge cooling, is very sensitive to the water vaporization, while changes in gamma are less sensitive.

Examining again Table 2 and Table 3 this seems at least plausible as the water has a very high enthalpy of vaporization on a mass basis, yet pure water vapor has a gamma only 0.07

lower than pure air, and the water injected cases are certainly not close to pure water. The water to air ratio can be determined according to Equation 28.

Equation 28: Water to Air Ratio.

$$\frac{W}{A} = \frac{\left(\frac{W}{F}\right)}{\left(\frac{A}{F}\right)}$$

Where :
W/F is the Water to Fuel Ratio
A/F is the Air to Fuel Ratio

Referring again to Figure 70, the nominal water to fuel ratio can be approximated as 3:1. For lambda = 1.0 operation with a fuel that has a stoichiometric A/F of approximately 14.5:1 the water to air ratio is nominally 0.20. Assuming gamma changes linearly with the addition of water vapor, the gamma of the mixture can be approximated by linear interpolation between pure air and pure water vapor. This results in a decrease in gamma be ***less than 0.015 if all of the water injected vaporized***. Based on this, and that it is unlikely that all of the water vaporized, it is plausible to see a change in volumetric efficiency without a significant corresponding change in gamma.

Another factor that should at least be considered is the change in saturation point after IVC. The polytropic index is calculated after IVC and before ignition, and over this period of time the saturation point of the air / fuel / water mixture is changing as a function of both temperature and pressure. The rise in pressure will tend to decrease the saturation point, while the corresponding rise in temperature will tend to increase it. So it ***might*** be possible for some water to condense back to a liquid during compression. To answer this definitively however requires further analysis of the psychrometric conditions inside the cylinder, and the compression work, as condensing water will transfer the enthalpy of vaporization back into the working fluid.

The final impact of the water injection on Net Thermal Efficiency and Indicated Thermal Efficiency is shown in Figure 87 and Figure 88 respectively. These two efficiency metrics differ by the differences in pumping work, as one is computed relative to net work, and one relative to indicated work (refer again to the section on key metrics used).

Although the magnitude of the efficiency is slightly different, the rank ordering is consistent between the two, as pumping work is overall relatively low compared to indicated work at this operating condition.

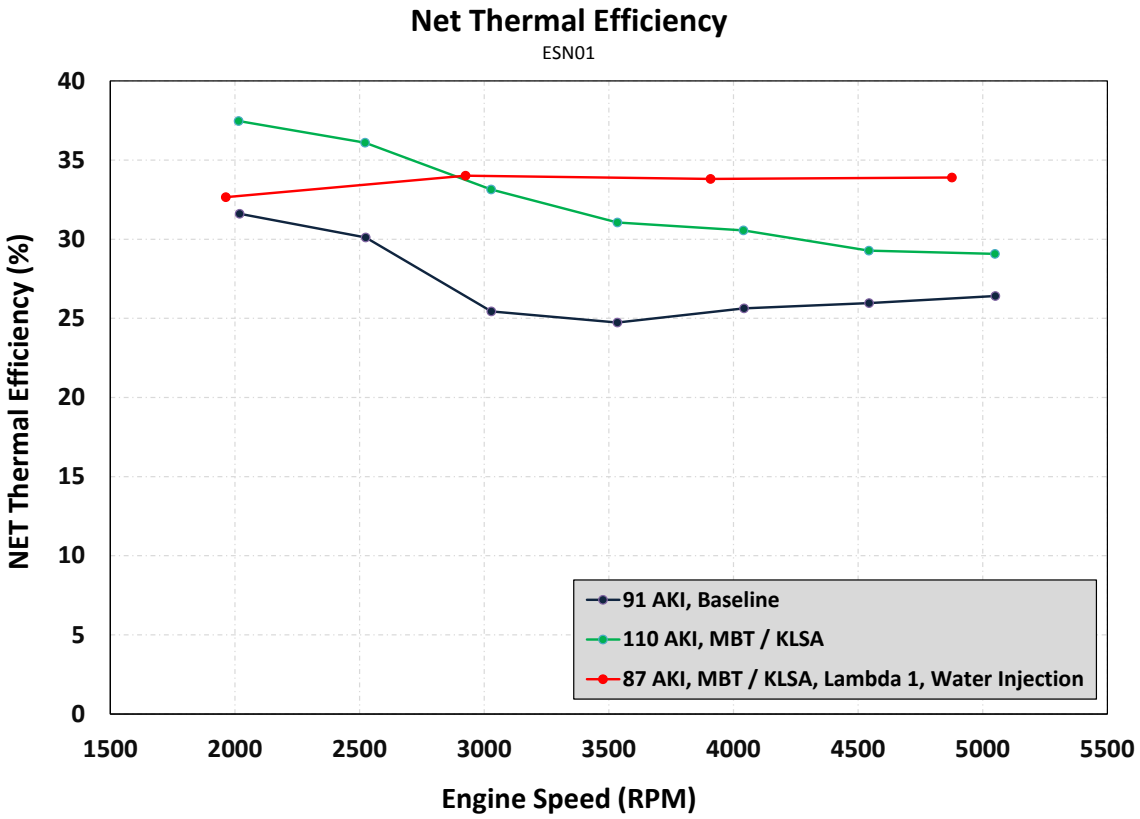

Figure 87: Impact of water injection on Net Thermal Efficiency. Reprinted with permission Copyright © 2017 SAE International. Further Distribution of this material is not permitted without prior permission from SAE. See 17 Appendix F for further details.

Here it is shown that the water injection resulted in a very significant improvement in efficiency over the baseline case. In terms of Net Thermal Efficiency, the maximum improvement is 34% at 3000 RPM. The maximum improvement in indicated efficiency is 35% at 3000 RPM. In both cases the improvement in efficiency comes primarily from a combination of more favorable combustion phasing and reduced fuel enrichment. Reduced combustion and expansion temperature will also reduce heat loss which would tend to improve efficiency. Recall from Equation 5 the change in gamma will actually tend to decrease ideal cycle efficiency. The reason the improvement was slightly less in Net Thermal Efficiency is because the water injection case required an increase in pumping work. Referring to Figure 80, water injected added as much as 3.9 kW in the power required to pump air / exhaust in and out of the engine at 5000 RPM and 1.8 kW at 3000 RPM. So in other words, the benefit of more advantageous combustion phasing, and stoichiometric A/F that is seen in the Indicated Efficiency comes at the price of increased pumping work, although the net result is still highly favorable.

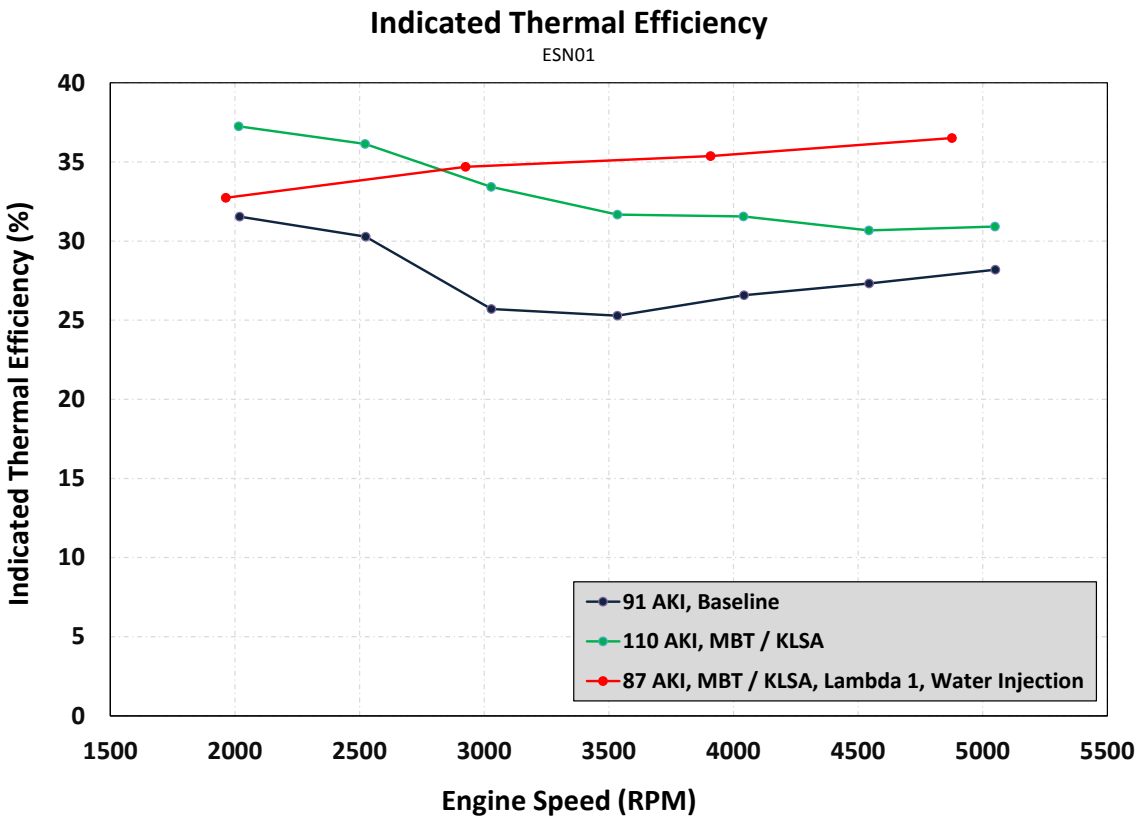

Figure 88: Impact of Water Injection on Indicated Thermal Efficiency.

These efficiency results are substantial. Although, on-cycle vehicle fuel consumption would not improve nearly this much because of the high amount of low load operation on the regulatory drive cycles, these results do show significant opportunity.

Knowing that the improvement in efficiency comes primarily from reduced heat transfer, improved combustion phasing, and elimination of fuel enrichment it is informative to attempt to separate out these effects. Because there was a water injection case run with fuel enrichment, an opportunity exists to further dissect these results. Figure 89 is the same data as Figure 88 except the water injection case that was run with fuel enrichment is included. Here it is shown that even with fuel enrichment, the water injection leads to an improvement in thermal efficiency over the baseline case. This is due to the improvement in combustion phasing (and presumably reduced heat loss). However, this improvement is less than half of the total improvement between the baseline and the water injected

stoichiometric case (this is in addition to the combustion phasing of the enriched water injection case being more optimal than the lambda 1 water injection case). Because this case also has the presumed reduction in heat loss, this implies the single biggest factor affecting thermal efficiency is the enablement of stoichiometric operation.

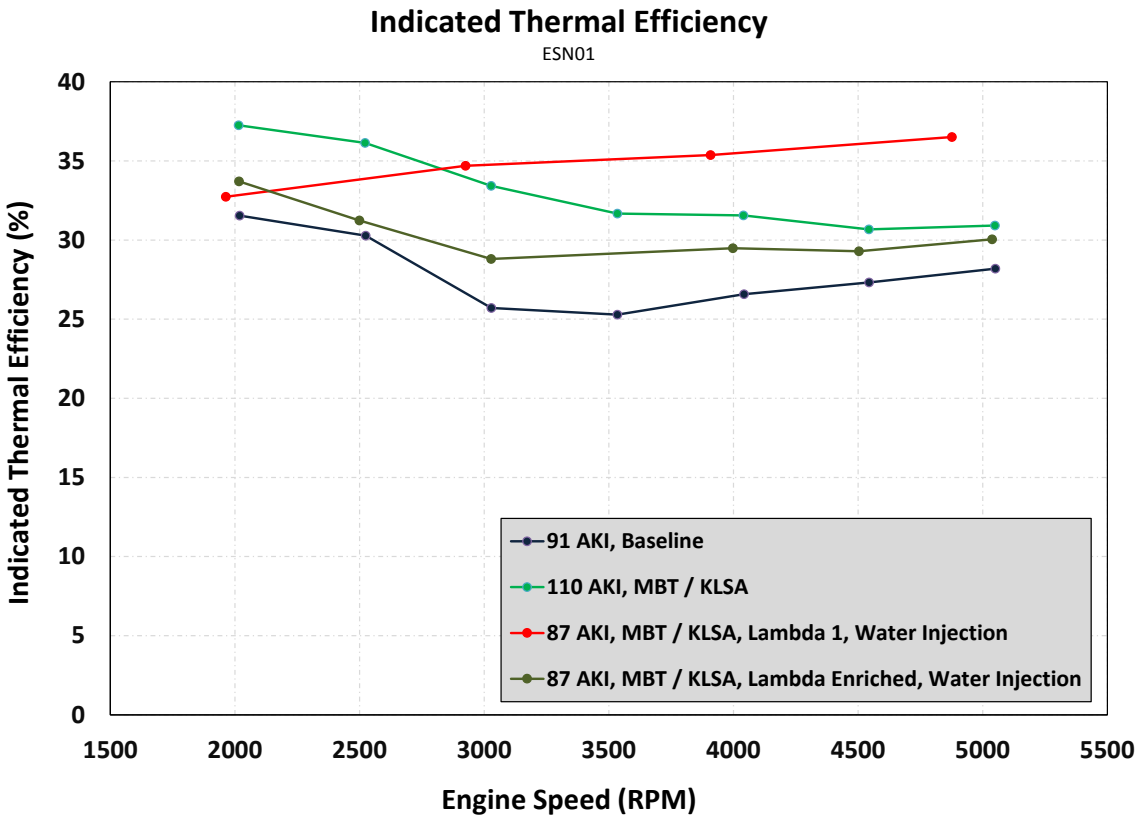

Figure 89: Impact of Water Injection on Indicated Thermal Efficiency, including water injection with and without fuel enrichment.

As was discussed in the section on experimental setup, it was expected that peak cylinder pressure may exceed the limit for the production pistons, which was recommended to be 150 bar (Blaxill 2015). Figure 90 plots the engine average (average of 4 cylinders) peak cylinder pressure averaged over the entire 300 cycle test. Here it is shown that the 110 AKI case is very close to the recommended design bogey, with cylinder pressure of 146 bar over much of the speed range tested. One must also realize with this plot being the average of 300 cycles of data, and the average of all four cylinders undoubtedly there are

many individual combustion events taking place that exceed (probably by a significant margin) the recommended upper cylinder pressure threshold. This data further reinforces the need to move to forged pistons for the testing at MAP > 250 kPa as was done with ESN02.

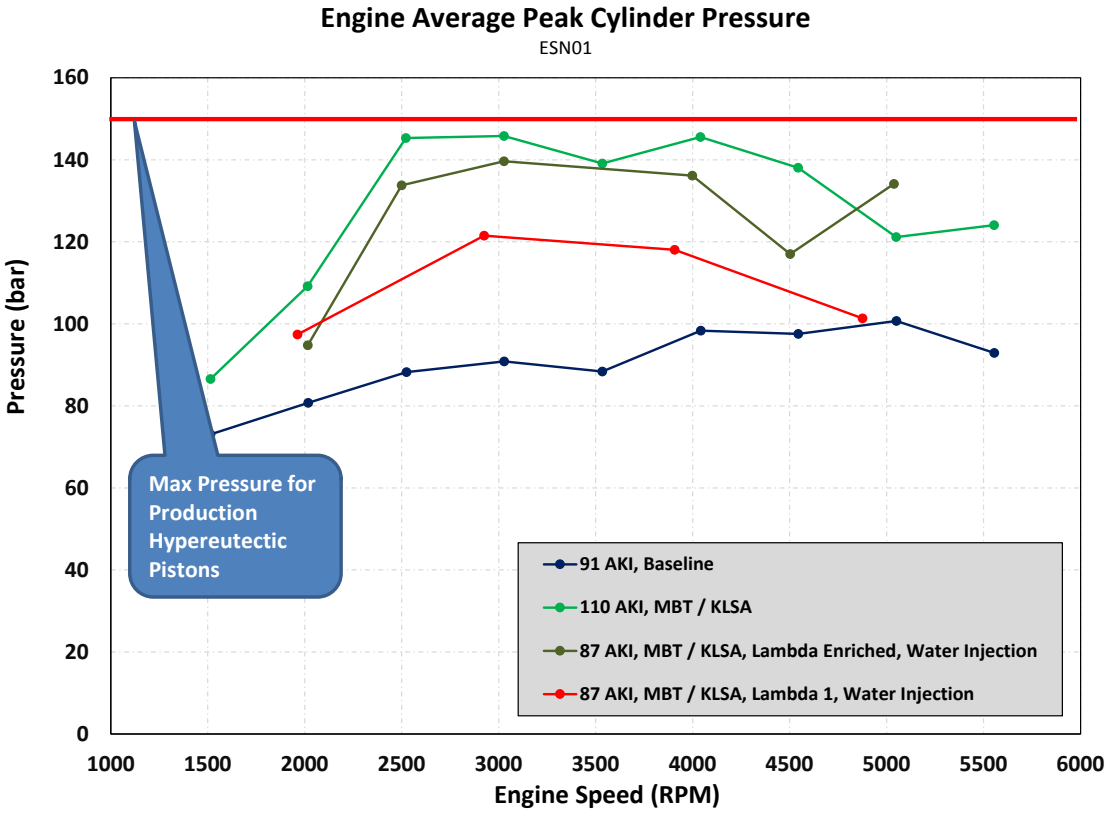

Figure 90: Engine Average Peak Cylinder Pressure.

6.2.2 Test Results at 300 kPa MAP

Engine 2 (ESN02) was setup and run in support of project objective 2.3, to demonstrate operation at manifold pressure levels at least 10% greater than current production for an engine at near best in class BMEP (i.e. the base engine for this work). Details on the build and setup of ESN02 are included in the experimental setup section. For these tests, the decision was made to run ESN02 at 300 kPa MAP, an increase of 20% over the baseline

case at 3000 RPM, and 50% over the baseline at 2000 RPM. As discussed previously, because of the limitations of available turbochargers, the engine was modified to remove the turbocharger and run an external boost rig. The decision was made to run this testing with 91 AKI fuel. Although considered a premium grade fuel, 91 AKI is widely available at filling stations, and is not typically the highest ON fuel at the pump, therefore is still considered a consumer grade fuel. The lambda for these tests, both with and without water, as set to 1.0 for all speeds. Spark timing was adjusted to MBT or KLSA whichever came first.

The comparison of observed (i.e. not corrected to standard SAE conditions) is shown in Figure 91. Here it can be seen that at 3000 RPM, brake torque reached 552 n-m[45].

[45] Although the dynamometer has steady state capacity to 800 n-m, the dynamometer would loose control, allowing the engine speed to rapidly increase if the boost was applied too abruptly. This made running this point difficult as the boost from the compressed air boost rig needed to be engaged rather quickly to avoid wasting the high pressure air stored in the buildings tanks. Much trial and error was required, and two operators were absolutely required.

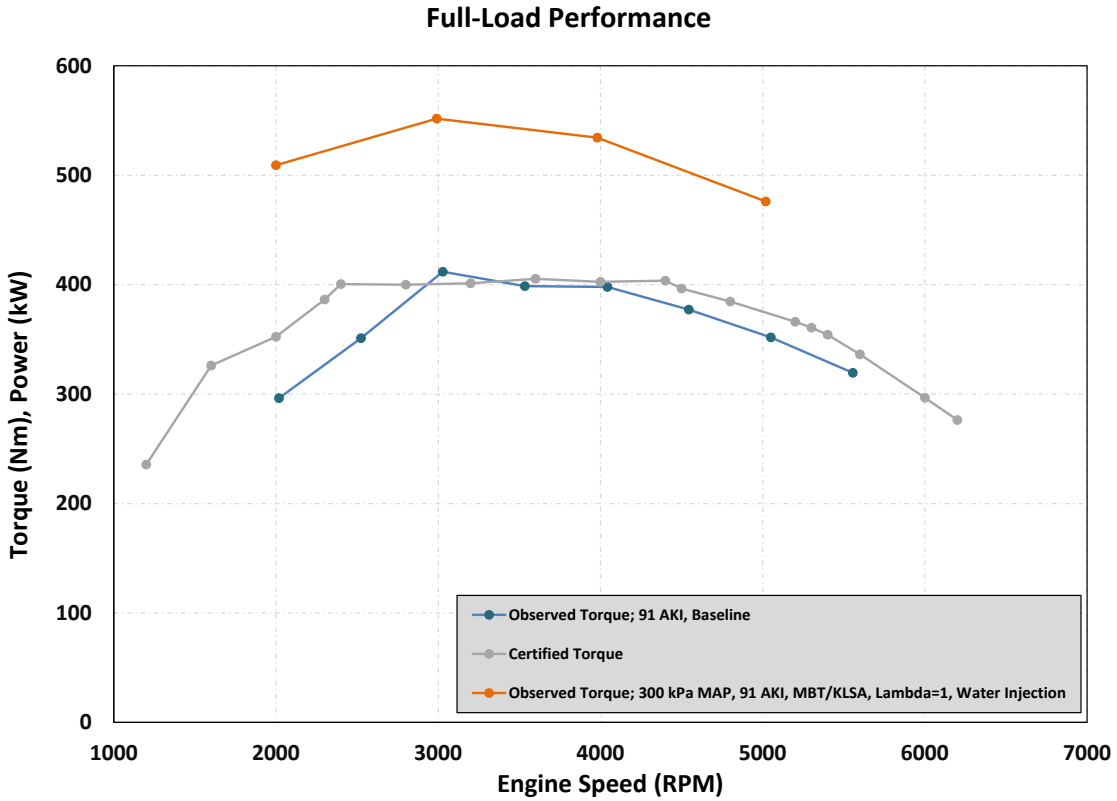

Figure 91: Comparison of Full Load Brake Torque between the SAE Certified and Baseline cases with the case boosted to 300 kPa MAP with Water Injection.

At 3000 RPM, the 20% increase in MAP resulted in a 35% increase in BMEP, with peak BMEP of ~35 bar, Figure 92. Moreover, this peak BMEP of 35 bar enabled by water injection is greater than the highest BMEP of 2017 MY production engines by a significant margin.

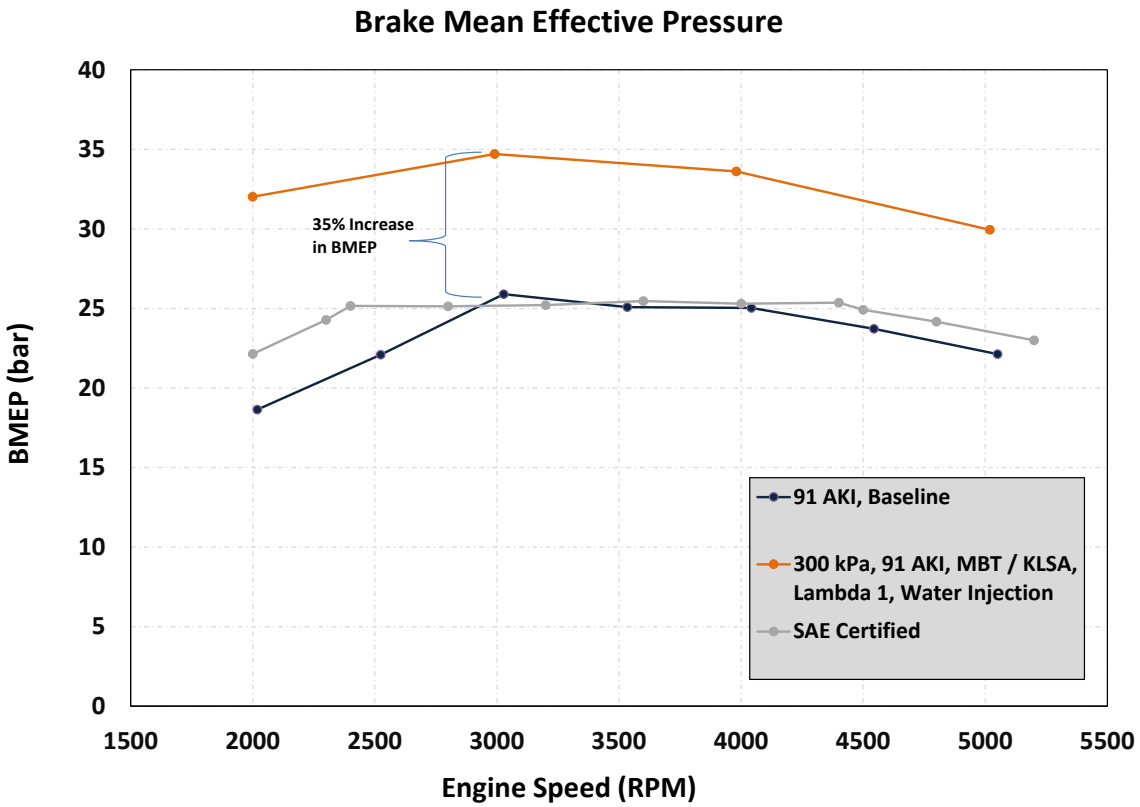

Figure 92: BMEP at 300 kPa MAP Compared to Baseline and SAE Certified BMEP.

Although Figure 92 is exciting, one must be careful with the results. It is important to remember that the 300 kPa MAP test was run with boost generated from an electric air compressor in the building, and there was not a turbine in the exhaust stream. As a result, PMEP was positive, effectively adding work on the intake stroke, without the penalty on the exhaust stroke that the turbine adds. Therefore, BMEP, and even NMEP are difficult to compare directly. The most direct comparison needs to be done with IMEP as is done in Figure 93. Here the improvement in IMEP on a percentage basis was less. 15% and 19.4% at 3000 RPM and 4000 RPM respectively.

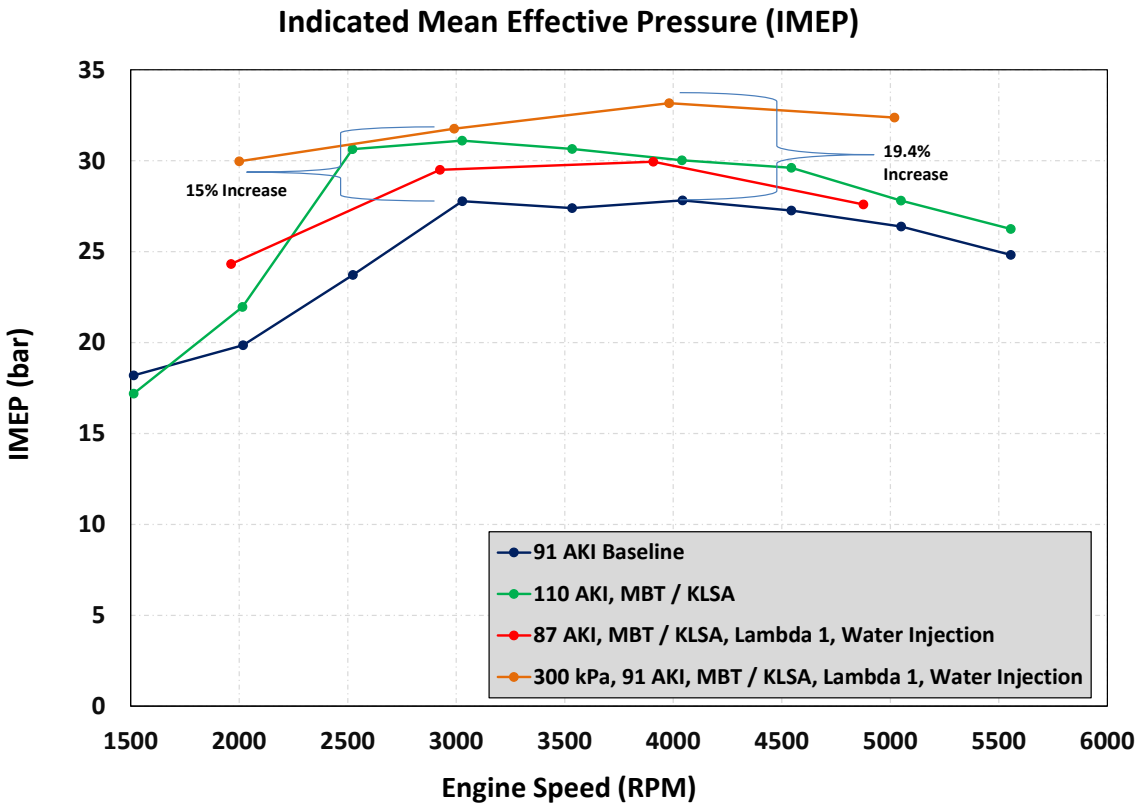

Figure 93: Comparison of IMEP between several cases run during this study.

On a percentage basis the increase in IMEP is much more in line with the increase in MAP, and in fact is slightly less. The same analysis that was done previously, by normalizing MEP to MAP, becomes even more important now with such a large change in MAP.

The IMEP normalized to MAP is shown in Figure 94. Here it is interesting to note that the 300 kPa MAP case resulted in the lowest normalized IMEP of any of the cases tested. Lower even than the baseline case. Therefore, although the increase in MAP did result in an increase in brake output, and even IMEP, the 300 kPa did not use the manifold pressure as effectively as the other cases.

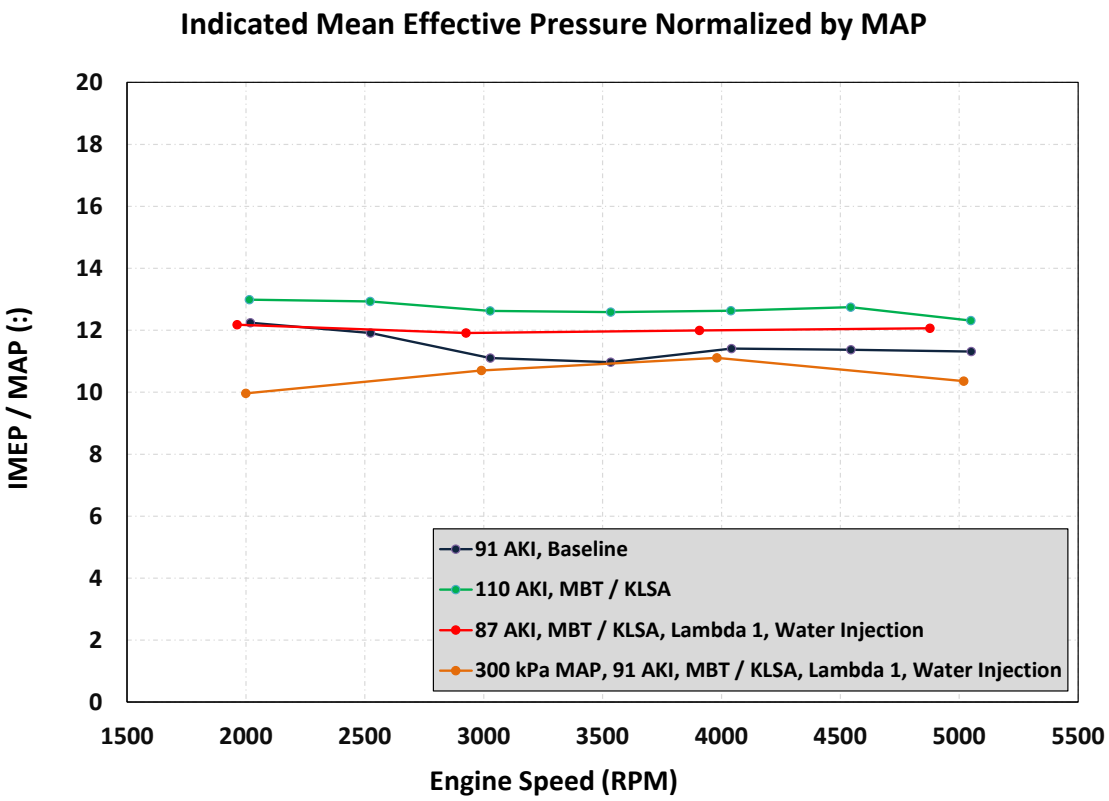

Figure 94: IMEP normalized by MAP for several cases in this study.

Pertinent flow rates are shown in Figure 95. As expected, the fuel flow rate was higher for the 300 kPa MAP test since both tests were run at lambda = 1. However, the water injection flow rate increased more than the fuel flow rate, resulting in a higher water to fuel ratio.

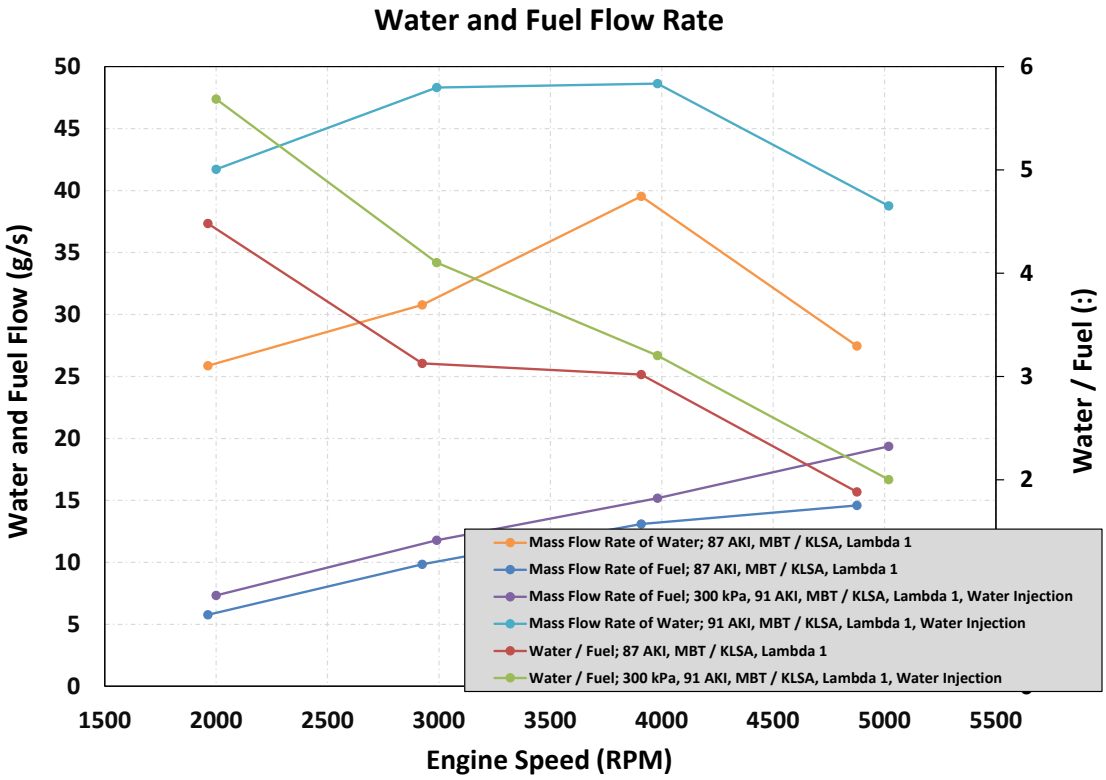

Figure 95: Comparison of the flow rates of water and fuel, and the Water to Fuel ratio between tests run at nominally 250 kPa MAP and 300 kPa MAP.

Combustion phasing, as indicated by CA50, is shown in Figure 96. Here it can be seen that combustion phasing was very close to MBT throughout most of the speed range. CA50 is rather late at 5000 RPM. For this particular base engine, 5000 RPM is not as robust from an ignition perspective as other speeds. This was observed early in the program, even when conducting baseline testing. With maximum amounts of water injection, as was the case in this testing, the combustion system exhibited high COV of IMEP, and even misfire at 5000 RPM as the combustion phasing was advanced. This high COV and misfire occurred well before the knock limit.

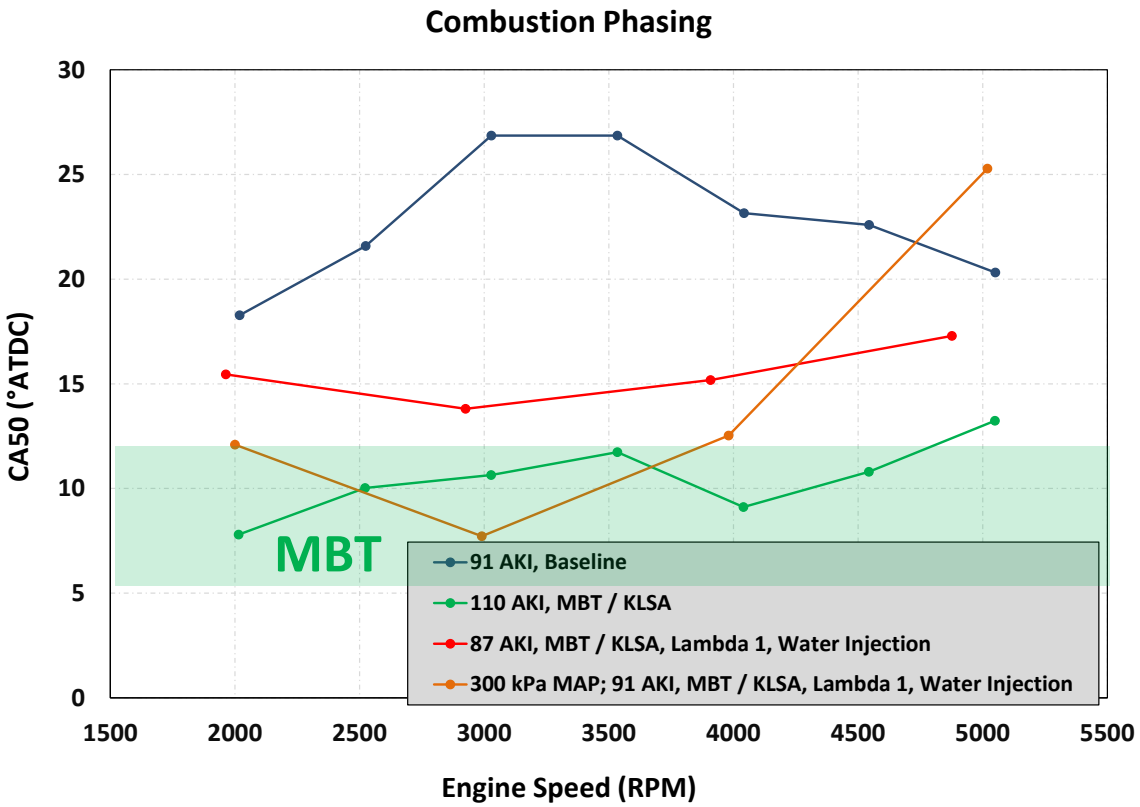

Figure 96: Comparison of Combustion phasing amount several test cases.

6.3 Water Vaporization

The discussion that follows includes a detailed analysis of the vaporization of the injected water in the engine cycle, and the implications on engine performance.

6.3.1 Water Vaporization during Intake and Compression

Figure 65 through Figure 67 and Figure 83 and Figure 84 suggest that not all of the water injected vaporizes prior to ignition. This notion will be explored in greater detail in this section. To simplify the analysis, the only operating condition that will examined will be 3000 RPM / Full Load. The analysis would be the same at other operating conditions.

Considering all of this testing is conducted with Port Injection of Water, a natural choice for an initial check is how much water the air inside the intake manifold will hold at its

saturation point. For the operating condition of interest (3000 RPM / Full Load) with the test case of 87 AKI, MBT / KLSA, and Lambda = 1.0, the air temperature in the intake manifold plenum immediately below the throttle body was 24.7°C, which will be approximated as 25°C. The pressure was the measured MAP of 248.5 kPa which will be approximated as 250 kPa. The most convenient analysis tool in this case is the psychrometric chart. The psychrometric chart for a water – air mixture was produced using the software package Engineering Equation Solver (EES) at 250 kPa (Klein 2017). This data is included in Figure 97 where the red cross hairs mark the saturation point at 25°C. The bottom of the figure tabulates the key data, where it can be seen that the humidity ratio (ω) is ~0.008 at the saturation condition. This indicates the air will hold 0.008 kg of water per kg of dry air without condensation, which is the Mass Water to Mass Air at saturation. Recall Equation 28, applied to this operating condition reveals a Water to Air ratio of 0.2. Furthermore, the computed Water to Air ratio of 0.2 does not account for the mass of water already in the induction air at ambient conditions. Therefore, the water to air ratio following injection in the intake manifold was more than 25 times greater than what could have actually vaporized into the intake air, and that assumes there was sufficient time to reach equilibrium. Based on this, there is no doubt that liquid water entered the cylinder. The conditions inside the cylinder at BDC are assumed to be exactly the same, relative to saturation, as no significant heat transfer is expected to take place at this speed and air flow rate.

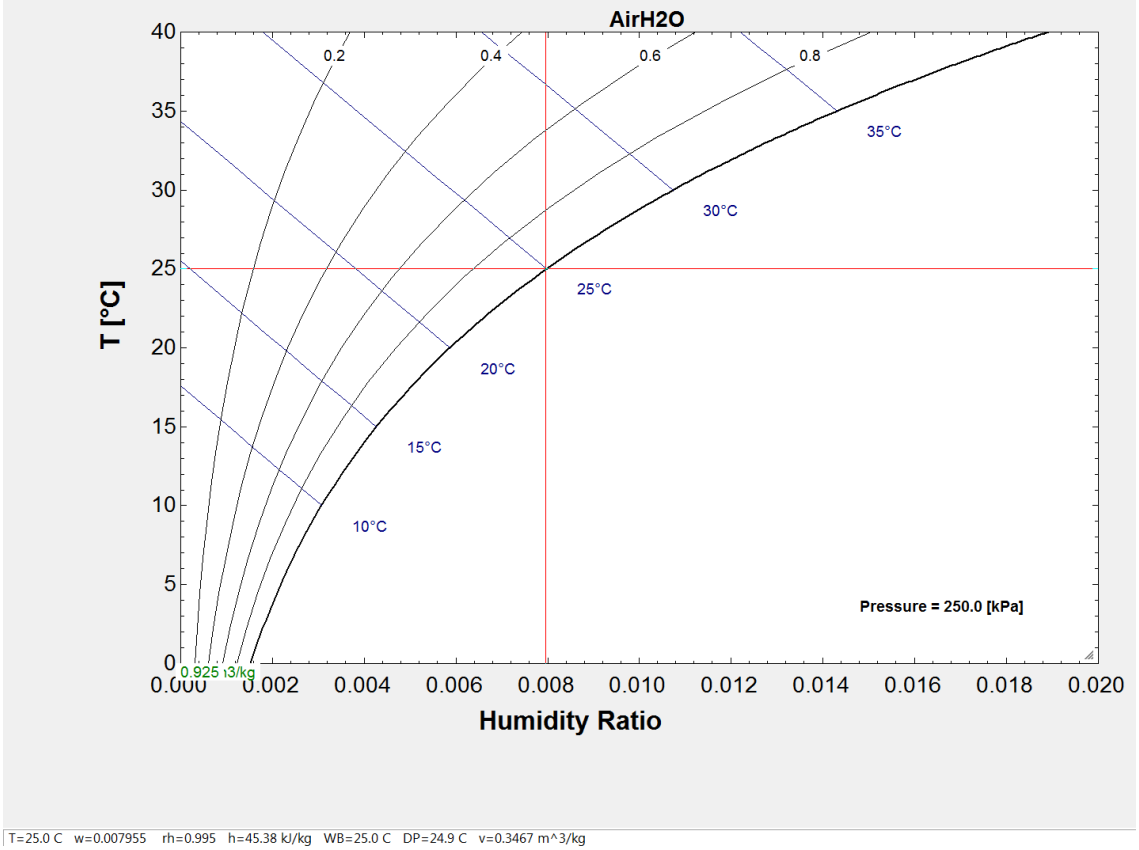

Figure 97: Psychrometric chart for an Air - Water Mixture at 250 kPa absolute pressure. Chart created using EES. Data source NASA Ideal Gas Database. Chart reproduced with permission; Klein, S.A., EES – Engineering Equation Solver, Version 10.278, 2017, F-Chart Software, http://fchart.com. See 17 Appendix F.

The next point that is natural to examine is Intake Valve Close (IVC). To do this, the pressure and temperature inside the cylinder at IVC must be determined. Figure 98 shows the cam lift for the intake and exhaust cam that was installed in ESN01 during this testing (production cams). This data is plotted such that the IMOP and EMOP are phased to match the production calibration under full-load operation at 3000 RPM, which is the same as was run during the experiment. Here the IVC point is taken as 235° CA $ATDC_{ge}$ which is the same as 125° CA BTDC. Referencing the tabulated Pressure and Volume data that generated Figure 65 reveals a cylinder pressure of 289 kPa and a cylinder volume of 4.8e-4 m^3.

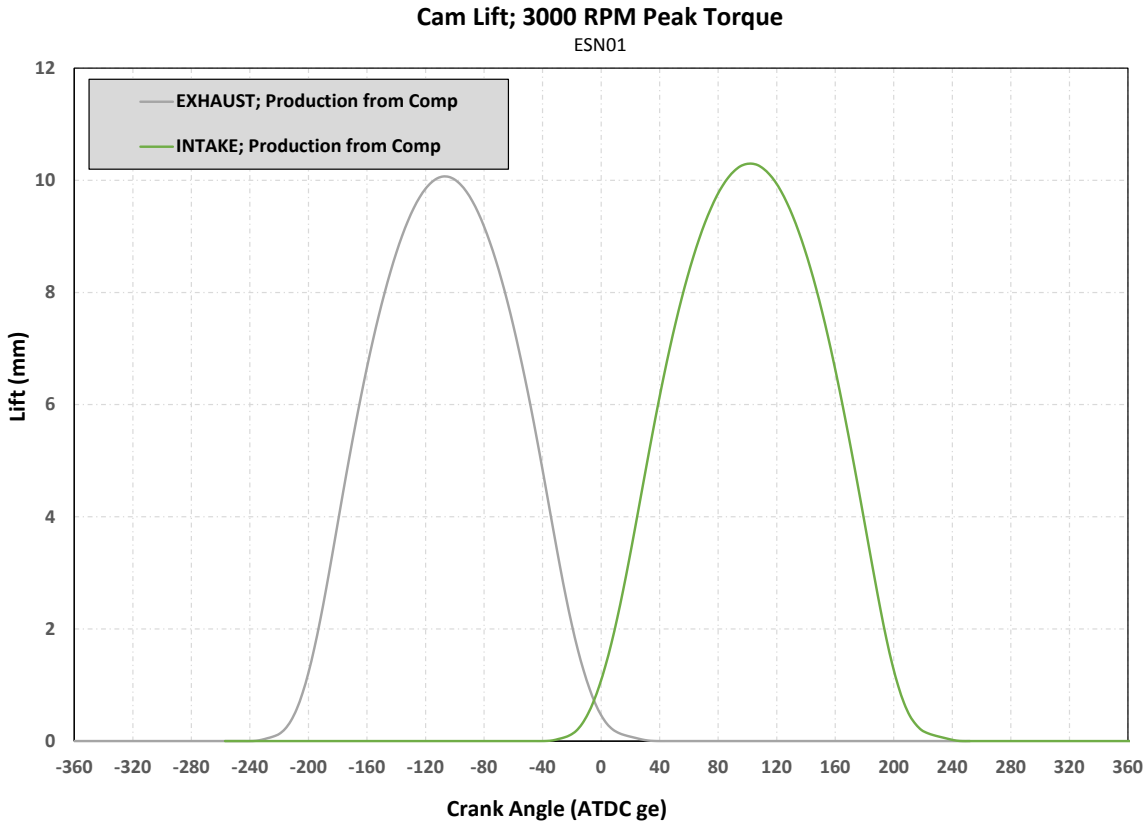

Figure 98: Intake and Exhaust cam lift, as phased according to the production calibration for peak torque at 3000 RPM.

The temperature can then be obtained through the Ideal Gas Law, Equation 29.

Equation 29: Ideal Gas Law solved for Temperature.

$$T = \frac{PV}{RM}$$

Where :

P = Pressure in kPa

V = Volume in m3

R = Gas Constant in kJ/kg - K

M = Total Mass of Gas

The mass used is the total mass inside the cylinder that behaves as an ideal gas. This is the mass of air, plus the mass of fuel, plus the mass of water that has vaporized. The mass of vaporized water is assumed to be the saturation mass at manifold conditions. The mass of air is obtained by Equation 22. With the mass of air known, the mass of fuel is obtained by Equation 30. Since the test was run at lambda = 1, the A/F is taken as 14.5:1.

Equation 30: Trapped Mass of Fuel.

$$m_{fuel} = \frac{m_{air}}{A/F}$$

The mass of water is not the mass of water injected, but rather the mass of water vaporized at this point. It is assumed that the air is saturated, thus the mass of vaporized water can be obtained by Equation 31. Here the ω for saturation is taken at 0.008, the value corresponding to intake manifold conditions.

Equation 31: Mass of Water Vapor at IVC.

$$m_{water} = m_{air} * \omega$$

Finally the total in-cylinder gas mass is obtained by Equation 32.

Equation 32: Total Mass In-Cylinder Behaving as an Ideal Gas.

$$m_{total\_gas} = m_{air} + m_{fuel} + m_{water}$$

Finally the temperature can be calculated, Equation 29, resulting in 48°C. The last step in fixing the water state in the cylinder is to determine the specific volume. In a liquid – vapor mix, the specific volume includes the mass of the liquid and vapor. Therefore in this case it is the total trapped water mass. The total trapped water mass is obtained in the same manner as the trapped air mass knowing the water flow rate and engine speed (Equation 22), resulting in $2.93e^{-4}$ kg of trapped total water. With the total trapped water mass and

cylinder volume at IVC known the specific volume is obtained by Equation 33 and is found to be 1.64.

Equation 33: Specific Volume of Water in the Cylinder.

$$v = \frac{V_i}{m_{water}}$$

Where :

V_i = Instantaneous Cylinder Volume at the Point of Interest

m_{water} = Total Mass of Water (Liquid + Vapor)

The equilibrium state at this condition is best assessed with a T-v diagram. EES was used to create a T-v diagram showing where the in-cylinder condition at IVC lies relative to saturation. This condition is depicted in Figure 99 where it can be seen that the in-cylinder conditions at IVC lie within the vapor dome[46]. It is important to note the Log scale, as the actual quality (x) is 0.12, lower than it appears at first glance. This means that at IVC, if equilibrium is reached, only 12% of the total trapped water mass has vaporized.

[46] The isobaric lines are saturation pressure not total pressure. They are included for reference. 1 kPa is the partial pressure of water at SAE standard engine test conditions at 101 kPa total barometric pressure, 3.2 kPa is the partial pressure at saturation at 25°C, and 11.2 kPa is the partial pressure for saturation at IVC conditions.

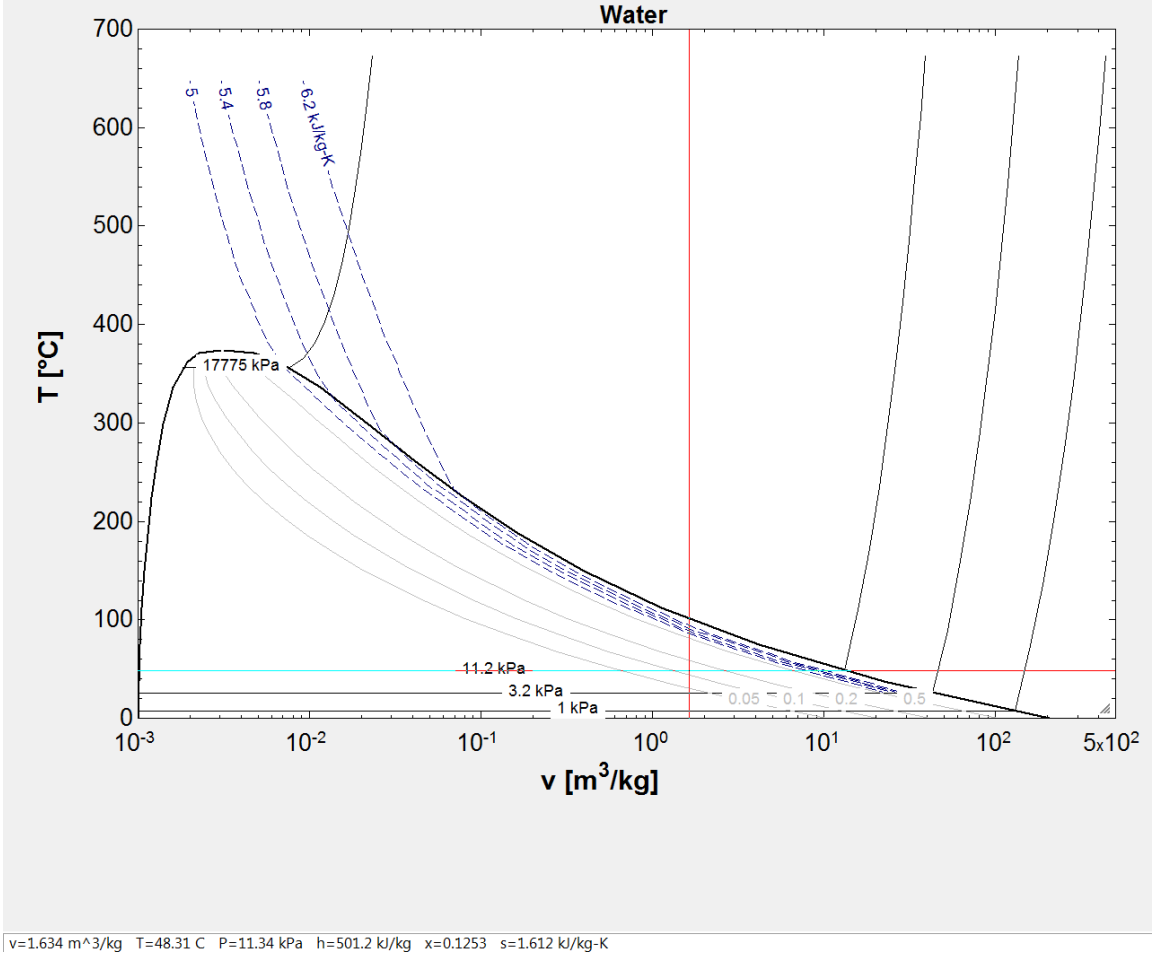

Figure 99: T-v diagram for Water. Cross-hairs indicate in-cylinder conditions at IVC. Chart created using EES. Data source NASA Ideal Gas Database. Chart reproduced with permission; Klein, S.A., EES – Engineering Equation Solver, Version 10.278, 2017, F-Chart Software, http://fchart.com. See 17 Appendix F.

The condition at ignition is evaluated next. The crank angle of ignition is known from the measured data. This is used to determine the cylinder pressure at ignition. The temperature at ignition is evaluated according to Equation 17, with the Polytropic Compression Index determined from Figure 83. This results in a temperature at ignition of 330°C. Specific volume is computed knowing the actual cylinder volume at Ignition, and the total mass of trapped water as previously discussed. The equilibrium state at this condition is depicted in Figure 100.

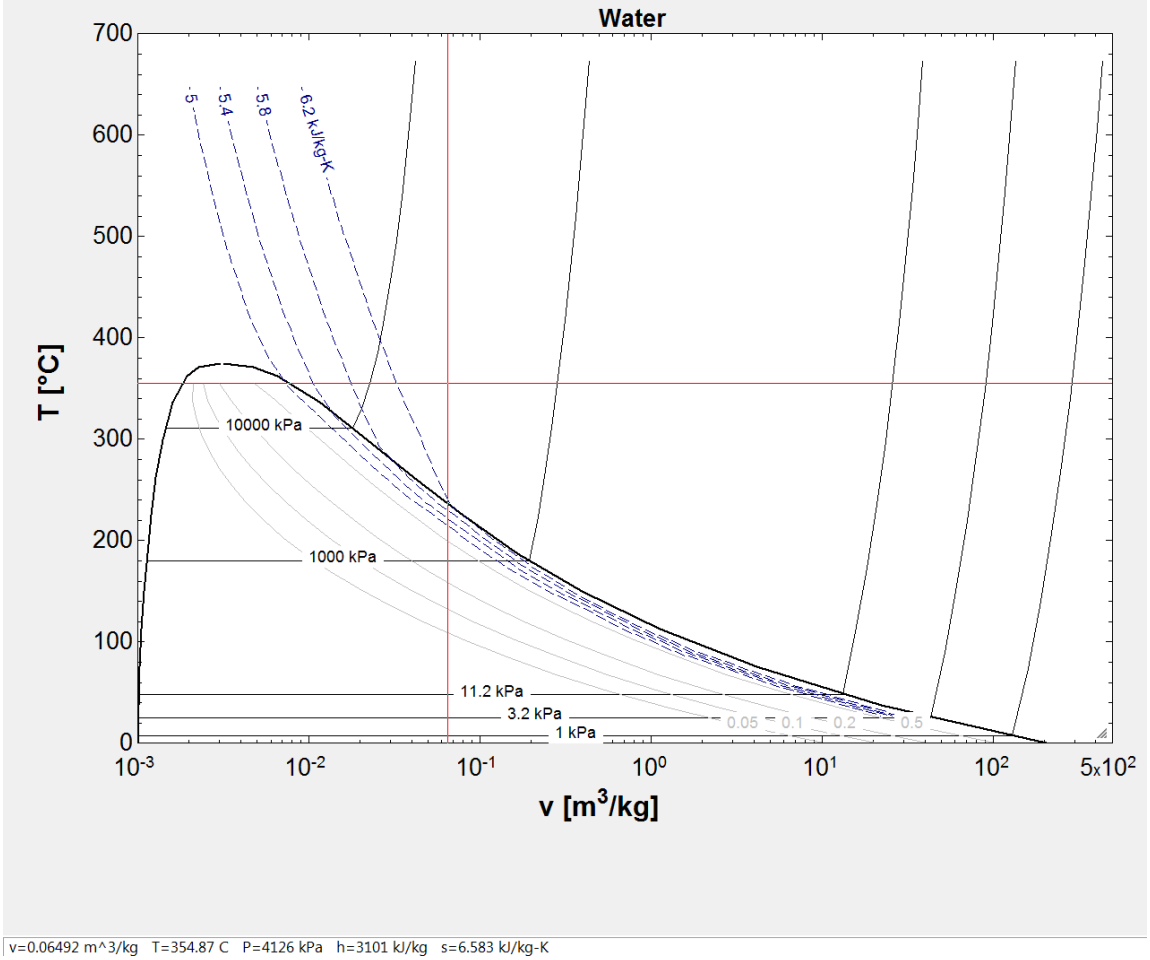

Figure 100: T-v diagram of water. Cross hairs depict state condition of water in the cylinder at the time of Ignition. Chart created using EES. Data source NASA Ideal Gas Database. Chart reproduced with permission; Klein, S.A., EES – Engineering Equation Solver, Version 10.278, 2017, F-Chart Software, http://fchart.com. See 17 Appendix F for further details.

The state at ignition is interesting because the conditions support full vaporization of water in equilibrium (the point is completely out of the vapor dome into the superheated region). However, it remains unclear how much water actually has vaporized to this point. Figure 65 through Figure 67 and Figure 83 do not show a noticeable difference in the Polytropic Index of Compression. In fact, the Log-Log plots in Figure 67 show very straight lines, indicating the Polytropic Index of Compression is not changing during the compression stroke, which may lead one to surmise water is not actually vaporizing, even though Figure 100 indicates it ***could*** vaporize.

Several factors must be considered. First, as the water vaporizes, the gamma of the mixture will decrease, as will the temperature due to the enthalpy of vaporization. Both of these factors would tend to reduce the Polytropic Index, but may be balanced by the increase in pressure from the additional mass in the gas phase, which would tend to increase the Polytropic Index. These factors may simply balance each other.

The other factor to consider is that although the water can fully vaporize ***if the system reaches equilibrium***, it might not ever reach equilibrium given the time scale during the compression stroke. As shown in Figure 99 and Figure 100, at IVC the equilibrium state is only 12% quality, so there is a significant amount of water that must be evaporated by ignition to reach the equilibrium state. The crank angle duration between IVC and Ignition at this condition is 100° CA. At 3000 RPM this occurs over a span of 0.56 ms as determined from Equation 34.

Equation 34: Time Interval Corresponding to a Crank Angle Interval

$$\Delta T = \frac{\Delta CA * 60 * 100}{N * 360}$$

Where :
ΔCA = Crank Angle Interval
N = Engine Speed in RPM

In assessing the feasibility of water to fully vaporize between IVC and IGN, a starting reference may be the familiar case of fuel injection. During Direct Injection of fuel, it is assumed common for all of the fuel to vaporize over a similar 0.56 ms duration, however, several factors are different and must be considered:

1. The mass of water to be vaporized over this time window exceeds the amount of fuel vaporized over a similar time window. Recall from Figure 70 that the water to fuel ratio at 3000 RPM is greater than 3:1[47].

2. When fuel is being vaporized it is assumed to be finely atomized spherical droplets. Since very little water vaporized in the intake port, the majority of the liquid water injected is likely condensed and pooled in the valve bowl area prior to IVO, and although there will be some breakup due to high velocity shear across the valve seat in the early stages of lift, the majority of the water is likely to enter the cylinder largely unatomized. Although the liquid water will be entering entrained with the charge air stream, it is assumed to largely fall out of suspension in the air stream when it impacts the cylinder wall and piston as part of the normal in-cylinder flow field (either as swirl or tumble), and therefore pooling on the piston and in the ring-pack crevice volume. This will result in the pool of water remaining cool (relative to a droplet suspended in hot compressed air), and with lower surface area to volume ratio than a spherical suspended droplet.

3. Full vaporization of a quantity of liquid cannot be complete until the enthalpy of vaporization has been transferred to the liquid. Table 2 points out that water has approximately 8 times more enthalpy of vaporization than gasoline, thus requiring more energy to be transferred into the liquid on a per unit mass basis than gasoline to achieve full vaporization.

[47] Even though some water is already in the vapor state at IVC, the quality is no greater than 12%.

To elaborate upon item 3 above; there is 2.9e-4 kg of water trapped in the cylinder, of which at most 12% has vaporized by IVC (equilibrium quality at IVC is 12%). Multiplying the mass by the enthalpy of vaporization[48] results in 655 J of energy required for this mass of water to vaporize compared to 33 J of energy required for the fuel mass to vaporize. This is a factor of 19 times more energy for the water. To put this into perspective further, the energy trapped within the cylinder from fuel is 4.2 kJ at this condition (assuming a typical 44 MJ/kg fuel LHV). Delivering this 655 J of energy over 0.56ms requires a power of 1169 kW. With the liquid water likely pooled on the cold piston and ring pack crevice, it is unlikely there will be enough Delta Temperature to deliver this power to the water. It is for these reasons, that even though the in-cylinder conditions support fully vaporized water at ignition in equilibrium, it is felt that the system has not yet reached equilibrium by the point of ignition, and thus there remains some quantity of liquid water in the cylinder.

6.3.2 Water Vaporization during Combustion and Expansion

It is also informative to examine the state of water during the combustion and expansion process.

The same analysis carried out previously for the intake manifold and compression process will be carried out during combustion and expansion. The state of the unburned end-gas, at TDC is shown in Figure 101 where it can be seen that even in the unburned zone of the end-gas, the equilibrium conditions are well into the superheated vapor region with a temperature of 547°C and a specific volume of 0.21 m^3/kg.

A point in the expansion stroke just prior to EVO results in a temperature of 1360° C with a specific volume of 1.65 m^3/kg. Despite the expansion that took place, because all of the fuel energy has been released by this point in the cycle this condition is even further into the superheated vapor region than the unburned end-gas at TDC. In fact, this point is not shown graphically because it is out of the range of the typical charts. So in other words, it

[48] The enthalpy of vaporization used is the tabulated value at 1 atm. At higher pressure the enthalpy of vaporization will be lower, as the condition is higher on the vapor dome, closer to the critical point. As a comparison however, the enthalpy of vaporization at 1 atm is used for both fuel and water in this comparison.

is not feasible to think that any water vapor present at TDC will condense back to liquid water during expansion. Furthermore, once blowdown occurs, the specific volume will continue to increase, moving the state further from the vapor dome. As long as the blowdown is not accompanied by a drastic change in temperature, the water will not condense during blowdown either. Referring back to the EGT plotted in Figure 82, it is conclusive that the temperature is sufficient to keep the gas away from the dewpoint.

It is assumed that all of the water is vaporized by the beginning of blowdown. At this point in the cycle several events have taken place leading to this assumption:

1. 1.4 ms have passed since IVC providing more time for vaporization,
2. Burned gases exceeding 2000 K have existed providing significant opportunity for heat transfer to the cooler liquid water,
3. Inertial forces on the pooled water as the piston slows may have propelled the liquid water away from the piston top and ring pack crevice, at least partially atomizing the liquid water, and entraining it into now hot gases[49]. It is hard to say how much water is propelled from the piston, as the cylinder gas is at high pressure, and very dense at this point, which will limit the penetration of the liquid into the gas.

[49] Note that the peak inertial forces occur at the peak piston deceleration point, which is NOT when the velocity is zero at TDC, but before TDC.

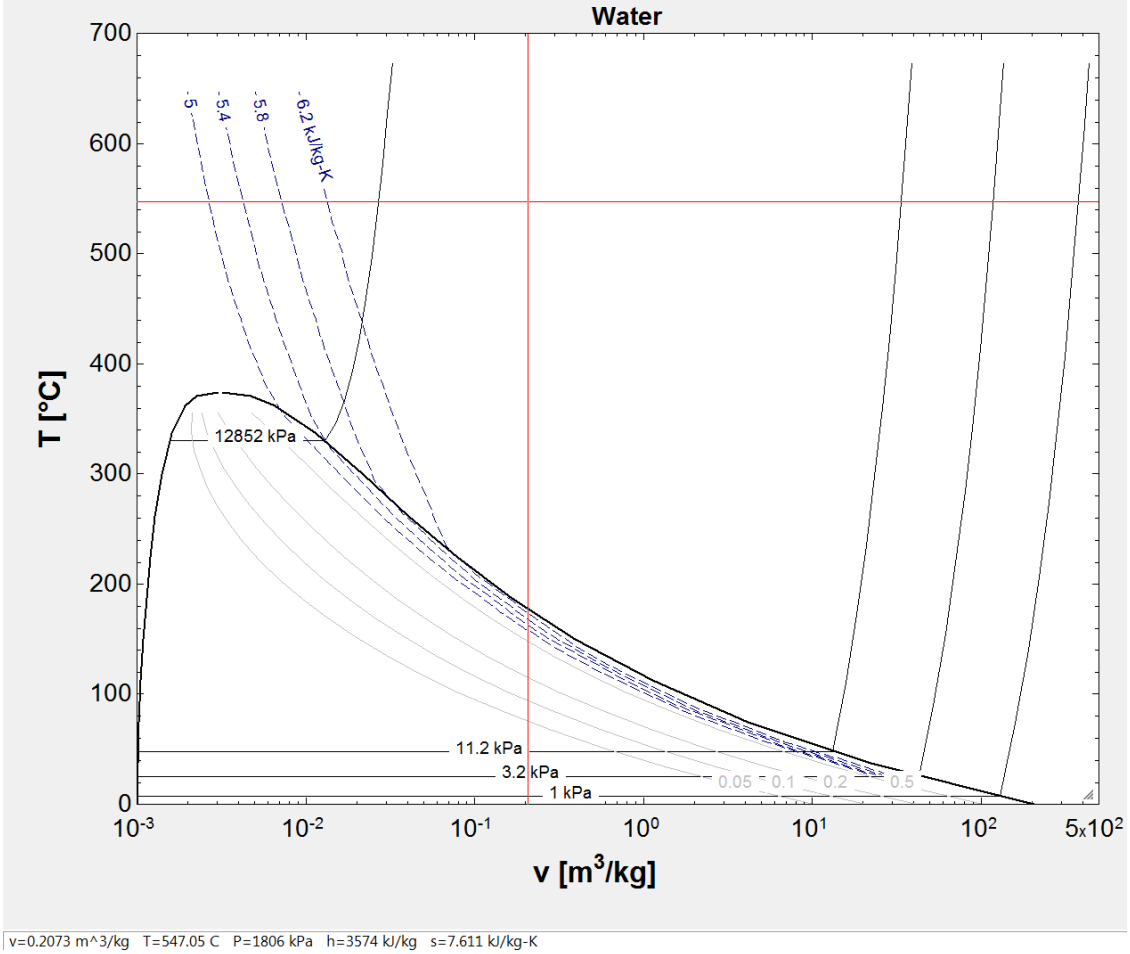

Figure 101: T-v diagram of water. Cross hairs depict state condition of water in the end-gas region at TDC. Chart created using EES. Data source NASA Ideal Gas Database. Chart reproduced with permission; Klein, S.A., EES – Engineering Equation Solver, Version 10.278, 2017, F-Chart Software, http://fchart.com. See 17 Appendix F for further details.

All five of the states analyzed are summarized in Table 13.

Table 13: Water Vapor Equilibrium States.

Location	Gas Temperature	Pressure	Equilibrium State
Intake Manifold Plenum	25° C	250 kPa	Liquid – Vapor Mixture
Cylinder @ IVC	48° C	298 kPa	Liquid – Vapor Mixture, x=0.12
Cylinder @ IGN	330° C	2588 kPa	Superheated Vapor
Cylinder @ TDC	547° C[50]	5800 kPa	Superheated Vapor
Cylinder @ EVO	1360° C	1437 kPa	Superheated Vapor

The pathway the water takes between the states shown in Table 13 is depicted in Figure 102. The equilibrium state at EVO is beyond the chart, and well into the superheated vapor region.

[50] Unburned Zone.

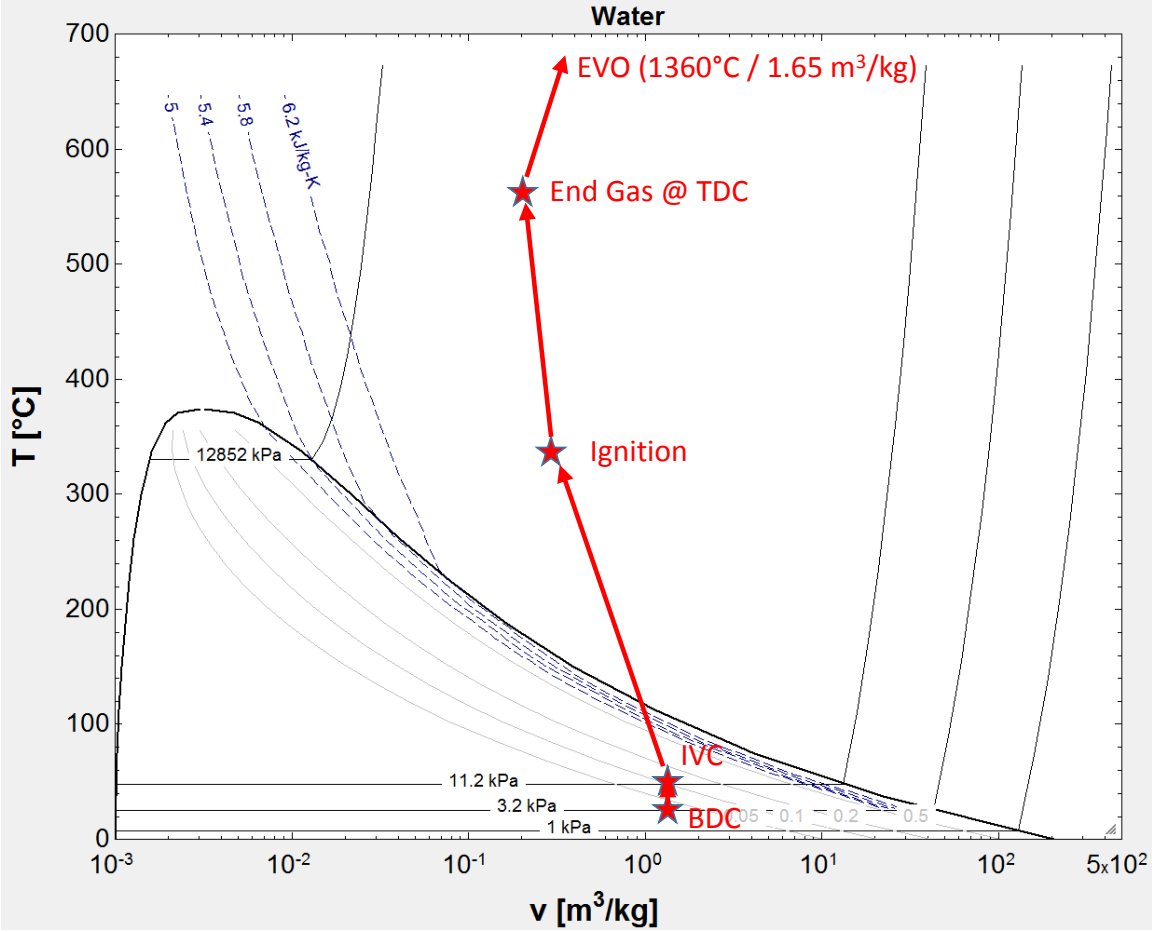

Figure 102: All of the States of Injected Water from Introduction to the Cylinder to Exit. Chart created using EES. Data source NASA Ideal Gas Database. Chart reproduced with permission; Klein, S.A., EES – Engineering Equation Solver, Version 10.278, 2017, F-Chart Software, http://fchart.com. See 17 Appendix F for further details.

6.4 Enthalpy Effects

A brief refresher on enthalpy of vaporization is prudent at this time, as it will support the discussion that follows. The enthalpy of vaporization is the difference between the enthalpy in the water at the saturated liquid point and the saturated vapor point as in Equation 35.

Equation 35: Enthalpy of Vaporization

$$h_{fg} = h_g - h_f$$

Where :

h_g = enthalpy at the saturated vapor point

h_f = enthalpy at the saturated liquid point

The enthalpy of vaporization is thus proportional to the distance between the saturated vapor and saturated liquid lines on a P-h diagram.

It is tempting to focus on the enthalpy of vaporization, h_{fg}. In doing so, one may observe that water vaporized further up on the vapor dome requires less enthalpy for the phase change between liquid and vapor, and thus surmise that a unit mass of liquid water vaporized near TDC will cause a smaller reduction in temperature of the working fluid, and thus provide a better tradeoff between an increased pressure during expansion (because total gas mass will have increased), and a decreased temperature. Although it is true that the actual phase change will result in a smaller temperature decrease for a unit mass of water vaporized at TDC vs the same unit mass of water vaporized at say, IVC, one must not lose sight of the fact that the water must increase in enthalpy more than just the phase change.

The water must increase in enthalpy from the point of introduction to the system to the point of exit from the system in the exhaust. It is assumed the water enters the intake system at 25°C and at a pressure equivalent to MAP, and that it exits the system at the temperature and pressure of the bulk gas at EVO. This change in enthalpy of the water between BDC and EVO is entirely independent upon the path taken. For illustrative purposes, Figure 103 shows that although the enthalpy of vaporization decreases when vaporization occurs at higher temperature and pressure, the overall enthalpy increase of the water is defined by the state at BDC and EVO, and that doesn't matter if the water vaporizes

early, then the steam continues to be superheated, or if the compressed water is first heated in the liquid phase, and is vaporized late in the cycle.

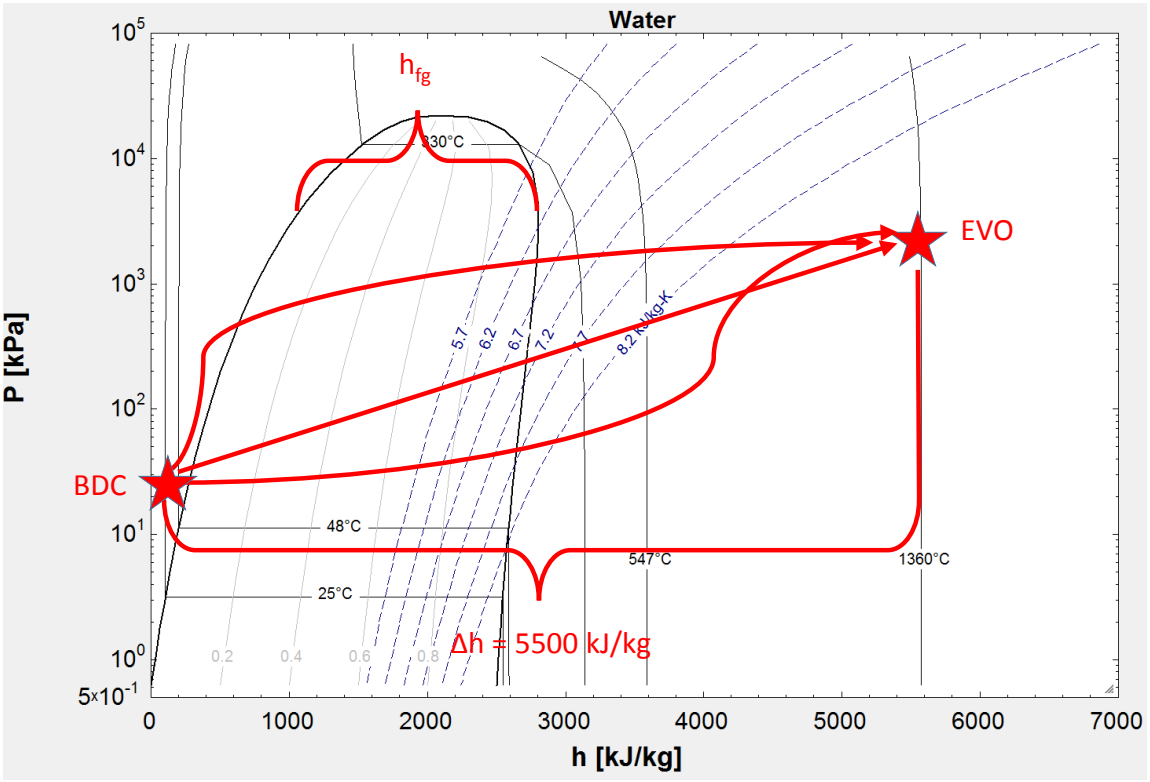

Figure 103: P-h diagram for water. Chart created using EES. Data source NASA Ideal Gas Database. Chart reproduced with permission; Klein, S.A., EES – Engineering Equation Solver, Version 10.278, 2017, F-Chart Software, http://fchart.com. See 17 Appendix F for further details.

Therefore, in the ideal case, the ideal gas law would indicate that the expansion pressure will increase as the mass of gas is higher during expansion than compression (liquid water turned to steam), however, the ideal gas law would also indicate that the expansion pressure will be lower as the temperature during expansion will be lower than it otherwise would be had the energy not been transferred to the water, see Equation 36. Recall that this temperature reduction is because of the total enthalpy transferred to the water in the liquid state, through vaporization, and as superheated steam.

Equation 36: Ideal Gas Law solved for Pressure.

$$P = \frac{mRT}{V}$$

That said, an additional factor may be considered, which is that the heat loss to the coolant and oil is a function of the temperature difference between the hot gas and the coolant and lube oil. With the water absorbing enthalpy, the bulk gas temperature is lower, and this will reduce the energy lost to the coolant and oil, thus keeping that energy in the piston – cylinder assembly.

One may consider that the enthalpy of the exhaust is equal to the enthalpy of the products of combustion, and the enthalpy of the water vapor. Along these lines, once can analyze alternative points at TDC and EVO with and without water injection. The total energy available is the mass of fuel multiplied by the Lower Heating Value of the fuel.

6.5 Impact of the Timing of Water Vaporization

As shown in Figure 103, the enthalpy of the water must increase between its state as injected, and when it is at equivalent pressure and temperature to the bulk gas at EVO. However, there is still some implications as to the timing of the injection. Since most of the enthalpy change at low temperature and pressure is from vaporization, there is not much gain in volumetric efficiency beyond the amount of water to saturate the intake charge prior to IVC. Additional water beyond saturation results in little temperature change, pools in the intake port, cylinder, and piston, degrading power cylinder durability and increasing oil dilution in the process and presumably ends up pooled on the piston by IVC, where it is cooling the piston more than the bulk gas. Therefore, it is recommended to inject only enough water prior to IVC to reach saturation, as this will maximize volumetric efficiency, minimize water consumption, and maximize long term durability. As the piston approaches TDC, and the cylinder conditions can support additional water vapor, additional water should be injected into the bulk gas to support rapid vaporization. This

will reduce gas temperatures, improving knock tolerance, and reducing heat loss to coolant. Of course this scenario requires water to be Direct Injected.

An interesting alternative, albeit at increased complexity, could be a port injector injecting relatively cold water to reduce temperature as much as possible to support increased volumetric efficiency and reduced knock tolerance, combined with a direct injector injecting water that has been significantly pre-heated by exhaust heat, with that injection occurring near TDC. If the water has been sufficiently pre-heated, then it may be more likely to produce a favorable P-T tradeoff during expansion. The key here is that the direct injected water is pre-heated with waste heat, as opposed to heat from the working fluid.

7 Hardware Failures and Issues

There were several hardware related failures and issues that were encountered during this project. As these are important, but are not the primary focus of this research, they will be discussed only briefly here.

7.1 Water Pump Drive System

There were multiple failures of the water pump drive system. This included two entirely severed water pump drive chains, and a failed chain tensioner. Both of these are production components, and therefore well vetted from a durability perspective. The assumption is that these components failed most likely due to dynamic issues (resonance, etc.) in the specific dynamometer, shaft, mount, setup being used for this research. An example of a failed chain is shown in Figure 104.

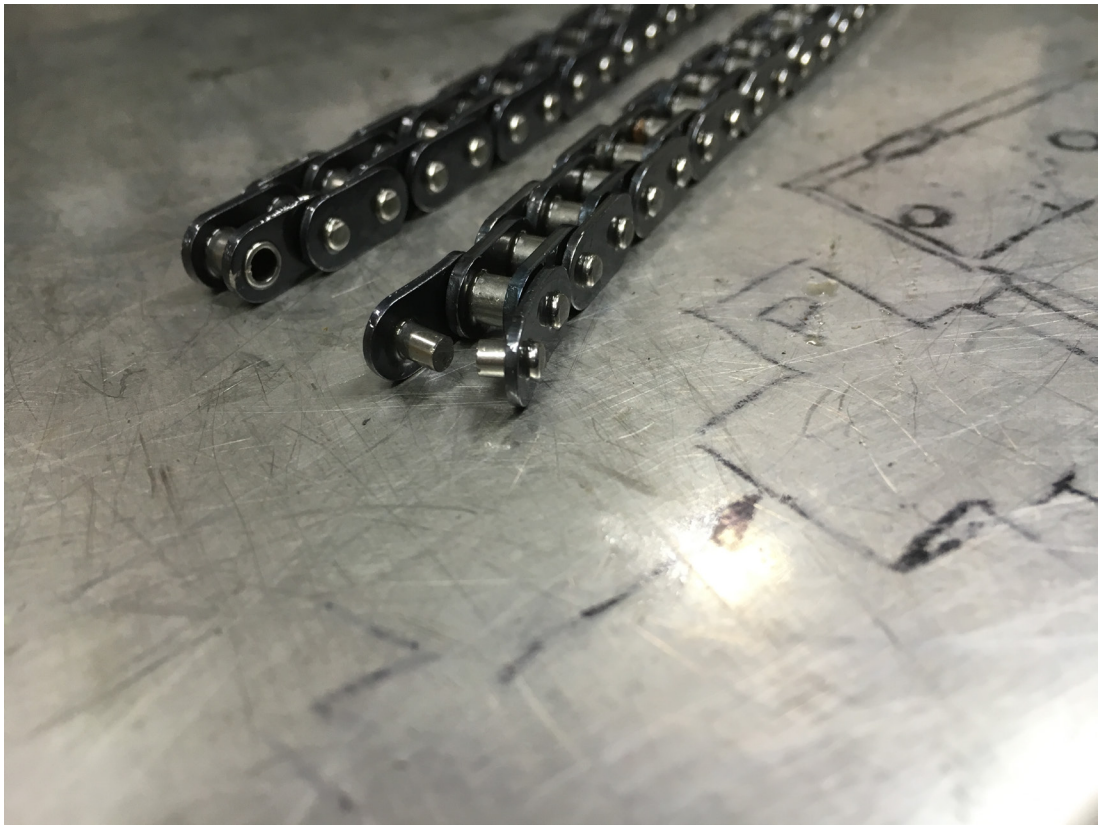

Figure 104: Failed Water Pump Chain from Engine ESN01.

7.2 Oil Cooler

Two different engine oil coolers failed. The failure mode was a fracture of the hose fitting where it attaches to the cooler fins. Since this is a well vetted production component, the root cause of the failure is assumed to be continual tension on the hose in combination with engine vibration.

7.3 Spark Plugs

Several spark plugs failed during the project. The failure mode was cracking, and missing pieces of the ceramic insulator inside the combustion chamber. At various times in the testing, the engine experienced heavy knock and pre-ignition. Both of these operating modes are known to cause this failure mode in spark plugs.

Figure 105: Example of failed spark plug. Note the broken and missing ceramic insulator.

7.4 Ignition Coil

One ignition coil failed during testing. The issue was a complete misfire, which was traced back to the failed coil. Again, these are highly validated production components. The coils were used in a harsh manner throughout the testing in debugging the control system. It is likely that the coil was energized for an extended period of time during debugging, which may have led to its failure during testing.

7.5 Throttle Body

Like the ignition coil, two throttle bodies failed during testing. This is assumed to result from abuse from a control perspective. Perhaps overdriving the actuation motor at WOT.

7.6 Optical Encoder

The optical encoder used to trigger the combustion analyzer experienced failure due to torsional vibration. At some engine speeds the vibration would resonate severely. This would cause the encoder cable to loosen, and break electrical contact. In its most severe case, the screws holding the encoder body together sheared, causing the encoder to mechanically come apart. Welding additional mass to the encoder mounting bracket did help the situation significantly. The problem was severely exacerbated whey the torsional damper in the driveshaft assembly would begin to fail (which occurred frequently). An image of the failed encoder can be seen in Figure 106.

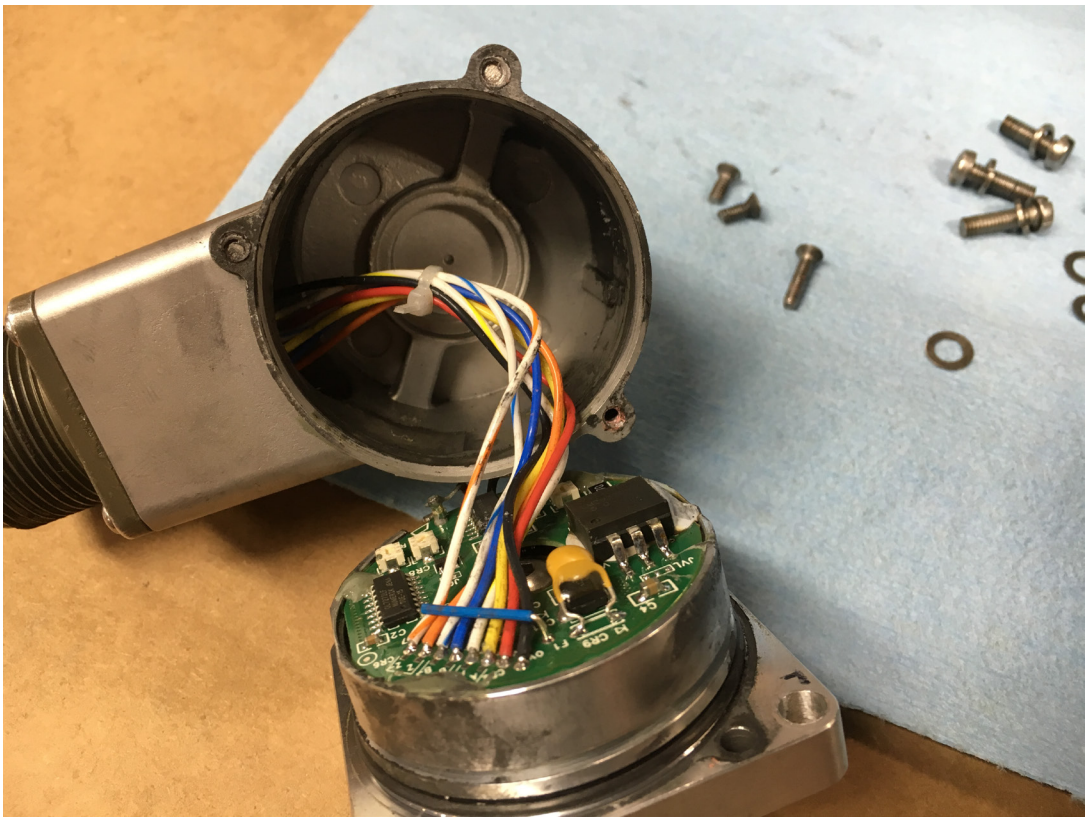

Figure 106: Encoder failed due to excessive torsional vibration. Note the sheared bolts that hold the encoder housing together.

7.7 Driveshaft

It was very common to fail the torsional damper located on the engine end of the driveshaft. The original unit failed several times. Modifications were made to the driveshaft to

upgrade to a torsional damper with increased torque capacity. This decreased the failure rate, but did still fail. When the dampers would begin to fail, other components in the system would resonate and fail. As discussed previously, this is believed to be the root cause for at least the encoder failure.

On one particular occasion when the damper was beginning to fail (as evidenced by increased vibration, and the beginnings of audible noise), the entire driveshaft failed in torsion. An image of the failed driveshaft is shown in Figure 107.

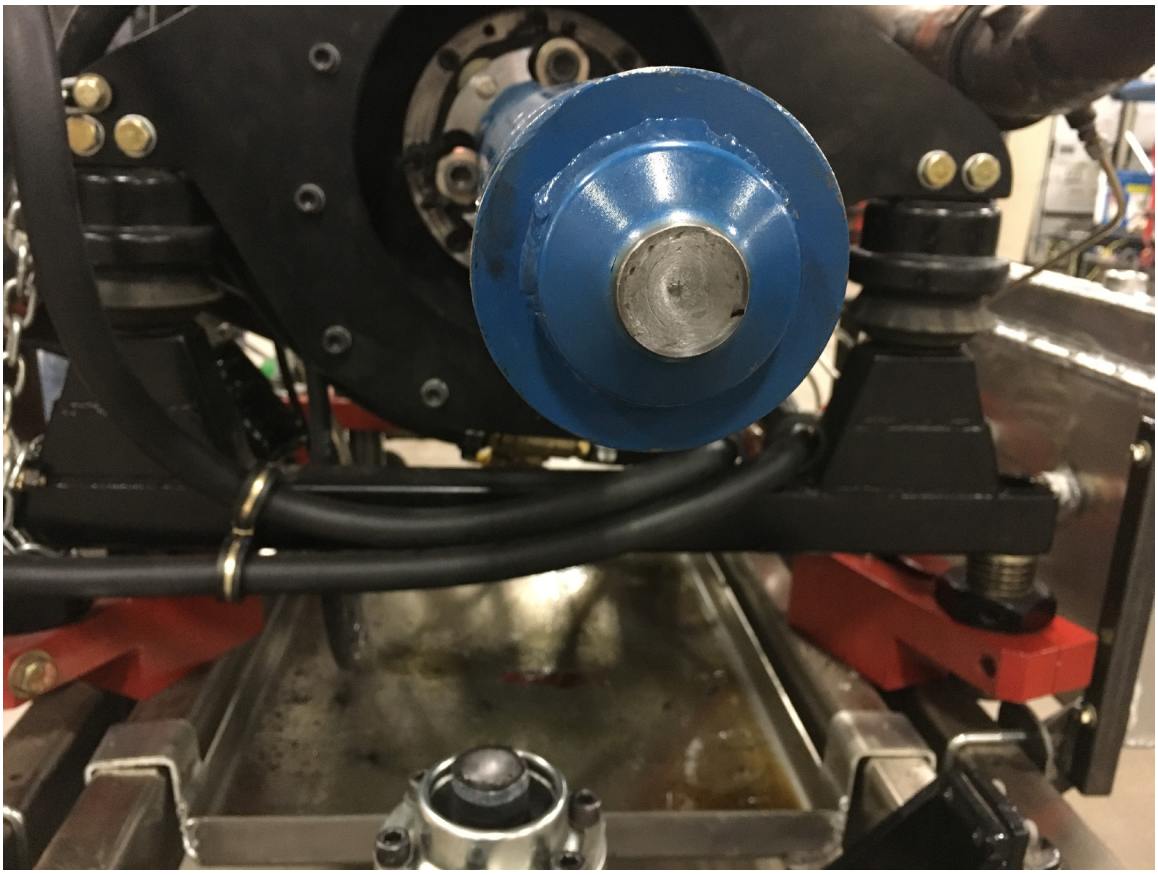

Figure 107: Driveshaft failed in torsion.

7.8 Cylinder Pressure Transducers

Several cylinder pressure transducers failed during testing. Although not intentionally, it was very common for a combustion cycle to result in heavy knock, or Pre-Ignition. When operating at the nominal cylinder pressure involved in this project, a single pre-ignition

event is capable of destroying the transducer. Several were sent back to the manufacturer for analysis, where it was determine the crystal was crushed and broken in to many pieces. On one particular occasion when testing at 300 kPa MAP, a transducer failed, with the failure mode being decreased sensitivity. This was caught immediately, however, since a spare transducer was not available, that cylinder was removed from the calculations in the combustion analyzer, and the data files, and testing continued on the other three cylinders. The failed transducer was left in the cylinder. Almost immediately there was a loud noise, the test cell camera showed extensive steam, and the engine had a complete miss. Inspection revealed the transducer was not to be found, and there was extensive damage to the cylinder head and transducer adaptor. The thought is that the transducer crystal failed from a pre-ignition event, allowing excessive deflection of the diaphragm, which very quickly failed. This created a pre-chamber effect, giving a nucleation site for further pre-ignition that proceeded to melt the transducer, adaptor, and cylinder head. The melted transducer adaptor and cylinder head are shown in Figure 108and Figure 109 respectively.

Figure 108: Transducer adaptor. Presumably failed due to pre-ignition.

Figure 109: Cylinder head failed at transducer adaptor penetration. Note the hole created by melted aluminum at the 3 o'clock position in the figure.

7.9 Lubrication Issues

As has been discussed, it is believed that a significant quantity of liquid water entered the cylinder during the intake stroke and was pooled on the top of the piston. A portion of this water migrated past the piston rings with the blow-by gases into the crank case. This resulted in an emulsion with the lubricating oil. This undoubtedly impacted the friction of the engine, as it likely changed the lubricity, viscosity, etc. of the oil. On one occasion the engine was untested for over a week with the emulsified oil. This resulted in severe corrosion of internal engine components. Images of a severely corroded camshaft and the water / oil emulsion are shown in Figure 110 and Figure 111 respectively.

Initially testing was begun with the oil temperature controlled to 90°C. Once this issue with excessive water in the crankcase was discovered, the oil temperature control setpoint was increased to 105°C, to intentionally raise the oil temperature above the boiling temperature of water at the pressure found in the crankcase. This helped significantly, but did not eliminate the problem. This was coupled with very frequent oil changes.

An experiment was conducted to determine if the water and oil were easily separated such that the oil could be re-used. However, once emulsified, it took several months for water to begin to separate from the emulsion that was left in a beaker at room temperature (elevated temperature may have sped up the process, but this was not investigated).

This observation with the oil gives further validation to the discussion above regarding the likelihood that liquid water is present in the cylinder.

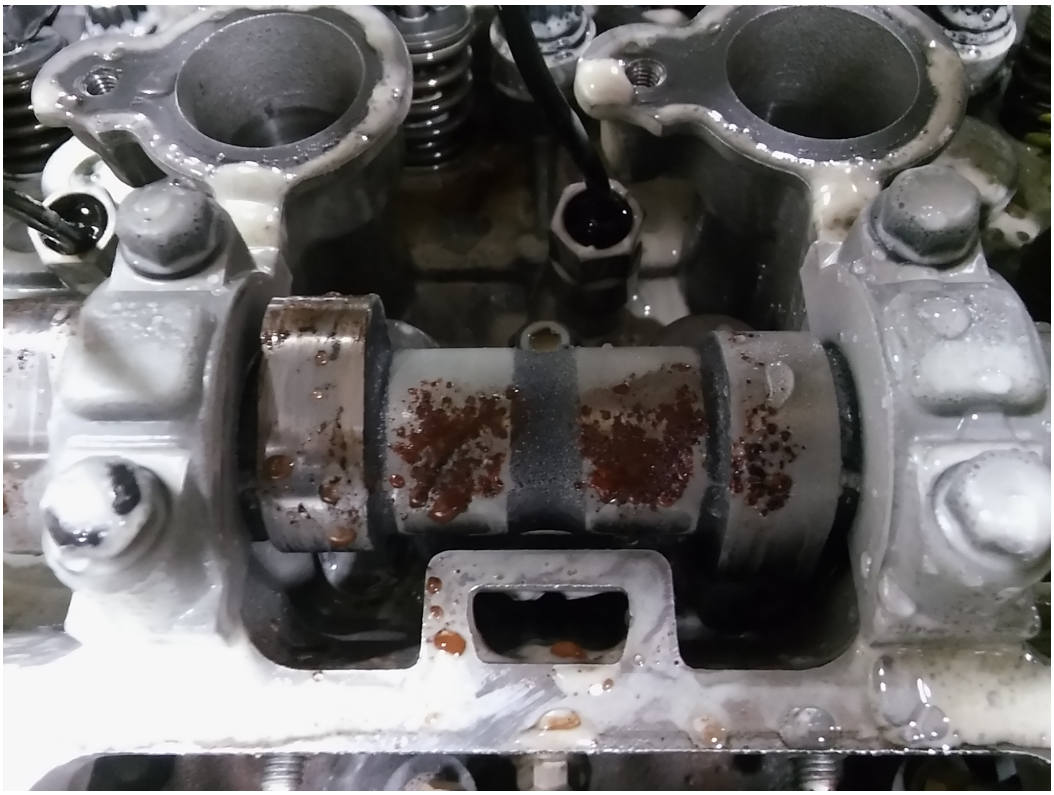

Figure 110: Corroded camshaft resulting from excessive water in the crankcase.

Figure 111: Water - Oil emulsion.

8 Publication Plans

As of the defense of this work (December 2017), one publication has been produced, (Worm 2017). This publication discusses the experimental results run with the production turbocharger and induction hardware. At least one additional publication is planned from this work, with the intended focus being on experimental results run with the external boosting system, and load exceeding current best-in-class.

9 Conclusions

The trend has been increasing specific load of engines through boosting. A limit to the degree of boosting and downsizing is imposed by the onset of auto ignition with current fuels. This not only limits maximum load, but reduces efficiency in the high load operating range as various measures are put in place to permit the engine to continue to operate in a knock prone region. Furthermore evidence has been presented in this dissertation showing that even today, there is a clear trend with a reduction in CR with increasing BMEP. Therefore, extending the knock limit can allow for higher CR, allowing engines to operate more efficiently throughout the entire speed / load range, and minimizing losses due to other knock mitigation strategies.

This project was undertaken to investigate the potential of water injection to extend the knock limit, while potentially providing other benefits to the operating cycle. Testing included a low, medium, and high octane fuel, with and without water injection, at two different loads, and over a range of engine speeds. This test matrix included speeds up to 5000 RPM and loads in excess of 30 bar BMEP; both of which are above (load is significantly greater) conditions previously run based on existing literature. The water to fuel ratio tested was nearly 6:1 at some conditions, also significantly greater than previously run based on existing literature.

Several specific conclusions can be drawn from this work. As applicable, the conclusions will be linked back to a specific stated objectives of this research.

1. Objective 1; Develop a testbed
    1.1. An extensive testbed has been created through this project. Holistically the testbed includes several major elements
        1.1.1. A system has been created to produce purified water, store the water, pressurize the water to both low (port injection) and high (direct-injection)

pressures, supply the water to an engine in a testcell, and measure the flow rate, pressure, temperature, etc.

1.1.2. An engine has been created existing of primarily production hardware with the exception of a port water injection system and instrumentation modifications.

1.1.3. An engine has been created with special consideration for operation under loads in excess of current production levels. The engine includes increased fuel flow capacity, stronger internal components, increased valvetrain capability, and port water injection.

1.1.4. A system has been designed and fabricated to provide externally generated boosted air to engines in a testcell. The system obtains compressed air from multiple air compressors and storage reservoirs, and uses multiple stages of pressure regulation. The system can be easily switched between naturally aspirated operation and boosted operation.

1.1.5. An engine control system has been implemented which provides a high degree of flexibility for operation of electronic throttle, direct or port injectors, cam phasers, turbochargers, etc.

1.1.6. A separate control system has been implemented for the control of water injectors.

2. Objective 2; Quantification of impacts of water injection & increased understanding of the thermodynamic processes involved.

2.1. Successful operation was demonstrated at production boost level of a near best-in-class engine from a BMEP perspective.

2.2. Successful operation was demonstrated at 20% higher boost compared to a near best-in-class engine from a BMEP perspective.

2.3. The timing of the water injection impacts engine operation

2.3.1. For a given quantity of water and spark timing, injection on a closed intake valve leads to faster burn rate, however, closed valve injection leads to increased knock amplitude. The explanation given is that during open valve

injection, the water increases very little in enthalpy in the port, with the major increase in enthalpy coming from the in-cylinder bulk gas and metal, thus leading to cooler end gas.

2.4. Generally speaking, water Injection was shown to be effective in reducing limitations due to knock, confirming observations by previous researchers.

2.4.1. At 3000 RPM, 250 kPa Manifold Pressure, water injection enabled knock limited CA50 to be advanced from 27° ATDC to 14° ATDC, with lambda being leaned from 0.78 to 1.0, and switching from 91 AKI fuel to 87 AKI fuel.

2.5. Although enabling advancement of CA50 in knock limited operating regimes, water injection was shown to increase both early, and bulk burn durations. 0% - 10% MFB duration was shown to increase by as much as 10°, while 10% to 90% MFB duration was shown to increase by as much as 18°.

2.6. Water injection was shown to increase NMEP relative to the baseline case. A 5.5% gain was observed at 3000 RPM. Although there are many factors, this gain is primarily due to advanced combustion phasing and secondarily due to increased volumetric efficiency.

2.7. The NMEP of the water injected case did not exceed the NMEP of the case run on non-knocking fuel, as the non-knocking fuel case was able to run MBT combustion phasing without the increased burn duration and other negative impacts of water injection.

2.8. The water injection resulted in a marked increase in pumping work; 4 kW more pumping work at 5000 RPM. The increase in pumping work comes from the exhaust process, not the intake process. The explanation given is that the majority of the water comes into the cylinder as a liquid and leaves as a vapor. This increases the flow requirement of the exhaust valves and ports, but not the intake.

2.9. Significant reductions in Exhaust Gas Temperature were observed; as much as 200°C. Although combustion phasing can be advanced with water injection, this is not the reason for the EGT reduction, as longer combustion duration means end of combustion does not change much. Rather the reduction in EGT comes as a result of decreased bulk gas temperature as the enthalpy of the water increases.

2.10. There is no significantly observable impact to the Polytropic Compression Index. The explanation given is that a limited amount of water vaporizes prior to ignition. This results in only minor changes to the gamma of the gas mixture, because the effect of additional water vapor is offset by a reduction of temperature and increased gas mass.

2.11. Pressure over the compression stroke is the same with and without water, and remains a straight line. This goes along with the conclusion above that the Polytropic Compression Index does not change, because either little water vaporizes during compression and / or any changes to gamma due to additional water vapor are offset by reductions in temperature. Furthermore, this clearly shows graphically that there is no change in compression work, which is something that multiple researchers had predicted or claimed.

2.12. The Polytropic Expansion Index shows a clear trend, whereby it is decreased with water injection. This suggests that the bulk of the water was vaporized during the combustion process.

2.13. There are clear improvements in Volumetric Efficiency with water injection. Although little water vaporizes prior to IVC, the specific heat capacity of water is substantial compared to air, thus even a small amount of water vaporization is sufficient to significantly drop the air temperature, densify the charge, and increase volumetric efficiency.

2.14. Thermal efficiency improved significantly with water injection; 35% at 3000 RPM. Approximately 1/3 of this improvement was from advancement of combustion phasing, and 2/3 from moving from an enriched to a stoichiometric lambda.

2.14.1. This has direct implications to real-world fuel consumption in driving cycle situations where the engine operates in knock limited regimes including trailer towing and climbing a grade.

2.15. Water injection enabled operation at boost levels 20% and greater beyond production boost levels (300 kPa MAP compared to 200 kPa to 250 kPa). The increased MAP resulted in increases in IMEP. However, the IMEP normalized to

MAP was lower with the 300 kPa water injected case than with any other case including the baseline case.

2.16. Based on a psychrometric analysis and phase analysis, very little of the total injected water can be vaporized prior to IVC because of the saturation point of the air. By ignition the in-cylinder conditions can support full vaporization in equilibrium, however, it is doubtful complete vaporization takes place based on the relatively short time scale and substantial amount of energy that must be transferred to water that is presumed to be pooled on the relatively cool piston. Evidence suggest that the bulk of the water vaporizes during the combustion phase. These statements are supported by the phase analysis of water, and the previously discussed combustion metric results.

2.17. Starting the cycle with liquid water and ending the cycle with vapor increases the mass of gas acting as an ideal gas, which directionally will increase pressure during the expansion stroke. However, this is counteracted with a reduction in gas temperature resulting from a substantial change in enthalpy of water as it moves from conditions as IVC to EVO, which directionally will decrease pressure during the expansion stroke. Heat rejection to the engines cooling system will be reduced as the delta T to the coolant will be lower. The net result of all of these effects on the pressure-volume history during expansion appears to be relatively negligible.

2.18. Once the combustion process takes place, the in-cylinder conditions are in the superheated vapor region, and remain in that region throughout expansion and blowdown. Therefore, once vaporized, water does not recondense as in-cylinder temperature drops during expansion.

2.19. From the perspective of increasing engine output (i.e. BMEP), the biggest benefit of water injection is increased volumetric efficiency and advanced knock limited combustion phasing

2.20. From the perspective of increasing engine efficiency, the biggest benefit of water injection is on advanced knock limited combustion phasing, reduced fuel enrichment, and increased compression ratio.

2.21. The W/F that was run as part of this work, may very well be beyond what is required for optimal performance.

In summary, water injection does appear to show merit in terms of increasing maximum engine load, increasing high load efficiency, and increasing low load efficiency (using water injection as an enabler for increased compression ratio). These opportunities for gain seem to outweigh the engineering challenges associated with addition an additional liquid injection system on-board automotive applications. Additional work is needed, both in terms of increasing the fundamental understanding of water injection, as well as development of production systems. Some of this is discussed in the next section.

10 Future Work

The conclusion section of this dissertation describes many benefits of water injection in terms of both peak load and engine efficiency. That said, the fundamental physics are far from fully understood, and water injection systems will need to be productionized. The following summarizes and describes future work that should be done in this area. The points that are described are not ranked in order of importance or chronology.

1. Determine optimal combustion phasing.
    a. A CA50 of 6°ATDC to 10° ATDC has been considered a sufficient indicator of optimal combustion phasing over the full range of engine operating conditions including speed, load, and dilution for years. This optimal CA50 is where a net balance of losses is maximum. In simplistic terms, increased heat loss with advanced combustion phasing is balanced against expansion losses with late combustion phasing. Water injection changes the in-cylinder temperature, pressure, and burn duration. This may impact the location of optimal CA50. Sweeps of W/F and combustion phasing should be conducted to determine if optimal CA50 changes with water injection, and how sensitive that change is to W/F
2. Determine optimal W/F
    a. This work showed that the engine operates remarkably well, with improvements in load and thermal efficiency at W/F ratios considerably higher than anything previously published on. That does not however mean best performance is found at the highest possible W/F. Although increasing W/F subdues knock enabling an advancement of combustion phasing toward MBT, it does so at the detriment of various factors including combustion robustness and burn rate. A sweep of W/F should be conducted examining the tradeoffs involved. The sweep should

include W/F ratio's significantly lower than what was run in this work (all the way to near zero), but also W/F greater than what was run in this work.

   b. This work showed there is a well-defined upper limit for the potential improvement in volumetric efficiency based on the saturation conditions prior to IVC. This upper limit in volumetric efficiency should be examined along with the tradeoffs in combustion.

3. Investigations should take place under further increases in boost pressure and load. In particular, one aspect that has not yet been answered in this work is why the increase in load with 300 kPa MAP and water injection was not as significant as expected.
4. Investigations should be conducted to specifically examine using water injection, not as an enabler for further increases in BMEP beyond today's levels, but rather from the standpoint of maintaining BMEP at today's levels and increasing CR to enable improvements in efficiency throughout the load range.
5. Investigations should be conducted to look at drive cycle effects and interactions.
   a. At what point in the operating range, as load is increased, does water injection begin to improve efficiency and how does that efficiency improvement change with further increases in load, and what is the impact of that part load efficiency increase on regulatory cycles and Real-World-Driving.
   b. Based on the load point that water injection begins to improve efficiency, determine the water consumption over typical regulated, and real world drive cycles. Determine the implication to water tank size, assuming on-board water recovery is not implemented.
6. Continue to develop simulation models, including simple 0-D, and 1-D, that can be used for further research and development.

7. Determine the impact to a typical three way catalyst. The thought being as long as the catalyst temperature remains greater than the light-off temperature, catalyst efficiency will remain high. This would suggest water injection can enable a significant reduction in high-load toxic emissions, where todays enrichment strategies result in very low conversion efficiencies. However, these interactions should be studied and verified.
8. Determine the impact to turbocharger performance. The turbocharger turbine extracts energy from the engine exhaust stream, and this energy is used to drive the compressor, or potentially for auxiliary purposes such as generation of electrical energy. Water Injection changes the exhaust enthalpy, and available energy that can be extracted by the turbine. Temperature for example decreases, while mass flow rate increases. The gas density / specific volume also changes. The net impact to available energy should be investigated.
9. Continued investigation of the phase of water throughout the engine operating cycle.
    a. The analysis presented in this dissertation suggested that although equilibrium conditions exist whereby the water is entirely vaporized, the real process may lag the equilibrium state due to transient limitations. These transient effects should be studied in greater detail to better understand the actual water phase vs crank angle.
    b. This analysis should include additional loads, as the equilibrium saturation conditions will change with not only inlet air temperature, but also MAP.
    c. Conducting additional experiments with heat flux probes on the piston and cylinder head may be helpful in determining the impact of water injection on heat transfer, and also may aid in validating the assumptions regarding the phase of the water and where liquid water may reside inside the cylinder.

d. Experiments can be carried out on an optical engine with common optical / laser diagnostics applied to visually determine the state of water in the cylinder at various points in the cycle.

10. A detailed breakdown of energy during the cycle should take place. This should include not only an analysis of compression and expansion work, but also exhaust and intake work, as the discussion in this dissertation revealed significant impacts of water injection on pumping work as well. Furthermore, it should begin with available energy in the incoming reactants, and conclude with available energy in the exhaust.
11. This work showed that the injection of water places increased demands on the exhaust side of the engine, as the changes in gas mass, density, etc., were shown to increase the pumping work substantially. An engineering exercise should be undertaken to optimize the lift, duration, and phasing of the exhaust cam, as well as the diameter of the exhaust valve (which may potentially require smaller intake valves), and the design of the exhaust port, manifold, and potentially even the turbine housing and turbine. Much of this work can be undertaken with a fully developed and validated 1D engine simulation model.
12. Continuation of the analysis that was conducted in this dissertation to examine the tradeoff between enthalpy absorbed by the water in the cycle, vs. increased gas mass for expansion.
    a. This should include calculation of the enthalpy in the exhaust. Although there are changes in temperature, the total exhaust enthalpy is a function of the enthalpy of the water and the enthalpy of the products of combustion.
    b. Although the water takes enthalpy from the system, much of this may be returned during expansion. As a first approximation, one may investigate the changes in state at TDC, and at EVO with and without water injection.
    c. This analysis should include estimates of energy exchanges with the cooling system. For example, although the water takes energy from the

working fluid in the cylinder, there is almost certainly a decrease in the energy transferred to the cooling system (and thus unavailable for expansion), as the peak in-cylinder temperature is lower with water injection. There are also some points in the cycle where the water is likely taking energy from the cooling system itself, which should be included.

13. Direct Injection of water should be investigated.
    a. As described in this dissertation, a relatively small amount of water can be held in vapor prior to IVC, and therefore any additional water injected beyond the saturation point at IVC is liquid, and is believed to be largely pooled in the ring pack crevice volume. The implication is that there is an upper limit on the improvement in volumetric efficiency possible, and any water injected into the port beyond this upper limit still has the potential to benefit the cycle, albeit at the expense of power cylinder durability. Through DI water, an amount of water up to the saturation point can be injected prior to IVC to maximum volumetric efficiency, then additional water can be added after IVC (once the equilibrium saturation point has increased), to further benefit the cycle (e.g. further reductions in knock tendency), without pooling of liquid water in the power cylinder. Furthermore, DI would allow for injection late, or even after combustion if that is found to be favorable from a temperature / pressure perspective, or to squelch NOx formation.
    b. A combined PI and DI water system (albeit highly complex) provides some interesting merit. The PI water can be used to increase volumetric efficiency, and provide some knock tolerance benefit. Water injected directly could be pre-heated with waste heat (from the exhaust perhaps), and injected near TDC. If sufficiently pre-heated, this water may improve the Pressure – Temperature tradeoff in the cylinder, as it will add to the gas mass in the cylinder, while taking less enthalpy out of the working fluid.

14. Additional work should focus on studying the impacts to combustion variation, and misfire limits. This should include a look at how combustion variation increases, where the actual misfire limit is, and ways to improve those limits through traditional techniques including ignition system improvements, in-cylinder flow, injector targeting, etc.
15. The impact of water on pre-ignition including Low Speed Pre-Ignition (LSPI) and Stochastic Pre-Ignition (SPI) should be studied.
16. Conduct a comparison with alternatives to water injection. This may include high octane gasoline, ethanol, butanol, methanol, etc.
17. Examine the potential of water injection used in conjunction with natural gas. Natural Gas has a very high Octane Number, but the gaseous fuel results in a reduction in volumetric efficiency (assuming it is not Direct Injected after IVC), and thus results in a reduction in engine output compared to gasoline. A relatively small quantity of water injection may improve the appeal and acceptance of Natural Gas powered engines.
18. The injection of water mixed with other chemicals, especially alcohols, should be studied. First and foremost would be ethanol and methanol. Both of these are highly soluble in water, making mixing easy, and both have their own advantages as a fuel. Furthermore, both ethanol and methanol would lower the freezing point of water thus acting as an antifreeze, which may have some advantages in the productionizing of a water injection system.
19. Determine the requirements for purity of the water to be injected. For this work, highly purified water was generated with a reverse osmosis water treatment system. This was done primarily to eliminate / reduce experimental variabilities. However, it is unclear if this is required in production. One aspect that may require purified water for production could be particulate emissions. Metals, salts, and various other minerals present in uncontrolled water sources could lead to an increase in exhaust particulate emissions. This should be investigated thoroughly, as there is a substantial cost and infrastructure implication to requiring purified water.

20. This dissertation showed the potential of water injection to be sufficiently high to justify design and development of a production intent water injection system. Although challenges exist, for the most part, this should be a fairly straight-forward engineering effort. Attention should be paid to several considerations including:
    a. Development of a suitable antifreeze solution, such as ethanol or methanol as discussed above.
    b. Consider the potential of designing the water injection system specifically to freeze at temperatures below 0°C. This would allow the end-user to use lower cost water (even if there is a requirement for it to be purified), as opposed to a pre-mixed solution of water and an antifreeze (such as ethanol or methanol).
        i. The system could be designed to be thawed by waste heat from the engine exhaust and / or cooling system, such that it may be frozen upon cold-start, but will thaw as the engine reaches operating temperature.
        ii. The system could be designed with thermal insulation which will not prevent freezing, but will delay freezing. It is not unreasonable to conceive an insulation solution that would delay freezing for 24 hours. When the vehicle is driven daily, little or no freezing will take place.
        iii. In application, the water will most likely be injected at high loads, and high load operation is significantly less likely at ambient temperatures less than 0°C in performance situations (because of traction limits), and even in trailering / hauling situations is reduced until the engine has reached operating temperature and some of the water has thawed.
    c. Consideration should be given to how precisely the water needs to be metered in a port injected application. It is possible the water could be administered through a venturi in the throttle body, similar to a

carburetor. If high precision metering is not required, introduction of water through a venturi has the potential to significantly reduce the cost of a production system, as it eliminates the need for electronic injectors, wiring, and drivers in the ECU. Even if the venturi is turned on with a valve, it can be a low cost valve actuated with a low cost digital output from the ECU. A potential compromise could be a single injector in the throttle body, similar to Throttle Body Injection (TBI) systems.

d. The additional of a water injection system has the potential to eliminate other systems. This may improve the business case for a water injection system not only from a pure cost perspective, but also from a packaging and mass perspective.
    i. The Charge Air Cooler (CAC) could be eliminated (or at least downsized). The elimination of the CAC results in a cost savings that can be applied to the water injection system. Furthermore the CAC tends to be a difficult component to package, whereas the water injection system has the potential to package easier, as the tank and pump can be remotely mounted, and can be mounted rearward of the front axle. Finally, the elimination of the CAC saves some mass, that can be applied to the water injection system, and the CAC mass is removed from the very front of the vehicle, while the water tank can be mounted further rearward, thus improving the overall weight balance of the vehicle.
    ii. Using water injection to reduce NOx (either port injection or direct injection) may have the potential to change the requirements of the catalyst. This could lead to a reduction in precious metal loadings in the catalyst substrate washcoat, which will reduce the cost of the catalyst. It should be noted however, that the HC emissions may increase. In addition to reducing catalyst requirements, an external EGR system, could

potentially be eliminated. The cost savings in eliminating the external EGR system is significant, especially if an EGR cooler is used, and the EGR cooler represents a packaging and mass opportunity as well.

iii. The addition of water injection may negate the need for piston oil squirters. This would allow a small piece cost savings in elimination of the squirter nozzles themselves, but there is also a cost savings in the machining of the cylinder block, and in the assembly process. Furthermore, there may be compounding improvements as the capacity of the oil pump can be reduced, and there degree of crankcase windage and oil aeration can decrease. All of these will decrease engine friction, improving engine efficiency across the entire engine speed and load range.

21. As has been shown and discussed in this dissertation, there are many impacts and causalities associated with water injection. A synopsis should be created (a table perhaps) to highlight and summarize these effects.

11 References

A&D (2016). A&D CAS User Manual. Hardcopy and Embedded Electronic, A&D.

Baines, N. C. (2005). Fundamentals of Turbocharging, Concepts NREC.

Bassett, M., Hall, J., Hibberd, B., Borman, S., Reader, S., Gray, K., Richards, B. (2016). "Heavily Downsized Gasoline Demonstrator." SAE International Journal of Engines.

Berni, F., Breda, S., D'Adamo, A., Fontanesi, S., Cantore, G. (2015). Numerical Investigation on the Effects of Water/Methanol Injection as Knock Suppressor to Increase the Fuel Efficiency of a Highly Downsized GDI Engine, SAE International.

Bethel, S. (2016). Personal Conversation Between Steve Bethel of Leadfoot Engineering and Jeremy Worm of APS LABS, Michigan Tech. J. Worm.

Bhagat, M., Cung, K., Johnson, J., Lee, S.-Y., Naber, J., Barros, S. (2013). Experimental and Numerical Study of Water Spray Injection at Engine Relevant Conditions, SAE International.

Blaxill, H. (2015). Personal conversation between Sam Barros of Nostrum Energy and Hugh Blaxill of Mahle Powertrain. S. Barros.

Boretti, A. (2012). "Water Injection in directly injected turbocharged spark ignition engines." Applied Thermal Engineering.

BorgWarner (2015). BorgWarner Performance Turbochargers, BorgWarner.

Bosch (2015). Function Manual, Project Code: MS6A_BASE_0404**:** User Manual for Bosch Motorsports Engine Control Unit. Available as pdf document.

Brooke, L. (2015). Bosch Developing New Water Injection System for Production Engines. Automotive Engineering, SAE International.

Brusca, S., Lanzafame, R. (2003). Water Injection in IC - SI Engines to Control Detonation and to Reduce Pollutant Emissions. International Spring Fuels & Lubricants Meeting. Yokohama, Japan, JSAE.

Busuttil, D., Farrugia, M., (2015). "Experimental Investigation on the Effect of Injecting Water to the Air to Fuel Mixture in a Spark Ignition Engine." Science Journal: 585-590.

By, A., Kempinski B., Rife J. M. (1981). Knock in Spark Ignition Engines, SAE.

Cengel, Y. A., Boles, M.A. (2008). Thermodynamics An Engineering Approach, McGraw-Hill Inc.

Davis, R. S., Patterson, G.J. (2006). Cylinder Pressure Data Quality Checks and Procedures to Maximize Data Accuracy. SAE World Congress and Exposition. Detroit, MI, SAE International.

Davis, R. S., Patterson, G.J. (2009). Geometric and Topological Considerations to Maximize Remotely Mounted Cylinder Pressure Transducer Data Quality. SAE World Congress and Exposition. Detroit, MI, SAE International.

Douaud A. M., E. P. (1978). "Four-Octane-Number Method for Predicting the Anti-Knock Behavior of Fuels and Engines." SAE Jornal of Transactions **87**.

Driver, C. a. (2017). Car and Driver Online Database of Vehicle Specifications. Car and Driver, Car and Driver.

Endress, B. (2016). Personal conversation between Jeremy Worm of Michigan Tech and Bob Endress of Vortech Industrial.

Fu, L., Wu, Z., Yu, X., Deng, J., Hu, Z., Li, L. (2015). Experimental Investigation of Combustion and Emission Characteristics for Internal Combustion Rankine Cycle Engine Under Different Water Injection Laws. The 12th International Conference on Combustion & Energy Utilisation - 12ICCEU, Energy Procedia.

Fuels, V. R. (2014). Specifications for VP Import.

Fuels, V. R. (2016). Specifications of VP110 Racing Fuel.

Gamma_Technologies (2016). User Manual for GT-Power**:** User Manual for GT-Power.

Harrington, J. (1982). Water Additon to Gasoline-Effect on Combustion, Emissions, Performance, and Knock, SAE.

Heywood, J. B. (1988). Internal Combustion Engine Fundamentals. New York, McGraw Hill, Inc.

HP_Tuners_User_Community (2016). Online Repository of Vehicle Calibrations Uploaded by Registered Users of HP Tuners (must have credentials to log-in).

Iacobacci, A., Marchitto, L., Valentino, G. (2017). "Water Injection to Enhance Performance and Emissions of a Turbocharged Gasoline Engine Under High Load Condition." SAE International Journal of Engines.

Joss, A. (2011). SAE Power Certification Form J2723 B; SAE J1349 Certified Power Results for LHU Engine in 2012 Model Year Buick Regal GS, General Motors Following SAE J1349 and J2723 Standards.

Kale V., S. H., Marriott C., Worm J.J., Naber J.D. (2012). Combustion Robustness Characterization of Gasoline and E85 for Startability in a Direct Injection Spark-Ignition Engine, SAE International.

Kim, J., Park, H., Bae, C., Choi, M., Kwak, Y. (2016). "Effects of Water Direct Injection on the Torque Enhancement and Fuel Consumption Reduction of a Gasoline Engine Under High-Load Conditions." International Journal of Engine Research **17**(7): 795-808.

Klein, S. A. (2017). Software Program, Engineering Equation Solver, EES, F-Chart Software, http://fchart.com.

Kohketsu S., M. K., Sakai K. (1996). Reduction of Exhaust Emission with New Water Injection System in a Diesel Engine, SAE.

Kuhring, M. S. (1938). "Water and Water-Alcohol Injection in a Supercharged Jaguar Aircraft Engine." Canadian Jornal of Research **16a**(8).

Lanzafame, R. (1999). Water Injection Effects in a Single Cylinder CFR Engine. SAE International Congress and Exposition. Detroit, MI, SAE International.

Lestz, S. S., Meyer, W.E., Colony, C.M. (1972). Emissions from a Direct-Cylinder Water Injected Spark-Ignition Engine, SAE.

Livengood J. C., W. P. C. (1955). Correlation of Autoignition Phenomena in Internal Combustion Engines and Rapid Compression Machines. Symposium (International) on Combustion.

Maehling, P., Oleski, S., et al. (2017). Separate personal conversations between Jeremy Worm of Michigan Tech, and Peter Maehling of AVL, Sam Oleski of Kistler, and group discussion during a scheduled special talk at SAE World Congress 2017. J. Worm.

Mello J. P., M., A. M., (1999). NOx Emissions from Direct Injection Diesel Engines with Water / Steam Dilution, SAE.

Miayamoto N., O. H., Wang J., Ohashi H. (1995). Significant NOx Reductions with Direct Water Injection into Sub - Chamber of an IDI Diesel Engine, SAE.

Mock, P., German, J., Bandivadekar, A., Riemersma, I., Ligterink, N., Lambrecht, U. (2013). From Laboratory to Road; A Comparison of Official and 'Real-World' Fuel Consumption and CO2 Values for Cars in Europe and The United States. International Council on Clean Transportation.

MotorTrend (2017). MotoTrend Vehicle Specifications. Online, MotoTrend.

MotoTron (2007). "MotoTron Training Manual."

Nande, A., M., Wallner, T., Naber, J. (2008). Influence of Water Injection on Performance and Emissions of a Direct-Injection Hydrogen Research Engine. Powertrains, Fuels and Lubricants Meeting, SAE International.

Nicholls, J. E., Messiri, E., Newhali, H.K. (1968). Inlet Manifold Water Injection for Control of Nitrogen Oxides – Theory and Experiment, SAE.

Odake, M., Koike, N., Tsukamoto, Y., Naurusawa, K., Yoshida, K. (1991). Effects of EGR with a Supplemental Manifold Water Injection to Control Exhaust Emissions from Heavy - Duty Diesel Powered Vehicles, SAE.

Pangborn, E. (2016). Analysis of Regular and Premium Pump Fuel**:** 4.

Pathak, S. K., Sood, V., Singh, Y., Channiwala, S.A. (2017). Impact of "Break In" Running on Exhaust Emissions and Fuel Consumption of a Portable Genset, SAE International.

Peters, B., Tebar, R. (1976). Water-Gasoline Fuels-Their Effect on Spark Ignition Engine Emissions and Performance, SAE.

Porter, J. C. (1950). Alcohol-Water Injection for High Compression Engines, SAE.

Randolph, A. (1990). Cylinder Pressure Transducer Mounting Techniques to Maximize Data Accuracy. SAE World Congress and Exposition. Detroit, MI, SAE International.

Randolph, A. (1990). Methods of Processing Cylinder Pressure Transducer Signals to Maximize Data Accuracy. SAE World Congress and Exposition. Detroit, MI, SAE International.

Ritchie A., B. D., Young A. (2016). "Controlling Low-Speed Pre-Ignition in Modern Automotive Equipment Part 3: Identification of Key Additive Component Types and Other Lubricant Composition Effects on Low-Speed Pre-Ignition." SAE International Journal of Engines.

Robert_Bosch_Gmbh (1996). Bosch Automotive Handbook. Germany, Robert Bosch GmbH.

Rohit, A., Satpathy, S., Choi, J., Hoard, J., Surnilla, G., Hakeem, M. (2017). Literature Survey of Water Injection Benefits on Boosted Spark Ignited Engines. SAE International Congress Detroit, MI, SAE International.

Rothrock, A. M., Kesek, A., Jones, A.W. (1942). The Introduction of Water to the Inlet Air as a Means of Internal Cooling in Aircraft-Engine Cylinders, NACA.

Ryu T.-Y., S. S.-Y., Lee E-H, Choi J-K (1997). Effects of Break-In of a Gasoline Engine on Heat Rejection to Coolant and Engine Metal Temperatures. International Fall Fuels and Lubricants Meeting and Exposition. Tulsa, Oklahoma, USA, SAE International.

SAE_International (2004). J1349; Engine Power Test Code - Spark Ignition and Compression Ignition - Net Power Rating, SAE International.

Schneider, E., Blossfeld, D., (2004). Effect of Break-In and Operating Conditions on Piston Ring and Cylinder Bore Wear in Spark-Ignition Engines. Powertrain & Fluid Systems Conference & Exposition. Tampa, FL, USA, SAE International.

Shimizu, M., Morita, Y., Matsumoto, H., Nozawa, R. (1991). Study of Friction Loss During Break-In Period in an Automotive Engine. JSAE Autumn Conference, SAE International.

Soyelmez, M., S., Ozcan, H. (2013). Water Injection Effects on the Performance of Four-Cylinder, LPG Fuelled SI Engine.

Speed Jr., L. (2015). Conversations and follow-up email between Lake Speed Jr. of Driven Racing Oil, and Jeremy Worm of Michigan Tech APS LABS Regarding Oil additives and specific products. J. Worm.

Speed_Jr., L. (2015). Conversations Regarding Oil Viscosity and Additives. J. Worm.

Stank, J. D. (2011). Analysis of In-Cylinder Pressure Transducer Data Quality Utilizing an SIDI Turbocharged Engine. Mechanical Engineering - Engineering Mechanics. Houghton, MI, Michigan Technological University. **MS**.

Taylor, C. (2016). Telephone conversation between Jeremy Worm of APS LABS, and Chris Taylor, Director of Specialty Chemicals, at VP Racing Fuels. J. Worm.

Tietge, U., Diaz, S., Mock, P., German, J., Bandivadekar, A., Ligterink, N. (2016). From Laboratory to road; A 2016 Update of Official and 'real-world' fuel consumption and CO2 values for Passenger Cars in Europe.

Tsao, K., Wang, C., Miller, E. (1984). Performance of Gasoline-Water Fuel in a Modified SI Engine, SAE.

Walsh, M. P. (1999). Global Trends in Diesel Emissions Control - A 1999 Update, SAE.

Wang, J. K., Li, J.L., Wu, M.H., Chen, R.H. (2009). Reduction of Nitric Oxide Emission from a SI Engine by Water Injection at the Intake Runner. ASME 2009 International Mechanical Engineering Congress & Exposition, Florida, USA, ASME.

Ward's Auto, M. (2017). Light Vehicle Engines: North American Availability & Specifications. W. s. A. a. Mahle. http://wardsauto.com/2017-light-vehicle-engine-chart-sponsored-mahle.

Weatherford, W. D., Quillian, R.D. (1970). Total Cooling of Piston Engines by Direct Water Injection, SAE.

Worm, J. J., Davis, R.S. (2007). Variable Cam Phasing Workshop, GM Powertrain Internal Document, General Motors Powertrain.

Worm, J. J., Dice, P., Jehlik, F., McFarland, J., Miers, S.A. (2013). The Effect of Individual Cylinder Fuel and Air Mixing in a High Performance Automotive Engine.

ASME Internal Combustion Engine Fall Technical Conference. Ann Arbor, MI, ASME Internal Combustion Engine Division.

Worm, J. J., Dice, P., Jehlik, F., McFarland, J., Miers, S.A. (2013). The Effect of Spark Plug Electrode Geometry in a High Performance Automotive Engine. ASME Internal Combustion Engines Fall Technical Conference. Ann Arbor, MI, ASME Internal Combustion Engine Division.

Worm, J. J., Duncan, J., Naber, J.D., Atkinson, W., Barros, S. (2017). "Water Injection as an Enabler for Increased Efficiency at High-Load in a Direct Injected, Boosted, SI Engine." SAE International Journal of Engines **10**(3).

12 : Appendix A: Critical Measurements during Assembly of ESN02

All Dimensions in Inches

Table 14: Critical Dimensions during Assembly of ESN02

Clearance Volumes

	thickness	diameter	volume
Deck Ht. W_9.2	0.0590	3.3867	8.7096
Deck Ht. W_11.0	0.0680	3.3867	10.0381
Deck Ht. Stock	0.0610	3.3867	9.0048
Head Gasket	0.0265	3.4330	4.0196
Top Land			0.8000
Wiseco Dish(9.2)			0.5000
Wiseco Dish(11)			-5.0900
Stock Dish			-1.8000
Cylinder Chamber			47.7000
Swept Volume	3.3860	3.3867	499.8405

Journal Diameters

Crankshaft Mains	+0.0001 taper
1	2.2045
2	2.2045
3	2.2043
4	2.2044
5	2.2045
Crankshaft Rods	+0.0001 taper
1	1.9298
2	1.9298
3	1.9298

4	1.9297	
Piston Skirts		
1	3.3824	
2	3.3825	3.38265
3	3.3828	
4	3.3829	
Wrist Pins		
1	0.9055	
2	0.9055	
3	0.9055	
4	0.9055	

Bore Diameters

Rod W/Insert	
1	1.9319
2	1.9317
3	1.9317
4	1.9317
Rod Pin Bushing	
1	0.9062
2	0.9063
3	0.9061
4	0.9062
Mains W/Insert	
1	2.2071
2	2.2068
3	2.2070
4	2.2075

5	2.2075
Cylinder 1	
Top	3.3871
Mid	3.3865
Bot	3.3864
Avg	3.3867
Out-of-Round	0.0013
Top-->Bottom Taper	0.0007
Cylinder 2	
Top	3.3875
Mid	3.3867
Bot	3.3867
Avg	3.3870
Out-of-Round	0.0015
Top-->Bottom Taper	0.0008
Cylinder 3	
Top	3.3877
Mid	3.3868
Bot	3.3866
Avg	3.3867
Out-of-Round	0.0014
Top-->Bottom Taper	0.0011
Cylinder 4	
Top	3.3878
Mid	3.3870
Bot	3.3867
Avg	3.3872
Out-of-Round	0.0013

Top-->Bottom Taper	0.0011

Oil Clearances

Main Bearings

1	0.0026
2	0.0023
3	0.0027
4	0.0031
5	0.0030

Rod Bearings

1	0.0021
2	0.0019
3	0.0019
4	0.0020

Rod Pin Bushings

1	0.0007
2	0.0008
3	0.0006
4	0.0007

Thrust and Side Clearances

Rods

1

2

3

4

Crankshaft End Play

Cylinder 1

1st Ring	0.0240
2nd Ring	0.0260
Piston-Wall	0.0043
Cylinder 2	
1st Ring	0.0240
2nd Ring	0.0260
Piston-Wall	0.0045
Cylinder 3	
1st Ring	0.0240
2nd Ring	0.0260
Piston-Wall	0.0039
Cylinder 4	
1st Ring	0.0240
2nd Ring	0.0260
Piston-Wall	0.0043

13 : Appendix B: Compression Ratio Analysis of ESN02

Table 15: Compression Ratio Data for ESN02.

Cylinder	Bore (mm)	Stroke (mm)	Top Ring Land Dia (mm)	Top Ring Land Depth (mm)	Piston Measurement Depth (TDC to Measurement Postion) (mm)	Measured Block Volume Above Piston (cm^3)	Block Side contribution to clearance volume (cm^3)	Gasket Dia (mm)	Gasket Thickness (mm)	Gasket Vol (cm^3)	Head Chamber Vol (cm^3)	Total Clearance Vol (cm^3)	Comp Ratio	Design Intent CR	CR Error	Otto Cycle Efficiency	Displaced Volume (cm^3)	Notes
1	86.022	86	85.1344	6.6802	4.270	34.2	10.173	87.198	0.673	4.020	47.7	61.89	9.076	9.20	-0.12	0.59	499.81	Wiseco 9.2
2	86.022	86	85.2106	5.486	5.321	38.5	8.172	87.198	0.673	4.020	47.7	59.89	9.345	9.20	0.15	0.59	499.81	Production 9.2
3	86.022	86	85.1281	6.6802	3.884	28.0	6.232	87.198	0.673	4.020	47.7	57.95	9.625	11.00	-1.38	0.60	499.81	Wiseco 11.0

14 : Appendix C: Transducer Passage Helmholtz Resonance Analysis

Table 16: Transducer Passage Helmholtz Resonance Analysis

Helmholtz Renonator Requency Calculation

Assume this calculator is for a small cylindrical pasage connecting to a large cylindrical chamber, as sho

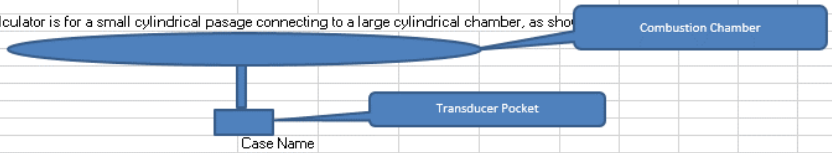

	Case Name											
	Nominal Dimensions											
Depth of Combustion Chamber Passage (mm)	13	12	11	10	9	8	7	6	5	4	3	2
Diameter of Combustion Chamber Passage (mm)	3	3	3	3	3	3	3	3	3	3	3	3
Depth of Transducer Face Pocket (mm)	1.27	1.27	1.27	1.27	1.27	1.27	1.27	1.27	1.27	1.27	1.27	1.27
Diameter of Transducer Face Pocket (mm)	3.3782	3.3782	3.3782	3.3782	3.3782	3.3782	3.3782	3.3782	3.3782	3.3782	3.3782	3.3782
Depth of Flame Arrestor Face Pocket (mm)	0.1524	0.1524	0.1524	0.1524	0.1524	0.1524	0.1524	0.1524	0.1524	0.1524	0.1524	0.1524
Diameter of Flame Arrestor Face Pocket (mm)	3.4036	3.4036	3.4036	3.4036	3.4036	3.4036	3.4036	3.4036	3.4036	3.4036	3.4036	3.4036
Flame Arrestor Depth into Transducer Pocket (mm)	1.143	1.143	1.143	1.143	1.143	1.143	1.143	1.143	1.143	1.143	1.143	1.143
Diameter of Flame Arrestor (mm)	3.3782	3.3782	3.3782	3.3782	3.3782	3.3782	3.3782	3.3782	3.3782	3.3782	3.3782	3.3782
Diameter of Flame Arrestor Holes (mm)	0.4572	0.4572	0.4572	0.4572	0.4572	0.4572	0.4572	0.4572	0.4572	0.4572	0.4572	0.4572
Length of Flame Arrestor Holes (mm)	1.4478	1.4478	1.4478	1.4478	1.4478	1.4478	1.4478	1.4478	1.4478	1.4478	1.4478	1.4478
Number of Flame Arrestor Holes	18	18	18	18	18	18	18	18	18	18	18	18
Ratio of Specific Heats (:)	1.36	1.36	1.36	1.36	1.36	1.36	1.36	1.36	1.36	1.36	1.36	1.36
Temperature (K)	900	900	900	900	900	900	900	900	900	900	900	900
Molecular Weight of Gas (kg/kmol)	28.97	28.97	28.97	28.97	28.97	28.97	28.97	28.97	28.97	28.97	28.97	28.97
Cross Sectional Area of Combustion Chamber Passa	7.0686E-06	7.0686E-06	7.0686E-06	7.0686E-06	7.1E-06	7.1E-06	7.1E-06	7.1E-06	7.1E-06	7.1E-06	7.1E-06	7.1E-06
Cross Sectional Area of a single flame arrestor Passa	1.6417E-07	1.6417E-07	1.6417E-07	1.6417E-07	1.6E-07	1.6E-07	1.6E-07	1.6E-07	1.6E-07	1.6E-07	1.6E-07	1.6E-07
Volume of Combustion Chamber Passage (m^3)	9.1892E-08	8.4823E-08	7.7754E-08	7.0686E-08	6.4E-08	5.7E-08	4.9E-08	4.2E-08	3.5E-08	2.8E-08	2.1E-08	1.4E-08
Volume of Transducer Pocket (m^3)	1.1383E-08	1.1383E-08	1.1383E-08	1.1383E-08	1.1E-08	1.1E-08	1.1E-08	1.1E-08	1.1E-08	1.1E-08	1.1E-08	1.1E-08
Volume of Transducer Pocket Less Flame Arrestor (m	1.1383E-09	1.1383E-09	1.1383E-09	1.1383E-09	1.1E-09	1.1E-09	1.1E-09	1.1E-09	1.1E-09	1.1E-09	1.1E-09	1.1E-09
Volume of Flame Arrestor Pocket (m^3)	1.3866E-09	1.3866E-09	1.3866E-09	1.3866E-09	1.4E-09	1.4E-09	1.4E-09	1.4E-09	1.4E-09	1.4E-09	1.4E-09	1.4E-09
Total Volume of Flame Arrestor Holes (m^3)	1.3548E-08	1.3548E-08	1.3548E-08	1.3548E-08	1.4E-08	1.4E-08	1.4E-08	1.4E-08	1.4E-08	1.4E-08	1.4E-08	1.4E-08
Total Pocket Volume (m^3)	1.6073E-08	1.6073E-08	1.6073E-08	1.6073E-08	1.6E-08	1.6E-08	1.6E-08	1.6E-08	1.6E-08	1.6E-08	1.6E-08	1.6E-08
Total Volume Added to Combustion Chamber (cc)	0.09441651	0.08734792	0.08027934	0.07321076	0.06614	0.05907	0.05201	0.04494	0.03787	0.0308	0.02373	0.01666
Speed of Sound (m/s)	594	594	594	594	594	594	594	594	594	594	594	594
as a single volume (i.e. flame arrestor pocket, plus flame arrestor holes, plus any volume between the flame arrestor and transducer) (Hz)	**17378**	**18087**	**18891**	**19813**	**20885**	**22152**	**23682**	**25579**	**28020**	**31328**	**36174**	**44304**
Helmholtz Frequency 2 (Only accounts for the flame arrestor pocket volume) (Hz)	**59165**	**61581**	**64319**	**67458**	**71107**	**75421**	**80628**	**87088**	**95401**	**106661**	**123162**	**150842**
resonator formed from a flame arrestor passage and the volume between the flame arrestor and transducer; but NOT accounting for the volume of the other	**29820**	**29820**	**29820**	**29820**	**29820**	**29820**	**29820**	**29820**	**29820**	**29820**	**29820**	**29820**

15 : Appendix D: Fuel Property Analysis Reports

MANY TESTS. ONE LABORATORY.

PARAGON Laboratories

ANALYTICAL RESULTS

Workorder: 207572 MICH TECH-041816

Lab ID: **2075720001** Date Collected: 4/15/2016 10:45 Matrix: Gasoline

Sample ID: FREEDOM 87 AKI Date Received: 4/18/2016 09:05

Sample Desc: PO:

Parameters	Qualifier	Result Units	Dilution Factor	Reporting Limit	Result Qualifier Min	Result Qualifier Max	Analyzed	By
Elemental Analysis								
Analytical Method: ASTM D5291 [A]								
Carbon (Wt%)		81.75 % m/m	1	0.05			4/20/2016 15:00	AKL
Hydrogen (Wt%)		14.33 % m/m	1	0.05			4/20/2016 15:00	AKL
Analytical Method: ASTM D5622 [A]								
Oxygen (Wt%)		3.92 % m/m	1	0.05			4/20/2016 08:43	DHN
Individual Parameters								
Analytical Method: ASTM D4052 [A]								
API Gravity at 15.56°C		65.4 °API	1	0.1			4/19/2016 16:16	AJB2
Density at 15.56°C		0.7179 g/mL	1	0.0001			4/19/2016 16:16	AJB2
Spec. Grav. at 15.56°C/15.56°C		0.7186	1	0.0001			4/19/2016 16:16	AJB2
Analytical Method: ASTM D240 [A]								
Gross Heating Value (BTU/lb)		19393 BTU/lb	1	175			4/28/2016 14:42	ALB
Gross Heating Value (MJ/kg)		45.109 MJ/kg	1				4/28/2016 14:42	ALB
Net Heating Value (BTU/lb)		18086 BTU/lb	1	175			4/28/2016 14:42	ALB
Net Heating Value(MJ/kg)		42.068 MJ/kg	1				4/28/2016 14:42	ALB
Octanes								
Analytical Method: ASTM D2699 & D2700 [A]								
Research Octane Number		90.6	1	1.0			4/22/2016 13:40	AKL
Motor Octane Number		85.0	1	1.0			4/22/2016 13:40	AKL
AKI Calculation		87.8	1	1.0			4/22/2016 13:40	AKL
Sensitivity		5.6	1	1.0			4/22/2016 13:40	AKL

[A] Paragon Laboratories, Inc. is accredited to ISO/IEC 17025 by A2LA for analytical methods referring to this footnote. (A2LA Cert. No. 2705.01 Expires 3/31/2017)
Paragon Laboratories, Inc. is certified by the Michigan DEQ to analyze Drinking Water. (MDEQ Lab No. 9901 Expires 2/25/2017)

Generated: 4/29/2016 11:29:49 AM

12649 Richfield Ct. Livonia, MI 48150 P 734.462.3900 F 734.462.3911 W http://www.paragonlaboratories.com

MANY TESTS. ONE LABORATORY.

PARAGON Laboratories

ANALYTICAL RESULTS

Workorder: 207572 MICH TECH-041816

Lab ID: **2075720002** Date Collected: 4/15/2016 10:45 Matrix: Gasoline

Sample ID: FREEDOM 91 AKI Date Received: 4/18/2016 09:05

Sample Desc: PO:

Parameters	Qualifier	Result	Units	Dilution Factor	Reporting Limit	Result Qualifier Min	Result Qualifier Max	Analyzed	By
Elemental Analysis									
Analytical Method: ASTM D5291 [A]									
Carbon (Wt%)		85.78	% m/m	1	0.05			4/20/2016 15:00	AKL
Hydrogen (Wt%)		14.22	% m/m	1	0.05			4/20/2016 15:00	AKL
Analytical Method: ASTM D5622 [A]									
Oxygen (Wt%)		<0.05	% m/m	1	0.05			4/20/2016 08:43	DHN
Individual Parameters									
Analytical Method: ASTM D4052 [A]									
API Gravity at 15.56°C		64.6	°API	1	0.1			4/19/2016 16:16	AJB2
Density at 15.56°C		0.7209	g/mL	1	0.0001			4/19/2016 16:16	AJB2
Spec. Grav. at 15.56°C/15.56°C		0.7216		1	0.0001			4/19/2016 16:16	AJB2
Analytical Method: ASTM D240 [A]									
Gross Heating Value (BTU/lb)		20164	BTU/lb	1	175			4/28/2016 09:52	ALB
Gross Heating Value (MJ/kg)		46.901	MJ/kg	1				4/28/2016 09:52	ALB
Net Heating Value (BTU/lb)		18866	BTU/lb	1	175			4/28/2016 09:52	ALB
Net Heating Value(MJ/kg)		43.883	MJ/kg	1				4/28/2016 09:52	ALB
Octanes									
Analytical Method: ASTM D2699 & D2700 [A]									
Research Octane Number		94.8		1	1.0			4/22/2016 14:00	AKL
Motor Octane Number		88.4		1	1.0			4/22/2016 14:00	AKL
AKI Calculation		91.6		1	1.0			4/22/2016 14:00	AKL
Sensitivity		6.4		1	1.0			4/22/2016 14:00	AKL

Generated: 4/29/2016 11:29:50 AM

12649 Richfield Ct. Livonia, MI 48150 P 734.462.3900 F 734.462.3911 W http://www.paragonlaboratories.com

MAKIN' POWER!™
www.vpracingfuels.com

Specification Sheet: VP110

(TYPICAL VALUES)

Specific Gravity: 0.720 – 0.735 @ 60°F/15.6°C

Color: Purple

MON: 107

RON:113

R+M/2: 110

RVP: 6.6 - 6.8psi/45.5 – 46.9kpa

Oxidation Stability (min.) 1440+

Distillation:
10% evap @145 -149°F/62.8 - 65°C
50% evap @ 208 - 215°F/97.8 – 101.7°C
90% evap @ 220 - 227°F/104.4 – 108.3°C
E.P. @ 243 - 263°F/117.2 – 128.3°C

H:C ratio = 2.12

Stoichiometric Ratio = 14.91

Production: Elmendorf, Texas USA

Availability: Sealed Drums

Rev 03/14

VP Racing Fuels, Inc. • P.O. Box 47878 San Antonio, TX 78265 • Phone: (210) 635-7744 • Fax: (210) 635-7799

MAKIN' POWER!™
www.vpracingfuels.com

Specification Sheet: VP Import

(TYPICAL VALUES)

Specific Gravity: 0.744 @ 60°F/15.6°C

Color: Clear

MON: 120+

RON:120+

R+M/2: 120+

RVP: 3.7psi/25.5kpa

Oxygen Content: 3.63% by weight

Oxidation Stability (min.) 1440+

Distillation:
10% evap @ 178.9°F/81.6°C
50% evap @ 218.2°F/103.4°C
90% evap @ 323.2°F/161.8°C
E.P. @ 350.9°F/177.2°C

Production: Elmendorf, Texas USA

Availability: Sealed Drums

Rev 03/14

VP Racing Fuels, Inc. • P.O. Box 47878 San Antonio, TX 78265 • Phone: (210) 635-7744 • Fax: (210) 635-7799

Email from VP Racing Fuels Regarding Heating Value

Hi Jeremy,

The net heating value for VP110 is 17,640 BTU/#. The net heating value for VP Import is 17,557 BTU/#. The oxygen content of VP Import comes from MTBE.

H:C ratio = 2.039 to 1

Stoichiometric A/F ratio = 14.11 to 1

Regards,

Duane Minazzi
Senior Chemist
VP Racing Fuels, Inc.
P. O. Box 47878
San Antonio, Texas 78265
Phone: (210) 635-7744
Fax: (210) 635-7999

16 . Appendix E: SAE Certified Power Results

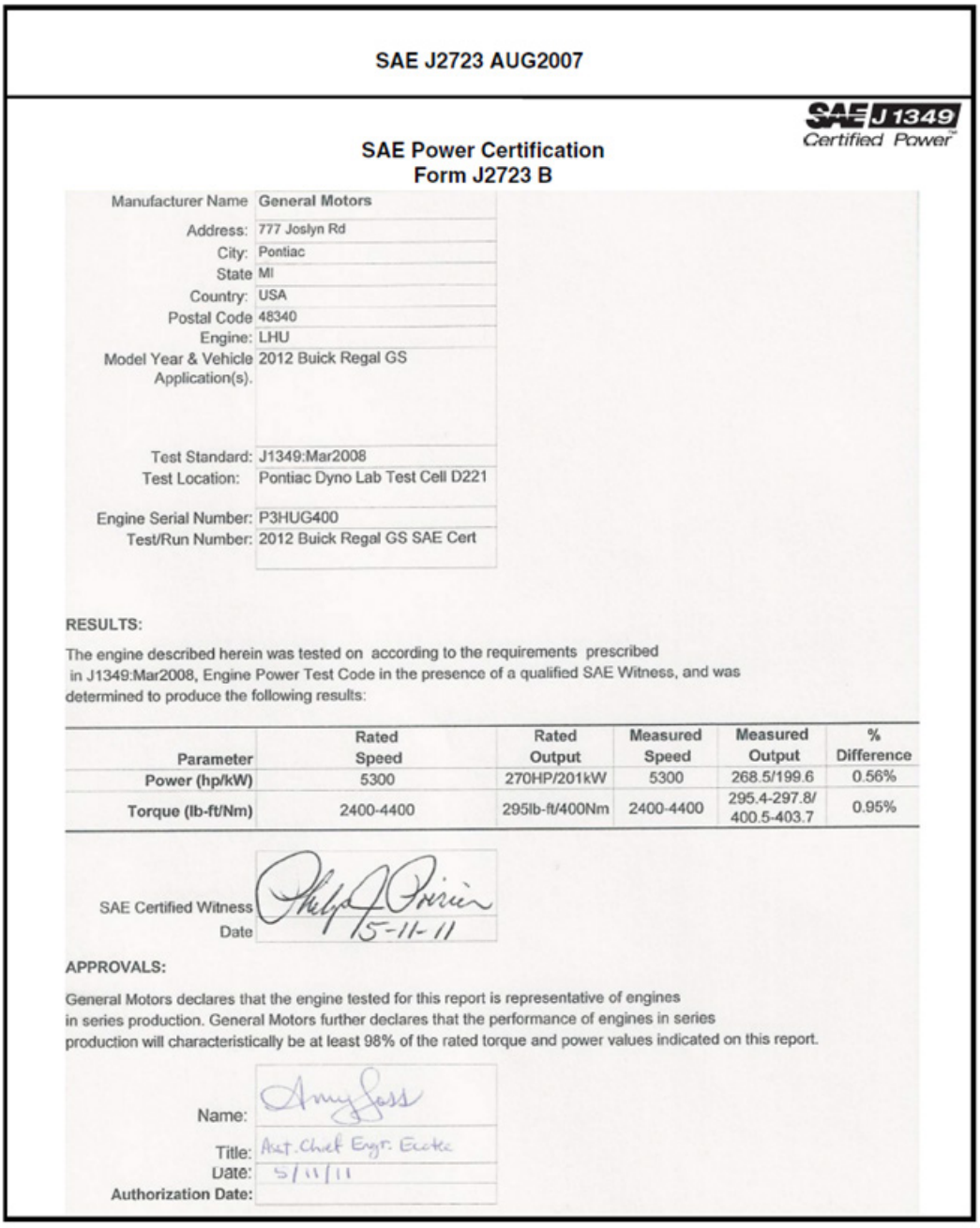

SAE J2723 AUG2007

SAE J1349 Certified Power™

SAE Power Certification
Form J2723 B

Manufacturer Name	General Motors
Address:	777 Joslyn Rd
City:	Pontiac
State	MI
Country:	USA
Postal Code	48340
Engine:	LHU
Model Year & Vehicle Application(s).	2012 Buick Regal GS
Test Standard:	J1349:Mar2008
Test Location:	Pontiac Dyno Lab Test Cell D221
Engine Serial Number:	P3HUG400
Test/Run Number:	2012 Buick Regal GS SAE Cert

RESULTS:

The engine described herein was tested on according to the requirements prescribed in J1349:Mar2008, Engine Power Test Code in the presence of a qualified SAE Witness, and was determined to produce the following results:

Parameter	Rated Speed	Rated Output	Measured Speed	Measured Output	% Difference
Power (hp/kW)	5300	270HP/201kW	5300	268.5/199.6	0.56%
Torque (lb-ft/Nm)	2400-4400	295lb-ft/400Nm	2400-4400	295.4-297.8/ 400.5-403.7	0.95%

SAE Certified Witness: Philip J. Perrin
Date: 5-11-11

APPROVALS:

General Motors declares that the engine tested for this report is representative of engines in series production. General Motors further declares that the performance of engines in series production will characteristically be at least 98% of the rated torque and power values indicated on this report.

Name: Amy Fass
Title: Asst. Chief Engr. Ecotec
Date: 5/11/11
Authorization Date:

WOT ENGINE POWER PLOT (as tested)

SAE J1349 Certified Power™

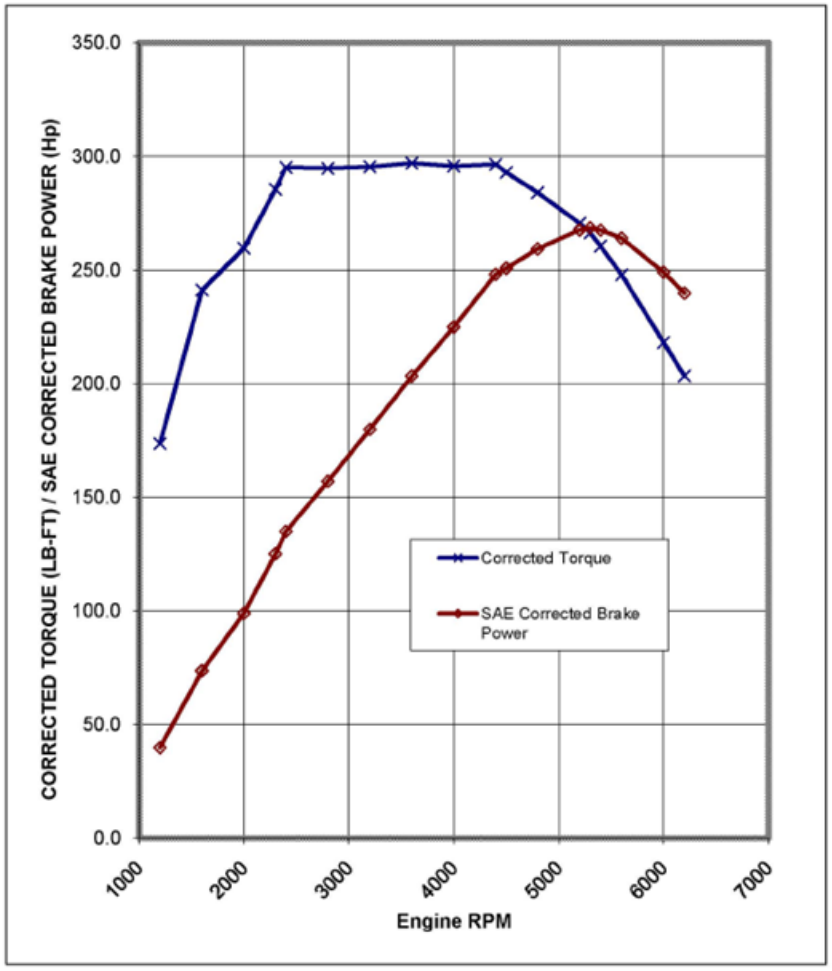

17 . Appendix F: Copyright documentation

17.1 Permission to reproduce Figure 1, from (Bassett 2016).

Order Details

SAE International journal of engines

Order detail ID: 70795783
Order License Id: 4232490897896

ISSN: 1946-3944
Publication Type: Journal
Volume:
Issue:
Start page:
Publisher: SAE International
Author/Editor: Society of Automotive Engineers

Permission Status: Granted
Permission type: Republish or display content
Type of use: Thesis/Dissertation

Hide details

Requestor type	Academic institution
Format	Electronic
Portion	chart/graph/table/figure
Number of charts/graphs/tables/figures	1
The requesting person/organization	Jeremy Worm / Michigan Tech
Title or numeric reference of the portion(s)	Figure 1
Title of the article or chapter the portion is from	Heavily Downsized Gasoline Demonstrator
Editor of portion(s)	NA
Author of portion(s)	Bassett, M., Hall, J., Hibberd, B., Borman, S., Reader, S., Gray K., Richards, B.
Volume of serial or monograph	N/A
Page range of portion	2
Publication date of portion	June 2016
Rights for	Main product
Duration of use	Life of current edition
Creation of copies for the disabled	no
With minor editing privileges	no
For distribution to	Worldwide
In the following language(s)	Original language of publication
With incidental promotional use	no
Lifetime unit quantity of new product	Up to 499
Title	The Impact of Water Injection on Spark Ignition Engine Performance Under High Load Operation
Instructor name	Jeremy Worm
Institution name	Michigan Technological University
Expected presentation date	Dec 2017

Note: This item will be invoiced or charged separately through CCC's **RightsLink** service. More info **$ 71.50**

Total order items: 1

This is not an invoice.

Order Total: 71.50 USD

17.2 Permission to use screen images and plots from GT-Power and GT-Post software produced by Gamma Technologies Incorporated.

Christopher Contag <C.Contag@gtisoft.com> 9:15 AM (12 minutes ago)

to me

Hello Jeremy,

Thank you for contacting us, you can of course use screen prints from your model and plots from GT-POST to show your results.

Congratulations on finishing your dissertation, please let us know, if you need any support from us.

Best Regards,
Chris

Christopher A. Contag
Senior Engineer
System Solutions Engineering
+1 (630) 537-9214
601 Oakmont Lane, Suite 220, Westmont, IL, 60559

From: Jeremy Worm [mailto:jjworm@mtu.edu]

Sent: Tuesday, November 21, 2017 7:07 AM

To: GT Leads Website <website_inbound@gtisoft.com>

Subject: Michigan Tech Information Request

Message Body:

Name: Jeremy Worm

Organization: Michigan Tech

Street Address: 1400 Townsend Dr, 815 R.L. Smith Mechanical Engineering Building

City: HOUGHTON

State: MI

Country: United States

Phone: 9064872686

Email: jjworm@mtu.edu

Inquiry type: Other

Reference source: Already a Customer

Comments:

Hello,

I am finishing my PhD dissertation and am requesting permission to use some images from GT-Power. Specifically 1) I would like to include a screen print of the GT-Power Model I used in my work. 2) I would like to include a plot from GT-Post.

Can you please grant me permission to reproduce those items in my dissertation? I will of course include a full credit to GTI.

Kind Regards,

Jeremy

--

This e-mail was sent from a contact form on Gamma Technologies (https://www.gtisoft.com)

17.3 Permission to use Property Plots from EES

F-Chart Software has included a statement on referencing EES on their Frequently Asked Questions list on their website: http://fchart.com/assets/downloads/faq.pdf. The response is as follows:

I Need to Reference EES in my publication

If you use EES to produce results that are to be published, you should reference the program as follows. Klein, S.A., EES – Engineering Equation Solver, Version XX.YYY, date F-Chart Software, http://fchart.com The version number and date are displayed on the EES startup screen.

Additionally, F-Chart software was contacted via the contact form on the website. The response is shown below:

Re: Requesting Permission to Reproduce Property Plots

Inbox x

S.A. Klein 11:10 AM (3 hours ago)

to me

Mr. Worm

You have my permission to include property plots from EES in your dissertation provided acknowledgement is provided.

Best wishes

S.A. Klein
On 11/21/2017 6:57 AM, Jeremy Worm wrote:
Hello,

I am finishing my PhD dissertation and I would like to include several property plots that I produced using EES. I would like to use some T-v, and T-h diagrams for water. I will of course give full credit and acknowledgement. Will you please provide permission for me to reproduce these property plots in my dissertation?

Kind Regards,

Jeremy Worm, P.E.
Director, Michigan Tech Mobile Lab
Advanced Power Systems Research Center
Department of Mechanical Engineering - Engineering Mechanics
Michigan Tech
Office: 906-487-2686
Cell: 906-369-0886

17.4 Permission to Use Images from Bosch Motorsports

Uwe Ostmann (XDI) 1:56 PM (47 minutes ago)

to me

Go ahead, Bosch confirmed.
Please just use the Block structure but not the decription or the page numbers etc.

Let me know if you need something else

Best Regards/Mit freundlichen Grüßen

Uwe Ostmann
Xtreme-DI LLC

Tel. +1(248)756-4715

This electronic message contains information, which may be confidential, legally privileged or otherwise protected from disclosure. This information is intended for the use of the addressee only. If you are not the intended recipient, you are hereby notified that any disclosure, copying, distribution, printing or any other use of, or any action in reliance on, the contents of this electronic message is strictly prohibited. If you have received this communication in error, please notify the sender by telephone at the number noted above and destroy the original message.

From: Jeremy Worm [mailto:jjworm@mtu.edu]
Sent: Tuesday, November 21, 2017 10:21 AM
To: Uwe Ostmann (XDI)
Subject: Seeking Permission to use a Screen Schot

Uwe,

I hope all is going well with you.

I am finishing up my dissertation on the work that I used the MS6.3 for. I would like to include some images.

Specifically I would like to use:

1) a screen print of a single page of the software description manual showing the Simulink block structure and,

2) a screen print of a single screen in Race Con showing what the test cell operator sees when running the engine.

Can you please grant me permission to reproduce those images in my dissertation? I will of course include full credit and acknowledgment.

Kind Regards,

Jeremy

Jeremy Worm, P.E.
Director, Michigan Tech Mobile Lab
Advanced Power Systems Research Center
Department of Mechanical Engineering - Engineering Mechanics
Michigan Tech
Office: 906-487-2686
Cell: 906-369-0886

17.5 Permission to Use Compressor Map for Production LNF / LHU Engine

RE: Turbo Information

Inbox x

khenderson@borgwarner.com 8:33 AM (23 hours ago)

to me

Hi Jeremy,

I would actually have to get approval myself to okay the reproduction… however, I pulled all of the BorgWarner logos etc. off the map so I see no harm in your using it in your dissertation. Good luck!

Thanks,
Kurt Henderson
Engineer – Accelerated Innovation
BorgWarner Turbo Systems
Fax: (800) 424-6464
Desk: (828) 684-4095
khenderson@borgwarner.com

Check us out at http://www.turbodriven.com & www.airwerksboosted.com

From: Jeremy Worm [mailto:jjworm@mtu.edu]
Sent: Monday, November 20, 2017 4:09 PM
To: Henderson, Kurt (Asheville)
Subject: Re: Turbo Information

Kurt,

I hope all is going well for you!

Thanks again for sending me this map.

I am in the final stages of my PhD Dissertation now. I would like to include this map in my dissertation in the section on the experimental setup for the baseline engine. I of course do not want to include this without proper permission. Can you reply to this email letting me know it is OK to reproduce this in my dissertation?

Kind Regards,

Jeremy

Jeremy Worm, P.E.
Director, Michigan Tech Mobile Lab
Advanced Power Systems Research Center
Department of Mechanical Engineering - Engineering Mechanics
Michigan Tech
Office: 906-487-2686
Cell: 906-369-0886

As an additional confidentiality measure, this author redacted all of the axis labels on both the x, and y-axis, rendering the compressor map ineffective for anything other than illustrative purposes only.

17.6 Permission to Use Figures From SAE 2017-01-0663

November 21, 2017

Jeremy Worm, P.E.
Director, Michigan Tech Mobile Lab
Advanced Power Systems Research Center
Department of Mechanical Engineering - Engineering Mechanics
Michigan Tech

Dear Jeremy,

Thank you for your email. Permission is granted for you to include content from your previously published technical paper 2017-01-0663, "Worm, J., Naber, J., Duncan, J., Barros, S. et al., "Water Injection as an Enabler for Increased Efficiency at High-Load in a Direct Injected, Boosted, SI Engine," *SAE Int. J. Engines* 10(3):951-958, 2017, https://doi.org/10.4271/2017-01-0663. It is my understanding that the thesis will not be available commercially.

The following conditions apply:

-A new copyright permission request is required for any further use of this material, other than that specified within your original request.

-The SAE material must be clearly identified and include the following statement *"Reprinted with permission Copyright © 2017 SAE International. Further distribution of this material is not permitted without prior permission from SAE."*

-Any language use, other than specified within your email, requires a new copyright request and additional fee.

Best regards,

Mandy L. May
Manager, Digital Publishing
Content Management

SAE INTERNATIONAL
400 Commonwealth Drive
Warrendale, PA 15096

o +1.724.772.8564
e mandy.may@sae.org
www.sae.org

17.7 Permission to use Installation Drawing of PCB Transducer

PCB PIEZOTRONICS
MTS SYSTEMS CORPORATION

November 22, 2017

Mr. Jeremy Worm, P.E.
Director, Michigan Tech Mobile Lab
Advanced Power Systems Research Center
Department of Mechanical Engineering - Engineering Mechanics
Michigan Tech University

Re: PCB Piezotronics, Inc.
Use of Image, Materials & Trademarks for PhD Dissertation

Dear Mr. Worm,

I write to confirm that PCB Piezotronics, Inc. ("PCB") has granted you permission to use a certain image that is the property of PCB, subject to the conditions stated in this letter. The image is PCB drawing number 50910, Rev C., which is the outline drawing for PCB pressure sensor model 115A04. This limited permission shall be effective upon PCB's receipt of a copy of this letter countersigned by you to acknowledge acceptance of these conditions.

This permission is limited to reproduction of such image for use in connection with your PhD dissertation. This permission does not extend to the reproduction or publication of such image in any other work without further written approval of PCB.

While the sensor in question is a charge mode sensor, any use of the acronyms "I.C.P." or "ICP", or the term "integrated-circuit piezoelectric", shall be made only in reference to PCB manufactured products.

Your dissertation shall include the following acknowledgment:
Image of [e.g., transducers] and other materials provided courtesy of PCB Piezotronics, Inc. and used with permission. The views expressed in this paper are those of the author and do not necessarily represent the views of PCB.

If applicable, the following shall also be included within your dissertation:
I.C.P.®, ICP® and PCB® are registered trademarks of PCB Piezotronics, Inc.

Very truly yours,

Joseph M. Marris
General Counsel

AGREED & ACCEPTED:

By: Aaron Worm

Dated: 11-22-2017

PCB PIEZOTRONICS, INC. — CORPORATE HEADQUARTERS
3425 Walden Avenue, Depew, New York 14043-2495 USA
Phone: 716-684-0001 Fax: 716-684-0987
E-mail: info@pcb.com
Web site: www.pcb.com
A2LA Accredited to ISO 17025

17.8 Permission to Use Image of MotoTune Screen Capture

RE: Requesting Permission to Reproduce a MotoTune Screen Shot

Inbox x

Mickey Swortzel <mswortzel@neweagle.net> Nov 22 (7 days ago)

to me, Communications

Jeremy

Thanks for asking and yes, please use the screen shots.

If we can help in the future, please let us know.

Mickey

For a faster response or to schedule time on my calendar, please contact my assistant, Taylor, at thageman@neweagle.net

---

Mary M. "Mickey" Swortzel
CFO
734.929.4557

Facebook | Twitter | LinkedIn | Web
https://www.linkedin.com/in/mickeyswortzel

From: Jeremy Worm [mailto:jjworm@mtu.edu]
Sent: Tuesday, November 21, 2017 2:18 PM
To: Communications <communications@neweagle.net>
Subject: Requesting Permission to Reproduce a MotoTune Screen Shot

Hello,

I am finishing up my PhD dissertation on a project that I used a MotoTron system for the experimental work. I would like to include a screen print of one of the calibration tables in MotoTune.

Can you please grant me permission to reproduce the screen shot image in my dissertation? I will of course include full credit and acknowledgment.

Kind Regards,

Jeremy

Jeremy Worm, P.E.
Director, Michigan Tech Mobile Lab
Advanced Power Systems Research Center
Department of Mechanical Engineering - Engineering Mechanics
Michigan Tech
Office: 906-487-2686
Cell: 906-369-0886

17.9 Permission to Use Image of ARP Fasteners

Re: Seeking permission to reproduce an image from the ARP Website
TRISH YUNICK Nov 28 (1 day ago)

to me

That's fine. Best wishes on getting it done!
trish
On Nov 28, 2017, at 2:34 PM, Jeremy Worm <jjworm@mtu.edu> wrote:

It has been a little while, but I do seem to recall using a lube packet that came with the kit. So I'm good with this image if you are OK with it.

Jeremy

Jeremy Worm, P.E.
Director, Michigan Tech Mobile Lab
Advanced Power Systems Research Center
Department of Mechanical Engineering - Engineering Mechanics
Michigan Tech
Office: 906-487-2686
Cell: 906-369-0886

On Tue, Nov 28, 2017 at 1:59 PM, TRISH YUNICK <trishyunick@me.com> wrote:
Did you use our Ultra Torque assembly lube as provided? Since you don't mention it in the text and it's not specifically pertinent, would you prefer the kit image without the lube packet?

Please credit: © 2017 AUTOMOTIVE RACING PRODUCTS, INC.
On Nov 28, 2017, at 1:52 PM, Jeremy Worm <jjworm@mtu.edu> wrote:

Trish,

Thanks for the fast reply! It always makes such huge difference when you finally find the right person to talk to!

Attached is the section from my dissertation where I talk about fasteners in the experimental build, and you can see the image that I am using.

Thanks!

Jeremy

Jeremy Worm, P.E.
Director, Michigan Tech Mobile Lab
Advanced Power Systems Research Center
Department of Mechanical Engineering - Engineering Mechanics
Michigan Tech
Office: 906-487-2686
Cell: 906-369-0886

On Tue, Nov 28, 2017 at 1:19 PM, TRISH YUNICK <trishyunick@me.com> wrote:
Hi Jeremy,

Can you tell me what image you'd like to use? As long as we're properly credited, it will be fine.
Thank you,
trish
On Nov 28, 2017, at 1:14 PM, Jeremy Worm <jjworm@mtu.edu> wrote:

Hi Trish,

I was given your name and email from the a person I talked to at ARP.

I am finishing a PhD dissertation on some experimental work I did running water injection on an engine. I used ARP head studs in the test engines. I would like to include a picture of the head studs from the ARP webpage in my dissertation.

Can you please grant me permission to reproduce a picture of a head stud kit from your website?

Thanks,

Jeremy

Jeremy Worm, P.E.
Director, Michigan Tech Mobile Lab
Advanced Power Systems Research Center
Department of Mechanical Engineering - Engineering Mechanics
Michigan Tech
Office: 906-487-2686
Cell: 906-369-0886

Trish Yunick
ARP, Inc
www.ARP-Bolts.com
Carbon Press
www.SmokeyYunick.com

<ARP Figure.Worm Dissertation.docx>

17.10 Permission to Use Turbocharger Compressor Maps From BorgWarner

Re: Seeking permission to reproduce compressor maps from catalog

Inbox x

jvincent@borgwarner.com 11:05 PM (13 hours ago)

to me

Hi Jeremy,

You are welcome to post the maps in your dissertation provided you use the proper citations. It would also be appreciated if you included www.borgwarnerboosted.com<http://www.borgwarnerboosted.com> in your citation. Lastly, it's recommended to use the latest maps found in the 2018 catalog vs. the 2015 version.

Thanks,

John Vincent
Regional Sales Manager, IAM
+1 828-458-3159 mobile ET
jvincent@borgwarner.com<mailto:jvincent@borgwarner.com>

Sent from my iPhone

On Nov 29, 2017, at 7:13 PM, Jeremy Worm <jjworm@mtu.edu<mailto:jjworm@mtu.edu>> wrote:

Hi John,

Just touching base with you on this to confirm you are OK with me reproducing these two compressor maps.

Thanks,

Jeremy

Jeremy Worm, P.E.
Director, Michigan Tech Mobile Lab
Advanced Power Systems Research Center
Department of Mechanical Engineering - Engineering Mechanics
Michigan Tech
Office: 906-487-2686
Cell: 906-369-0886

On Tue, Nov 28, 2017 at 3:42 PM, Jeremy Worm <jjworm@mtu.edu<mailto:jjworm@mtu.edu>> wrote:
John,

Dissertations are public documents, so although they are not published in the same sense that a paper is through SAE or some journal, it is published in the sense that anyone could access it if they wanted.

As for the catalog, I pulled the images out of the 2015 Catalog, Edition 3. Is that OK?

Thanks,

Jeremy

Jeremy Worm, P.E.
Director, Michigan Tech Mobile Lab
Advanced Power Systems Research Center
Department of Mechanical Engineering - Engineering Mechanics
Michigan Tech
Office: 906-487-2686<tel:(906)%20487-2686>
Cell: 906-369-0886<tel:(906)%20369-0886>

On Tue, Nov 28, 2017 at 2:52

PM, jvincent@borgwarner.com<mailto:jvincent@borgwarner.com>
<jvincent@borgwarner.com<mailto:jvincent@borgwarner.com>> wrote:
Hi Jeremy,

Thanks for the additional information. Will this be published anywhere? Also, please confirm that your maps came from the 2018 catalog which is posted here:

http://www.turbos.bwauto.com/aftermarket/downloads.aspx

[cid:image001.png@01D36858.396816D0]

Thank you,

John Vincent
Regional Sales Manager
North American Aftermarket

BorgWarner Turbo Systems
1849 Brevard
Rd.<https://maps.google.com/?q=1849+Brevard+Rd.%0D+Arden,+NC+28704&entry=gmail&source=g>
Arden, NC
28704<https://maps.google.com/?q=1849+Brevard+Rd.%0D+Arden,+NC+28704&entry=gmail&source=g>
Tel: +1 828-458-3159<tel:(828)%20458-3159>
jvincent@borgwarner.com<mailto:pharcourt@borgwarner.com>

From: Jeremy Worm [mailto:jjworm@mtu.edu<mailto:jjworm@mtu.edu>]
Sent: Tuesday, November 28, 2017 1:41 PM
To: Vincent, John (Asheville)
Subject: Seeking permission to reproduce compressor maps from catalog
Hi John,

Thanks for getting back to me. I was on the phone when you called.

Please find attached a document that gives a little more information and also shows the two figures that I am seeking permission to use.

Thanks!

Jeremy

Jeremy Worm, P.E.
Director, Michigan Tech Mobile Lab
Advanced Power Systems Research Center
Department of Mechanical Engineering - Engineering Mechanics
Michigan Tech
Office: 906-487-2686<tel:(906)%20487-2686>
Cell: 906-369-0886<tel:(906)%20369-0886>

17.11 Permission to Use Compressor Map from Garrett

COPYRIGHT LICENSE AGREEMENT (AS IS)

This Agreement made and entered into as of the 4th day of December, 2017 between Honeywell International Inc., with offices at 115 Tabor Road, NJ 07950 (the "Owner") and Jeremy Wohm (the "Licensee"). The Owner and Licensee hereby agree as follows:

1. Licensee is permitted to reproduce and use the works described in Exhibit A attached hereto (the "Material") on a non-exclusive basis to be used in connection with PhD Dissertation.

2. Licensee acknowledges that the Material IS PROVIDED "AS IS" WITHOUT WARRANTY OF ANY KIND, EITHER EXPRESS OR IMPLIED, INCLUDING BUT NOT LIMITED TO, THE IMPLIED WARRANTIES OF MERCHANTABILITY, FITNESS FOR A PARTICULAR PURPOSE, OR NON-INFRINGEMENT. Owner does not warrant or represent that it is the owner of the Material. Licensee acknowledges that Owner will not be liable, to Licensee or otherwise, for any damages of any kind, including without limitation, lost revenues or lost profits, which may result from the use of the Material (in whole or in part) by Licensee, even if Owner, or its representatives thereof, are advised of the possibility of such damages, losses or expenses.

3. This permission is granted on a royalty free basis and will endure for a period of 3 years from the date above.

4. Owner will not make a claim that Licensee's use of the Material as permitted herein infringes Owner's rights.

5. Any rights not expressly granted to Licensee are expressly retained Owner which may fully exercise and exploit the same at all times.

IN WITNESS WHEREOF, the Parties have caused this agreement to be signed by their respective officers thereunto duly authorized.

Honeywell International Inc.

By Jeremy Wohm

Name Jeremy Wohm

Date 12-04-2017

By _____

Name _____

Date _____